Effect and Position of Molecularly Engineered Bipropylenedioxythiophene-Bridged Donor/Acceptor Dyes in Dye-Sensitized Solar Cells (DSSC): Homo and Hetero-Dimeric Di-anchoring Organic Dyes For Panchromatic Light Absorption with Controlled Dye Aggregation and Reduced Charge Recombination

Thesis Submitted to the AcSIR for the Award of the Degree of

DOCTOR OF PHILOSOPHY

In Chemical Sciences

AcSIR

By
Manik Chandra Sil
(Registration Number: 10CC12A26004)

Under the guidance of
Dr. Jayaraj Nithyanandhan

Physical and Materials Chemistry Division
CSIR-National Chemical Laboratory
Pune-411008, India

June 2018

To My Parents

For their love, endless support, encouragement & sacrifices

सीएसआईआर – राष्ट्रीय रासायनिक प्रयोगशाला

(वैज्ञानिक तथा औद्योगिक अनुसंधान परिषद)

डॉ. होमी भाभा मार्ग, पुणे - 411 008, भारत

CSIR - NATIONAL CHEMICAL LABORATORY

(Council of Scientific & Industrial Research)

Dr. Homi Bhabha Road, Pune - 411 008, India

CERTIFICATE

This is to certify that the work incorporated in this Ph.D. thesis entitled "**Effect and Position of Molecularly Engineered Bipropylenedioxythiophene-Bridged Donor/Acceptor Dyes in Dye-Sensitized Solar Cells (DSSC): Homo and Hetero-Dimeric Di-anchoring Organic Dyes for Panchromatic Light Absorption with Controlled Dye Aggregation and Reduced Charge Recombination**" submitted by **Mr. Manik Chandra Sil** to Academy of Scientific and Innovative Research (AcSIR) in fulfillment of the requirements for the award of the Degree of Doctor of Philosophy in Chemical Sciences, embodies original research work under my supervision. I further certify that this work has not been submitted to any other University or Institution in part or full for the award of any degree or diploma. Research material obtained from other sources has been duly acknowledged in the thesis. Any text, illustration, table etc., used in the thesis from other sources, have been duly cited and acknowledged.

Research Student

Manik Chandra Sil

Research guide

Dr. Jayaraj Nithyanandhan

Senior Scientist

DECLARATION

I, hereby declare that the research work in this thesis entitled, "**Effect and Position of Molecularly Engineered Bipropylenedioxythiophene-Bridged Donor/Acceptor Dyes in Dye-Sensitized Solar Cells (DSSC): Homo and Hetero-Dimeric Di-anchoring Organic Dyes for Panchromatic Light Absorption with Controlled Dye Aggregation and Reduced Charge Recombination"** submitted for the degree of Doctor of Philosophy in Chemical Sciences to the Academy of Scientific & Innovative Research (AcSIR), has been carried out at the Physical and Materials Chemistry Division of CSIR-National Chemical Laboratory, Pune, India under the guidance of **Dr. Jayaraj Nithyanandhan**. Research material obtained from other sources has been duly cited and acknowledged in the thesis. The work is original and has not been submitted in part or full by me for any other degree or diploma to other University.

Date: 13/06/2018   **Manik Chandra Sil**

Physical and Materials Chemistry Division   Research Student

CSIR-National Chemical Laboratory,

Pune - 411008, India.

CONTENTS

Chapter 5:   **Orthogonally Functionalized Molecular Dyad Containing D-π-A Dye and Hole Transport Moiety for Dye-Sensitized Solar Cell**

Chapter 6:   **Summary and Future Outlooks**

, Sandeep Sharma, Swechchha, Dr. Shanti Dr. Sandip and many others for making this journey so wonderful.

Finally, I dedicate this thesis to the people who mean the most to me, my father **Sri. Anil Chandra Sil** *and mother* **Smt. Kalpana Bhowmik (Sil).** *Their patience and sacrifices are always a main source of my inspiration and will remain throughout my life, motivating me to pursue still higher goals. I am also thankful to my sister* **Smt. Anima Rani Shil** *and brother-in-law* **Sri. Swapan Sil** *for giving me constant encouragement and guidance throughout my life.*

Manik Chandra Sil

List of Abbreviations

AM	Air mass
CDCA	Chenodeoxycholic acid
CV	Cyclic Voltammetry
DFT	Density functional theory
DPV	Differential Pulse Voltammetry
DSSCs	Dye-sensitized solar cells
D-π-A	Donor-π-bridge-acceptor
EIS	Electrochemical Impedance Spectroscopy
FTO	Fluorine-doped-tin oxide
HOMO	Highest occupied molecular orbital
ICT	Intramolecular charge transfer
IPCE	Incident photon-to-current conversion efficiency
IR	Infrared
NIR	Near Infrared
J-V	Current-Voltage
LHE	Light harvesting efficiency
LUMO	Lowest unoccupied molecular orbital
MALDI-TOF	Matrix-assisted laser desorption ionization-time of flight
MLCT	Metal-to-ligand charge transfer
PCE	Power conversion efficiency
IPCE	Incident photon to current conversion efficiency
PV	Photovoltaic
UV-Vis	Ultraviolet-visible
NMR	Nuclear magnetic resonance
DCM	Dichloromethane
DMF	N,N-Dimethylformamide
DMA	N,N-Dimethylacetamide
EtOAc	Ethyl acetate
THF	Tetrahydrofuran
$CDCl_3$	Chloroform-d
MeOH-d_4	Methanol-d_4
DMSO-d_6	Dimethyl sulfoxide-d_6
E_g	Energy band gap
E_{CB}	Conduction band edge
ff	Fill factor
J_{SC}	Short-circuit currentdensity

V_{OC}	Open-circuit voltage
R_{ct}	Charge transfer resistance
C_μ	Chemical capacitance
η	Power conversion efficiency
τ	Electron lifetime
ε	Extinction coefficient
s	Singlet
d	Doublet
t	Triplet
m	Multiplet
MS	Mass spectrometry
M^+	Molecular ion
mmol	Millimole
MHz	Megahertz
ppm	Parts per million
Å	Angstrom
λ	Wavelength
eV	Electron volt
ºC	Degree Celsius
min	Minute(s)
h	Hour (s)
g	Gram
mg	Miligram
mL	Mililitre
kW	Kilowatt
GW	Gigawatt

ABSTRACT

Dye-sensitized solar cells have emerged as potential device architecture to harvest the solar energy due to easy device fabrication and diversity in key components such as semiconductors, dyes, electrolytes and cathode materials. Ever since the discovery of homoleptic metallated ruthenium-based dyes with 7.12% device efficiency by O'Regan and Grätzel, last two and half decade research on the functional materials provided deeper understanding of device structure and various pathways associated with interfacial charge transfer and recombination processes. Dye design with panchromatic absorption, avoiding both charge recombination and dye aggregation achieved high device efficiencies by increasing the J_{sc} and V_{oc} besides the choice of electrolyte having minimum loss-in-potentials. The structure-property relationship of organometallic and metal-free organic dyes have been carried out, so far the best conversion efficiency of about 13% was achieved for zinc-porphyrin dye and 12.5% for indenoperylene dye with cobalt (II/III) redox couple. One of the advantages of having D/A metal free organic dyes is that it utilizes simple precursors to tune the optical and electrochemical properties and which developed high molar absorptivity dyes with strong intermolecular charge transfer (ICT). Dyes with D-π-A, and D-A-π-A configurations provided good harvesting efficiency in the visible and far-red regions, respectively, whereas few chromophores such as polymethine, porphyrin, and phthalocyanine dyes have been explored for photo-current generation in near infrared (NIR) region.

The main disadvantages in DSSC are charge recombination, back electron transfer, dye aggregation and self-quenching of dyes. Tethering or substitution of long or bulky alkyl chain on donor moiety or π-spacer moiety in plane or out-of-plane may sort out this aggregation problem. Unfortunately, the concentration of dye loading in a unit area may reduce on that TiO_2 surface due to this modification. This decrease of dye loading used to reduce the J_{sc} value of DSSC devices.

DSSC dyes containing two anchoring groups were found potential candidates to settle down the above mention problem. It has seen that, those dyes reduce the aggregation as well as charge recombination. It has also seen that dianchoring dyes can bind with semiconductor in a bi-dentate fashion, which may lead to increase the charge injection capacity from LUMO of dye to conduction band of the semiconductor.

Hence, it was particularly focused on to synthesize of spiro-dyes containing two dye strands connected by a flexible spiro-linker (spiroBiProDOT). **In chapter 2**, it was observed that dimeric dianchoring dye **D_1-D_1** and **D_2-D_2** showed better device efficiency than that of its mono-congener **D_1** and **D_2** respectively. The flexible nature of spiro-unit lead to better charge passivation on TiO_2 surface as well as due to the presence of two di-anchoring group increases the charge injection and light harvesting efficiency for dimeric dyes. All the dyes were synthesized by using Pd-catalyzed direct arylation reaction. To get panchromatic absorption **D_1-D_2** was synthesized where two different dyes were connected through spiro linker. Finally to increase the solubility of **D_1-D_2** in some common organic solvent **D_2-D_4** was synthesized by introducing 2-ethyl hexyl chain. The highest efficiency was observed in homodimeric spiro-dye **D_1-D_1** with power conversion efficiency (PCE), of 7.6% with a V_{oc} and J_{sc} of 0.672 V and 16.16 mA/cm^2, respectively.

In chapter 3, two derivatives of symmetric (**D_{sq}-D_{sq}**) and asymmetric (**D_1-D_{sq}**) spiro squaraine dyes were synthesised and its photo-physical, electrochemical and photovoltaic properties were characterised. In order to comparison with dimeric dyes, a model squaraine dye **D_{sq}** was synthesised and characterised. In **D_{sq}-D_{sq}** dye, two **D_{sq}** monomeric unit was attached through 2H,2'H,4H,4'H-3,3'-spirobi[thieno[3,4-b][1,4]dioxepine] unit. On the other hand in **D_1-D_{sq}** contain two different dyes namely monomeric **D_{sq}** unit and **D_1** (donor-π-acceptor) unit. **D_1-D_{sq}** dye showed better device performance of 3.9% with V_{oc} = 0.652 V, J_{sc}

= 8.89 mA/cm^2, *ff* = 69% under 1 sun, AM1.5G rather than that of **D$_{sq}$-D$_{sq}$** of 2.8 % PCE with the open circuit voltage (*V$_{oc}$*) of 0.607 V, short-circuit current density *J$_{sc}$* of 6.62 mA/cm^2. Effective charge passivation plays an important role to increase the *V$_{oc}$* of DSSC device incorporating spiro-dyes. At the same time effective dipole moment of **D$_1$-D$_{sq}$** may increase shift the conduction band of TiO2. Due to aforementioned issues has been lead to increase the PCE of **D$_1$-D$_{sq}$** than that of **D$_{sq}$-D$_{sq}$**.

In chapter 4, a series of homo spiro-dimeric D-π-A dyes based on bithiophene and terthiophene spacers with two-anchoring group containing dyes, **TT$_1$**, **T$_1$T**, **TT$_1$T** were designed and synthesized by Pd-catalysed successive Suzuki coupling followed by direct arylation reactions. In between two structural isomeric dyes **TT$_1$** and **T$_1$T**, the spiro spacer branching unit (spiroBiProDOT) was placed near and away from the anchoring carboxylic acid unit, respectively. The better efficiency with higher photovoltaic parameters (PCE of 3.9 % with a *V$_{oc}$* and *J$_{sc}$* of 0.593 V and 9.09 mA/cm^2) was observed in **T$_1$T**, in which the branching unit was placed far away from anchoring group than that of **TT$_1$** (PCE of 2.45 % with *V$_{oc}$* of 0.568 V and *J$_{sc}$* of 6.25 mA/cm^2). Based upon the above results it was decided to design a new dye **TT$_1$T** by incorporating an extra thiophene unit in between the donor and π-spacer. The maximum efficiency was observed in **TT$_1$T** with PCE of 4.29 % with *V$_{oc}$* of 0.589 V, *J$_{sc}$* of 9.8 mA/cm^2.

In chapter 5, a D-π-A dye and hole transport moiety connected through spiro-linker (**D$_1$-HTM**) has been synthesized and characterized by photo-physical, electrochemical methods and fabricated DSSC devices for dye-sensitized solar cell. In order to increase the dye regeneration process, a triarylamine based electron donor was introduced and attached with D-π-A dye unit. The best efficiency of **D$_1$-HTM** was found by using 5 equivalent of co-adsorbent CDCA of 2.24 % (*V$_{oc}$* and *J$_{sc}$* of 0.590 V and 5.27 mA/cm^2).

Introduction to Dye Sensitized Solar Cell (DSSC)

1.1 Introduction

Electricity generated from renewable energy sources increased from 13 to 16.7 % in the year 2012 and it will exceed 22 % in 2020 according to the international energy agency. The generation of renewable energy sources are becoming the global challenging for the development of nation as well as the world. At the same time higher the practice of renewable energy resources (**Figure 1**) can save the whole earth in terms of global warming and the mask layer present in the above of earth atmosphere.[1]
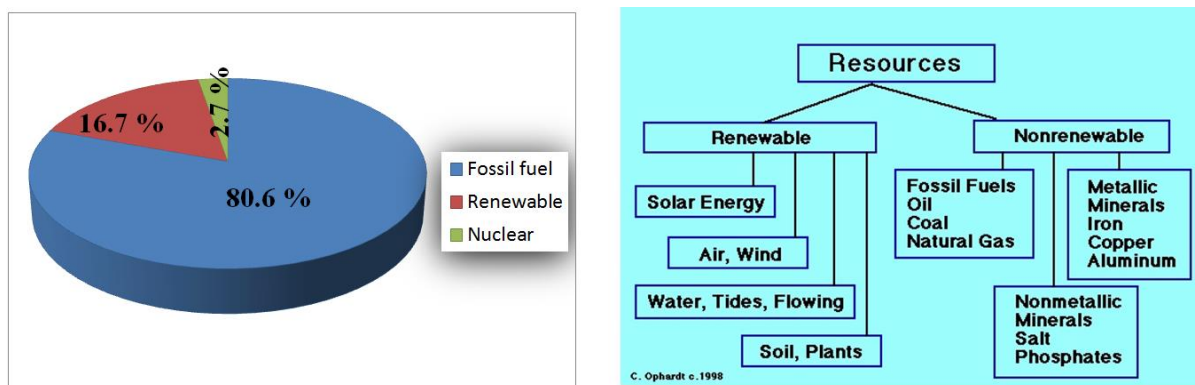
Figure 1. Pie-graph of consumption of renewable and non-renewable energy distribution and types of energy sources.

The percentage of using different types of renewable energy sources in 2015 are

- 12.35% from biomass and bio fuel

- 3.34% as hydroelectricity

- 0.001% as a tidal power

- 0.51% from wind energy

- 0.46% from solar power

1.2 Necessity of renewable energy

1.2.1 Limited fossil fuel

The first and main reason for why governments and businesses are keen to move to renewable energies as soon as possible is that fossil fuels are a finite resource and come to end near future. This is true that, fossil fuels will run out eventually and it will take some 10,000,000 years to replenish whatever used in around 150 years. As the human population increases, our rate of consumption of these fossil fuels also increases.[2] Geologists and others whose job it is to locate access these pockets of crude oil and finding its availability become difficult to locate and extract new sources. Now it is impossible to control the rate of consumption of crude petroleum and oil without any better substitution.

1.2.2 Greenhouse effect

The most immediate problem has been taken seriously in United Nations Climate Change Conference (COP21) agreement of 2016. The serious object was the global warming effect which had seen in the last 150 years. The carbon emission is the main reason of that climate change and the solid reason for warming the planet. In the last few years especially, no part of the world has been untouched by unusual weather conditions. Most continents have recorded record high temperatures in summer, record lows in winter and increased frequency of typhoons and hurricanes, record dry spells, drought and flooding. There is no doubt that these irregular weather conditions are affecting every country.[3]

For the above reasons the harness of renewable energy sources, and the technology is essential to maintain the useful weather in this planet is necessary. In most cases, once installed it has to minimal or no carbon output and can still provide our energy needs. It is not possible to make this earth carbon neutral, as it takes resources to make a lot of solar panel, build a dam and so on, but still it is a critical and significant reduction of our carbon output. Therefore it is necessary to take some steps to control carbon footprint for international regulations, to help those in the developing world, and to protect ourselves against the abnormal weather. It is also well known that the ice caps are melting and the sea levels are rising which creates food shortages and national instability as well as being an expensive situation for our insurance.

1.2.3 Economic stability

To maintain the economic condition and sustained with the global economic system with greater stability it is necessary for constant and sustained energy supply such as hydroelectric, wave power, biofuel and solar energy. In some cases energy developed from renewable sources is cheaper than that of non-renewable sources. For example Idaho and Texas generated more electricity from geothermal and wind energy respectively rather than that of non-renewable energy sources.[4]

1.2.4 Environmental damage

Now a days it is harder to achieved new pockets of oil and also a challenging job to drill longer and deeper to get it. However there is always a conflict between environmental groups and industry and between governments and both groups when local wildlife and environmentally sensitive areas are threatened.

1.2.5 Public health

The level of pollution and the toxicity due to harmful gases and liquid by oil, gas and coal drilling and mining is the main concern of each government. It has taken decades about the knock on effect of industrial processes for public health. There are few renewables are entirely emission-free, but their output is much lower than conventional fossil fuel acquisition and processing.

1.3 Types of renewable energy sources

It would be not technically correct for the clear division of renewable energy sources because of their unlimited classification but it is important to note that not all forms are environmentally friendly. Here, it was discussed the most common types (**Figure 2**) of renewable energy and discuss their advantages and limitations.[5]

Figure 2. Pie-graph of world consumption of renewable energy sources.

1.3.1 Hydroelectricity

Using water's motion power to generate electricity is not a new concept. It has been established so far around one hundred years ago. Generally hydroelectricity is produced by

processing and controlling the current of water through a dam. This is one of the most powerful forms of renewable energy. Hydropower is the leading renewable source for electricity generation globally, supplying 21% of all renewable electricity. Reaching 1,064 GW of installed capacity in 2016, it generated 3.34% of the world's electricity from all sources.[6]

Advantages: The main advantages of this process are that the power generation can be tailored depending on the needs of the community. During times of low use output may be reduced, and increased during times of high output need, these changes can be made quickly compared to oil production which has a delay due to the need to refine the raw product. The momentum with which these input and output of hydroelectricity used to change is a major advantage of growing energy needs. However during the construction of high level building and maintaining of these dam produces carbon emission in the atmosphere but still this process gives a significant reduction of burning fossil fuels. The relative cheapness of construction and maintenance, and the low cost of generation mean it is used increasingly in both the developed and the developing world. Dams are not only useful for power generation although it can be regulate water supply during floods and maintain water supplies during a draught. For an example in the year of 1980, Aswan dam prevented drought in Egypt whereas the other countries around them (Sudan, Ethiopia) suffered horrific drought.

Disadvantages: It will take a high level of cost to build a dam and also it should be keep in mind to the construction of a new building on that site by the environmental engineers. Building of a dam can destroy an area of landscape and may changes the ecology downstream. Dam building can also destroy the cultural landscapes and sometimes this can be unavoidable. For an example Aswan dam created a problem when, the river valley flooded to create the high water table that would sit behind the dam destroyed an important

archaeological landscape. However many relics were saved and features recorded as well as the movement of Philae temple was done by international community.[7] Even though the cultural landscape around this original site is lost forever. On the other hand high level of methane is produced in the area of reservoirs but this has been put down to the higher levels of anaerobic chemical reaction. Finally, the potential for failure of a dam is catastrophic. Should it burst, any settlement in the valley below would be flooded, leading possibly to loss of human life, destroyed houses, disrupted power supply to all the homes affected and possibly flooding of the winder landscape beyond, more ecological damage, more loss of human life.

1.3.2 Tidal power

With the help of ebb and flow of the oceans the power generation is possible which is termed as tidal power, yet it is not so common. This a common form of power generation across the Atlantic, in the eastern US states and Western Europe. Tidal power generators come in three general types.[8]

(a) Stream generators use the water flow to power a turbine which then generates electricity.

(b) Tidal lagoons are still in development, but it has to work in a similar fashion to the barrage but is completely artificial.

(c) Dynamic tidal power is still theoretical and has not been tried, but requires the building of dams that are tens of kilometres long to regulate water flow.

Advantages: The better predictable coordination of the moon and earth makes more accurate measurement of tidal power rather than that of other renewable energy resources. First of all, it can be measured accurately the number of high and low tide times. This has always helped plan a number of maritime functions and now it is helping us begin to generate electricity. Secondly, the volume of water on the planet is fairly constant and unlikely to run out, even without a significant temperature rise way beyond the 2-3 ^{0}C predicted by climate scientists. Fortunately melting of ice caps is not effected the tidal changes by a prominent figure, but moon is only the influencing factor of this high and low tide fluctuation. Finally, most important of this energy production is that, high output energy can be produced by applying low input of human strength.

Disadvantages: The main disadvantage of this technology is that, it is limited only in coastal region. Unfortunately this technology has largely not been taken up due to high cost and other cheaper technology is available instead of this technology. As mentioned above, the technology is limited to those areas of the world with a wide variation in its tidal range to warrant harnessing the power of the sea - this includes the eastern seaboard of North America and Western Europe but few other places.

1.3.3 Wind power

This technology of harnessing unlimited power generated by natural process is very common in most of the countries of this world. This kind of energy is most commonly used to drive a ship on the ocean. The same principle has been used to generate the electricity through the turbines of wind farm. The same principle is behind the generation of electricity through the turbines of wind farms. At sea or on land, these giant spinning windmills capture the power of the air around it. In 2015, Denmark broke its own world record by producing

over 40% of its national power from wind energy. Wind power is far more popular in Europe than in North America, with nearly have of the global capacity produced across various European countries. Many of these are at sea where most of the wind power is produced.[9]

Advantages: Most advantage of this wind power due to constant weather cycles on Earth and nowhere in this planet is untouched by wind. There is greater levels of wind at sea as the topography does not act as wind breaks as it does on land, this means greater potential to harness energy and most wind farms are at sea. Turbines can be altered for maximum efficiency of use to generate as much energy as possible, because it is efficient and also very low cost compared to most others - including other forms of renewable energy, arguably the cheapest form available.

Disadvantages: The best place to produce wind energy is coastal areas and those land having high level of wind sources. However these areas are highly far away from common populated areas. The optimum siting of wind farms is often counterintuitive to the needs of the people that will use the energy it generates. Wind sources are best out at sea where there are no cities, and on large, expansive plains which are far from the settlements that will need it. It does mean that there should be great investment of transport energy from the place of generation to the place of consumption if wind power is controlled as a major power source.

1.3.4 Biofuel & biomass

Biofuel is the production of the types of fuel that has use in vehicles from plants or other organic matter rather than from the fossil fuels extracted from the ground. Biofuels are produced in one of two ways:

(a) Directly processing a raw plant material, such as extracting its natural oils, and processing it into a type of fuel

(b) Extraction of residues or decomposing matter as a result of natural anaerobic processes (such as broken down by bacteria or algae into an alcohol substance – bioethanol)

On the other hand biomass is different from biofuel, where waste organic material such as wood and other plant matter. Here the energy is produced by burning the chopped wood, grasses, leaves, brush, scrub and other organic raw materials including animal dung. In the past, and indeed in areas where there are few trees to burn as fuel (Arctic Circle) people may burn bone or as a source of fuel.[10]

Advantages: One of the most advantages of energy generation from biofuel and biomass is flexibility especially when liquid fuel such as ethanol can be generated from this process. Different topographies are suitable for different types of crop, which means that most countries should be able to produce biofuels as it is not limited to one crop type of crop cultivation. It can be easily produced it in moderate areas of the US as well as more tropical or arid locations. Another advantage is that supply of this fuel to vicinity of populated area is very easy as well as it is not depend on the international trade for fuel. This facility will have lower carbon footprint for having eliminated the transportation process of getting fuel from source to consumer which will increase the energy security.

Disadvantages: It is true to improvise most of the bio fuels until or unless there has some substituted which is cleaner and greener than ethanol. The energy generated from biofuels and biomass is much lower than that of conventional fossils fuels and required to generate

high quantity. Unfortunately, more areas of land are required to produce biofuels and biomass but our land is limited or constant in this Earth. Half of the world will face problem like starving if the major quantity of the land is used for biofuel and biomass energy generator.

1.3.5 Solar energy

It may be argued that sun is not renewable energy because it has a finite end but it is a matter of fact that it has 4.5 billion years lifetime and not an immediate cause of worry. Solar light offers climate-friendly, easily available and clean energy to all over the glove which is well-spread. However the availability depends upon the climate of that region. Fortunately it is more or less available in the whole world. Solar energy is up growing due to its cost effectiveness and availability in each every door. In many islands and sunny countries solar thermal electricity (STE) and photovoltaic energy are making a healthy competition with the energy developed from oil and natural gas. There are two basic types of solar energy.

(a) Photovoltaic solar technology is a method in which sunlight's can be directly converted into electricity using panels of semiconductor cells.[11]

(b) Solar thermal technology in which after the storage of the sun's heat can directly or converted into mechanical energy which also converted electrical energy. This can be use directly or can be converted into mechanical energy to generate electricity.[12]

Advantages: One of the most important advantages of solar energy is that it can be used to produce electricity as long as the sun exists. This energy can be harnessed by installing solar panels that can reduce our dependence on other countries for consistent supply of coal to produce electricity. Solar energy is the way to minimize carbon footprint by making the atmosphere carbon free. Solar energy is an alternative for fossil fuels as it is non-polluting,

clean, reliable and renewable source of energy. It does not pollute the air by releasing harmful gases like carbon dioxide, nitrogen oxide or sulphur oxide. So, the risk of damage to the environment is reduced. Solar energy also does not require any fuel to produce electricity and thus avoids the problem of transportation of fuel or storage of radioactive waste. Secondly, solar energy is also cost effective and far cheaper now a day. Here it does representing long term investment with minimum savings. Moreover it is noise free and can work all the time. Finally it is true that solar energy is an important form up growing resource which may lead to most efficient system near future.

Disadvantages: There are three major disadvantages to solar energy. Firstly, their efficiency became less in cloudy days as well as winter and stormy season. However the new technology of photovoltaic system is more efficient than that of the previous system and research is going on to make it more efficient. In this way it can be more applicable in sunnier climes as well as less sunshine zone. The second disadvantage solar panel is tough to place in a direction considering the rotation of earth. The rotation of the Earth doesn't need to be explained here beyond the understanding that the sun does not remain in the same place all day. It rises in the east and sets in the west. Therefore an expensive system is required by which to rotate your panels with definite time period. The third and important one is to get maximum power efficiency through out that solar PV panels.

1.4 Types of solar cells and application

The name of the solar cell is considered with the semiconductor by which these made of. Those materials contained certain characteristic properties of photon absorption from the solar light. Some solar technology can optimize the sunlight that reaches the earth's surface, while others are optimized for use in space.[13] Solar cells can be made of one single layer of

light-absorbing material (single-junction) or multiple physical configurations (multi-junctions), which may lead to take advantage of broad absorption in solar spectrum and charge separation mechanisms. Solar cells are classified into first, second and third generation solar cells. The first generation cells are conventional, traditional and wafer-based cells which are made of crystalline silicon, the commercially photovoltaic technology. These materials are based on polysilicon and monocrystalline silicon. Second generation cells are consists of thin film solar cells which include amorphous silicon, CdTe and CIGS cells. These solar cells are commercially significant in utility-scale photovoltaic power stations. The third generation of solar cells includes multilayer of thin-film technologies which have not yet been commercially applied and are still in the research or development phase. Use of organometallic compounds as well as inorganic substances such as ruthenium complexes with organic ligand can be used as a sensitizer to absorb light and these are considered as a fourth generation of solar cell. However perovskite, polymer and organic solar cell are recently in developing stage. Few companies already developed polymer solar cell in commercial stage (Krebs, Denmark). Different types of solar cells are given below.

1.4.1 Amorphous silicon solar cell (A-Si)

Amorphous silicon (A-Si) is the non-crystalline form of silicon.[14–17] It is well developed of the thin film technologies had commercialized. It is widely used in pocket calculators, but it also powers some private homes, buildings, and remote facilities. One of the most disadvantages of this solar cell is degradation in their power output when it exposed to sunlight. The power conversion efficiency of this type of cell reaches up to 26.6 % till the date.

1.4.2 Copper indium gallium selenide solar cells (CI(G) S)

One of the most challenging and promising in solar is Copper-Indium-Gallium-Selenide (CIGS). A copper indium gallium selenide solar cell (or CIGS cell, sometimes CI(G)S or CIS cell) is a thin film solar cell used to convert sunlight into electrical energy.[18–21] Thin layers of copper, indium, gallium and selenium which are coated on glass surface along with the electrodes helps to generate electricity. The film using in this method is much thinner because the material has high absorption coefficient. CIGS is one of the powerful candidates among thin-film PV technologies compared to the other two cadmium telluride and amorphous silicon. CIGS solar cell efficiency reached up to 23.1% efficiency whereas CdTe got 22.1% efficiency according to NREL.

1.4.3 Cadmium telluride solar cell (CdTe)

Cadmium telluride (CdTe) photovoltaics was developed by using of cadmium telluride on thin film semiconductor, which absorbed the light and convert into electric energy.[22–26] This technology is better than that of silicon technology in terms of carbon foot print. One the most disadvantage of this technology is the toxicity of cadmium and the life time of CdTe. This type of cells is used in some of the world's largest photovoltaic power stations. The power conversion efficiency of this cell reaches up to 22.7 % in 2017.

1.4.4 Multi-junction cells

The only difference between a concentrating photovoltaic (CPV) with the common conventional photovoltaic technology is a concentrator (an advanced optical system) by which a large area of sunlight can be focused into a small area of cell to get maximum efficiency.[24,27–29,29,30] Depends upon concentration factor it was classified into two different ways, such as low-concentration (LCPV) and high concentration (HCPV). On the other hand

conventional photovoltaic systems contain lenses and curved mirrors to focus sunlight into small area of multi-junction. Multi-junction photovoltaic solar cell is also classified into two, three and four junction solar cell (using concentrator, or non-concentrator). In these technologies, solar trackers and cooling system has been used to increase the efficiency. Concentrated two junctions and four junction solar cell were reached up to 44 and 46% efficiency respectively and the day is nearby when multi-junction solar cell will completely with the race against conventional fossils fuels. Concentrating photovoltaic systems work by converting solar light into electricity. Traditional rooftop solar modules rely on the same basic concept to generate electricity. The concentration factor in multi-junction solar cell reduces the semiconductor area more than thousands times. Out of different multi junction solar cell, four-junction solar cell showed highest 46 % solar efficiency in 2017.

1.4.5 Single junction GaAS solar cell

Gallium arsenide is composed of gallium and arsenic. The velocity and the mobility of the electron will be increased in GaAs semiconductor rather than that of Si window itself. GaAs semiconductor can emit light efficiently due to the presence of direct band gap.[31–34] High level optical windows, IR-LED, integrated circuits (microwave frequency and monolithicmicrowave), laser diodes has been made of GaAS semiconductor. GaAS solar cell has been classified into three different categories e.g. single crystal, concentrator and thin-film crystal. One of the most advantages of this semiconductor is that it contains a higher breakdown voltage. Breakdown voltage is the minimum (reverse) voltage applied that can cause to make a part of the component electrically conductive (or conduct in reverse). All of these described above factors made this semiconductor a good candidate for applying in cellular telephones, satellites, communicative satellites and solar power. The concentrator is

giving highest efficiency of 29.3 % out of three different type of single junction GaAS solar cell in 2017.

1.4.6 Monocrystalline solar cell (Mono-Si)

All electronic equipment's and devices are based on silicon chips containing monocrystalline silicon (or "single-crystal silicon", "single-crystal Si", "mono c-Si", or just mono-Si). In solar cell this silicon chips also used as photovoltaic, light-absorbing material. Mono-Si can be prepared intrinsic consisting only of exceedingly pure silicon, or doped, containing very small quantities of other elements added to change its semiconducting properties[35–39]. In present days, due to the availability and affordable cost single-crystal silicon chips are widely use in electronic and informative technical devices. Monocrystalline silicon differs from other allotropic forms, such as the non-crystalline amorphous silicon which is used in thin-film solar cells, and polycrystalline silicon, that consists of small crystals of silicon. Monocrystalline solar cell is also divided into two parts e.g. concentrator and non-concentrator. Non-concentrator is giving highest efficiency of 27.6 %.

1.4.7 Perovskite-sensitized solar cells

Highly efficient light- harvesting characteristics was developed in perovskite $CH_3NH_3PbI_3$ sensitizer.[40] After discovery the high light absorbing properties of these inorganic crystals got a greater attention to use them as a sensitizer.[40] In the beginning metal chalcogenides have been reported with solid-state dye-sensitized solar cells, where the best power conversion efficiency of 6%. In this technology submicrometer-thick TiO_2 film is required to deliver sufficient internal surface area to absorb sufficient dye in order to absorb most of incident sunlight.[41–47] In 2012 $CH_3NH_3PbX_3$ (X = Cl, Br, or I) perovskite sensitizer made a first

breakthrough in solid-state solar cells after getting 10 % power conversion efficiency. After

that a rapid efficiency of power conversion was developed in perovskite-sensitized solid-state

mesoscopic solar cells and reached up to 22.1 % till the date.

A schematic of the perovskite-sensitized titania and the spectral response of the ensuing solar

cell are shown in **Figure 3**.
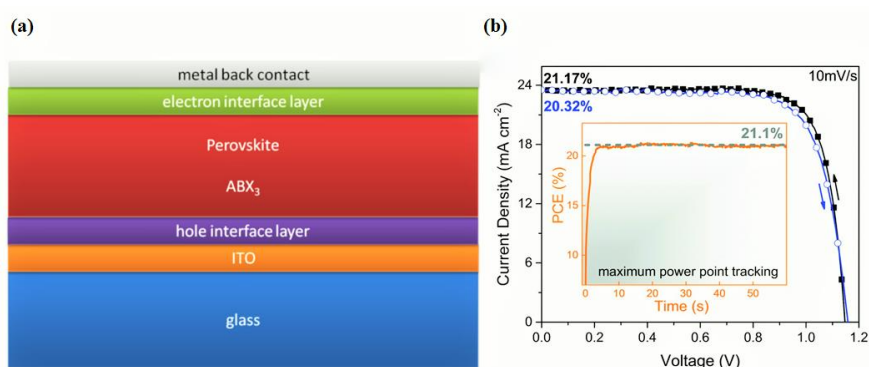
Figure 3. (a) A general structure of perovskite solar cell, and (b) the PCE curve of highest

efficiency perovskite solar cell till date (on applied and reverse vias at 10 mV/s rate).

1.4.8 Quantum dot sensitized solar cells (QDSCs)

Quantum dot sensitized solar cells (QDSCs), also defined as a third generation solar

cells, are optimistic candidates for solar energy harvester due to have prominent

optoelectronic properties by efficient light harvesting and reduced cost.[48–50] Most importantly

the bulk and heavy materials like silicon, copper indium gallium selenide (CIGS) or cadmium

tellurium (CdTe) were replaced by simply synthesized quantum dots. One of the most

important advantages of this solar device is that, the band gap can be tuned with wide range

by changing the size of quantum dots. Generally, As (III), Sb (III) quantum dots are

incorporating for multi-photon absorption from the solar system. Therefore the proportion of

light harvesting in different region of the solar spectrum were done by varying the size of

quantum dots in different layer of multi-junction solar cell. The power conversion efficiencies have been increased from less than 5% to the state-of-the-art 13.6% in 2017.

1.4.9 Organic photovoltaic (OPV)

Another important technology, which converts solar energy to electrical energy, is called organic photovoltaics.[51–54] A general OPV device is consisted with two electrodes (**Figure 4**) and several photoactive materials (donor and acceptor part). Upon shining light, light is absorbed in the photoactive layers composed with donor and acceptor materials. The donor material acts as an electron donor or hole transporter and at the same time an acceptor material act as an electron acceptor or electron transporter.
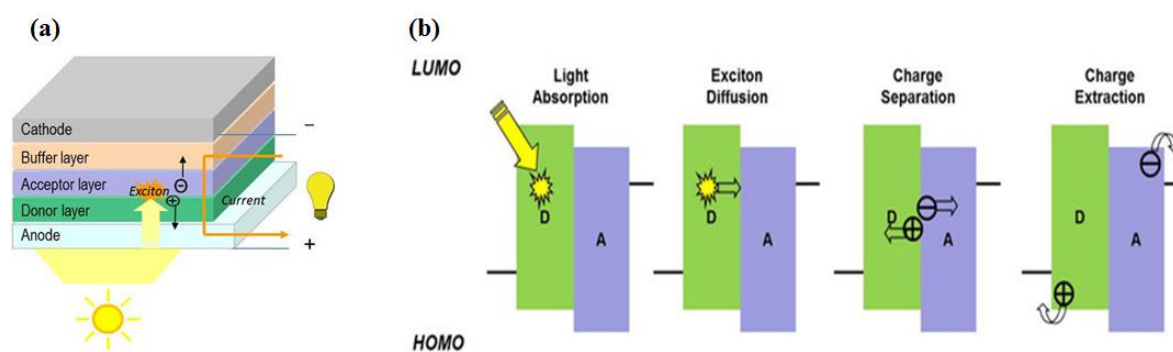
Figure 4. (a) Structure of a bilayer organic photovoltaic device, (b) general mechanism of a bilayer organic photovoltaic (D = donor, A = acceptor).

On shining the light, photoactive materials harvest photons from sunlight to form excitons, by exited the electrons from the HOMO (highest occupied molecular orbital) into the LUMO (lowest unoccupied molecular orbital). On higher concentration on light absorption, those excitons diffuse in the interfaces of donor and acceptor materials. In this way the charge is separated into free holes and electrons. Upon charge extraction by different

opposite phase due to the movement of electron and holes towards particular electrodes afford to generate photovoltaic current. The significant improvement of OPV device performance has been accomplished by introducing various OPV architectures, such as bulk-heterojuction (BHJ) as well as inverted device structures and by developing low band gap conjugated polymers and innovative organic small donor materials. The power conversion efficiency has been increase up to 14.2% till the date.[55]

1.4.10 Dye sensitized solar cell

For more than 22 years, dye sensitized solar cells (DSSC) have been under extensive research. Since the efficiency of the device can be easily varied by choosing different dyes and cells on flexible substrates have been already demonstrated, DSSCs are especially attractive for Building Integrated Photovoltaic (BIPV). The cell concept is believed to reduce the production cost and energy payback time significantly compared to standard silicon cells or other thin film cells. The conversion efficiency varies between 6 -10% depending on the module size and the technology is currently on the pilot plant scale. First the main impediments for large-scale production are presented and then different approaches to improve the hole conduction in the electrolyte and the light harvesting of the dye are introduced. But since iodine corrodes most metals and generates a problem of scaling up of the device. A lot of research is going on to get hole conductors materials.

1.5 Components use in DSSC (TiO$_2$, redox electrolyte, light absorbing dye)

DSSCs are composed of three main components, (A) mesoporous n-type TiO$_2$ that is sensitized with a (B) redox-active electrolyte (C) light-absorbing dye and (D) Cathode materials.

(A) Mesoporous n-type TiO₂: TiO$_2$ is a wide band gap semiconductor with a gap of 3-3.2 eV, therefore is transparent to the visible region of light. The common crystal structures of TiO$_2$ are rutile, anatase and brookite. Rutile crystallizes in the tetragonal system, in which six oxygen atoms form a distorted octahedral around the titanium with four shorter and two longer Ti-O bonds. Anatase is slightly different from octahedral structure. Rutile to anatase transformation occurs in the temperature range of 700-1000 °C depending on crystal size and impurities. The main difference between the two allotropic forms is the band gap which is of about 3 eV for rutile and of 3.2 eV for anatase. The valence band is composed of oxygen 2p orbitals hybridized with titanium 3d orbitals, whereas the conduction band is composed primarily of titanium 3d orbitals. Titanium dioxide is chemically inert, nontoxic and biocompatible. It is easy to produce in large scale at low cost. Due to the high surface affinity toward carboxylates, salicylates, phosphonates and boronates, it can be sensitized by a large variety of dyes, some of them allowing incident photon/electron conversion efficiency close to unity.

(B) Redox-active electrolyte
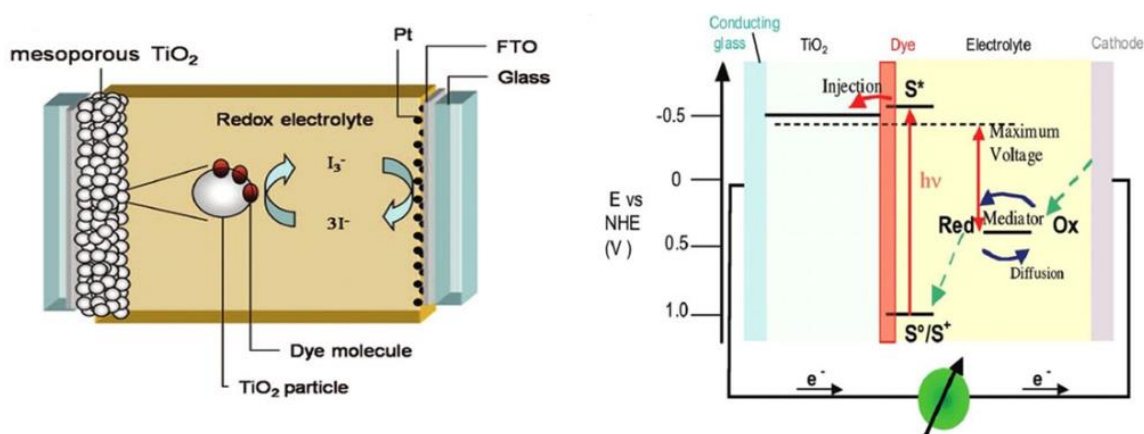
Figure 5. Schematic diagram representation of DSSCs employing the iodide/triiodide redox couple is given above (http://www-g.eng.cam.ac.uk/CMMPE/lcddss.html).

DSSCs consist of three processes (I) light absorption, (II) electron- and (III) hole transport between three different materials. Light is absorbed by a dye which transfers the electrons into the conduction band of a mesoporous metaloxide, usually TiO_2. The dye is then regenerated by a hole transporting material (HTM) which is infiltrated into the (**Figure 5**) mesoporous network and transports the hole to the respective electrode. DSSCs have conventionally incorporated an iodide/triiodide (I^-/I_3^-) liquid electrolyte as the HTM. The main disadvantages of cell using iodide/triiodide electrolyte system are

1. Such cells suffer from potential leakage problems associated with the corrosive and volatile nature of the liquid electrolyte and, thus, may be impractical for large-scale applications.

2. More importantly, the over potential required for dye regeneration by the I^-/I_3^- redox couple limits the maximum obtainable voltage of the system.

3. The triiodide ion absorbs a significant part of the visible light when employed in high concentrations, its low redox potential limits the open-circuit voltage available, and

4. Its aggressiveness towards silver prevents the use of this metal as current collector in large cells.

The use of alternative redox couples and their photovoltaic performance has been reviewed to examine the cell performance. Organic redox couples investigated includes halogens, pseudo halogens, inter halogens, hydroquinone's, nitroxide radicals and sulfur-based systems. Many of these redox couples investigated, such as Br^-/Br_3^-, $SCN^-/(SCN)_3^-$, $SeCN^-/(SeCN)_3^-$ and thiolate/disulfide redox couples, involves, like iodide/triiodide, the

interchange of 2 electrons. The complicated regeneration mechanism for most halogens and pseudo halogens redox couples has thus been suggested to limit the solar cell performance.

Co (III) and Co (III) redox couple of cobalt complex also used instead of using triiodide system to get better current efficiency.[56] The one-electron-transfer redox mediator [Co (dbbip)$_2$](ClO$_4$)$_2$ (2, 6-bis (1-butylbenzimidazol-2$^/$-yl) pyridine) performed best among the compounds investigated. The E$_{1/2}$ value of cobalt complexes influences V_{OC}, which increases with higher E$_{1/2}$ values. In spite of slow dye regeneration kinetics for step 3, the enhanced photovoltaic performances observed with this dye are due to steric and electrostatic effects. With the design of novel heteroleptic hydrophobic ruthenium dyes and optimized electrolyte solutions, it was able to reach incident photon to-current conversion efficiencies of over 80% in the visible region.

There are many requirements to be fulfilled by an alternative redox mediator in order to obtain high efficiency DSSCs:

(a) The redox potential should be as positive as possible to optimize the photovoltage of the devices, meanwhile maintaining a sufficient driving force for regeneration of the oxidized dye molecules.

(b) Slow interfacial electron recombination kinetics.

(c) High diffusion coefficient to avoid mass transport limitations.

(d) Fast electron transfer kinetics at the counter electrode.

(e) Negligible visible light absorption.

(f) Non-corrosiveness towards metal contacts.

(g) Good photo-electrochemical stability.

(C) Light-Absorbing Dye: In the last 15–20 years a lot of effort has been done to the synthesis and characterisation of materials for Dye sensitised solar cells. Working principles of dye sensitized solar cell can easily understand by using modelling electrical and optical properties as well as by advanced characterization techniques. Sensitizers used for DSSCs can be grouped into two broad areas: (1) Functional ruthenium (II)–polypyridyl complexes such as N3, N719 (TBA$^+$=tetra-n-butyl ammonium), Z907, and black dye and (2) metal-free organic donor–acceptor (D–A) dyes. The former class of compounds contains expensive ruthenium metal and requires careful synthesis and tricky purification steps. On the other hand, the second classes can be prepared rather inexpensively by following established design strategies. The major advantages of these metal-free dyes are their tuneable absorption and electrochemical properties through suitable molecular design. T. Miyasaka and co-workers came up with a new idea has used in DSSCs in between 2007.[57] $CH_3NH_3PbI_3$ and $CH_3NH_3PbBr_3$ absorbers were employed in (3) perovskite-sensitized solar cells.

(D) Counter electrode: Platinum deposited on fluorine-doped tin oxide (FTO) plate act as a counter electrode in dye sensitized solar cell. This cathode material in DSSC helps in the regeneration of oxidized dye by catalysing the I$^-$ reformation from I_3^- ion in redox couple. However, the facet and surface of the platinum electrode are playing an important rule of DSSC device efficiency. The cost of platinum is an important disadvantage in DSSC device. However, graphite and carbon black has been introduced instead of platinum electrode in liquid organic DSSC.[58–61]

1.6 DSSC - operation principle

Dye-sensitized solar cells have emerged as potential device architecture to harvest the solar energy due to easy device fabrication and diversity in key components such as semiconductors, dyes, electrolytes and cathode materials. Ever since the discovery of homoleptic metallated ruthenium-based dyes with 7.12% device efficiency by O'Regan and Grätzel, last two and half decade research on the functional materials provided deeper understanding of device structure and various pathways associated with interfacial charge transfer and recombination processes. Dye design with panchromatic absorption, avoiding both charge recombination and dye aggregation achieved high device efficiencies by increasing the J_{sc} and V_{oc} besides the choice of electrolyte having minimum loss-in-potentials. The structure-property relationship of organometallic and metal-free organic dyes have been carried out, so far the best conversion efficiency of about 13% was achieved for zinc-porphyrin dye and 12.5% for indenoperylene dye[62] with cobalt (II/III) redox couple. The main problem was that a monolayer of dye molecules on a flat surface can only absorbed up to 1 % of the incident light. Introduction of nano porous TiO_2 electrodes with a roughness factor of ca. 1000 dramatically increased the light harvesting efficiency and in 1991 solar cells of 7 % efficiency were introduced[63].
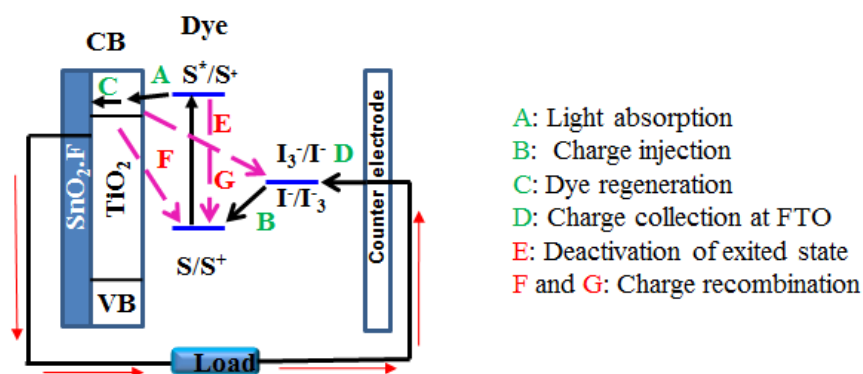
Figure 6. General mechanism in dye sensitized solar cell.

Step 1. (A) Upon photo-excitation, a photo-excited electron is injected from the excited state (LUMO) of the dye into the conduction band of the TiO_2 (**Figure 6**). The lifetime of the excited state is in the nano second range. At high iodine concentration reductive quenching might deactivate the excited state representing a loss channel. The dye injects an electron into the conduction band of the TiO_2. The corresponding injection rate constants are in the femtosecond range (singlet state) and about one order of magnitude slower for the triplet state. Since the energy level of the triplet state is only slightly above the conduction band edge of TiO_2, both the driving force for electron injection and the electron transfer probability is lower, which is believed to the reason for the relatively slow injection rate. For efficient charge injection the energy level of the dye has to be between 0.2 V and 0.3 V above the TiO_2 conduction band edge, which corresponds to -0.5 V vs. NHE on the electrochemically energy scale. The back reaction, the reduction of oxidized sensitizer molecules by conduction band electrons occurs in the μs - ms range and is thus several orders of magnitude slower. This huge difference is the main reason for the efficient charge separation in the device.

Step 2. (B) The oxidized dye molecules are then regenerated by the electrolyte leaving the oxidized electrolyte in the system. The regeneration of the oxidized dye occurs in the nanosecond range, which are typically 100 times faster than any recombination reaction and about 10^8 times faster than the intrinsic lifetime of the oxidized dye. It is a two-step electron transfer with a large driving force. I_2^- then undergoes disproportionate reaction into I_3^- and I^-.

$$2I^- + D^+ \xrightarrow{K_3} I_2^- + D$$

$$2I_2^- \xrightarrow{K_4} I_3^- + I^-$$
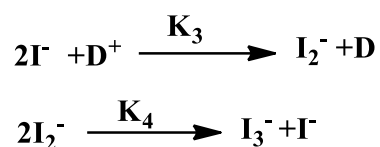
Step 3. (**C**) The injected electron in TiO₂ percolates through the film and collected at a transparent conductive layer of fluorine-doped tin oxide (FTO) glass substrate, on which the TiO₂ film is formed.

Step 4. (**D**) After passing through an external circuit, the electron is reintroduced into the DSSC device at the Pt cathode, where the oxidized electrolyte is reduced to regenerate the electrolyte. At the counter electrode the electron is transferred to a hole conducting medium (HTM). In most DSSC an iodide/iodine redox couple is employed. The reduction is catalysed by a thin layer of platinum.

$$I_3^- + 2e^- \xrightarrow{Pt, K_2} 3I^-$$
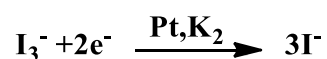
The efficiency of a DSSC is based on different rate constants for iodine reduction at the front and counter electrode. The iodine reduction at the counter electrode (K_2) has to be orders of magnitudes faster than the recombination at the TiO₂/electrolyte interface (K_1).

Step 5. (**E**) If the distance between the neighbour dye molecules is very close then LUMO of dye can quench the HOMO of dye molecule. This process is also known as self-quenching.

Step 6. (**F**), (**G**) The electron of the conduction band may directly inject towards the oxidized dye or hole transporting material which is also termed as recombination.

1.7 Metal complexes based dye

The high efficiencies of the ruthenium (II)–polypyridyl (Figure 6) DSSCs can be attributed to their wide absorption range from the visible to the near-infrared (NIR) regime. In addition, the carboxylate groups attached to the bipyridyl moiety lower the energy of the ligand π^* orbital. Since the electronic transition is a metal-to-ligand charge transfer (MLCT), excitation energy is effectively channelled to the carboxylate group, from which electron injection into the conduction band of the semiconductor takes place. Molar extinction co efficient of these metal based dyes is very low.

Due for this low absorptivity the thickness of the nanostructure titanium dioxide (TiO$_2$) layer on top of transparent conductive glass coated with a fluorine-doped tin oxide (FTO) layer can be adjusted to absorb nearly all the incident light. However, high extinction coefficients for all organic donor–acceptor dyes can be achieved from the structure–property relationships well-known in dye chemistry. In contrast to ruthenium (II) complexes[64], different light absorbing groups can be incorporated into the organic framework to tune the absorption over a broad spectral range and to achieve high extinction coefficients.
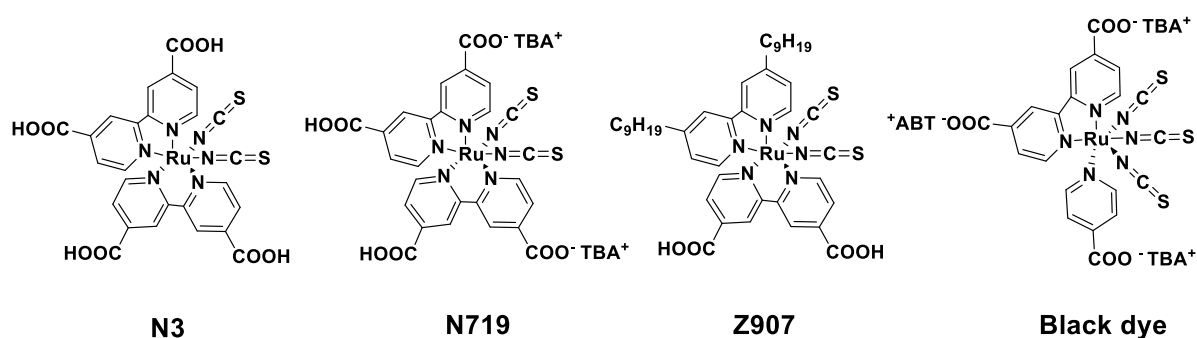
Figure 7. Structure of metal organic dyes having good efficiency.

1.8 Metal free organic dye

Organic dyes as an alternative to the noble Ru complexes sensitizers exhibit many advantages. (a)The molecular structures of organic dyes are in diverse form and can be easily designed and synthesized. (b) Concerning the cost and environment issues, organic dyes are superior to noble metal complexes. (c) The molar extinction coefficients of organic dyes are usually higher than those of Ru complexes, making them attractive for thin film and solid-state DSSCs. Generally, donor-π-bridge-acceptor (D-π-A) structure is the common character of these organic dyes (**Figure 7**). With this construction it is easy to design new dye structures, extend the absorption spectra, tuning the HOMO and LUMO levels and complete the intramolecular charge separation. When a dye absorbs light, intramolecular charge transfer occurs from subunit D to A through the π-bridge. For n-type DSSCs, the excited dye injects the electron into the conduction band of the semiconductor via the electron acceptor group. Many efforts have been made to change the different parts of organic dyes to optimize DSC performance. To date, hundreds of n-type organic dyes, including coumarin dyes [65], indoline dyes [66], tetrahydroquinoline dyes [67], triarylamine dyes [68], anthracene dyes [69], hemicyanine dyes [70], merocyanine dyes [71], squaraine dyes [66,72], perylene dyes [73], anthraquinone dyes [74], boradiazaindacene (BODIPY) dyes [75], oligothiophene dyes [76], polymeric dyes [77], and natural dyes [78] have been adopted to act as sensitizers for DSSCs and have obtained impressive efficiencies. Discussions are described in the order of absorption, electron injection, dye regeneration, recombination, and controlled aggregation.

1.8.1 Dye design regarding absorption

The fundamental requirement for photovoltaic energy conversion is the collection of as much sunlight as possible. However, the main absorption ranges of typical all-organic dyes

are limited within 200 nm, because it is determined by the molecular orbital hybridization through a conjugated dye frame. Photon flux density indicates the number of photons that can excite ground-state electrons with corresponding energy at the wavelength, has a noticeable distribution, and the highest photon flux region stands around 600 to 800 nm. For example, if a dye can completely absorbs solar radiation from 280 to 500 nm it can produce 5.1 mAcm^{-2}.
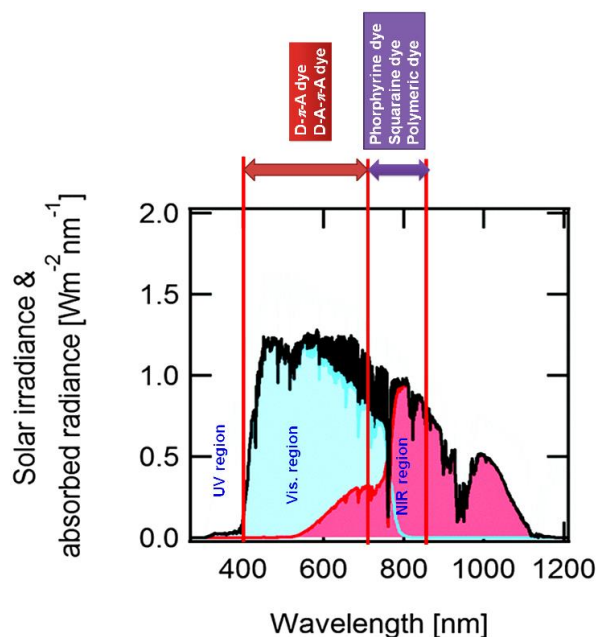
Figure 8. Different types of dye absorbed different region of the solar spectrum.

This current density is even smaller than the expected current density (6.5 mAcm^{-2}) of a dye which can cover only from 600 to700 nm, because of the unique distribution of the photon flux density of solar radiation. In this regard, the dye absorption range should match the high photon flux region of the solar spectrum, thus the ability to tailor the optical band-gap of dyes for DSSC application is crucially important for efficient solar-light harvesting. One of the common tools to tailor the absorption of all organic dyes is the extension of the effective conjugation length, because the absorption band of π-conjugated materials originates from the degree of interaction between π orbital's. However, the degree of π-

orbital interaction is also strongly affected by chain conformation, which limits the practical implication of the conjugation length in tuning the absorption range of dyes. Another efficient way to control a dyes absorption range is by combining an electron-donating (donor, D) and an electron-accepting (acceptor, A) moiety. Within the same conjugated framework. The D-π-A structure induces intramolecular charge transfer (ICT), which facilitates π-orbital overlap via the quinoid resonance structure and produces consequent red shift absorption of the dye.[79,80] Various kind of dyes can be engineered by changing the D-π-A structure of the dye so that it can absorbed different region of the solar spectrum (**Figure 8**). Although the D-π-A structure of all-organic dyes has the advantage of modulating the absorption range, their poor light-to-electric-energy conversion efficiency has limited their wide application for DSSCs. When a strong electron withdrawing group is located at the proximity of the anchoring moiety, as exemplified with benzo[c]-1, 2, 5-thiadiazole in **Figure 9a**, the electron-injection efficiency into TiO$_2$ from the excited dye was critically damaged, because of the charge entrapment effect around the withdrawing group or the strong recombination.[81,82] The role of the π-bridge in D-π-A dyes is to extend the absorption range of the dyes to the visible region. Since the π bridge is the channel through which electrons move from donor to acceptor moieties, it should have a (quasi) planar geometry for efficient electron transfer. However, the planar geometry tends to induce inter chain aggregation of the dyes on the semiconducting oxide surface, resulting in the decrease of electron-injection yield. Thus, the π–bridge should be selected carefully after considering liability of aggregation.
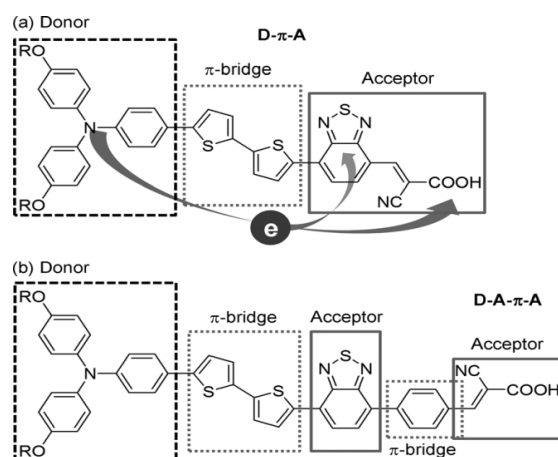
Figure 9. Representative examples of (a) D–A-type dye resulting in back electron transfer and (b) modified D–A-π-A type organic dye.

To overcome these drawbacks while preserving the merit of easy absorption modulation, an additional π-bridge (D–π–A–π–A) was recently introduced between the electron-withdrawing and anchoring groups. As shown in **Figure 9b**, the insertion of an additional phenyl ring dramatically improved the light-to-electric-energy conversion efficiency. The incident photon-to-current conversion efficiency (IPCE) was enhanced from 20 to over 90% at their maximum absorption region with subtle absorption blue shift, leading to over 6.5 times higher power conversion efficiency (PCE. 8.21%). Although there was no significant difference in the electron-injection efficiency when the phenyl ring was added, the reduction behaviour of the oxidized dye on TiO_2 in the absence of electrolyte was noticeably retarded, indicating slow recombination and prevent back electron transfer.

1.8.2 Dye design regarding dye regeneration

The driving force for dye regeneration in DSSCs is originated from the potential-energy difference between the oxidized dyes HOMO level and the redox potential of applied electrolyte in the DSSC. It has been reported that an insufficient driving force for dye

regeneration causes a low open-circuit voltage (V_{oc}) and poor photocurrent generation, because of fast recombination between the injected electrons and the photo oxidized dye molecules.[83] The photo oxidized dye should also be regenerated rapidly to avoid charge recombination between the hole on the oxidized dye and the injected electron to the electrode and minimize chemical degradation during the DSSC operation cycle. Since the V_{oc} of the DSCC is limited by the difference between the E_{CB} of the semiconducting oxide electrode and the redox potential of the electrolyte, higher voltages can be theoretically achieved by using a redox shuttle with a higher redox potential. The HOMO- LUMO energy level can be tolerated by maintain the extended π bond, conformational structure, conjugation length.[83]

1.8.3 Dye design regarding panchromatic absorption

It is very difficult task to design a sensitizer which can absorbs efficiently over the entire visible and NIR region of the absorption spectra. There is a possibility to get wide and broad range absorption. The only way to tolerate this is to make a combination in between two different dyes. This type of combination in between multiple dyes is a promising approach to get a panchromatic absorption. In that type of combination it is necessary to maintain the complementary absorption of these dyes for getting panchromatic sensitization. Panchromatic absorption can be get into two different ways. (a) Mixing with metal sensitisation with non-metal sensitizer. For example Zhang and colleagues have shown that squarylium cyanine dye in cocktail with N3 dye improved the efficiency by 12% relative to that of single N3 by extending the absorption range into the red.

(b) Panchromatic absorption by a complex compound or design the dye model in such a way that can absorb the wide region of the spectra. For example the spectral property in Ru-based dye can be tuned towards the red part of the visible spectrum by introducing a ligand with

low lying π^* molecular orbital by using a strong donor ligand. In this way the HOMO-LUMO gap can be reduced and form a NIR region absorption band. The other way it can be done in organic sensitizer case by modifying the different part of D-π-A model. For example Sun and his co-workers designed a new TH304 where phenoxazine act as an elector donor and co-rhodamine as the electron acceptor and connected by a π- conducting bridge. Although it having an absorption band at NIR region yet it shows only 3% efficiency. It was reported that the mixing of two different types of dyes may increase the PCE of the cell. (**Figure 10**).
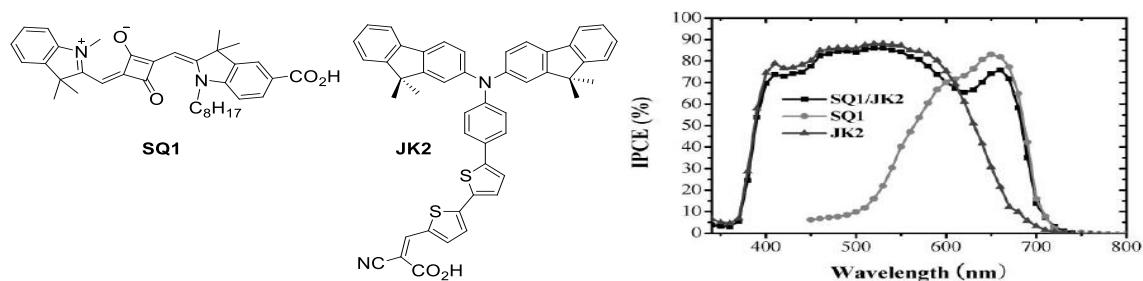
Figure 10. Molecular structure and Photocurrent action spectrum of SQ1 and JK2.

The efficiency of SQ1 and JK2 is 4.23 and 7.02 respectively but after mixing of these two dyes it became 7.36 %. An external afford has been done[84] to get panchromatic absorption by synthesized a multichromophoric dye contains two different solar spectrum absorption moieties (**Figure 11**). At the same time it was trying to mixing two different dyes with proper ratio to get the same effect.[85–89]
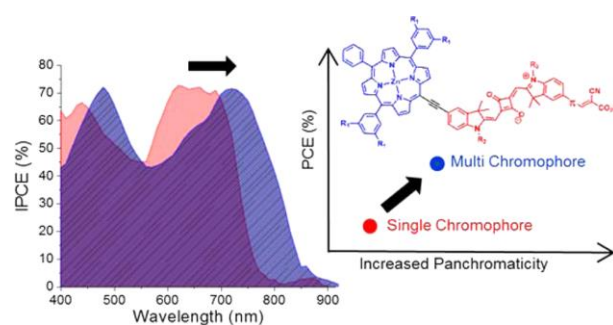
Figure 11. Molecular structure and efficiency of SQ1, D, T and their efficiency.

1.8.4 Dye design regarding recombination

There are two different types of improper recombination in DSSCs. One is charge recombination between the semiconducting oxide electrode and the dye cation (inner-path recombination), which decrease electron-injection efficiency of organic dyes and leads to the decrease in photocurrent. The mechanism of the inner-path recombination is that the electron injected from a dye to the E_{CB} of an oxide electrode recombines again with the dye cation before the dye regeneration.
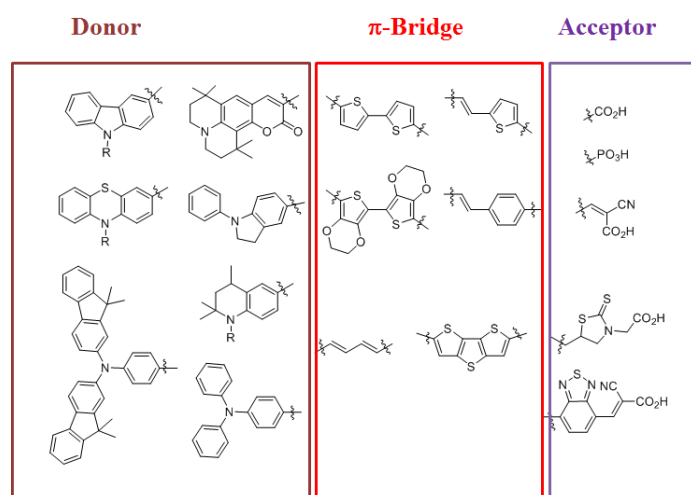
Figure 12. Schematic illustration of D-π-A type organic dye and representative examples of donor, π−bridge, and acceptor.

The rate of inner recombination strongly depends on the molecular structure of the organic dyes and their arrangement on the surface of the oxide electrodes. The recombination rate can be determined by means of Transient Absorption Spectroscopy by using two different laser spectrometers. To prevent this charge recombination, the produced positive charge density on all-organic dyes by the electron injection should be spatially separated from the oxide electrode (TiO_2).[90] As shown in **Figure 12**, inserting a π bridge into asymmetric D-π-A type dyes facilitates charge transfer and subsequent charge separation between the donor and acceptor moieties in the excited state, which could effectively retard charge recombination. The spatial isolation of positive charge density from the oxide electrode is also largely determined by the dyes geometry and resulting arrangement on the surface.

As shown in **Figure 13**, the dye orientation on the surface of TiO_2 is affected by the design of the anchoring units, although the rest of chemical nature of the applied dyes is essentially the same. Geometry optimization by using computational calculations showed that the cyanoacrylic acid induces vertically oriented dye geometry when it binds to TiO_2 surface, while the rhodanine aceticacid orients the dye with a tilt angle, resulting in a relatively shorter distance between the donor moiety of the dye and theTiO_2 surface.
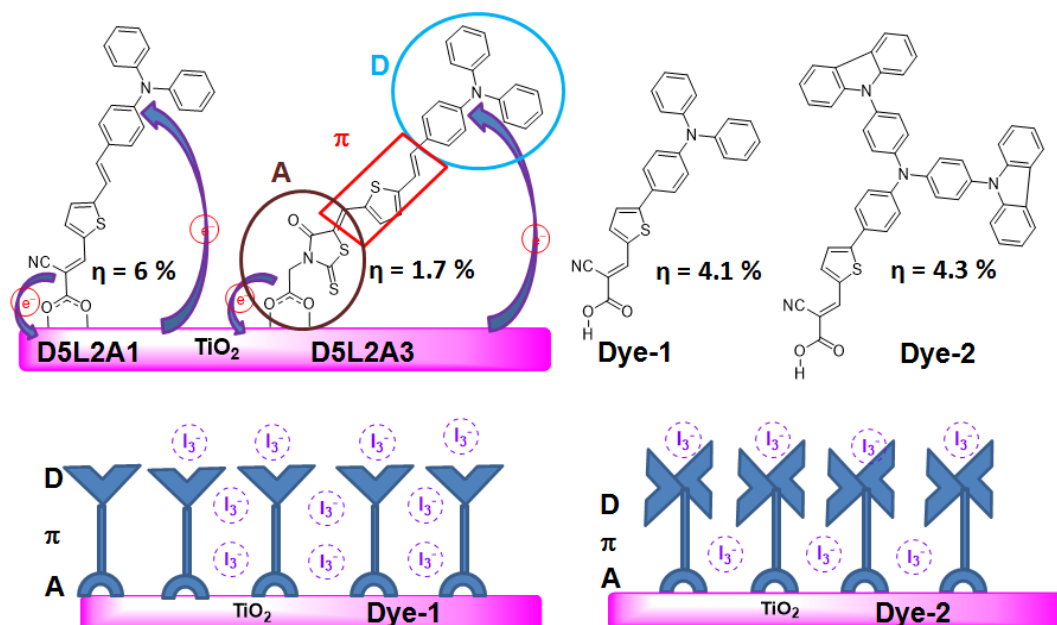
Figure 13. Anchoring units affect dyes orientation on the surface of TiO$_2$.

Thus, dye cations with rhodanine acetic acid as an anchoring unit are prone to experience more inner-path recombination with the injected electrons. Therefore the selection of an anchoring unit of all organic dye is important to prevent the degree of inner-path recombination.[91,92]

The other type of charge recombination in DSSCs occurs between the semiconducting oxide electrode and the electrolyte (outer-path recombination). This recombination decreases the theoretical potential difference between the oxide electrode and the electrolyte, resulting in a reduced V_{oc}. [91–93] One of the common strategies to suppress this improper recombination path is preventing the electrolyte from approaching the surface of the semiconducting oxide electrode. Because most electrolytes in DSSCs are hydrophilic, inserting hydrophobic alkyl side chains or π bridges into the dye framework could inhibit the approach of the electrolytes to the oxide electrode surface. Densely packed hydrophobic all-organic dyes on the oxide electrode could coat the electrode surface from the electrolytes, although the nature of the

semiconducting oxide is hydrophilic. This strategy effectively suppresses charge recombination, resulting in enhanced V_{oc} values and an extended electron lifetime.

It is known that introducing the star-burst triarylamine as a donor in a D-π-A type dye provided higher V_{oc} than similar dyes with a simple triarylamine donor. As illustrated in **Figure 13**, the dye containing a hydrophobic and extra-bulky triarylamine derivative as a donor group is superior in coating the TiO$_2$ surface from the penetration of I$_3^-$ of the electrolyte, which decreases charge recombination between TiO$_2$ and I$_3^-$ and provides better device performance including a higher V_{oc}.[94] However, one drawback of this dye design is that the sterically hindered dye structure reduces the number density of the adsorbed dyes on the oxide electrode surface, which decreases the absolute amount of injected electrons from the dyes to the electrode, resulting in poorer photocurrent generation in DSSCs.

1.8.5 Dye design regarding dye aggregation

Another most important part to design the organic dye in such a way that dyes aggregation should prevent because it reduces electron-injection efficiency from the dye to the semiconducting oxide through intermolecular energy transfer, resulting in low solar-to-electric-energy conversion efficiency. Many attempts have been made to design efficient organic sensitizers through structural modifications in order to prevent the aggregation of dyes. Dye aggregation can be restrained via molecular design that changes the molecular structure from planar to non planar or twisted. The presence of lengthy rod like structures, however, can lead to aggregation and, therefore, self-quenching and inefficient electron injection into theTiO$_2$.

A new type of spiro dye[95] has been designed, in which the bridging of two chromophores perpendicularly via a sp³-hybridized atom into a spiro configuration allows the constituted π-systems to retain their individual electronic properties (e.g., absorption and emission characteristics).
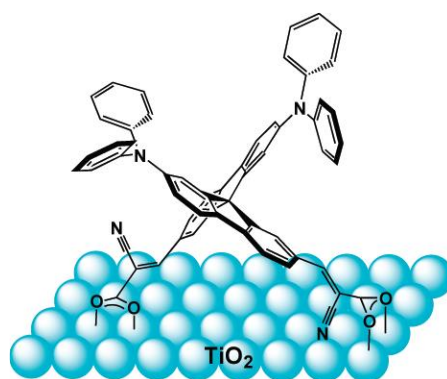
Figure 14. Co facially attached SSD1 dye on TiO₂.

In addition, the high steric demand resulting from the rigid structure efficiently suppresses intermolecular interactions, thereby diminishing the tendency to form aggregates. Spiro-configured compounds have higher solubility than their single components. Spiro linkages are particularly beneficial for fluorescent emitters, suppressing the excimer formation that is frequently encountered in the solid state. Spirobifluorene-based bipolar dye SSD1 featuring a diphenylamino (DPA) group as the donor and a 2-cyanoacrylicacid unit as the acceptor, with a fluorene bridge was synthesized and characterized (**Figure 14**) ensuring efficient donor-acceptor interactions.

This dye possesses several unique features that are potential advantages for application in DSSCs. SSD1 is composed of two D/A branches in a rigid cross-shaped molecular structure, which not only doubles the light absorption efficiency but also minimizes dye aggregation. In addition, two anchoring carboxylate groups are presents one at

each electron acceptor sites to improve dye adsorption on basic TiO_2 surfaces and to direct the photo induced electron injection.

A new dye has been designed incorporating rotaxane-like molecular wires [96] with an inner polythiophene core and outer circle rings were linked by covalent bond to control the aggreagtion. These outer rings not only prevent the polythiophene core from participating in intermolecular π–π interaction but also fix the dihedral angles between the thiophene moieties, resulting in planer π conjugation and efficient light harvesting. The intermolecular interaction is suppressed by the outer circle chain, which also prevents the approach of acceptors (I_3^- ions) to the TiO_2 surface, thus increasing the electron lifetimes and V_{OC}. Three dyes were synthesized and characterized namely LJ-1, LJ-2, and LJ-3 (**Figure 15**)
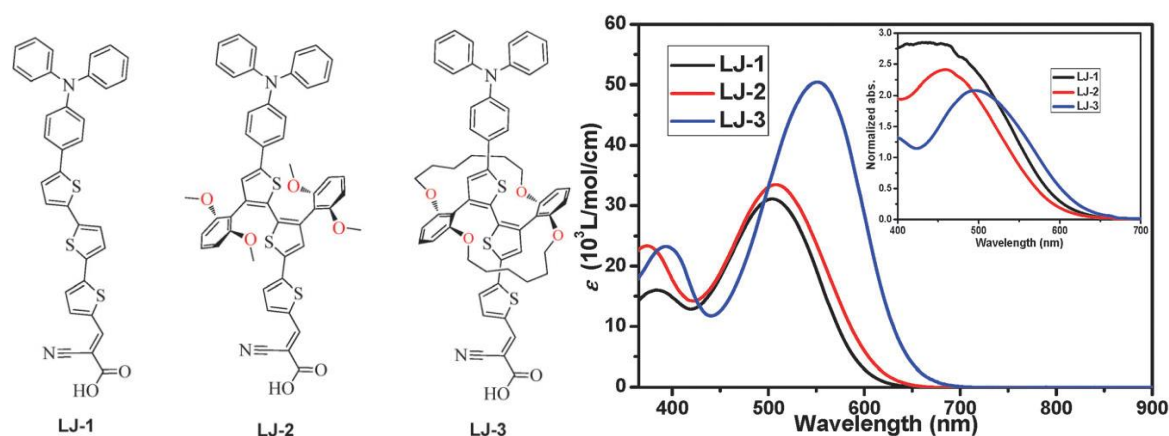
Figure 15. Molecular structures and Absorption spectra of LJ-1, LJ-2 and LJ-3 in CH_2Cl_2 and anchored on a transparent TiO_2 film (inset).

It was concluded that the rigid circle chain fixes the π-spacer of LJ-3 in a coplanar configuration, which increases the probability of the ICT transition from the donor to the acceptor. Due to the absence of bulky rigid ring in LJ-1, intermolecular π–π interactions exist, which might lead to the formation of aggregates on the TiO_2 film. In contrast,

intermolecular π–π interactions in both LJ-2and LJ-3 are suppressed by the bulky substituents linked to the π-conjugated backbone as well as dye aggregation.

1.8.6 Dye design to modulate the conduction band position of TiO$_2$ to control the V_{oc}

The V_{oc} of DSSC also directly depends on the conduction band of TiO$_2$. Therefore to increase the V_{oc} dye can be design in such a way to tailored the conduction band position of V_{oc}. There are two ways by which conduction band position of TiO$_2$ can be modulated.

(a) Dipole moment of the additives: To increase the photocurrent and suppressed the charge recombination along with upshifted conduction band, bromo-benzene has been used as an additives. After using the additives, which increase the amount of dye coverage on the active area of DSSC cell. This must be useful to increase the J_{sc} value along with the dye density on TiO$_2$. Therefore due to the high concentration of dye on TiO$_2$ surface has been upshifted the conduction band of TiO$_2$ due to increase the uniform resultant dipole moment.[97]

(b) Dipole moment of the dye: Open circuit photo-voltage can be regulated by using the resultant dipole moment of chemisorbed dyes on TiO$_2$. The resultant dipole moment of unidirectional dye molecule on TiO$_2$ surface can modulate the conduction band of TiO$_2$ which in turns changing the V_{oc} of the solar cell. The most important mechanism to tailor the V_{oc} has been correlated with the dye arrangement and its direction with respect to E_{CB} of TiO$_2$. The dipole moment of the dye can be generated by the probability of electronic localization in the excited state of dye molecule. In general, the direction of dipole has been established in from more electron localized part to less localized part in case of donor-π-acceptor dyes. This is because of the probability of finding electron density is

maximum in acceptor unit in excited state of the dyes. Therefore in these cases the directions of resultant dipole moments of dyes are away from the conduction band of TiO_2. This arrangement helps to increase the V_{oc} by upshifted the E_{CB} of TiO_2. A new strategy has been developed to tailoring the energy level of conduction band by changing the orientation of dipole of the incorporated π-spacer.[98] It was succeeding to increase the dipole moment by changing the dipole direction of the aromatic unit attached to that π-spacer of the dye. On the other hand, the direction of dipole moments towards the conduction band of TiO_2 can decrease the V_{oc} by lowered the energy level of conduction band. By introducing of hemicyanine dye in presence of lithium ion in I^-/I_3^- without any additives causes downward shift of the energy level of TiO_2 conduction band.[99] A general idea of modulate the V_{oc} by changing the energy level of conduction band was showed below (**Figure 16**).
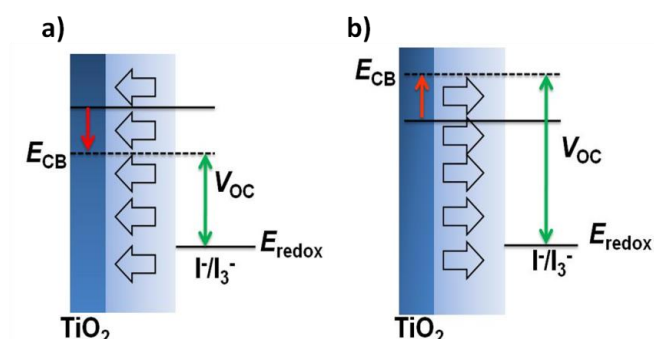
Figure 16. Changing of V_{oc} by (a) downward and (b) upward shifted of conduction band.

1.8.7 Avoiding dye aggregation by introducing in-plane and out-of-plane alkyl groups

Aggregation and back electron transfer can be minimized by attaching bulky alkyl group through sp^3-C atom (out-of-plane) or sp^2-C atom (in-plane). Such approach allowed positioning the alkyl groups in donor, π-spacer, and acceptor moieties to have the

hydrophobic units near or far away to the TiO$_2$ surface. The maximum efficiency of dyes was achieved by introducing this method was given below (**Figure 17**). That steric hindrance can be shown by the bulky groups, which is either in plane or out of the plane with respect to the conjugated backbone of the dyes. [62,66,100,101]

C272 ($\eta = 10.6$ %)   **YD2** ($\eta = 11$ %)   **SQ 5** ($\eta = 9.1$ %)

C275 ($\eta = 12.5$ %)   **YD2-*O*-C8** ($\eta = 12.6$ %)   **Y6** ($\eta = 12.6$ %)
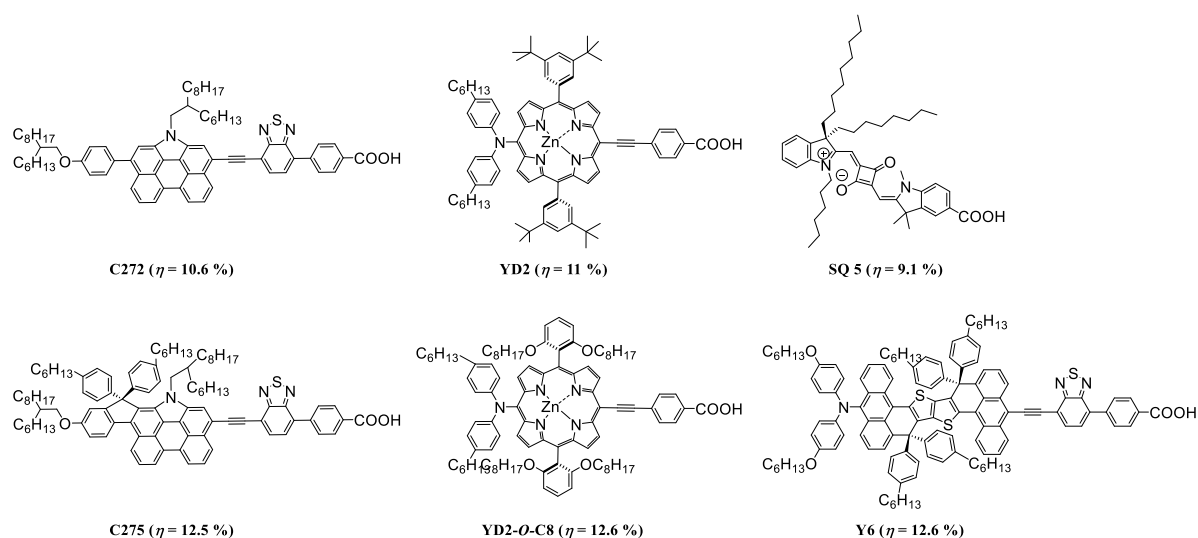
Figure 17. Chemical structures of dyes containing bulky group in- plane and out-of -plain.

1.9 Thesis Objective

Out of various interfaces at DSSC, dye-TiO$_2$ interface plays an important role for charge injection and dye regeneration besides aggregation of dye on the TiO$_2$ surface. Charge injection from aggregated structure that contributes to the device performance is varied and which can be modulated by co-adsorbing the dyes with optically transparent CDCA. Hence, controlling the dye-dye interaction on the TiO$_2$ surface has become one of the challenging tasks for synthetic chemists besides having desired optical band gap of dyes, which governs both charge injection and dye regeneration. Dimeric dyes that are connected through spiro-π-spacer showed better device efficiency than corresponding monomeric units. Generally, for panchromatic absorption, two or more dyes with complementary absorption properties were adsorbed to enhance the light harvesting properties over solar spectrum. In the present

approach, this critical problem is solved by connecting two structurally different dyes through spiro-linkage. Spiro-based π-spacer spiroBiProDOT has been explored to synthesize dimeric dyes with orthogonal orientation.

1.9.1 Thesis Outline

Chapter 1: In this chapter, it was provided background to motivate our investigations on solar cell efficiency by using organic sensitizers.

Chapter 2: π-framework forms closely packed monolayers on photoanode in dye-sensitized solar cell (DSSC), because of the limitation to control the orientation and the extend of intermolecular π-π interaction, self-aggregation of dyes leads to reduced cell performance. In this chapter, a series of homodimeric (**D_1-D_1** and **D_2-D_2**) and heterodimeric (**D_1-D_2** and **D_2-D_4**) donor/acceptor (D/A) dyes containing spiroBiProDOT π-spacer were designed and synthesized by utilizing Pd-catalyzed direct arylation reaction and correlates the device performance with monomeric dyes (**D_1** and **D_2**) (**Figure 18**). Both the thiophenes (π-spacer) of spiroBiProDOT were functionalized with same or different donor groups which led to homodimeric and hetero dimeric chromophores in a single sensitizer. The homodimeric spiro-dye **D_1-D_1** showed higher power conversion efficiency (PCE), of 7.6% with a V_{oc} and J_{sc} of 0.672 V and 16.16 mA/cm^2, respectively. On the other hand, the monomeric **D_1** exhibited a PCE of 3.2 % (V_{oc} of 0.64V and J_{sc} of 7.2 mA/cm^2), which is lower by 2.4 fold compared to dimeric **D_1-D_1** analogue. The spiro-unit provides flexibility between the incorporated chromophores to orient on TiO$_2$ surface due to four sp^3-centers, which arrest the molecular motions after chemisorption. This study showed a new molecular approach to incorporate two different chromophores in the dimeric dye possessing complementary absorption characteristics towards panchromatic absorption. The attenuated charge

recombination at TiO₂/Dye/redox couple interface in case of **D₁-D₁**, owing to better passivation of TiO₂ surface, was elucidated through electrochemical impedance spectroscopy. The FT-IR spectrum of **D₁-D₁** adsorbed on TiO₂ film indicated both the carboxylic units were involved in chemisorption which makes strong coupling between dye andTiO₂.
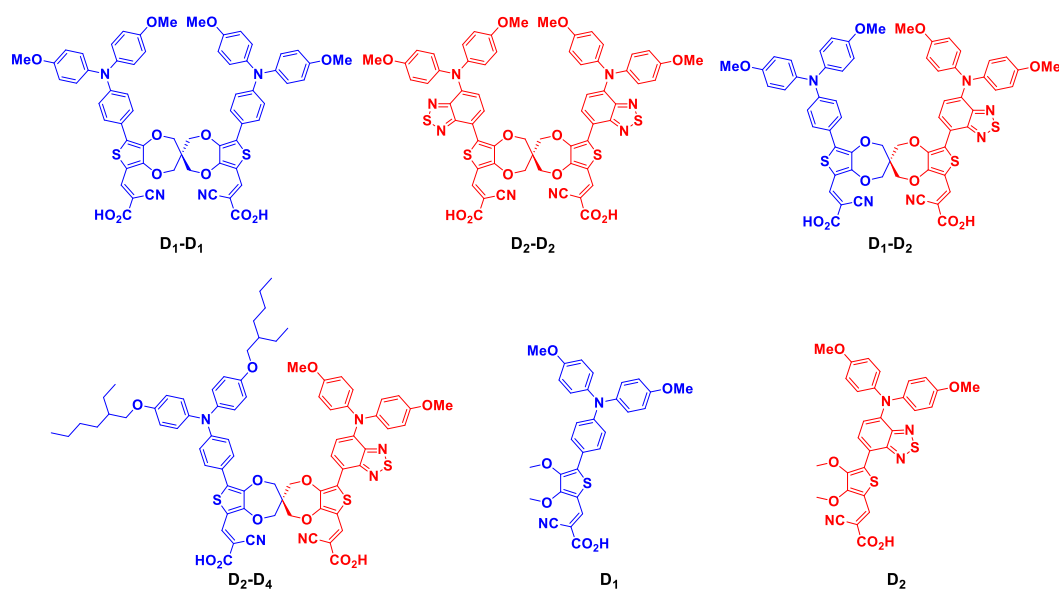
Figure 18. Homo- (**D₁-D₁** and **D₂-D₂**) and heterodimeric (**D₁-D₂** and **D₂-D₄**) and model donor/acceptor (D/A) dyes.

Chapter 3: Dye design for panchromatic light absorption has attracted much attention in the field of dye-sensitized solar cells. One of the methods to achieve the panchromatic light absorption is that utilizing mixture of complementary light absorbing dyes besides dyes with specific anchoring groups that facilitate interfacial charge transfer with TiO₂. Dipole-dipole interaction between the dye molecules on surface leads to broaden the spectrum which leads to decreased DSSC device performance. However controlled aggregation of dyes facilitate both broadening the spectral profile along with an efficient charge injection from the aggregated state. To control the dye-dye interaction a homo dimeric, **D_sq-D_sq** and a hetero dimeric, **D₁-D_sq** spiro dyes were synthesized with spirolinker by direct arylation method

(**Figure 19**). A model monomeric squaraine dye **D$_{sq}$** was also synthesized and characterized. Photo-physical, electrochemical properties were evaluated for the feasibility of charge injection and dye regeneration processes which is required for utilizing the synthesized dyes as an active material for DSSC device fabrication. Absorption spectra of **D$_{sq}$-D$_{sq}$, D$_1$-D$_{sq}$** were broadened in solution compared to model dye **D$_{sq}$** indicates the dye-dye interaction is prominent in solution. In **D$_1$-D$_{sq}$** excitation energy transfer between photoexcited **D$_1$** and **D$_{sq}$** was explained by using Förster resonance energy transfer (FRET). Homo dimeric dye showed the device performance of 2.8 % with the open circuit voltage (V_{oc}) of 0.607 V, short-circuit current density J_{sc} of 6.62 mA/cm^2, and fill factor (ff) = 69% under 1 sun, AM1.5G, whereas **D$_1$-D$_{sq}$** dye showed the V_{oc} = 0.652 V, J_{sc} = 8.89 mA/cm^2, ff = 69% and η = 3.9%. The increased photocurrent for **D$_1$-D$_{sq}$** is due to the panchromatic IPCE response compared to **D$_{sq}$-D$_{sq}$**. The increased V_{oc} is due to the effective passivation of TiO$_2$ surface by the spiro-linker, and the effective dipole moment that shift the conduction. Hence, the open circuit potential, V_{oc}, for the devices of **D$_{sq}$, D$_1$-D$_{sq}$** and **D$_{sq}$-D$_{sq}$** have been been systematically modulated by controlling the intermolecular π-π and intramolecular dipole-dipole interactions of the dimeric dyes.
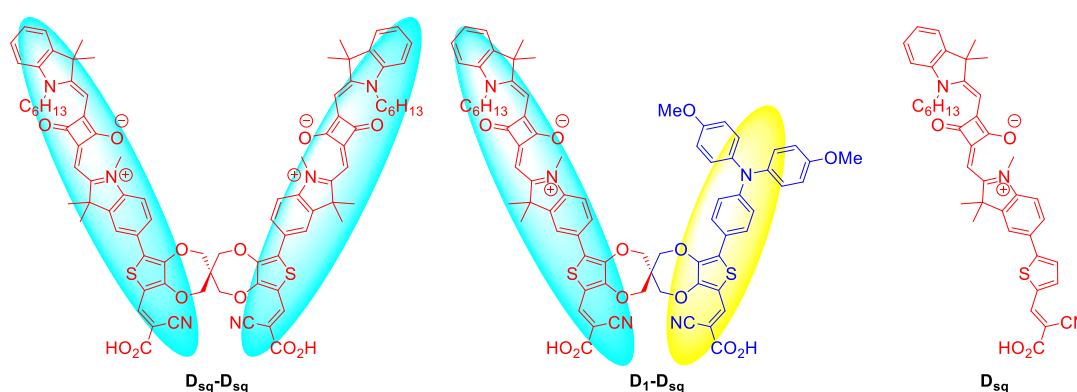
**Figure 19.** Structures of homo-dimeric (**D$_{sq}$-D$_{sq}$, D$_1$-D$_1$**), hetero-dimeric (**D$_1$-D$_{sq}$**) and model dyes (**D$_1$** and **D$_{sq}$**).

Chapter 4: Improper orientation and aggregation of dyes on TiO_2 are the main disadvantages at the dye-TiO_2 interface which governs charge injection and dye regeneration processes. In this chapter, a series of homo spiro-dimeric D-π-A dyes based on bithiophene and terthiophene spacers with two-anchoring group containing dyes, **TT$_1$, T$_1$T, TT$_1$T** were designed and synthesized by Pd-catalysed successive Suzuki coupling followed by direct arylation reactions (**Figure 20**). The position of branching centre in **TT$_1$** and **T$_1$T** was systematically varied, where the spiro unit was placed near and away from the anchoring carboxylic acid unit, respectively. The dimeric spiro-dye **T$_1$T** showed higher power conversion efficiency (PCE), with a 1.6 fold higher than its structural isomeric analogue **TT$_1$**, of 3.9 % with a V_{oc} and J_{sc} of 0.593 V and 9.09 mA/cm^2, respectively, whereas the isomeric analogue **TT$_1$** a PCE of 2.45 % (V_{oc} of 0.568 V and J_{sc} of 6.25 mA/cm^2) under simulated AM 1.5G illumination (100 mW/cm^2). The improved V_{oc} for the **T$_1$T** compared to **TT$_1$** dye was ascribed to the dipole moment exerted by the dye on TiO_2 surface. Further the PCE of 4.16 % (V_{oc} and J_{sc} are 0.589 V and 9.79 mA/cm^2 respectively) maximum was observed, when an extra thiophene unit was inserted in between the donor and π-spacer in **TT$_1$T.** The shifting the position of branching spiroBiProDOT π-spacer makes an impact on the device performance by synergistically enhancing both V_{oc} and J_{sc}. This study shows new molecular approaches in which two chromophores were attached through spiroBiProDOT at different position, further examined with photo-physical, electrochemical and photovoltaic parameters. The charge recombination reduced at TiO_2-dye/electrolyte couple interface in case of **T$_1$T** and **TT$_1$T**, allowing to better passivation of TiO_2 surface was explored through impedance spectroscopic analysis.
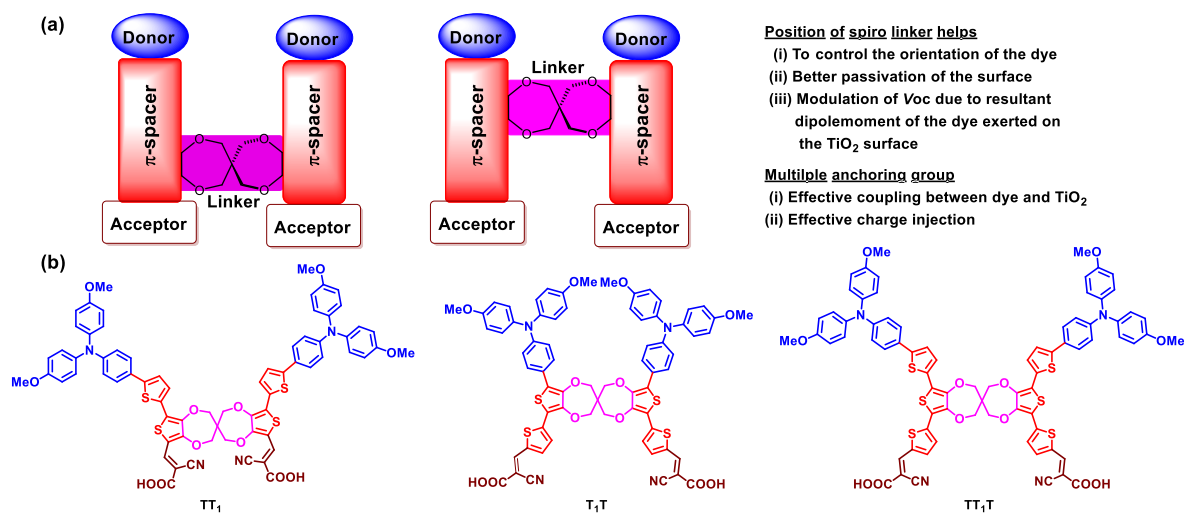
Figure 20. (a) Design of spiro- dyes and (b) molecular structures of **TT$_1$**, **T$_1$T** and **TT$_1$T** spiro dyes.

Chapter 5: Among various interfaces in dye-sensitized solar cells (DSSCs), dye-TiO$_2$ interface plays a vital role in governing charge injection and dye regeration process. To enhance the dye regeneration process, a triarylamine based electron donor was functionalized with a D-π-A dye through a spiro-linker is designed. Hence an orthogonally functionalized molecular dyad containing D-π-A dye and hole transport moiety (**D$_1$-HTM**) for dye-sensitized solar cell was synthesized and characterized (**Figure 21**) by photo-physical, electrochemical methods and fabricated DSSC devices. Dye regeneration may be faster due to faster hole transfer from oxidized dye (D-π-A) to I$^-$/ I$_3^-$ system through HTM part. Fluorescence quenching experiments indicated the feasibility of that electron transfer from hole transporting material (**PTS1**, **HTM-1**) to excited **D$_1$-D$_1$** and **D$_1$** dye. Photovoltaic studies showed that the net efficiency 2.24 % (**V$_{oc}$** and **J$_{sc}$** of 0.590 V and 5.27 mA/cm^2) was obtained of **D$_1$-HTM** by using 5 equivalent of co-adsorbent CDCA.
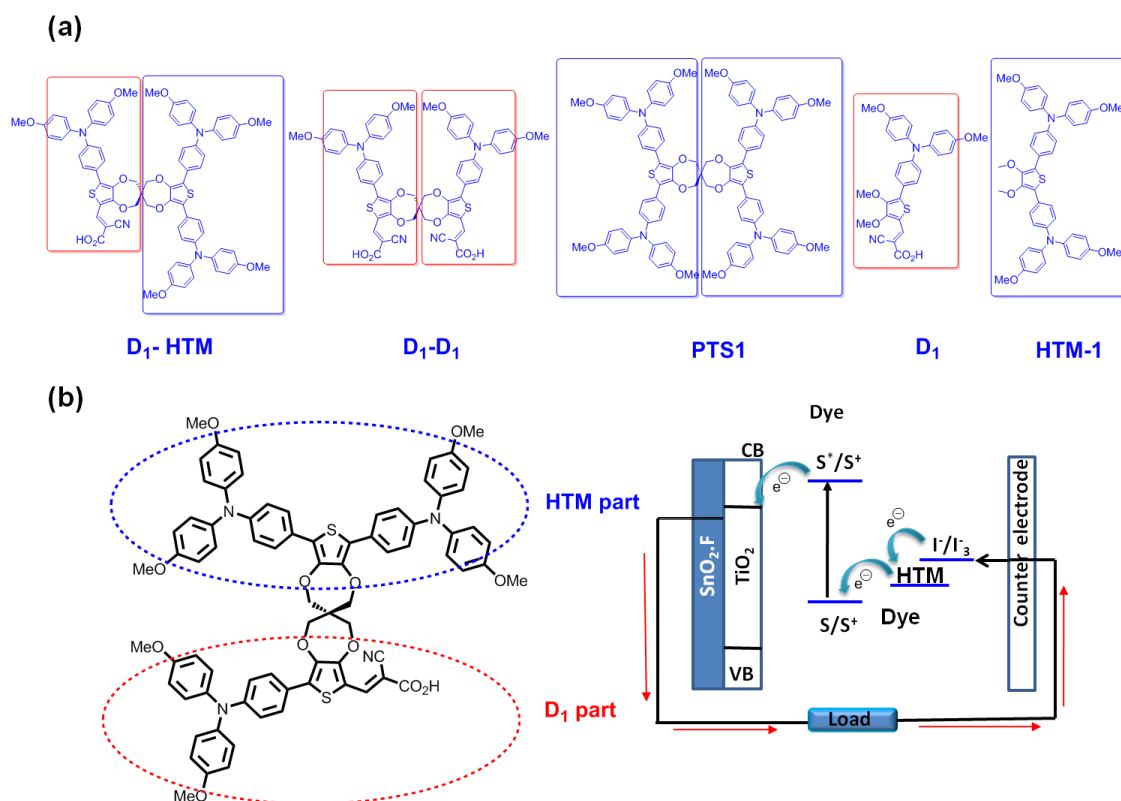
Figure 21. Structures of **D₁-HTM**, **D₁-D₁**, **PTS1**, **D₁**, **HTM-1**(a).Separation of dye and HTM parts in **D₁-HTM** (b).Possible mechanism dye regeneration and electron injection.

1.10 References

(1)   Panwar, N. L.; Kaushik, S. C.; Kothari, S. Role of Renewable Energy Sources in Environmental Protection: A Review. *Renewable and Sustainable Energy Reviews* **2011**, *15*, 1513–1524.

(2)   Hubbert, M. K. Energy from Fossil Fuels. *Science* **1949**, *109*, 103–109.

(3)   Anderson, T. R.; Hawkins, E.; Jones, P. D. CO₂, the Greenhouse Effect and Global Warming: From the Pioneering Work of Arrhenius and Callendar to Today's Earth System Models. *Endeavour* **2016**, *40*, 178–187.

(4)   Wackernagel, M.; Schulz, N. B.; Deumling, D.; Linares, A. C.; Jenkins, M.; Kapos, V.; Monfreda, C.; Loh, J.; Myers, N.; Norgaard, R.; et al. Tracking the Ecological Overshoot of the Human Economy. *PNAS* **2002**, *99*, 9266–9271.

(5)   Sommer, A. Burning Fossil Fuels: Impact of Climate Change on Health. *Int J Health Serv* **2016**, *46*, 48–52.

(6)   Barros, N.; Cole, J. J.; Tranvik, L. J.; Prairie, Y. T.; Bastviken, D.; Huszar, V. L. M.; del Giorgio, P.; Roland, F. Carbon Emission from Hydroelectric Reservoirs Linked to Reservoir Age and Latitude. *Nature Geoscience* **2011**, *4*, 593–596.

(7)   Frampton, A. H. Hydroelectric Power Plants. *Electrical Engineering* **1946**, *65*, 151–159.

(8)   Egbert, G. D.; Ray, R. D. Significant Dissipation of Tidal Energy in the Deep Ocean Inferred from Satellite Altimeter Data. *Nature* **2000**, *405*, 775–778.

(9)   Amer, M.; Daim, T. U. Application of Technology Roadmaps for Renewable Energy Sector. *Technological Forecasting and Social Change* **2010**, *77*, 1355–1370.

(10)   Lee, R. A.; Lavoie, J.-M. From First- to Third-Generation Biofuels: Challenges of Producing a Commodity from a Biomass of Increasing Complexity. *Anim Fron* **2013**, *3*, 6–11.

(11)   Chow, T. T. A Review on Photovoltaic/Thermal Hybrid Solar Technology. *Applied Energy* **2010**, *87*, 365–379.

(12)   Kraemer, D.; Poudel, B.; Feng, H.-P.; Caylor, J. C.; Yu, B.; Yan, X.; Ma, Y.; Wang, X.; Wang, D.; Muto, A.; et al. High-Performance Flat-Panel Solar Thermoelectric Generators with High Thermal Concentration. *Nature Materials* **2011**, *10*, 532–538.

(13)   Lewis, N. S.; Nocera, D. G. Powering the Planet: Chemical Challenges in Solar Energy Utilization. *PNAS* **2006**, *103*, 15729–15735.

(14) Derkacs, D.; Lim, S. H.; Matheu, P.; Mar, W.; Yu, E. T. Improved Performance of Amorphous Silicon Solar Cells via Scattering from Surface Plasmon Polaritons in Nearby Metallic Nanoparticles. *Appl. Phys. Lett.* **2006**, *89*, 093103.

(15) Green, M. A. Thin-Film Solar Cells: Review of Materials, Technologies and Commercial Status. *J Mater Sci: Mater Electron* **2007**, *18*, 15–19.

(16) Tsakalakos, L.; Balch, J.; Fronheiser, J.; Korevaar, B. A.; Sulima, O.; Rand, J. Silicon Nanowire Solar Cells. *Appl. Phys. Lett.* **2007**, *91*, 233117.

(17) Pillai, S.; Catchpole, K. R.; Trupke, T.; Green, M. A. Surface Plasmon Enhanced Silicon Solar Cells. *Journal of Applied Physics* **2007**, *101*, 093105.

(18) Liska, P.; Thampi, K. R.; Grätzel, M.; Brémaud, D.; Rudmann, D.; Upadhyaya, H. M.; Tiwari, A. N. Nanocrystalline Dye-Sensitized Solar Cell/Copper Indium Gallium Selenide Thin-Film Tandem Showing Greater than 15% Conversion Efficiency. *Appl. Phys. Lett.* **2006**, *88*, 203103.

(19) Hetzer, M. J.; Strzhemechny, Y. M.; Gao, M.; Contreras, M. A.; Zunger, A.; Brillson, L. J. Direct Observation of Copper Depletion and Potential Changes at Copper Indium Gallium Diselenide Grain Boundaries. *Appl. Phys. Lett.* **2005**, *86*, 162105.

(20) Li-Kao, Z. J.; Naghavi, N.; Erfurth, F.; Guillemoles, J. F.; Gérard, I.; Etcheberry, A.; Pelouard, J. L.; Collin, S.; Voorwinden, G.; Lincot, D. Towards Ultrathin Copper Indium Gallium Diselenide Solar Cells: Proof of Concept Study by Chemical Etching and Gold Back Contact Engineering. *Prog. Photovolt: Res. Appl.* **2012**, *20*, 582–587.

(21) Shah, A.; Torres, P.; Tscharner, R.; Wyrsch, N.; Keppner, H. Photovoltaic Technology: The Case for Thin-Film Solar Cells. *Science* **1999**, *285*, 692–698.

(22) Nakayama, N.; Matsumoto, H.; Yamaguchi, K.; Ikegami, S.; Hioki, Y. Ceramic Thin Film CdTe Solar Cell. *Jpn. J. Appl. Phys.* **1976**, *15*, 2281.

(23) Aramoto, T.; Kumazawa, S.; Higuchi, H.; Arita, T.; Shibutani, S.; Nishio, T.; Nakajima, J.; Tsuji, M.; Hanafusa, A.; Hibino, T.; et al. 16.0% Efficient Thin-Film CdS/CdTe Solar Cells. *Jpn. J. Appl. Phys.* **1997**, *36*, 6304.

(24) Gur, I.; Fromer, N. A.; Geier, M. L.; Alivisatos, A. P. Air-Stable All-Inorganic Nanocrystal Solar Cells Processed from Solution. *Science* **2005**, *310*, 462–465.

(25) Gupta, A.; Compaan, A. D. All-Sputtered 14% CdS⁄CdTe Thin-Film Solar Cell with ZnO:Al Transparent Conducting Oxide. *Appl. Phys. Lett.* **2004**, *85*, 684–686.

(26) Kuribayashi, K.; Matsumoto, H.; Uda, H.; Komatsu, Y.; Nakano, A.; Ikegami, S. Preparation of Low Resistance Contact Electrode in Screen Printed CdS/CdTe Solar Cell. *Jpn. J. Appl. Phys.* **1983**, *22*, 1828.

(27) Yan, B.; Yue, G.; Sivec, L.; Yang, J.; Guha, S.; Jiang, C.-S. Innovative Dual Function Nc-SiOx:H Layer Leading to a >16% Efficient Multi-Junction Thin-Film Silicon Solar Cell. *Appl. Phys. Lett.* **2011**, *99*, 113512.

(28) You, J.; Dou, L.; Yoshimura, K.; Kato, T.; Ohya, K.; Moriarty, T.; Emery, K.; Chen, C.-C.; Gao, J.; Li, G.; et al. A Polymer Tandem Solar Cell with 10.6% Power Conversion Efficiency. *Nature Communications* **2013**, *4*, 1446.

(29) Yamaguchi, M.; Takamoto, T.; Araki, K.; Ekins-Daukes, N. Multi-Junction III–V Solar Cells: Current Status and Future Potential. *Solar Energy* **2005**, *79*, 78–85.

(30) Dresselhaus, M. S.; Thomas, I. L. Alternative Energy Technologies. *Nature* **2001**, *414*, 332.

(31) Hubbard, S. M.; Cress, C. D.; Bailey, C. G.; Raffaelle, R. P.; Bailey, S. G.; Wilt, D. M. Effect of Strain Compensation on Quantum Dot Enhanced GaAs Solar Cells. *Appl. Phys. Lett.* **2008**, *92*, 123512.

(32) Krogstrup, P.; Jørgensen, H. I.; Heiss, M.; Demichel, O.; Holm, J. V.; Aagesen, M.; Nygard, J.; Fontcuberta i Morral, A. Single-Nanowire Solar Cells beyond the Shockley–Queisser Limit. *Nature Photonics* **2013**, *7*, 306–310.

(33) Kosten, E. D.; Atwater, J. H.; Parsons, J.; Polman, A.; Atwater, H. A. Highly Efficient GaAs Solar Cells by Limiting Light Emission Angle. *Light: Science & Applications* **2013**, *2*, e45.

(34) Yoon, J.; Jo, S.; Chun, I. S.; Jung, I.; Kim, H.-S.; Meitl, M.; Menard, E.; Li, X.; Coleman, J. J.; Paik, U.; et al. GaAs Photovoltaics and Optoelectronics Using Releasable Multilayer Epitaxial Assemblies. *Nature* **2010**, *465*, 329–333.

(35) Saga, T. Advances in Crystalline Silicon Solar Cell Technology for Industrial Mass Production. *NPG Asia Materials* **2010**, *2*, 96–102.

(36) Knuesel, R. J.; Jacobs, H. O. Self-Assembly of Microscopic Chiplets at a Liquid–liquid–solid Interface Forming a Flexible Segmented Monocrystalline Solar Cell. *PNAS* **2010**, *107*, 993–998.

(37) Kaltenbrunner, M.; White, M. S.; Głowacki, E. D.; Sekitani, T.; Someya, T.; Sariciftci, N. S.; Bauer, S. Ultrathin and Lightweight Organic Solar Cells with High Flexibility. *Nature Communications* **2012**, *3*, 770.

(38) Zeng, L.; Bermel, P.; Yi, Y.; Alamariu, B. A.; Broderick, K. A.; Liu, J.; Hong, C.; Duan, X.; Joannopoulos, J.; Kimerling, L. C. Demonstration of Enhanced Absorption in Thin Film Si Solar Cells with Textured Photonic Crystal Back Reflector. *Appl. Phys. Lett.* **2008**, *93*, 221105.

(39) Guo, X.; Zhou, N.; Lou, S. J.; Smith, J.; Tice, D. B.; Hennek, J. W.; Ortiz, R. P.; Navarrete, J. T. L.; Li, S.; Strzalka, J.; et al. Polymer Solar Cells with Enhanced Fill Factors. *Nature Photonics* **2013**, *7*, 825–833.

(40)   Park, N.-G. Organometal Perovskite Light Absorbers Toward a 20% Efficiency Low-Cost Solid-State Mesoscopic Solar Cell. *J. Phys. Chem. Lett.* **2013**, *4*, 2423–2429.

(41)   Burschka, J.; Pellet, N.; Moon, S.-J.; Humphry-Baker, R.; Gao, P.; Nazeeruddin, M. K.; Grätzel, M. Sequential Deposition as a Route to High-Performance Perovskite-Sensitized Solar Cells. *Nature* **2013**, *499*, 316–319.

(42)   Kim, H.-S.; Lee, C.-R.; Im, J.-H.; Lee, K.-B.; Moehl, T.; Marchioro, A.; Moon, S.-J.; Humphry-Baker, R.; Yum, J.-H.; Moser, J. E.; et al. Lead Iodide Perovskite Sensitized All-Solid-State Submicron Thin Film Mesoscopic Solar Cell with Efficiency Exceeding 9%. *Scientific Reports* **2012**, *2*, 591.

(43)   Liu, M.; Johnston, M. B.; Snaith, H. J. Efficient Planar Heterojunction Perovskite Solar Cells by Vapour Deposition. *Nature* **2013**, *501*, 395–398.

(44)   Jeon, N. J.; Noh, J. H.; Kim, Y. C.; Yang, W. S.; Ryu, S.; Seok, S. I. Solvent Engineering for High-Performance Inorganic–organic Hybrid Perovskite Solar Cells. *Nature Materials* **2014**, *13*, 897–903.

(45)   Heo, J. H.; Im, S. H.; Noh, J. H.; Mandal, T. N.; Lim, C.-S.; Chang, J. A.; Lee, Y. H.; Kim, H.; Sarkar, A.; Nazeeruddin, M. K.; et al. Efficient Inorganic–organic Hybrid Heterojunction Solar Cells Containing Perovskite Compound and Polymeric Hole Conductors. *Nature Photonics* **2013**, *7*, 486–491.

(46)   Liu, D.; Kelly, T. L. Perovskite Solar Cells with a Planar Heterojunction Structure Prepared Using Room-Temperature Solution Processing Techniques. *Nature Photonics* **2014**, *8*, 133–138.

(47)   Malinkiewicz, O.; Yella, A.; Lee, Y. H.; Espallargas, G. M.; Graetzel, M.; Nazeeruddin, M. K.; Bolink, H. J. Perovskite Solar Cells Employing Organic Charge-Transport Layers. *Nature Photonics* **2014**, *8*, 128–132.

(48) Albero, J.; Clifford, J. N.; Palomares, E. Quantum Dot Based Molecular Solar Cells. *Coordination Chemistry Reviews* **2014**, *263–264*, 53–64.

(49) Kamat, P. V.; Tvrdy, K.; Baker, D. R.; Radich, J. G. Beyond Photovoltaics: Semiconductor Nanoarchitectures for Liquid-Junction Solar Cells. *Chem. Rev.* **2010**, *110*, 6664–6688.

(50) Wang, W.; Jiang, G.; Yu, J.; Wang, W.; Pan, Z.; Nakazawa, N.; Shen, Q.; Zhong, X. High Efficiency Quantum Dot Sensitized Solar Cells Based on Direct Adsorption of Quantum Dots on Photoanodes. *ACS Appl. Mater. Interfaces* **2017**, *9*, 22549–22559.

(51) Pivrikas A.; Sariciftci N. S.; Juška G.; Österbacka R. A Review of Charge Transport and Recombination in Polymer/Fullerene Organic Solar Cells. *Progress in Photovoltaics: Research and Applications* **2007**, *15*, 677–696.

(52) Bronstein, H.; Chen, Z.; Ashraf, R. S.; Zhang, W.; Du, J.; Durrant, J. R.; Shakya Tuladhar, P.; Song, K.; Watkins, S. E.; Geerts, Y.; et al. Thieno[3,2-b]Thiophene−Diketopyrrolopyrrole-Containing Polymers for High-Performance Organic Field-Effect Transistors and Organic Photovoltaic Devices. *J. Am. Chem. Soc.* **2011**, *133*, 3272–3275.

(53) Tang, C. W. Two-layer Organic Photovoltaic Cell. *Appl. Phys. Lett.* **1986**, *48*, 183–185.

(54) Nelson, J. Organic Photovoltaic Films. *Current Opinion in Solid State and Materials Science* **2002**, *6*, 87–95.

(55) Li, S.; Ye, L.; Zhao, W.; Yan, H.; Yang, B.; Liu, D.; Li, W.; Ade, H.; Hou, J. A Wide Band Gap Polymer with a Deep Highest Occupied Molecular Orbital Level Enables 14.2% Efficiency in Polymer Solar Cells. *J. Am. Chem. Soc.* **2018 (ASAP)**.

(56) Nusbaumer, H.; Zakeeruddin, S. M.; Moser, J.-E.; Grätzel, M. An Alternative Efficient Redox Couple for the Dye-Sensitized Solar Cell System. *Chemistry* **2003**, *9*, 3756–3763.

(57) Kojima, A.; Teshima, K.; Shirai, Y.; Miyasaka, T. Organometal Halide Perovskites as Visible-Light Sensitizers for Photovoltaic Cells. *J. Am. Chem. Soc.* **2009**, *131*, 6050–6051.

(58) Bönnemann, H.; Khelashvili, G.; Behrens, S.; Hinsch, A.; Skupien, K.; Dinjus, E. Role of the Platinum Nanoclusters in the Iodide/Triiodide Redox System of Dye Solar Cells. *J Clust Sci* **2007**, *18*, 141–155.

(59) Murakami, T. N.; Grätzel, M. Counter Electrodes for DSC: Application of Functional Materials as Catalysts. *Inorganica Chimica Acta* **2008**, *361*, 572–580.

(60) Papageorgiou, N.; Maier, W. F.; Grätzel, M. An Iodine/Triiodide Reduction Electrocatalyst for Aqueous and Organic Media. *J. Electrochem. Soc.* **1997**, *144* (3), 876–884.

(61) Thomas, S.; Deepak, T. G.; Anjusree, G. S.; Arun, T. A.; Nair, S. V.; Nair, A. S. A Review on Counter Electrode Materials in Dye-Sensitized Solar Cells. *J. Mater. Chem. A* **2014**, *2*, 4474–4490.

(62) Yao, Z.; Zhang, M.; Wu, H.; Yang, L.; Li, R.; Wang, P. Donor/Acceptor Indenoperylene Dye for Highly Efficient Organic Dye-Sensitized Solar Cells. *J. Am. Chem. Soc.* **2015**, *137*, 3799–3802.

(63) O'Regan, B.; Grätzel, M. A Low-Cost, High-Efficiency Solar Cell Based on Dye-Sensitized Colloidal TiO$_2$ Films. *Nature* **1991**, *353*, 737–740.

(64) Grätzel, M. Photoelectrochemical Cells. *Nature* **2001**, *414*, 338.

(65) Venkatraman, V.; Abburu, S.; Alsberg, B. K. Artificial Evolution of Coumarin Dyes for Dye Sensitized Solar Cells. *Phys. Chem. Chem. Phys.* **2015**, *17*, 27672–27682.

(66)   Alagumalai, A.; Kavungathodi, M. F. M.;Vellimalai, P.; Sil, M. C.; Nithyanandhan, J. Effect of Out-of-Plane Alkyl Group's Position in Dye-Sensitized Solar Cell Efficiency: A Structure–Property Relationship Utilizing Indoline-Based Unsymmetrical Squaraine Dyes. *ACS Appl. Mater. Interfaces* **2016**, *8*, 35353–35367.

(67)   Chen, R.; Yang, X.; Tian, H.; Wang, X.; Hagfeldt, A.; Sun, L. Effect of Tetrahydroquinoline Dyes Structure on the Performance of Organic Dye-Sensitized Solar Cells. *Chem. Mater.* **2007**, *19*, 4007–4015.

(68)   Holliman, P. J.; Mohsen, M.; Connell, A.; Davies, M. L.; Al-Salihi, K.; Pitak, M. B.; Tizzard, G. J.; Coles, S. J.; Harrington, R. W.; Clegg, W.; et al. Ultra-Fast Co-Sensitization and Tri-Sensitization of Dye-Sensitized Solar Cells with N719, SQ1 and Triarylamine Dyes. *J. Mater. Chem.* **2012**, *22*, 13318–13327.

(69)   Teng, C.; Yang, X.; Yang, C.; Li, S.; Cheng, M.; Hagfeldt, A.; Sun, L. Molecular Design of Anthracene-Bridged Metal-Free Organic Dyes for Efficient Dye-Sensitized Solar Cells. *J. Phys. Chem. C* **2010**, *114*, 9101–9110.

(70)   Stathatos, E.; Lianos, P.; Laschewsky, A.; Ouari, O.; Van Cleuvenbergen, P. Synthesis of a Hemicyanine Dye Bearing Two Carboxylic Groups and Its Use as a Photosensitizer in Dye-Sensitized Photoelectrochemical Cells. *Chem. Mater.* **2001**, *13*, 3888–3892.

(71)   Meyer, T.; Ogermann, D.; Pankrath, A.; Kleinermanns, K.; Müller, T. J. J. Phenothiazinyl Rhodanylidene Merocyanines for Dye-Sensitized Solar Cells. *J. Org. Chem.* **2012**, *77*, 3704–3715.

(72)   Kim, S.; Mor, G. K.; Paulose, M.; Varghese, O. K.; Baik, C.; Grimes, C. A. Molecular Design of Near-IR Harvesting Unsymmetrical Squaraine Dyes. *Langmuir* **2010**, *26*, 13486–13492.

(73)   Yang, L.; Chen, S.; Zhang, J.; Wang, J.; Zhang, M.; Dong, X.; Wang, P. Judicious Engineering of a Metal-Free Perylene Dye for High-Efficiency Dye Sensitized Solar Cells: The Control of Excited State and Charge Carrier Dynamics. *J. Mater. Chem. A* **2017**, *5*, 3514–3522.

(74)   Li, C.; Yang, X.; Chen, R.; Pan, J.; Tian, H.; Zhu, H.; Wang, X.; Hagfeldt, A.; Sun, L. Anthraquinone Dyes as Photosensitizers for Dye-Sensitized Solar Cells. *Solar Energy Materials and Solar Cells* **2007**, *91*, 1863–1871.

(75)   Erten-Ela, S.; Yilmaz, M. D.; Icli, B.; Dede, Y.; Icli, S.; Akkaya, E. U. A Panchromatic Boradiazaindacene (BODIPY) Sensitizer for Dye-Sensitized Solar Cells. *Org. Lett.* **2008**, *10*, 3299–3302.

(76)   Hara, K.; Wang, Z.-S.; Sato, T.; Furube, A.; Katoh, R.; Sugihara, H.; Dan-oh, Y.; Kasada, C.; Shinpo, A.; Suga, S. Oligothiophene-Containing Coumarin Dyes for Efficient Dye-Sensitized Solar Cells. *J. Phys. Chem. B* **2005**, *109*, 15476–15482.

(77)   Nogueira, A. F.; Longo, C.; De Paoli, M.-A. Polymers in Dye Sensitized Solar Cells: Overview and Perspectives. *Coordination Chemistry Reviews* **2004**, *248*, 1455–1468.

(78)   Sathyajothi, S.; Jayavel, R.; Dhanemozhi, A. C. The Fabrication of Natural Dye Sensitized Solar Cell (Dssc) Based on TiO$_2$ Using Henna And Beetroot Dye Extracts. *Materials Today: Proceedings* **2017**, *4*, 668–676.

(79)   Kleinhenz, N.; Yang, L.; Zhou, H.; Price, S. C.; You, W. Low-Band-Gap Polymers That Utilize Quinoid Resonance Structure Stabilization by Thienothiophene: Fine-Tuning of HOMO Level. *Macromolecules* **2011**, *44*, 872–877.

(80)   Nazeeruddin, M. K.; Humphry-Baker, R.; Liska, P.; Grätzel, M. Investigation of Sensitizer Adsorption and the Influence of Protons on Current and Voltage of a Dye-Sensitized Nanocrystalline TiO$_2$ Solar Cell. *J. Phys. Chem. B* **2003**, *107*, 8981–8987.

(81) Kim, B.-G.; Zhen, C.-G.; Jeong, E. J.; Kieffer, J.; Kim, J. Organic Dye Design Tools for Efficient Photocurrent Generation in Dye-Sensitized Solar Cells: Exciton Binding Energy and Electron Acceptors. *Adv. Funct. Mater.* **2012**, *22*, 1606–1612.

(82) Haid, S.; Marszalek, M.; Mishra, A.; Wielopolski, M.; Teuscher, J.; Moser, J.-E.; Humphry-Baker, R.; Zakeeruddin, S. M.; Grätzel, M.; Bäuerle, P. Significant Improvement of Dye-Sensitized Solar Cell Performance by Small Structural Modification in π-Conjugated Donor–Acceptor Dyes. *Adv. Funct. Mater.* **2012**, *22*, 1291–1302.

(83) Daeneke, T.; Mozer, A. J.; Kwon, T.-H.; Duffy, N. W.; Holmes, A. B.; Bach, U.; Spiccia, L. Dye Regeneration and Charge Recombination in Dye-Sensitized Solar Cells with Ferrocene Derivatives as Redox Mediators. *Energy Environ. Sci.* **2012**, *5*, 7090–7099.

(84) Jradi, F. M.; O'Neil, D.; Kang, X.; Wong, J.; Szymanski, P.; Parker, T. C.; Anderson, H. L.; El-Sayed, M. A.; Marder, S. R. A Step Toward Efficient Panchromatic Multi-Chromophoric Sensitizers for Dye Sensitized Solar Cells. *Chem. Mater.* **2015**, *27*, 6305–6313.

(85) Shi, Y.; Hill, R. B. M.; Yum, J.-H.; Dualeh, A.; Barlow, S.; Grätzel, M.; Marder, S. R.; Nazeeruddin, M. K. A High-Efficiency Panchromatic Squaraine Sensitizer for Dye-Sensitized Solar Cells. *Angewandte Chemie* **2011**, *123*, 6749–6751.

(86) Han, L.; Islam, A.; Chen, H.; Malapaka, C.; Chiranjeevi, B.; Zhang, S.; Yang, X.; Yanagida, M. High-Efficiency Dye-Sensitized Solar Cell with a Novel Co-Adsorbent. *Energy Environ. Sci.* **2012**, *5*, 6057–6060.

(87) Nazeeruddin, M. K.; Péchy, P.; Renouard, T.; Zakeeruddin, S. M.; Humphry-Baker, R.; Comte, P.; Liska, P.; Cevey, L.; Costa, E.; Shklover, V.; et al. Engineering of

Efficient Panchromatic Sensitizers for Nanocrystalline TiO$_2$-Based Solar Cells. *J. Am. Chem. Soc.* **2001**, *123*, 1613–1624.

(88) Paek, S.; Choi, H.; Kim, C.; Cho, N.; So, S.; Song, K.; Nazeeruddin, M. K.; Ko, J. Efficient and Stable Panchromatic Squaraine Dyes for Dye-Sensitized Solar Cells. *Chem. Commun.* **2011**, *47*, 2874–2876.

(89) Sil, M. C.; Sudhakar, V.; Kavungathodi, M. F. M.; Punitharasu, V.; Nithyanandhan, J. Orthogonally Functionalized Donor/Acceptor Homo- and Heterodimeric Dyes for Dye-Sensitized Solar Cells: An Approach to Introduce Panchromaticity and Control the Charge Recombination. *ACS Appl. Mater. Interfaces* **2017**, *9*, 34875–34890.

(90) Tian, H.; Yang, X.; Chen, R.; Pan, Y.; Li, L.; Hagfeldt, A.; Sun, L. Phenothiazine Derivatives for Efficient Organic Dye-Sensitized Solar Cells. *Chem. Commun.* **2007**, *0*, 3741–3743.

(91) Tang, J.; Hua, J.; Wu, W.; Li, J.; Jin, Z.; Long, Y.; Tian, H. New Starburst Sensitizer with Carbazole Antennas for Efficient and Stable Dye-Sensitized Solar Cells. *Energy Environ. Sci.* **2010**, *3*, 1736–1745.

(92) Tashiro, K.; Kobayashi, M.; Kawai, T.; Yoshino, K. Crystal Structural Change in Poly(3-Alkyl Thiophene)s Induced by Iodine Doping as Studied by an Organized Combination of X-Ray Diffraction, Infrared/Raman Spectroscopy and Computer Simulation Techniques. *Polymer* **1997**, *38*, 2867–2879.

(93) Planells, M.; Pellejà, L.; Clifford, J. N.; Pastore, M.; Angelis, F. D.; López, N.; Marder, S. R.; Palomares, E. Energy Levels, Charge Injection, Charge Recombination and Dye Regeneration Dynamics for Donor–acceptor π-Conjugated Organic Dyes in Mesoscopic TiO$_2$ Sensitized Solar Cells. *Energy Environ. Sci.* **2011**, *4*, 1820–1829.

(94) Liang, Y.; Cheng, F.; Liang, J.; Chen, J. Triphenylamine-Based Ionic Dyes with Simple Structures: Broad Photoresponse and Limitations on Open-Circuit Voltage in Dye-Sensitized Solar Cells. *J. Phys. Chem. C* **2010**, *114*, 15842–15848.

(95) Heredia, D.; Natera, J.; Gervaldo, M.; Otero, L.; Fungo, F.; Lin, C.-Y.; Wong, K.-T. Spirobifluorene-Bridged Donor/Acceptor Dye for Organic Dye-Sensitized Solar Cells. *Org. Lett.* **2010**, *12*, 12–15.

(96) Liu, J.; Numata, Y.; Qin, C.; Islam, A.; Yang, X.; Han, L. Circle Chain Embracing Donor–acceptor Organic Dye : Simultaneous Improvement of Photocurrent and Photovoltage for Dye -Sensitized Solar Cells. *Chemical Communications* **2013**, *49*, 7587–7589.

(97) Buhbut, S.; N. Clifford, J.; Kosa, M.; Y. Anderson, A.; Shalom, M.; Thomas Major, D.; Palomares, E.; Zaban, A. Controlling Dye Aggregation, Injection Energetics and Catalytic Recombination in Organic Sensitizer Based Dye Cells Using a Single Electrolyte Additive. *Energy Environ. Sci.* **2013**, *6*, 3046–3053.

(98) Clark, C. C.; Meyer, G. J.; Wei, Q.; Galoppini, E. Tuning Open Circuit Photovoltages with Tripodal Sensitizers. *J. Phys. Chem. B* **2006**, *110*, 11044–11046.

(99) Karjule, N.; Kavungathodi, M. F. M.; Nithyanandhan, J. Molecular Control of the Band Edge Movement and the Recombination Process in Donor–Acceptor Hemicyanine-Sensitized Solar Cells. *J. Phys. Chem. C* **2017**, *121*, 21836–21847.

(100) Yella, A.; Lee, H.-W.; Tsao, H. N.; Yi, C.; Chandiran, A. K.; Nazeeruddin, M. K.; Diau, E. W.-G.; Yeh, C.-Y.; Zakeeruddin, S. M.; Grätzel, M. Porphyrin-Sensitized Solar Cells with Cobalt (II/III)-Based Redox Electrolyte Exceed 12 Percent Efficiency. *Science* **2011**, *334*, 629–634.

(101) Ren, Y.; Sun, D.; Cao, Y.; Tsao, H. N.; Yuan, Y.; Zakeeruddin, S. M.; Wang, P.; Grätzel, M. A Stable Blue Photosensitizer for Color Palette of Dye-Sensitized Solar Cells Reaching 12.6% Efficiency. *J. Am. Chem. Soc.* **2018**, *140*, 2405–2408.

Orthogonally Functionalized Donor/Acceptor Homo- and Heterodimeric Dyes for Dye-Sensitized Solar Cells: An Approach to Introduce Panchromaticity and Control the Charge Recombination

2.1 Introduction

Organic sensitizers-based dye cells have emerged as a potential device architecture to harvest the solar energy due to easy device fabrication of dye sensitized solar cells and diversity in key components such as semiconductors, dyes, electrolytes and cathode materials.[1] Ever since the discovery of homoleptic metallated ruthenium-based dyes with 7.12% device efficiency by O'Regan and Grätzel, last two and half decade research on the functional materials provided deeper understanding of device structure and various pathways associated with interfacial charge transfer and recombination processes.[2] Dye design with panchromatic absorption,[3–5] avoiding both charge recombination[6–11] and dye aggregation achieved high device efficiencies by increasing the J_{sc} and V_{oc} besides the choice of electrolyte having minimum loss-in-potentials.[12] The structure-property relationship of organometallic and metal-free organic dyes have been carried out, so far the best conversion efficiency of about 13% was achieved for zinc-porphyrin dye[13] and 12.5% for indenoperylene dye[14] with cobalt (II/III) redox couple. One of the advantages of having D-π-A metal free organic dyes is that it utilizes simple precursors to tune the photophysical and electrochemical properties which developed high molar absorptivity dyes with strong intramolecular charge transfer (ICT) transitions.[15] Dyes with D-π-A,[16] and D-A-π-A[17] configurations provided good harvesting efficiency in the visible and far-red regions, respectively, whereas few chromophores such as polymethine,[18] porphyrin,[19–23] and phthalocyanine dyes[24] have been explored for photo-current generation in near-infrared (NIR) region. Though organic conjugated dyes possess sharp transitions with high extinction coefficient in solution, due to short and long range interaction between the dyes on the surface leads to aggregation of dyes resulting in broadening of the absorption spectrum.[25] The head-to-head (H-type) and head-to-tail (J-type) arrangements of dyes leads to hypsochromic and bathochromic shifts, respectively in the

absorption spectrum on TiO_2.[26–29] However the charge injection from aggegated structure that contributes to the device performance (**Figure 1a**) is varied and which can be modulated by co-adsorbing the dyes with optically transparent CDCA (**Figure 1b**).[30–32]
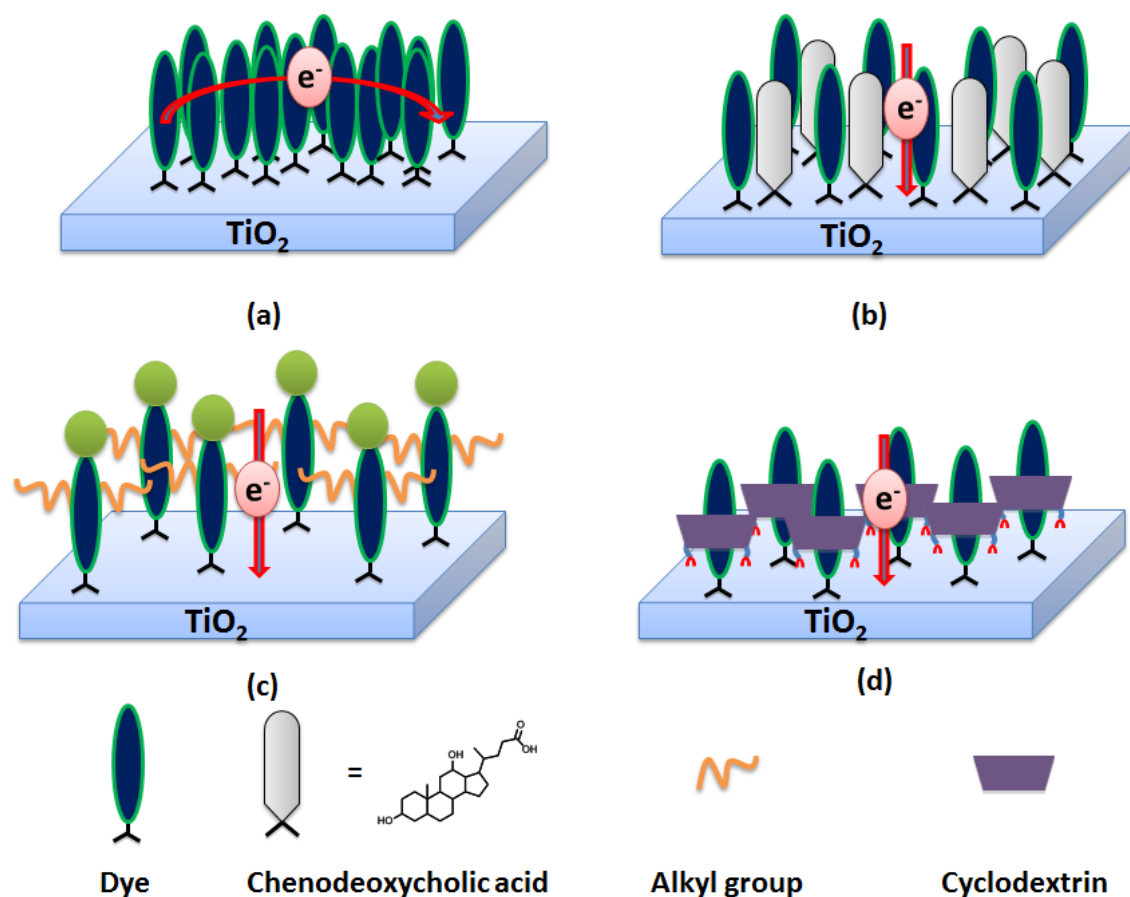

Figure 1. (a) Charge injection from aggregated dye molecule, controlling of dye-dye aggregation by (b) addition of CDCA, (c) functionalization of dyes with alkyl groups, (d) encapsulation by cyclodextrin.

Hence, controlling the dye-dye interaction on the TiO_2 surface has become one of the challenging tasks for synthetic chemists besides having desired optical band gap of dyes, which governs both charge injection and dye regeneration. Functionalization of dyes with alkyl groups (**Figure 1c**) showed better device efficiency with reduced charge recombination by passivating the TiO_2 surface and diminishing the dye aggregation. Out-of-plane[33] (through

sp^3-C atom) alkyl group functionalization provided better device efficiency than the in-plane (through sp^2-C atom) alky groups.[34] Such approach allowed positioning the alkyl groups in donor, π-spacer, and acceptor moieties to have the hydrophobic units near or far away to the TiO$_2$ surface. Structure-device efficiency correlation has been observed by keeping the alkyl groups in different positions of D-π-A[35] or D-A-D[25] conjugated backbone. Another important approach to control the aggregation of dye on TiO$_2$ was realised by anchoring Ru(II) complexes and organic dyes on the surfaces with suitable linkers and anchoring groups which increases footprint of the molecules.[36-39] This molecular engineering is more attractive, as it allows controlling the orientation and distribution of the dyes on the surface than use of a co-adsorbent. Other than this molecular approach, supramolecular approaches have been explored for circumventing the aggregation phenomenon by isolating the dyes from the bulk by molecular encapsulation. Cyclodextrin and cavitand containers have been explored to control the interfacial electron transfer process and encapsulated JK2 dye with cyclodextrin showed better device efficiency (**Figure 1d**).[40] An in-built cyclic alkyl group around the planar π-spacer in a D-π-A dye has been designed to avoid the dye aggregation. Such processes may also decrease the amount of dye on the surface that correlates with the current density. Further, atomic layer deposition method (ALD) has been utilized to diminish the aggregation of dyes on the surface.[41] Apart from the above mentioned designs, DSSCs with dye containing two anchoring groups were synthesised to increase the electronic coupling between TiO$_2$ and dye for an efficient charge injection and reduced charge recombination which in turn increase V_{oc} and J_{sc}.[42] **Figure 2a** and **Figure 2b** shows the general design of dyes with di anchoring groups, in which two dye moieties are connected with each other to provide a configuration that avoid aggregation of dyes by a conjugate/non-conjugate linkers through either donor or π-spacer component of the dye.[43-52] A cross-shaped D-π-A dye, FNE92 (**Figure 2a**) reduced the intermolecular interaction in rod-shaped monomeric FNE91

and which increased both J_{sc} (ΔJ_{sc} = 4.1 mA/cm^2) and V_{oc} (ΔV_{oc} = 100 mV).[51] Similar observation was made for JY07 (**Figure 2b**), orthogonal conformation minimize the intermolecular aggregation and consequently achieved 1.2-fold higher efficiency than monomer JY06.[53] The photophysical and photovoltaic properties are also influenced by the distance between two anchoring unit and flexibility of linker that connects two dye units. Thus to attain high efficiency dimeric dyes an optimal distance and flexibility is required.
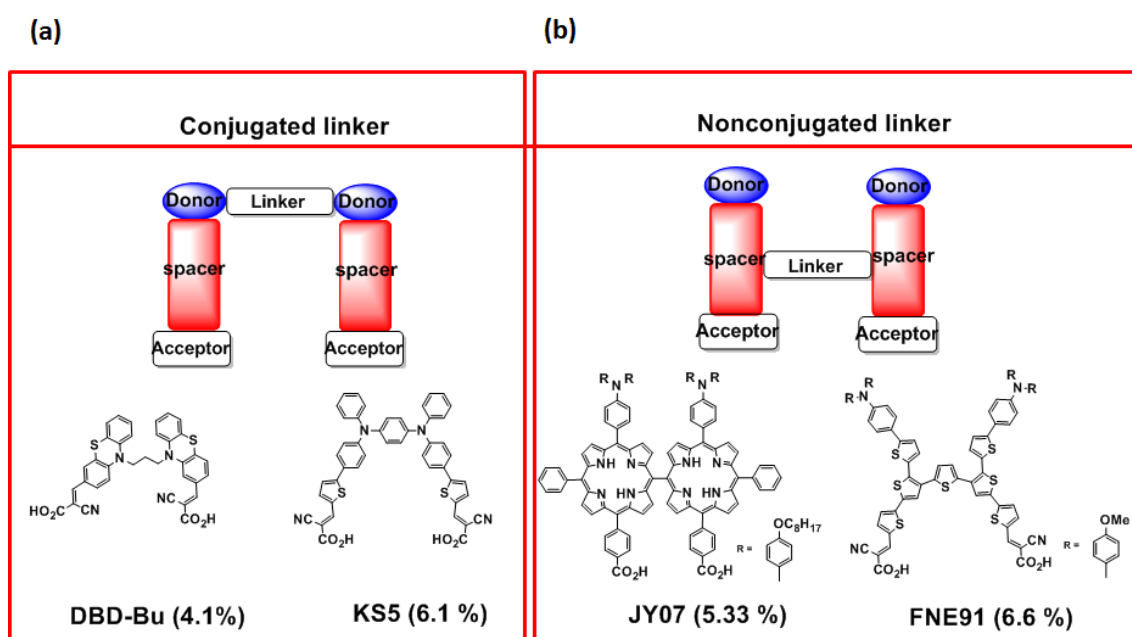
Figure 2. Dimeric dye connected by conjugated or non-conjugated linker through aggregation by (a) donor part and (b) π-spacer part.

Dimeric dyes that are connected through spiro π-spacer showed better device efficiency than corresponding monomeric units (**Figure 3b**). Generally, for panchromatic absorption, two or more dyes with complementary absorption region were mixed. This approach may have competitive adsorption of dyes on the TiO$_2$ surface with respect to the strength of anchoring group or solubility of dyes in the dipping solvent. In the present approach, this critical problem is solved by connecting two structurally different dyes through spiro-linkage

(**Figure 3c**). Spiro-based π-spacer has been explored to synthesize dyes as the sp^3-C that separate the two dye units bring the orthogonal orientation between the dye units. Distance between the two dye molecules can be varied by the choice of spiro-branching units. It was judiciously utilized the 2H,2'H,4H,4'H-3,3'-spirobi[thieno[3,4-b][1,4]dioxepine] (spiroBiProDOT)[54] based π-spacer to connect two dyes with four additional sp^3-C atoms at the branching unit that may offer better flexibility, dictates the distance between the dyes that helps in anchoring, diminish the aggregation of dyes and better passivation of surface. The tetrahedral sp^3 hybridized carbon in between the two propylenedioxythiophenes adopts a spiro conformation. However, the two seven-membered alkylenedioxy rings are large enough to reduce the distortion than five membered rings of SCPDT1.[55] Therefore, although the four carbon atoms directly connecting to the spiro carbon do not lie in a plane, the two thiophene rings and four oxygen atoms are almost coplanar and with proper substitution the conformation of spiroBiProDOT units were changed.[56]
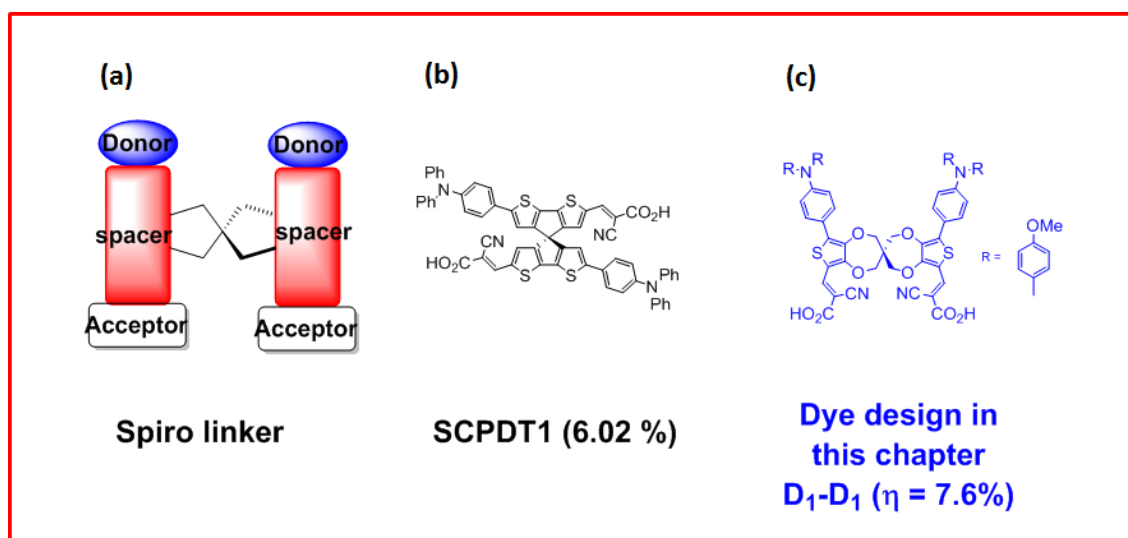
Figure 3. (a) Dimeric dye connected by spiro-linker, (b) structure of spiro-dimeric dye SCPDT1, and (c) Structure of **D$_1$-D$_1$**.

In the present chapter, D-π-A based dimeric dyes with spiroBiProDOT based π-spacer were synthesized by employing Pd-catalyzed direct arylation reaction, as conventional C-C bond formation through Pd catalyzed reaction requires boronic acid, stannylated derivatives for Suzuki and Stille coupling reactions, respectively. However direct arylation method utilized in material synthesis as it reduces the number steps and it is very cost effective. Sequential direct arylation reactions have been utilized to synthesize unsymmetrical spiro-dyes by which two different D-π-A dyes can be stitched by spiroBiProDOT unit. This method is very effective in synthesizing dyes with panchromatic light absorption by judicious choice of dyes that possess complementary absorption properties. Out of four spiro dyes, dye **D$_1$-D$_1$** exhibits the V_{oc} of 0.672 V, J_{sc} of 16.16 mA/cm^2 with the device efficiency of 7.6%, under simulated AM 1.5G illumination (100 mW/cm^2) whereas the corresponding model monomeric **D$_1$** showed an efficiency of 3.2% with V_{oc} of 0.64 V, J_{sc} of 7.26 mA/cm^2.

2.2 Results and discussion

2.2.1 Dye design and synthesis. The main strategy was to design and synthesize dimeric D-π-A dyes connected through a spiro skeleton with flexible bonds to control the dye aggregation. Two different or same dye molecules can be covalently connected in a spiro carbon atom for extended absorption in the visible regions so that a panchromatic responsive dye can be judiciously designed by selecting two complementary dyes. The flexible nature of spiro units ensures the anchoring of both the dye molecules as well as passivates the TiO$_2$ surface which avoids the charge recombination process. Two anchoring groups can bind strongly to TiO$_2$ to enhance the coupling of dye and TiO$_2$ that enhance the charge injection process. The targeted structures of the dimeric and monomeric dyes are presented in **Figure 4**.
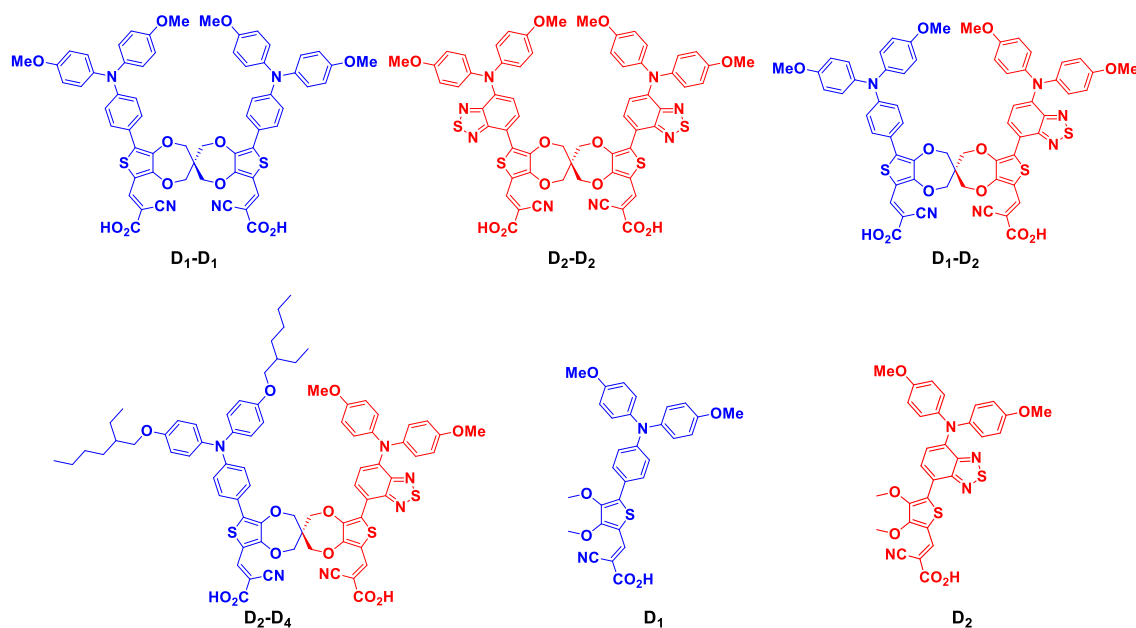
Figure 4. Structures of targeted homo and hetero-dimeric dyes.

2.2.2 Synthesis of spiro dyes. 2H,2'H,4H,4'H-3,3'-spirobi[thieno[3,4-b][1,4]dioxepine] (spiroBiProDOT) was selected as a π-spacer for synthesizing the D-π-A dyes containing two anchoring groups.
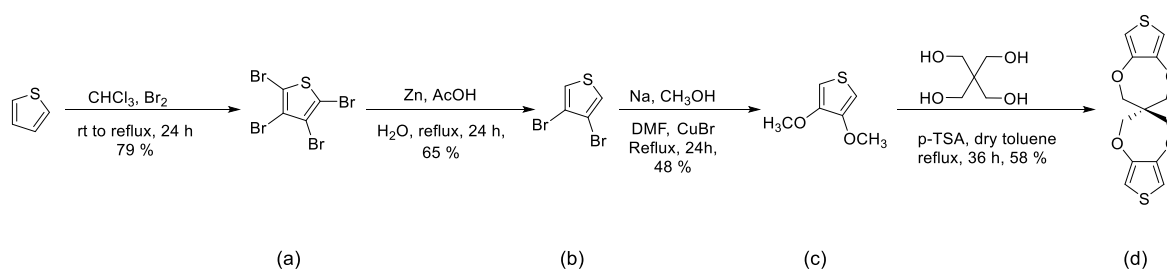

Scheme 1. Synthesis of 2H,2'H,4H,4'H-3,3'-spirobi[thieno[3,4-b][1,4]dioxepine].

SpiroBiProDOT was synthesized from *trans*-etherification of 3,4-dimethoxythiophene (**Scheme 1**). Vilsmeier-Haack formylation of spiroBiProDOT afforded the symmetric mono-formylated dialdehyde, **1** in good yield. Homo and hetero dimeric dyes have been synthesized by Pd[2+]catalyzed direct arylation reaction[58-60] of suitable triaryl halide **2** and **5** with

dialdehyde **1** to afford the corresponding aldehyde and further Knoevenagel condensation with cyanoaceticacid. Synthesis of homo spiro-dialdehyde requires stoichiometric equivalent of aryl bromide whereas for hetero dimeric spiro-dyes requires successive direct arylation reaction to afford the corresponding unsymmetric dialdehyde. Such methodology helps in installing two different dye units in a same compound. In this method the classical Suzuki or Stille coupling was avoided to get coupling product which helped to reduce number of steps. The donor triaryl amines are attached to the aldehyde derivative of spiroBiProDOT moiety by direct arylation method using catalytic amount of Pd(OAc)$_2$, PCy$_3$, PivOH with the moderate reaction conversion of **D$_1$-D$_1$** dialdehyde within 55% yield. Yield for the synthesis of **D$_1$-D$_1$** dialdehyde, **3** was 55%. Finally, **D$_1$-D$_1$** dialdehyde was condensed with cyanoaceticacid in the presence of ammonium acetate to afford the target spiro dye **D$_1$-D$_1$** in 65% yield via a Knoevenagel reaction (**Scheme 2**). Dyes **D$_2$-D$_2$** and **D$_1$-D$_2$** are synthesized moderate yields (**Scheme 2** and **Scheme 3**).
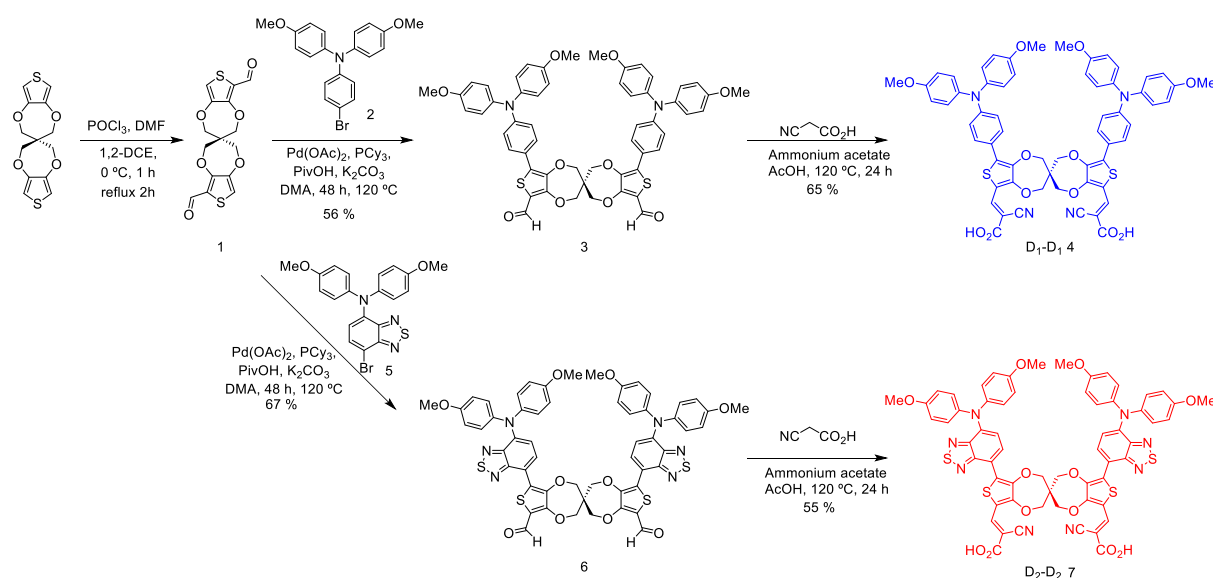
Scheme 2. Synthesis of **D$_1$-D$_1$** and **D$_2$-D$_2$** of homo-dimeric dyes by direct arylation method.
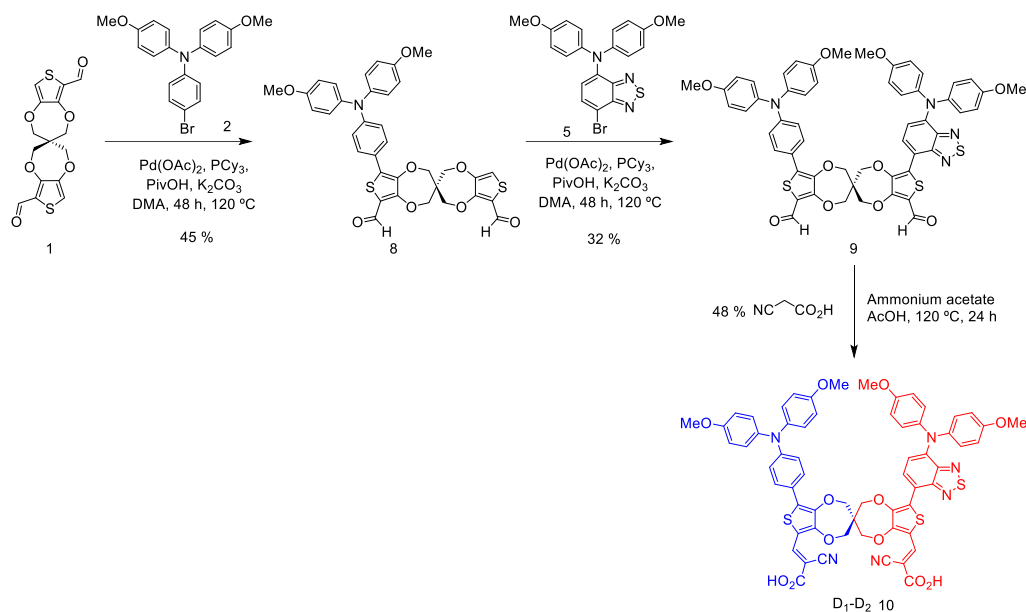
Scheme 3. Synthesis of hetero-dimeric **D₁-D₂** dye by direct arylation method.

Organic sensitizers applied in DSSCs are required to possess a good solubility in common organic solvent like MeOH and CH₃CN. **D₁-D₁** was solubilised in EtOH whereas **D₁-D₂** and **D₂-D₂** were soluble only in DMSO. So as to increase the solubility of all the dyes in MeCN/EtOH, branched ethylhexyl group was introduced in **D₂-D₄** and synthesized by successive direct arylation reactions and Knoevenagel condensation reaction (**Scheme 4**).
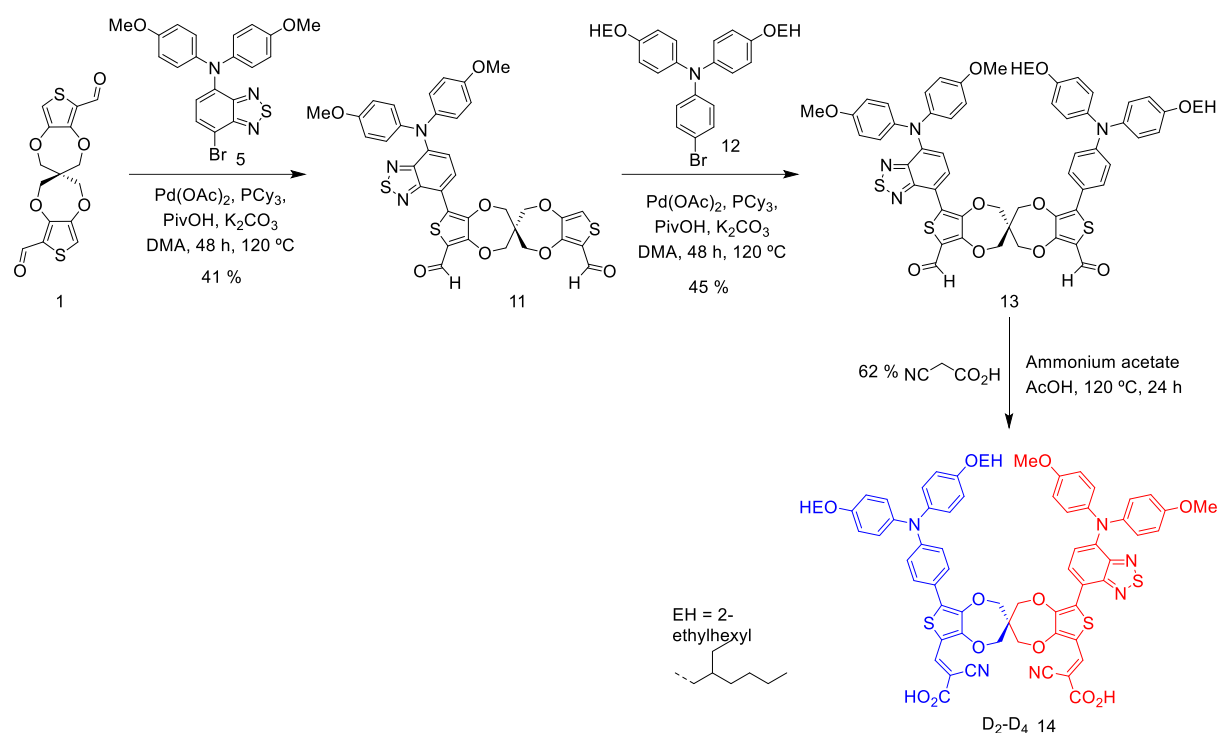
Scheme 4. Synthesis of hetero-dimeric **D₂-D₄** dye by direct arylation method.

Introduction of ethyl hexyl group in **D₂-D₄** increased the solubility in common organic solvent with panchromatic light absorption as benzothiadiazole, an electron deficient auxiliary acceptor moiety is a component of **D₄**. Model dyes are also synthesized as mentioned in **Scheme 5** by employing direct arylation and Knoevenagel condensation.
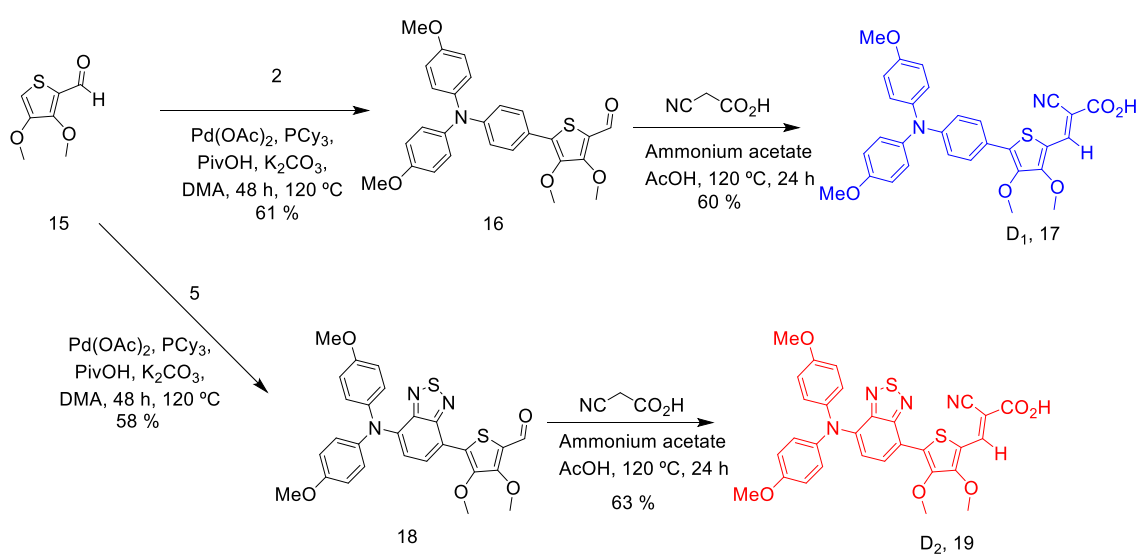
Scheme 5. Synthesis of model dyes **D₁** and **D₂**.

2.2.3 Photophysical properties. Optical properties of spiro-dyes were recorded in solution (DMSO) and on thin mesoporous TiO_2 film. The absorption spectrum of monomeric dyes **D₁** and **D₂** showed single and double bands, respectively. **Figure 5a** shows the absorption spectra of all the dimeric spiro (except **D₂-D₄**) and monomeric model dye, and the corresponding data are summarized in **Table 1**. The dye **D₁-D₁** and **D₁** showed the absorption maxima of 437 nm and 433 nm are corresponding to the intramolecular charge transfer (ICT) transition from donor to acceptor. It is confirmed that the extinction coefficient of **D₁-D₁** ($\varepsilon = 4.37 \times 10^4$ M^{-1} cm^{-1}) is four fold higher than the corresponding monomer **D₁** ($\varepsilon = 1.11 \times 10^4$ M^{-1} cm^{-1}), because of the presence of two D-π-A chromophores, which in turn responsible for better light harvesting. Two distinct bands were observed for three dyes (**D₂-D₂**, **D₂** and **D₁-D₂**) containing benzothiadiazole group in the donor side. The band located at shorter wavelength (401, 391 and 402 nm corresponding to **D₂-D₂**, **D₁-D₂** and **D₂**, respectively) for these three dyes attributed to π-π* electron transition of the chromophores and the other at longer wavelength (555, 537 and 552 nm corresponding to **D₂-D₂**, **D₁-D₂** and **D₂,** respectively) is responsible to the intramolecular charge transfer (ICT) from donor to acceptor.
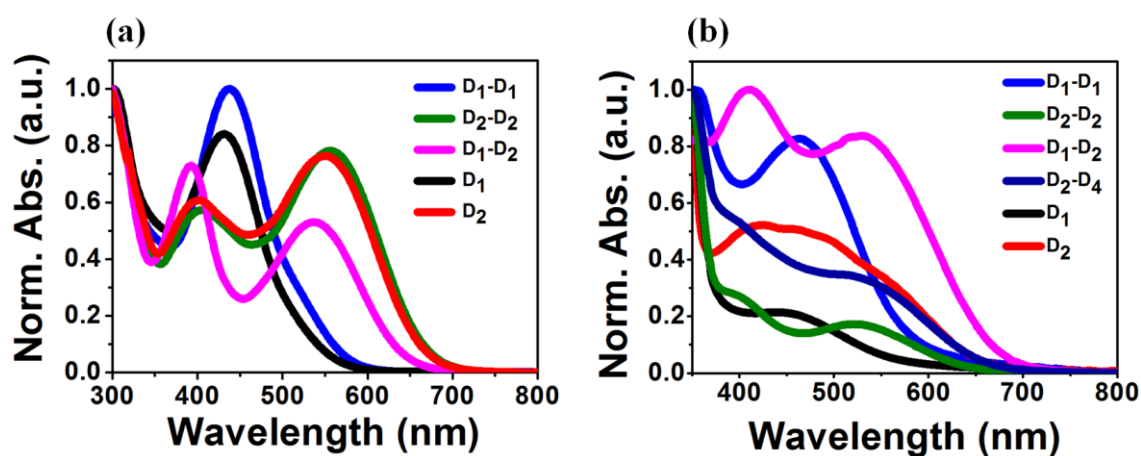
Figure 5. (a) Normalized UV-vis absorption spectra of dimeric and monomeric dyes in solution, (b) Normalized absorption spectra on TiO$_2$ thin film (thickness 6 μM, [dye] = 0.2 mM and dipping time 60 min).

To understand the aggregation property of spiro dyes, UV-vis spectra of all sensitizers adsorbed on to a transparent nanocrystalline TiO$_2$ film was carried out (**Figure 5b**). In general when anchored to the TiO$_2$ surface dye can aggregate and form H-type aggregates, which usually results in absorption bands shifted to lower wavelength (blue shifted) relative to the corresponding monomer peaks in solution, or edge-edge π-aggregates (J-aggregates), which usually gives red shifted absorption band. Besides deprotonation of carboxylic acid[61] of **D$_1$-D$_1$** and **D$_1$** on crystalline TiO$_2$, the ICT transitions of these two dyes were almost 27 nm and 40 nm red shifted respectively. On the other hand in **D$_2$-D$_2$** ($\Delta\lambda$ = 31 nm), **D$_2$** ($\Delta\lambda$ = 62 nm) and **D$_1$-D$_2$** ($\Delta\lambda$ = 5 nm) were blue shifted on TiO$_2$ surface. Therefore it may be concluded that in **D$_1$-D$_1$** and **D$_1$** case J-aggregation is possible, reverse is possible in other dyes despite keeping a spiro linker between the dyes.

In case of **D$_2$-D$_2$** *vs* **D$_2$** the molar extinction coefficient was followed the same trend as observed in **D$_1$-D$_1$** *vs* **D$_1$**. The molar extinction coefficient of **D$_2$-D$_2$** (ε = 3.02 $\times 10^4$ M^{-1} cm^{-1}) corresponding to ICT band is 1.3 fold higher than **D$_2$** (ε = 2.32 $\times 10^4$ M^{-1} cm^{-1}).
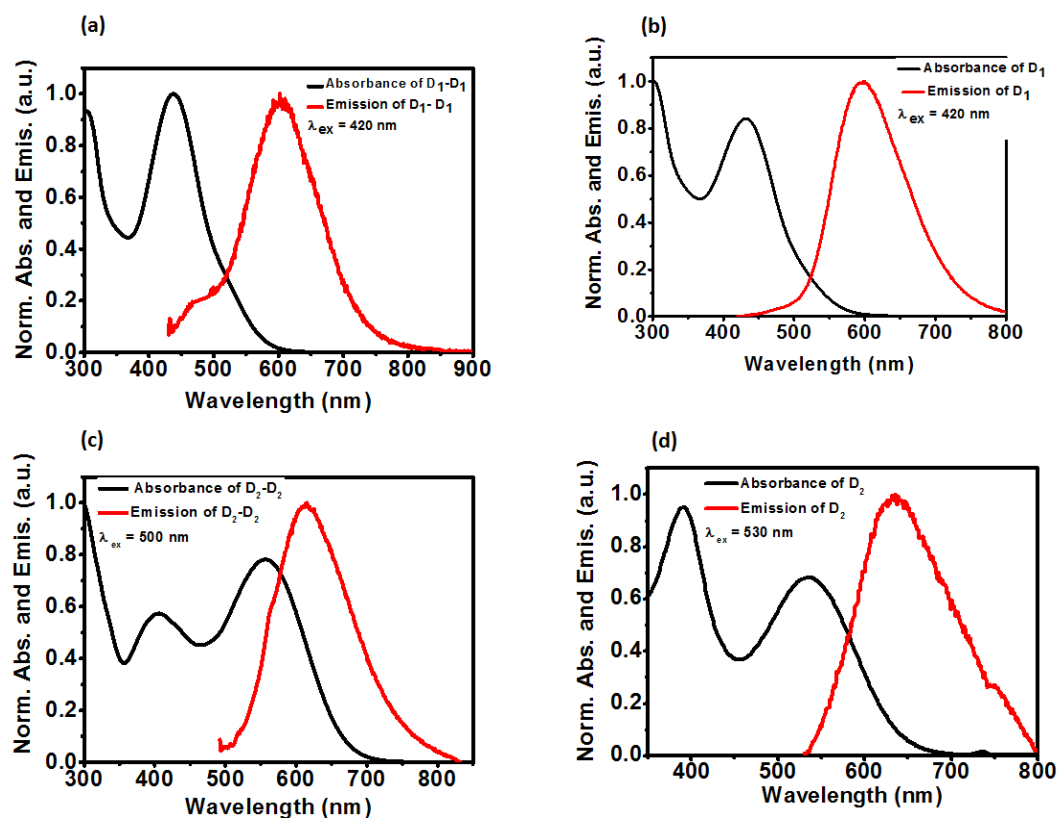
Figure 6. (a) Normalized UV-Vis absorption and emission spectra of (a) **D₁-D₁**, (b) **D₁**, (c) **D₂-D₂** and (d) **D₂** dyes.

Excitation of **D₁-D₁** and **D₁** at 420 nm showed the emission at 606 nm and 598 nm respectively (**Figure 6a and 6b**). In **D₂-D₂** and **D₂** case excitation wavelength were 500 and 530 nm to get emission maxima at 613 nm and 620 nm respectively (**Figure 6c** and **Figure 6d**).
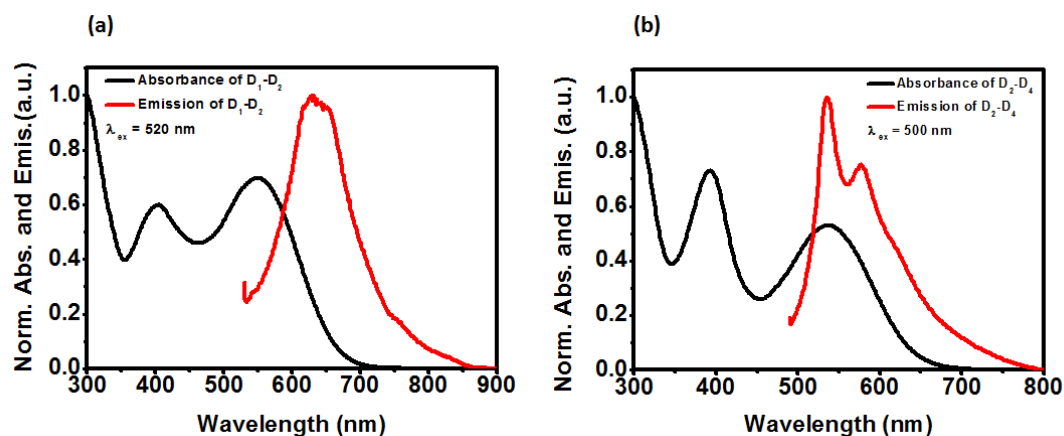
Figure 7. (a) Normalized UV-Vis absorption and emission spectra of (a) **D₁-D₂** and **D₂-D₄** dyes.

In **D₁-D₂** the emission maxima was 630 nm when it exited at 520 nm (**Figure 7a** and **Figure 7b**). Solubility of **D₁-D₂**, **D₂-D₂** and **D₂** was decreased in EtOH, MeOH and chlorinated solvent due to the incorporation of benzothiadiazole group, and solubilized in DMSO.

Different modes of dye anchoring is possible on TiO₂, if dye bind with the TiO₂ though carboxylic acid group, then the following two modes of anchoring is possible, monodentate or bidentate. To prove the interaction in between carboxylic groups of **D₁-D₁** and TiO₂ FTIR studies on chemisorbed TiO₂ powder was carried out. **Figure 8** shows the FTIR spectra of **D₁-D₁** in EtOH solution and **D₁-D₁** adsorbed on the TiO₂ surface. Dye carbonyl peaks were located at 1700 cm⁻¹ for **D₁-D₁**. Upon adsorption on TiO₂ film, the carbonyl peaks corresponding to the free carboxylic acid groups disappeared but asymmetric stretching (v_{as},1584 cm⁻¹) and symmetric stretching(v_s,1389 cm⁻¹) bands for carboxylate units appeared in spectrum. The absence of free carbonyl group corresponding to carboxylic groups and presence of asymmetric and symmetric stretching frequency corresponding to

carboxylate units observed in FTIR is a good indication of the dianchoring bidentate adsorption of **D₁-D₁** on the TiO₂ surface.
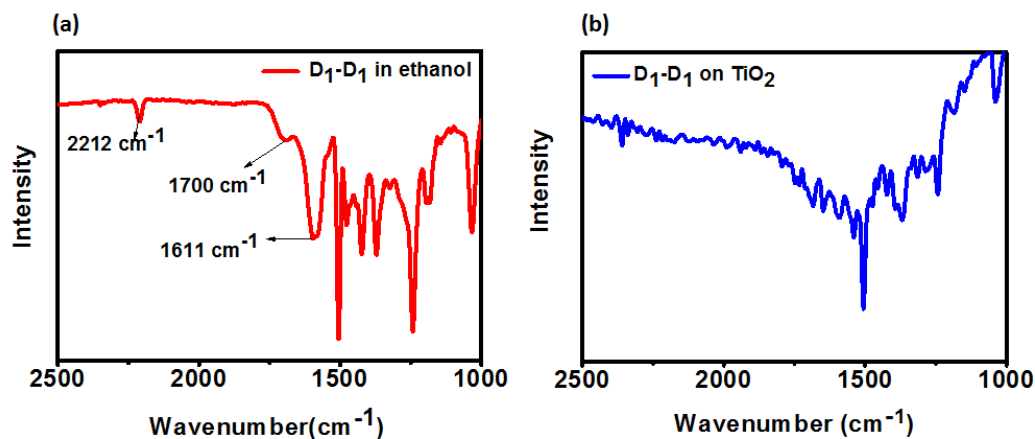
Figure 8. FTIR spectra of **D₁-D₁** in (a) EtOH and (b) **D₁-D₁** in TiO₂.

2.2.4 Electrochemical studies. DPV experiments were carried out to understand the efficacy of charge injection and dye regeneration processes. For the efficient charge injection process, the LUMO energy level of the dye should be above to the conduction band of TiO₂. Whereas the HOMO level of the dye should be below to the electrolyte redox potentials for the dye regeration process. The electrochemical properties of dyes were investigated by DPV (**Figure 9**) in DMSO using 0.1 M tetrabutylammoniumperchlorate. The highest occupied molecular orbital (HOMO) of all these dyes (-5.04 eV to -5.1 eV) are lying below the energy level of I⁻/I₃⁻ redox couple (-4.9 eV)[62,63], so that the oxidized dye formed after electron injection into the conduction band of TiO₂ can be effectively regenerated by accepting electrons from the redox couple. Furthermore the LUMO of the dyes (-3.24 eV to 2.8 eV) is situated above the Fermi level of TiO₂ (-4.2 eV) which facilitates an efficient electron injection from the LUMO of dyes to the conduction band of TiO₂. The zero-zero excitation (E_{0-0}) was estimated from the onset of UV-vis absorption spectrum. E_{LUMO} energy level was calculated by addition of both E_{0-0} and E_{HOMO}. Minimum over potentials of 100-150 mV is required for electron

injection; these dyes showed a significant potential loss (around 1 eV) for the LUMO to conduction band edge electron transfer. Incorporation of benzothiadiazole moiety observed a more negative shift in the LUMO levels of D_2 and D_2-D_2.
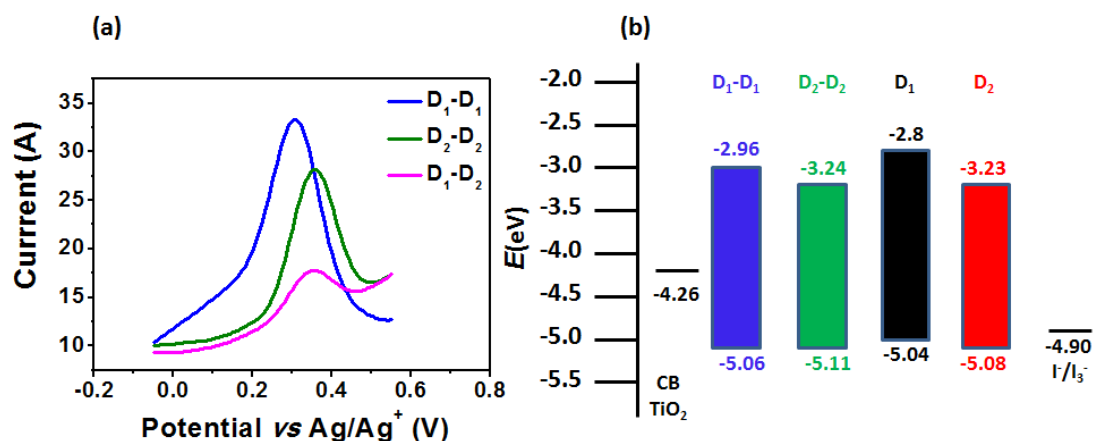
Figure 9. Electrochemical properties of three different spiro dyes. (a) Differential pulsevoltammograms of heterodimeric dyes and (b) schematic energy level representation of spiro-based dye cell.

2.2.5 Density functional theory calculations. To understand the electron distribution of spiro dye, DFT calculations were performed with Gaussian 09 programme using B3LYP/6-31 G (d,p) level. From the frontier molecular orbital calculation it has seen that HOMO of D_1-D_1 is localised mostly on amino phenyl groups whereas LUMO is localised on the cyanoacrylic acid units. Thus, it was anticipated that efficient photoinduced charge separation and the relatively stronger anchoring effect would enhance the degree of electron injection to the TiO$_2$ electrode. The HOMO and LUMO energy level of D_1-D_1 calculated from DFT -4.93 eV and -2.63 eV (**Table 1**) respectively, which is closely related to the result obtained from CV and UV-Vis study (**Figure 10**). DFT calculation was also performed for dimeric (D_2-D_2, D_1-D_2) and monomeric dyes (D_1 and D_2) and shown in **Table 2** and **Table 3**.

(a)   **(b)**

HOMO : - 4.93 eV   LUMO : - 2.63 eV
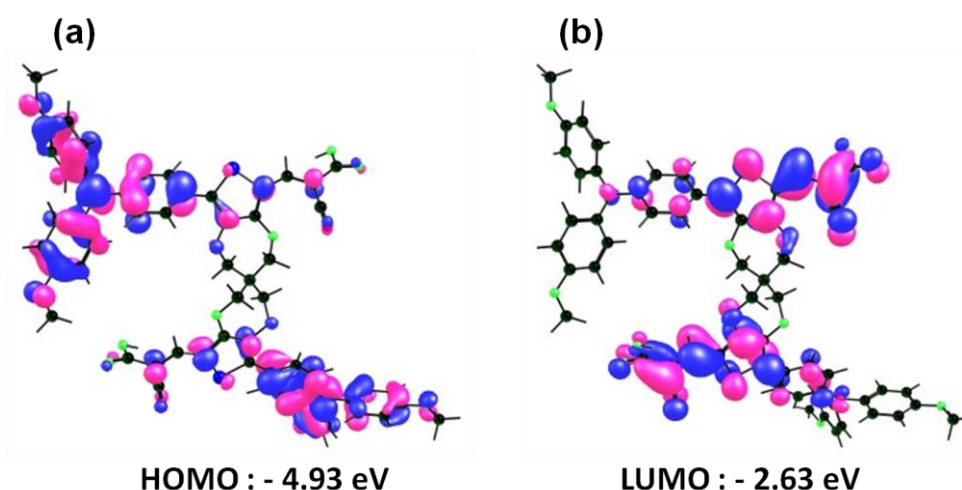
Figure 10. Optimized structure of $\mathbf{D_1}$-$\mathbf{D_1}$ by DFT calculation.

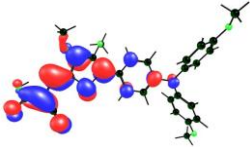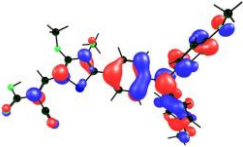**Table 1. Photophysical and electrochemical properties of the dyes**
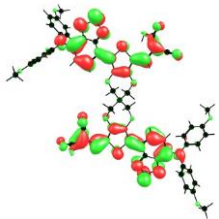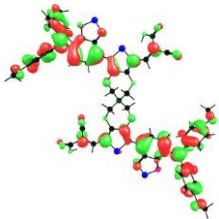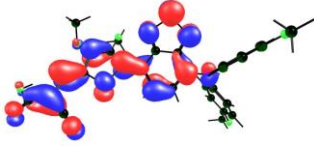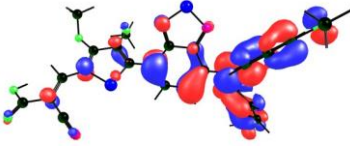
Dye	λ_{max} (nm)[a]	λ_{max} (nm)[b]	λ_{em} (nm)[c]	$\mathcal{E}$ (10^4 $M^{-1}cm^{-1}$)	E_{HOMO}[d] (eV)	E_{LUMO}[e] (eV)	ΔE_{0-0}[f] (eV)	E_{HOMO}[g] (eV)	E_{LUMO}[g] (eV)
$\mathbf{D_1}$-$\mathbf{D_1}$	437	464	606	4.37	–5.06	- 2.96	2.14	-4.93	-2.63
$\mathbf{D_2}$-$\mathbf{D_2}$	401, 555	396, 524	613	3.02	-5.11	- 3.24	1.85	- 5.03	- 2.91
$\mathbf{D_1}$-$\mathbf{D_2}$	391, 537	410, 532	630	1.7	- 5.10	- 3.23	1.86	- 5.03	- 2.90
$\mathbf{D_1}$	433	458	598	1.11	- 5.04	-2.80	2.24	-4.96	-2.46
$\mathbf{D_2}$	402,552	423, 460, 490	634	2.32	- 5.08	-3.23	1.85	-5.08	-2.65

[a]Absorption maxima of dye in DMSO. [b]Absorption maxima of absorbed dye on TiO_2 (thickness 6 μm, dye concentration 0.1 mM in DMSO, dipping time 60 min. [c]Emission maxima of dye in DMSO (excitation, for $\mathbf{D_1}$, $\mathbf{D_1}$-$\mathbf{D_1}$ = 420 nm, for $\mathbf{D_2}$, $\mathbf{D_2}$-$\mathbf{D_2}$ = 530 and 500 nm, for $\mathbf{D_1}$-$\mathbf{D_2}$ = 520 nm. [d]The oxidation potentials were measured by DPV in DMSO with 0.1 M TBAP as supporting electrolyte, Fc^+/Fc as an internal standard, scan rate 200 mV/sec, potential window -0.05 to 0.55 V and supporting electrolyte is tetrabutylammonium perchlorate. HOMO energy level was calculated from ($E_{HOMO} = -$ {E_P [Dye] – $E_{1/2}$ [Fc^+/Fc]} + 4.8). [e]The excited-state oxidation potentials (E_{LUMO}) for the dyes were calculated from the

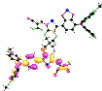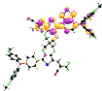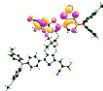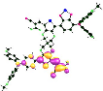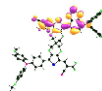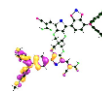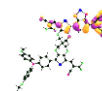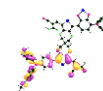equation $E_{LUMO} = -\{E_{HOMO} - E_{g/opt}\}$. [f]Experimental band gap. [g]E_{HOMO} and E_{LUMO} by DFT calculation (B3LYP, 6-31 G (d,p) level).

Table 2. DFT calculation of dimeric (**D₂-D₂**) and monmeric (**D₁, D₂**) dyes

Dye	Molecular orbital of LUMO	Molecular orbital of HOMO	E_{LUMO}	E_{HOMO}
D₂-D₂			-2.91	-5.03
D₁			-2.46	-4.96
D₂			-2.66	-5.08

Table 3. DFT calculation of **D₁-D₂** dye

Description	LUMO + 1 of D₁ in D₁-D₂	LUMO + 2 of D₂ in D₁-D₂	LUMO + 1 of D₂ in D₁-D₂	LUMO of D₁ in D₁-D₂	LUMO of D₂ in D₁-D₂	HOMO of D₁ in D₁-D₂	HOMO of D₂ in D₁-D₂	HOMO - 1 of D₁ in D₁-D₂
Molecular orbital								
Energy (eV)	-0.70	-0.75	-2.25	-2.58	-2.87	-4.91	-5.11	-5.92

2.2.6 Photovoltaic studies. The photocurrent density-voltage (*J-V*) measurements of the cells were carried out under an irradiance of 100 mW/cm^2 simulated AM 1.5G sunlight. Solubility of these dye were varied in different solvents, best solvents and corresponding *J-V* characteristics are shown in **Table 4**. Overall performance of dimeric dyes was compared with monomeric systems. Monomeric **D$_1$** and **D$_2$** showed efficiency of 3.2% (in EtOH) and 2.8% (in DMSO), respectively. Homodimeric sensitizers of **D$_1$** and **D$_2$** performed better than heterodimeric **D$_1$-D$_2$** or **D$_2$-D$_4$**, and monomers (**Figure 12a**). Despite similar UV-vis absorption properties in solution and on thin film, homodimeric **D$_1$-D$_1$** (η =7.6%) showed 2.4 fold increase in PCE having double than **D$_1$** (η = 3.2%). This significant improvement in performance is correlated with both J_{sc} and V_{oc} of the cells. As shown in **Table 4**, the enhanced PCE of **D$_1$-D$_1$** was mainly because of the significant improvement in J_{sc} (about 9 mA/cm^2), which is attributed to the high electron injection efficiency of well oriented structures in the chemisorbed monolayer. Orientation of dyes on the TiO$_2$ surface plays an important role in controlling the charge recombination reactions that impact on the photovoltaic performance.[64,65] It may be plausible that spiro dyes with two anchoring groups fix the **D$_1$-D$_1$** dye with smaller tilt angle on TiO$_2$ compared to **D$_1$**, which leads to slower charge recombination between the oxidized dye and the injected electron in TiO$_2$. Besides that the large dipole moment exerting on the surface from dimeric dyes and better passivation of surface showed a 32 mV increase in V_{oc}. The similar trend is observed in **D$_2$-D$_2$** case, but overall efficiency of **D$_2$-D$_2$** (η=3.4%) was lesser than **D$_1$-D$_1$**, and showed higher PCE than **D$_2$** (η=2.8%). The insertion of benzothiadiazole in dye molecule reduce the solubility in most of the common organic solvent like EtOH, MeOH, MeCN and halogenated solvent like CH$_2$Cl$_2$ or CHCl$_3$. Heterodimeric dye, **D$_1$-D$_2$**, in DMSO further reduced the efficiency (η=1.4%) and which was less than monomers **D$_1$** and **D$_2$**. To make this dye more soluble in common organic solvent the methyl group (from methoxy) of triarylamine was replaced by ethyl hexyl

group. Introduction of ethyl hexyl group make it soluble in EtOH and J_{sc} (8.34 mA/cm^2) was increased more than double amount than that of **D$_1$-D$_2$** (J_{sc}= 4.02 mA/cm^2) as well as IPCE. The IPCE is also depending upon the dielectric constant of the solvent that used in the dye bath in which the TiO$_2$ electrode is immersed for dye loading. For better device performance the dielectric constant of the dipping solvent has to be around 18 to 20.[66] Dielectric constants of EtOH and DMSO are 24.5 and 46.7, respectively.
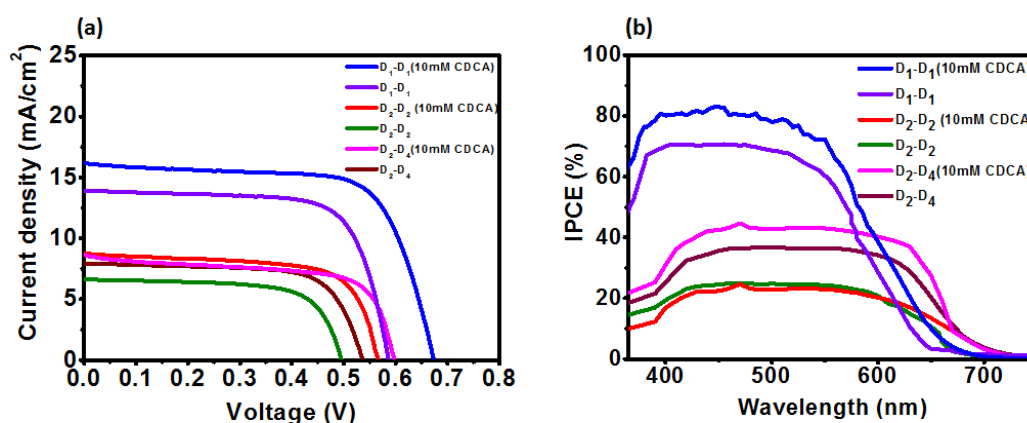
Figure 11. (a) Current density-voltage curve (dye dipping solvent mentioned in **Table 4**), (b) IPCE of spiro and model dyes in DMSO:EtOH (1:3) with and without CDCA.

The influence of solvent was further examined by mixing two solvents. Interestingly J_{sc} and V_{oc} were increased when a mixture of solvent (DMSO/EtOH) was used as a solvent in an optimized ratio (1:3) and **D$_2$-D$_2$** exhibited η = 4.7%. The J_{sc} of **D$_1$-D$_1$** and **D$_2$-D$_2$** in the same solvent ratio were 14 mA/cm^2 and 10.2 mA/cm^2, respectively (**Figure 11**). After mixing equal concentration of dyes the J_{sc} increases with respect to **D$_2$-D$_2$** but at the same time decreases with respect to homodimeric dye (**Figure 12c**). The **D$_1$-D$_1$** dye performs much better than the corresponding monomers dye (**D$_1$**) and similar dye reported in the literature.[66]
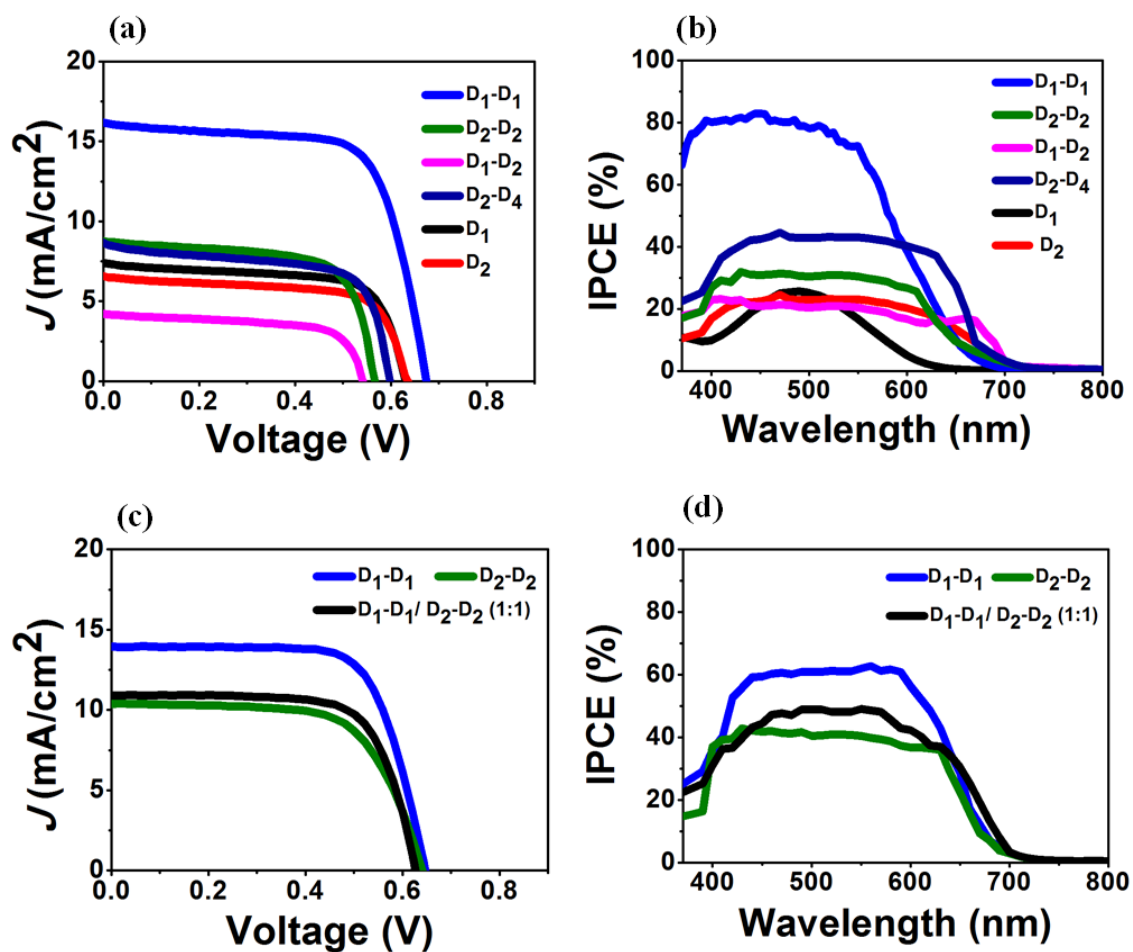
Figure 12. (a) Current density-voltage curve (dye dipping solvent mentioned in **Table 4**), (b) IPCE of spiro and model dyes (c) Current density and voltage of **D₁-D₁** and **D₂-D₂** in DMSO:EtOH (1:3) (d) IPCE of **D₁-D₁** and **D₂-D₂** in DMSO:EtOH (1:3).

Table 4. Photovoltaic parameters[a] of dimeric and monomeric dyes

Dyes	V_{oc} (V)	J_{sc}(mA/cm^2)	FF	η(%)
D₁-D₁ (EtOH)[b]	0.570±0.015	14.0±0.2	0.69±0.02	5.51±0.24
D₁-D₁ (EtOH)	0.66±0.013	16.01±0.15	0.683±0.017	7.22±0.38
D₂-D₂ (DMSO)[b]	0.483±0.012	6.4±0.25	0.662±0.016	2.05±0.18
D₂-D₂ (DMSO)	0.55±0.017	8.5±0.31	0.682±0.013	3.19±0.28
D₁-D₂ (DMSO)	0.53±0.021	3.7±0.22	0.637±0.015	1.24±0.16

D$_2$-D$_4$ (EtOH) [b]	0.518±0.018	7.65±0.25	0.68±0.021	2.69±0.30
D$_2$-D$_4$ (EtOH)	0.58±0.017	8.34±0.34	0.67±0.02	3.24±0.24
D$_1$ (EtOH)	0.62±0.02	7.0±0.21	0.685±0.01	2.96±0.25
D$_2$ (DMSO)	0.63±0.021	6.24±0.18	0.664±0.014	2.61±0.19
D$_1$-D$_1$ (EtOH, DMSO) [c]	0.63±0.012	14.0±0.15	0.66±0.022	5.8±0.32
D$_2$-D$_2$ (EtOH,DMSO)	0.63±0.019	10.18±0.23	0.67±0.02	4.4±0.3
D$_1$-D$_1$ + D$_2$-D$_2$ (EtOH, DMSO)	0.61±0.021	11.0±0.2	0.685±0.015	4.6±0.29
N719 (EtOH)	0.69±0.021	17.6±0.32	0.69±0.02	8.8±0.2

[a]TiO$_2$ thickness 8+5 μm and 0.235 cm^2, [dye] = 0.2 mM, and [CDCA] = 10 mM dipping solvent EtOH, dipping time 16 h, under AM 1.5 illumination (100 mW/cm^2) and the average device parameters from 10 devices is provided, [b]dye adsorption without CDCA on TiO$_2$, [c]Solvent ratio of EtOH and DMSO (3:1).

Incident photon-to-electron conversion efficiencies (IPCE) of homo- and heterodimeric dyes were recorded to understand the conversion efficiency of monomeric and aggregated structures on TiO$_2$, corresponding profiles are shown in **Figure 12b**. **D$_1$** show IPCE of 23%, whereas **D$_1$-D$_1$** shows an IPCE of 80% at 500 nm. **D$_1$-D$_1$** sensitizer exceeds 80% in the spectral range from 400 to 510 nm. The origin of 4 fold higher J_{sc} of **D$_1$-D$_1$** can be correlated with this significant enhancement of photon-to-electron conversion. Monomer **D$_1$** has better chance to have strong intermolecular π-π interaction, which leads to self-quenching of exited states and hence reduce its electron injection capacity. As a result, **D$_1$** based cell produce lower IPCE. In comparison **D$_1$-D$_1$** has orthogonally attached two **D$_1$**-monomers and reasonably has weak intermolecular π-π interaction. Therefore, **D$_1$-D$_1$** based cell generates 4 fold higher IPCE than that of **D$_1$**. This effect is very less in case of **D$_2$-D$_2$** *vs* **D$_2$**. At 460 nm

the IPCE of D_2-D_2 maximum reaches to 31% while in case of D_2 it reaches to 23%. But still

IPCE of D_2-D_2 is higher than that of D_2 at the same wavelength. In D_1-D_2, where two

different type of chromophores D_1 and D_2 are orthogonally attached to each other is not

showing much improvement on IPCE (20% in 510 nm) value. Whereas introduction of ethyl

hexyl group instead of methyl group to D_1 chromophore in D_2-D_4, the IPCE increased to 43

% at the same wavelength. To get the higher IPCE value and panchromatic absorption several

solar cell devices were made by mixing of two spiro dyes D_1-D_1 and D_2-D_2 (**Figure 12d**) in a

solvent mixture of EtOH and DMSO (3:1). The IPCE value of D_1-D_1 was individually

reduced to 60% but increased in D_2-D_2 from 31 to 40% in that particular solvent mixture at

510 nm. Furthermore the IPCE maximum of mixed dyes (D_1-D_1 and D_2-D_2) reaches to 48%

at 510 nm. J_{sc} and V_{oc} of the mixed dyes reached to 11.20 mA/cm^2 and 0.631 V and

ultimately giving 4.9 % efficiency.

2.2.7 Electrochemical impedance spectroscopy. Impedance analysis was carried out to

understand the significant improvement in V_{oc} and J_{sc} of homodimeric D_1-D_1 which results in

2.4 fold increase in PCE than monomeric D_1. The impedance of electrons in the photo

electrochemical cell at the forward bias was analysed by electrochemical impedance

spectroscopy (EIS). The electrochemical impedance spectra of spiro-dyes are recorded for the

DSSC devices under a forward bias of 0.4, 0.5 and 0.6 V in the dark. The Nyquist plots of six

dyes are shown in **Figure 13**. In a typical Nyquist plot, there are three semicircles associated

with the charge transfer processes, first the high frequency region associated with the counter

electrode /electrolyte interface, the mid frequency large semicircle for the charge transfer at

the TiO$_2$-dye-electrolyte interface and the third at low frequency part indicates ion diffusion

resistance or Warburg diffusion coefficient in the electrolyte. Here, the major semicircle is

related to the charge transport process at the interfaces between TiO$_2$ and the electrolyte

because of the experiment carried out in dark.[67,68]

The charge transfer resistance (R_{ct}) on the TiO_2 surface denoted the charge recombination between the electrons resides on TiO_2 at forward bias and electrolyte [69] which is measured by the large semicircle area. A large R_{ct} means a small charge recombination. The R_{ct} values for homodimeric (**D₁-D₁** and **D₂-D₂**) and heterodimeric (**D₁-D₂** and **D₂-D₄**) dyes-based DSSCs were calculated and presented in **Table 5** at 0.4 V.

Among the series **D₁-D₁** showed high impedance of 35 ohm and for its monomeric analogue (**D₁**) R_{ct} was reduced to 18 ohm. The heterodimeric dyes accelerated the charge recombination than **D₁-D₁** and **D₂-D₂** (**Figure 13a**) and the reason has to be analysed further.
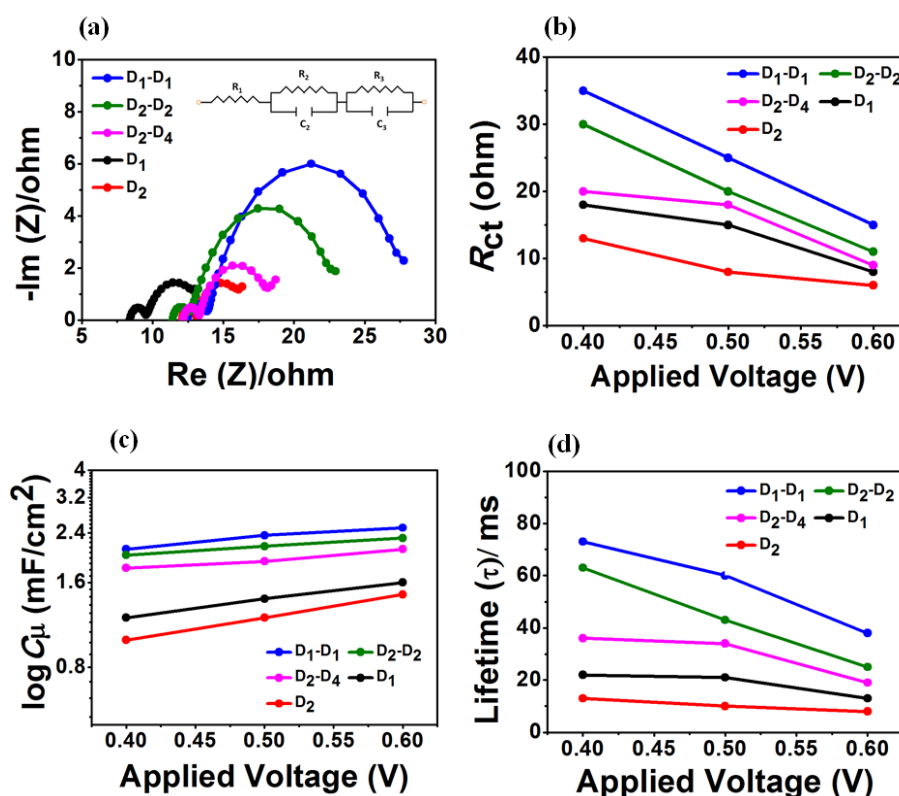
Figure 13. Impedance analysis of spiro spacer connected D-π-A dyes. (a) Nyquist plot, (b) capacitance, (c) charge transfer resistance and (d) electron lifetime *vs* applied potential.

Table 5. Electrochemical impedance parameters of spiro dyes at applied bias of 0.4 V[a,]

Dyes	R_{ct} (ohm)	C_μ (F/cm^2)	τ_n (ms)[b]
D$_1$	18	1.2×10^{-3}	22
D$_2$	13	1×10^{-3}	13
D$_1$-D$_1$	35	2.1×10^{-3}	73
D$_1$-D$_2$	7	1.1×10^{-3}	8
D$_2$-D$_2$	30	2.1×10^{-3}	63
D$_2$-D$_4$	20	1.8×10^{-3}	36

[a]TiO$_2$thickness 8+5 μm and 0.235 cm^2, [dye] = 0.2 mM, and [CDCA] = 10 mM dipping solvent EtOH, dipping time 16 h, [b]Electron lifetime was calculated from capacitance and charge transfer resistance: Life time (τ) = $R_{ct} \times C_\mu$.

The main factors altering the dye cell voltage is conduction band shift and capacitance, as given in **Equation 1** and **Equation 2**; where k_B is the Boltzmann constant, T is the absolute temperature (293 K), n_c the free electron density, and N_c the density of accessible states in the conduction band. The chemical capacitance (C_μ) has been, thus, extrapolated from fitting the experimental data with an equivalent circuit model showed in inset of **Figure13a** [70]. High capacitance of **D$_1$-D$_1$** dye indicates the long lifetime and more number of electrons present in the conduction band. Whenever the electron deficient donor groups coupled with **D$_1$** structure through spiro linkage poor capacitance was showed but **D$_2$-D$_2$** exhibited better capacitance and which in turn increased lifetime of electrons present on TiO$_2$. Evidently, the electron lifetime in TiO$_2$ for the homodimeric dyes, **D$_1$-D$_1$** (73 ms), and **D$_2$-D$_2$** (63 ms) are higher than that of corresponding monomeric dyes **D$_1$** (22 ms) and **D$_2$** (13 ms). Comparatively strong dipole moment of **D$_1$-D$_1$** can be influence the V_{oc} by exerting an upward shift in position of conduction band of TiO$_2$,[71,72]

$$V_{oc} = E_{(F,redox)} - E_{(F,n)} \quad\quad\quad (1)$$

$$E_{(F,n)} = E_{CB} + k_B \, T \, \ln(n_c/N_c) \quad\quad\quad (2)$$

Figure 14 shows a schematic representation of effect of dye structure on conduction band. Electron lifetime was increased same as the observed trend in R_{ct} and C_μ and which are linearly increased with the applied potential, upward shift of capacitance and high charge transfer resistance improved the V_{oc}. This trend appears to be consistent with the values of device V_{oc}. The long electronic lifetime and better passivation of surface infers the high J_{sc} of **D$_1$-D$_1$** than other dyes in series.
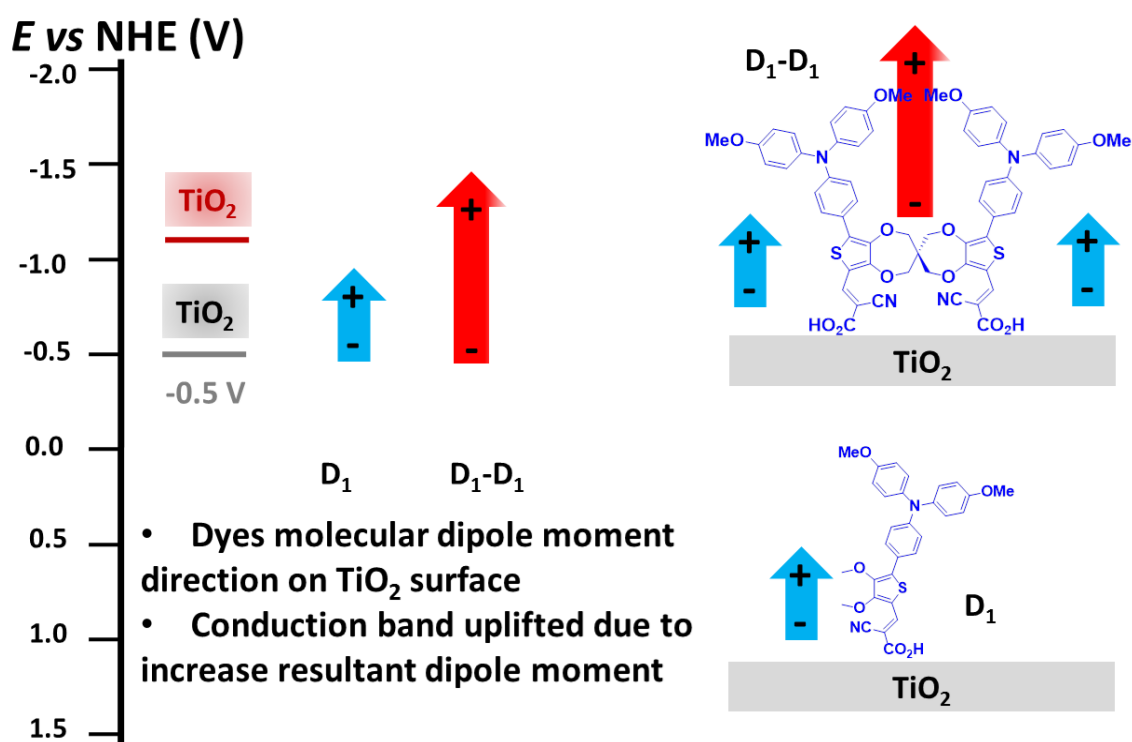
Figure 14. Postulated diagram of uplifted conduction band of **D$_1$-D$_1$** absorbed TiO$_2$ compare to **D$_1$** absorbed TiO$_2$.

2.3 Conclusion

Homo and Hetero dimeric spiro dyes were synthesised by using direct arylation method to avoid traditional Suzuki and Stille coupling. Both the thiophenes (π-spacer) of spiroBiProDOT were functionalized with same or different donor groups which led to homodimeric (**D$_1$-D$_1$** and **D$_2$-D$_2$**) and heterodimeric (**D$_1$-D$_2$** and **D$_2$-D$_4$**) chromophores in a single sensitizer. Due to the flexible linker connecting two dyes reduced dye aggregation and recombination. J_{sc} of dimeric dye **D$_1$-D$_1$** (16.16 mA/cm^2) is 2.24 times higher than that of **D$_1$** (7.2 mA/cm^2) which implies the double amount of charge injection on TiO$_2$ conduction band will also be high in case of **D$_1$-D$_1$**. The V_{oc} of the dimeric spiro-dye **D$_1$-D$_1$** (0.672 V) is also higher than that of **D$_1$** (0.64 V) may be result of increased resultant dipole moment of **D$_1$-D$_1$**,and reduced charge recombination due to the orientation of dyes on the TiO$_2$.The two anchoring groups of these dimeric dyes facilitates strong binding with TiO$_2$ surface which renders controlled orientation and reduced the deactivation process of excited state. This study shows a new molecular approach to incorporate two chromophores in a dimeric dye possessing complementary absorption characteristics for panchromatic absorption and to be studied further by increasing solubility.

2.4 Experimental section

2.4.1 Materials and reagents. All the reagents and solvents were purchased from Aldrich and TCI chemicals and used without further purification. Required precursor 3,4-dimethoxy thiophene[57] was synthesised from thiophene and converted into 2H,2'H,4H,4'H-3,3'-spirobi[thieno[3,4-b][1,4]dioxepine][48] according to the reported literature procedure. All oxygen- and moisture-sensitive reactions were performed under nitrogen atmosphere. The other materials were of the common commercial level and used as received. PhMe was dried over Na/benzophenone ketyl and freshly distilled prior to use.

2.4.2 Characterization. ^{1}H NMR spectra were recorded on a 200 MHz (Bruker AC-200) or 400 MHz (JEOL ECX-400) or 500 MHz (Bruker DRX-500) spectrometers, using DMSO-d_6. All chemical shifts were reported in parts per million (ppm). ^{1}H NMR chemical shifts were referenced to TMS (0 ppm). ^{13}C NMR chemical shifts were referenced to DMSO-d_6 (39.9 ppm), and recorded on either 100 MHz or 125 MHz NMR spectrometer, except where noted. TFA (trifluoroacetic acid) was used to solubilize **D₁-D₂** in DMSO-d_6. MALDI-TOF-MS was recorded on ABSciex 5800 MALDI TOF mass spectrometer. Absorption spectra were recorded on Analytikjena (SPECORD 210 PLUS) UV-Vis spectrophotometer. Cyclic voltammetry (CV) and differential pulse voltammetry (DPV) were performed on BioLogic SP300 potentiostat, where platinum wire was used as a working electrode, a platinum foil was used as a counter electrode, and dyes were dissolved in dry DMSO prior to experiment. CV measurements were carried out at a scan rate of 50 mV/s containing 0.1 M n-Bu$_4$NClO$_4$ as the supporting electrolyte. All potentials were recorded versus Ag/Ag$^+$ reference electrode and calibrated with the redox couple of Fc$^+$/Fc under the same experimental conditions. Electrochemical impedance measurements were performed using a BioLogic SP300 potentiostat equipped with frequency response analyser. Electrochemical impedance analysis was carried out in a frequency range from 1 MHz to 10 mHz with AC amplitude of 10 mV in the dark by applying different potentials. $I-V$ characteristics of the cells were measured under clean room conditions using PHOTO EMISSION TECH (PET, CT200AAA, USA) solar simulator. To measure the short-circuit current, an external bias of AM 1.5G light was applied using a xenon lamp (450 W, USHIO INC, Philippines), and $I-V$ characteristics were recorded using Keithley digital source meter (2420, Keithley, USA) at room temperature. IPCE measurements for the device with area 0.235 cm^2 were carried out with a Newport QE measurement kit by focusing a monochromatic beam of light from 300 W Xe lamp onto the spiro-based DSSC.

2.4.3 Fabrication of dye sensitized solar cells. Commercial fluorine doped tin oxide (FTO) glass (F-doped SnO_2 glass; 6−8 Ω/sq; Pilkington TEC 7) was used as transparent conducting photoanode substrate, which cleaned in an ultrasonic bath using a detergent solution, acetone and ethanol, respectively (each step was 20 min). In the next step plates were immersed into a 40 mM aqueous $TiCl_4$ solution at 70 °C for 30 min and washed with water and ethanol. Then FTO plates are sintered at 500°C for 30 min. Subsequently, 6-8 μm thick layer of commercial TiO_2 paste (Ti-Nanoxide T/SP, Solaronix) with an average particle diameter of 20 nm was deposited over the substrate and sintered at gradually heated under air flow at 325 °C for 5 min, at 375 °C for 5 min, at 450 °C for 15 min, and 500 °C for 15 min. Then a 4-6 μm thick layer of 400 nm scattering layer were deposited over the of 20 nm sized TiO_2 particles and gradually heated under air flow condition at 325 °C for 5 min, at 375 °C for 5 min, at 450 °C for 15 min, and 500 °C for 15 min. After that, the FTO plates are again treated with 40 mM aqueous $TiCl_4$ solution at 70 °C for 30 min and washed with water and ethanol and FTO plate are sintered at 500°C for 30 min. The annealed photo anodes were immersed in a 0.2 mM spiro-dye solution containing 10 mM CDCA (Solaronix, Switzerland) at room temperature for 16 h, for dye adsorption on the TiO_2 surface. After dye loading photoanodes are washed with ethanol solution and dried by air flow. Finally, electrolyte (AN-50, Solaronix, Switzerland) solution was introduced into the space between the photoanodes and Pt sheet counter electrode. Photovoltaic parameters are measured without mask, active area 0.235 cm^2.

2.4.4 Characterization of synthetic compound

Tetrabromo thiophene, a: To a stirred mixture of thiophene (13 g, 0.154 mol), bromine (54g, 0.338 mol) in dry $CHCl_3$ (120 mL) was added, drop wise during 5 h at 0 °C. After 5 h the reaction mixture was allowed to reflux overnight at 55-60 °C temperature. Then a

saturated solution of NaOH solution was added in to the reaction mixture and refluxed further for 2 h. The reaction mixture was extracted with 250 mL of CH_2Cl_2 and washed with 150 mL of water. The organic layer was dried over anhydrous Na_2SO_4 and concentrated with rotary evaporator. The concentrated oily organic compound cooled below 5 °C to induce precipitation of the product. This solid was collected, dissolved in CH_2Cl_2, washed with sodium bisulphite to remove unreacted bromine and recrystallized from hexane. White crystals of tetrabromothiophene were collected and dried under vacuum. Yield 50 g (79%)

3, 4-Dibromo thiophene, b: Tetrabromothiophene (50 g, 0.125 mol) was taken in a 250 mL 2 neck round bottom flask under nitrogen atmosphere. A solution of glacial acetic acid in water at a ratio of 1:2 was added to that tetra bromo thiophene and refluxed overnight it at 100 °C under nitrogen atmosphere. The reaction mixture was washed with ice water and extracted three times with Et_2O. Et_2O was removed by rotary evaporator and the product was distilled under vacuum as a colourless liquid. Yield 20 g (65%); bp 90 - 95 °C at 8 mmHg extracted with 100 mL of Et_2O.

3, 4-Dimethoxy thiophene, c: Sodium metal (10.8 g, 0.470 mol) was dissolved in anhydrous methanol (120 mL, 3.75 mol) in a two neck 250 mL round bottomed flask attached with a Dean-Stark apparatus under nitrogen atmosphere in an ice bath. Dry DMF (100 mL) was added to that solution and the temperature was raised to 100 °C where methanol was distilling and allowed to collect in that Dean stark apparatus. The solution then allowed to cooling at room temperature. 3, 4-dibromothiophene (20 g, 0.083 mol) and CuBr (12 g, 0.083 mol) were added respectively and refluxed it overnight under nitrogen atmosphere at 110 °C. The reaction progress was monitored with TLC. Once the reaction was complete, the reaction mixture was allowed to cool down to room temperature. Water (100 mL) was added under stirring and the product was extracted with Et_2O (5 times). The Et_2O layers were combined

and dried over anhydrous sodium sulphate. Et$_2$O was removed with a rotary evaporator and the residual oil was distilled under vacuum to obtain a yellow colour liquid which further purified by column chromatography using 10% ethyl acetate in pet. ether as an elutent. The reaction mixture then allowed to cool at room temperature and concentrated by rotary evaporator. It was washed with 120 mL of water and extracted by 100 ml of Et$_2$O. Yield: 5.9 g, 48 %. ^{1}H NMR (200 MHz, CDCl$_3$, δ (ppm): 3.87 (s, 6 H), 6.20 (s, 2H).

2H,2'H,4H,4'H-3,3'-Spirobi[thieno[3,4-b][1,4]dioxepine], d: A 500 mL oven dried round bottom flask, equipped with soxhlet extractor containing 4 Å molecular sieves, and an Argon inlet was charged with 250 mL dry PhMe, pentaerythritol (11.3 g, 0.083 mol), 3, 4-dimethoxy thiophene (2 g, 0.014 mol), *p*- toluenesulphonic acid (0.26 g, 1.38 mmol). The mixture was then refluxed under Argon for 72 h. The black mixture was then cooled and washed with 200 mL water. The organic layer was dried over sodium sulphate and the solvent was removed by rotary evaporation. The resulting yellow solid was eluted through silica gel plug with CH$_2$Cl$_2$ to yield (58%) yellow crystal. ^{1}H NMR (200 MHz, CDCl$_3$) δ: 4.06 (s, 8 H), 6.48 (s, 4 H).

2H,2'H,4H,4'H-3,3'-Spirobi[thieno[3,4-b][1,4]dioxepine]-6,6'-dicarbaldehyde, 1: To an ice cooled solution of 2H,2'H,4H,4'H-3,3'-spirobi[thieno[3,4-b][1,4]dioxepine] (500 mg, 1.7 mmol) in anhydrous1,2-DCE (20 mL), DMF (26 µL, 4 mmol) and POCl$_3$ (32 µL, 4 mmol) were added by syringe under nitrogen atmosphere. The solution was stirred for 1 h at 0 °C then allowed to warm to room temperature and left an additional hour before heating to reflux for 2 h. The reaction mixture was cooled to room temperature, aqueous 1M AcONa was added and the refluxing mixture was stirred under heating for 4 h. The mixture was washed with water (200 mL) and extracted with CH$_2$Cl$_2$ (150 mL). Solvents were removed under reduced pressure and purified by column chromatography by using ethyl acetate and pet.

ether as an eluent to give compound 1 as a yellow solid. Yield: 650 mg, 75%. Mp149-158 °C; FT-IR (dry film, cm^{-1}): 2956 (w), 2922 (s), 2853 (s), 1643 (s), 1458 (s), 1415 (w); ^{1}H NMR (400 MHz, CDCl$_3$) δ:4.15 (q, J_A= 1.6 Hz, J_B= 1.6 Hz, 4 H), 4.34 (q, J_A= 4 Hz, J_B= 1.2 Hz, 4 H), 6.97 (s, 2 H), 9.96 (s, 2 H); ^{13}CNMR (400 MHz, CDCl$_3$) δ: 50.3, 70.9, 115.6, 122.6, 148.4, 154.6, 180.3; MALDI-TOF m/z calcd for [M+Na]$^+$ [C$_{15}$H$_{12}$O$_6$S$_2$Na]$^+$374.9968, found 375.1316.

6,6'-Bis(4-(bis(4-methoxyphenyl)amino)phenyl)-2H,2'H,4H,4'H-3,3'-spirobi[thieno[3,4-b][1,4]dioxepine]-8,8'-dicarbaldehyde, 3: Precursor **1** (100mg, 0.28 mmol), **2** (254 mg, 0.57 mmol), K$_2$CO$_3$ (85 mg, 0.62 mmol), Pd(OAc)$_2$ (0.5 mol%), PCy$_3$ (0.5 mol%), and PivOH (0.15 mol%) were taken in a Schlenk tube under nitrogen atmosphere. Anhydrous DMA (5 mL) was added to that and kept the reaction at 120 °C temperature under the same atmosphere for 24 h. After 24 h, monitoring the reaction conversion by TLC showed disappearance of compound **1**. The reaction mixture cooled and was washed with 100 mL of water and extracted with 100 mL of CH$_2$Cl$_2$. Solvents were removed under reduced pressure and purified by column chromatography by using ethyl acetate and pet. ether as an eluent to give compound 3 as an orange solid. Yield: 125 mg, 56%. Mp 175-182 °C; FT-IR (dry film, cm^{-1}): 2955 (w), 2923 (s), 2856 (m), 1732 (s), 1646 (m), 1599 (w); ^{1}H NMR (200 MHz, CDCl$_3$) δ: 3.82 (s, 12 H), 4.21 (d, J = 4 Hz, 4 H), 4.35 (s, 4 H), 6.85-6.92 (m, 12 H), 7.09-7.13 (m, 8 H), 7.57 (d, J = 10 Hz, 4 H), 9.92 (s, 2H);^{13}C NMR (100 MHz, CDCl$_3$) δ: 55.5, 70.9, 112.3, 114.2, 114.8, 115.7, 122, 126.6, 131.8, 140.6, 147.9, 156.0, 180.8. MALDI-TOF (m/z) calcd for [M]$^+$[C$_{55}$H$_{46}$N$_2$O$_{10}$S$_2$]$^+$958.2594, found 958.0824.

D$_1$-D$_1$, 4: A mixture **4** (100 mg, 0.1 mmol), cyanoacetic acid (54 mg, 0.63 mmol), NH$_4$OAc (33 mg, 0.44 mmol) and glacial CH$_3$COOH (15 mL) was heated under reflux reaction conditions for 12 h. The reaction mixture was washed with water, methanol and Et$_2$O

thoroughly. The dark red solid **D$_1$-D$_1$** was partially soluble in PhMe, EtOAc, CH$_2$Cl$_2$, CHCl$_3$ and completely soluble in DMSO and EtOH, MeOH. Compound was purified by washing and yield was 125 mg, 65%. Mp 240-243 °C; FT-IR (dry film, cm^{-1}): 2960-2850 (br), 2216 (s), 1676 (s), 1567 (w), 1507 (m); ^{1}H NMR (200 MHz, DMSO-d_6) δ : 3.78 (s, 12 H), 4.23-4.30 (m, 4 H), 4.39-4.47 (m, 4 H)6.79 (d, J = 8 Hz, 4 H), 6.97 (d, J = 8 Hz, 8 H), 7.13 (d, J = 8 Hz, 8 H), 7.62 (d, J = 8 Hz, 4 H), 8.25 (s, 2 H);^{13}C NMR (100 MHz, DMSO-d_6) δ: 29.5, 55.7, 56.3, 72.1, 107.0 115.1, 118.0, 119.2, 122.5, 127, 128, 129.7, 131.4, 132.8, 139.6, 144.9, 149.4, 156.8, 172.5 ;MALDI-TOF m/z calcd for [M+Na] $^+$[C$_{61}$H$_{48}$O$_{12}$N$_4$NaS$_2$+ Na] $^+$1115.2602, found 1115.2604.

7-Bromo-N, N-bis (4-methoxyphenyl)benzo[c][1,2,5]thiadiazol-4-amine, 5: *tert*-BuOK (1.3 g, 11.5 mmol), Pd$_2$(dba)$_3$ (200 mg, 0.22 mmol), PCy$_3$ (0.24 g, 0. mmol) were taken in a 2 necked 100 mL round bottom flask adjusted with a reflux condenser under inert atmosphere. Anhydrous dry PhMe (30 mL) added to it. Compound **5** (1.5 g, 5.2 mmol) and bis(4-methoxyphenyl)amine (600 mg, 2.6 mmol) added to that under inert atmosphere and the reaction mixture kept overnight by heating at 65° C. The reaction was followed by TLC. The reaction mixture was washed with water (200 mL) and extracted by CH$_2$Cl$_2$ (100 mL). The organic layer was dried by Na$_2$SO$_4$ and concentrated by reducing pressure. The reaction mixture was purified by column chromatography using pet. ether and CH$_2$Cl$_2$ (10:1) as an eluting agent to give compound 5 as deep brown solid. Yield: 910 mg, 65 %. ^{1}H NMR (200 MHz, CDCl$_3$) δ : 3.80 (s, 6 H), 6.79-6.83 (m, 5 H), 6.99 (d, J = 8 Hz, 4 H), 7.61 (d, J= 8 Hz, 1 H);^{13}C NMR (100 MHz, CDCl$_3$) δ: 55.5, 114.6, 114.7, 120.2, 125.9, 126.1, 132.7, 141.1, 156.3; MALDI-TOF m/z calcd for[M] $^+$[C$_{20}$H$_{16}$BrN$_3$O$_2$S] $^+$441.0147, found 440.9442.

6,6'-Bis(7-(bis(4-methoxyphenyl)amino)benzo[c][1,2,5]thiadiazol-4-yl)-2H,2'H,4H,4'H-3,3'-spirobi[thieno[3,4-b][1,4]dioxepine]-8,8'-dicarbaldehyde, 6: A mixture of precursor **1**

(100 mg, 0.28 mmol), **5** (380 mg, 0.57 mmol), K_2CO_3 (125 mg, 0.62 mmol), $Pd(OAc)_2$ (0.5 mol%), PCy_3 (0.5 mol%), and PivOH (0.15 mol%) were taken in a Schlenk tube under nitrogen atmosphere. Anhydrous DMA (5 mL) was added to that and kept the reaction at 120 °C temperature under the same atmosphere for 24 h. After 24 h TLC was checked in 30% EtOAc in PhMe. The reaction mixture was washed with 200 mL of water and extracted with 150 mL of CH_2Cl_2. Solvents were removed under reduced pressure and purified by column chromatography by using EtOAc and pet. ether as an eluent to give compound 6 as brown solid. Yield: 121 mg, 67%. Mp 203-210 °C; FT-IR (dry film, cm^{-1}): 2954 (s), 2922 (s), 2851 (s), 1730 (s), 1642 (m), 1535 (w); ^{1}H NMR (200 MHz, CDCl$_3$) δ: 3.83 (s, 12 H), 4.27-4.37 (m, 4 H), 4.42 (s, 4 H), 6.85-6.88 (m, 8 H), 6.95 (d, $J = 10$ Hz, 2 H), 7.03-7.06 (m, , 8 H), 8.16 (d, $J = 10$ Hz, 2 H) 10.02 (s, 2 H);^{13}C NMR (125 MHz, CDCl$_3$) δ: 50.4, 55.5, 70.9, 71.2, 114.6, 116.8, 118.2, 120.6, 126.5, 129.4, 130.6, 140.7, 141.5, 144.7, 149.6, 153.9, 154.5, 156.6, 168.7, 180.6;MALDI-TOF m/z calcd for[M] $^+$[C$_{55}$H$_{42}$N$_6$O$_{10}$S$_4$] $^+$1074.1845, found 1073.8605.

Synthesis of D$_2$-D$_2$, 7: A mixture **6** (100 mg, 0.084 mmol), cyanoacetic acid (63 mg, 0.53 mmol), NH$_4$OAc (70 mg, 0.5 mmol) and glacial AcOH (10 mL) was heated under reflux for 12 h during which time the aldehyde is completely consumed as indicated by TLC. After 12 h the reaction mixture was washed with water, CH$_3$OH and Et$_2$O repeatedly. Deep brown D$_2$-D$_2$ was partially soluble in PhMe, EtOAc, CH$_2$Cl$_2$, and CHCl$_3$ and completely soluble in DMSO. Compound was purified by washing with Et$_2$O. Yield: 58 mg, 55%. Mp 287-289 °C; FT-IR (dry film, cm^{-1}): 3384 (br), 2961-2853 (br), 2213 (s), 1691 (s), 1565 (m), 1538 (m), 1502 (s); ^{1}H NMR (200 MHz, DMSO-d_6) δ: 3.77 (s, 12 H), 4.36 (s, 4 H), 4.45 (s, 4 H), 6.88-6.92 (m, 10 H), 7.03 (d, $J = 10$ Hz, 8 H), 8.31 (s, 2 H), 8.40 (d, $J = 10$ Hz, 2 H);^{13}C NMR (100 MHz, DMSO-d$_6$) δ: 47.4, 55.7, 72.1, 111.1, 115.2, 116.2, 118.3, 127, 128.2, 140.6,

141.6, 145.7, 149.2, 153.7, 156.8, 161.7, 164.5;MALDI-TOF *m/z* calcd for[M+Na] $^+$[$C_{61}H_{44}N_8O_{12}S_4$+Na] $^+$1231.1854, found 1230.8029.

6'-(4-(Bis(4-methoxyphenyl)amino)phenyl)-2H,2'H,4H,4'H-3,3'-spirobi[thieno[3,4-b][1,4]dioxepine]-6,8'-dicarbaldehyde, 8: Dialdehyde derivative, **1** (200 mg, 0.56 mmol), **2** (208 mg, 0.56 mmol), K_2CO_3 (185 mg, 0.62 mmol), Pd(OAc) $_2$ (0.5 mol%), PCy$_3$ (0.5 mol%), and PivOH (0.15 mol%) were taken in a Schlenk tube and purged with nitrogen. Anhydrous DMA (5 mL) was added to that and kept the reaction at 120 $^\circ$C temperature under the same atmosphere for 24 h. The reaction mixture was washed with 200 mL of water and extracted with 150 mL of CH_2Cl_2. Solvents were removed under reduced pressure and purified by column chromatography by using EtOAc and pet. ether as an eluent to give compound **8** as yellow solid. Yield: 148 mg, 45%. Mp 171-180 $^\circ$C; FT-IR (dry film, cm^{-1}): 2953 (w), 2923 (s), 2853 (m), 1641 (s), 1606 (m), 1585 (s), 1503 (s), 1482 (s); ^{1}H NMR (200 MHz, CDCl$_3$) δ: 3.82 (s, 6 H), 4.14-4.20 (m, 4 H), 4.23- 4.35 (m, 4 H), 6.84-6.91 (m, 6 H), 6.96 (s, 1 H), 7.08- 7.13 (m, 4 H),7.56 (d, *J* = 10 Hz, 2 H), 9.91 (s, 1 H), 9.94 (s, 1 H);^{13}C NMR (125 MHz, CDCl$_3$) δ: 50.4, 55.5, 70.9, 114.8, 114.9, 115.7, 116.8, 118.8, 127.3, 127.9, 128.1, 131.6, 139.2, 139.8, 148.4, 155.3, 156.6, 157.0, 180.0, 180.8; MALDI-TOF *m/z* calcd for[M] $^+$[$C_{35}H_{29}NO_8S_2$] $^+$ 655.1335, found 655.0026.

6-(7-(Bis(4-methoxyphenyl)amino)benzo[c][1,2,5]thiadiazol-4-yl)-6'-(4-(bis(4-methoxyphenyl)amino)phenyl)-2H,2'H,4H,4'H-3,3'-spirobi[thieno[3,4-b][1,4]dioxepine]-8,8'-dicarbaldehyde, 9: Compound **8** (130 mg, 0.09 mmol), **5** (228 mg, 0.1 mmol), K_2CO_3 (115 mg, 0.62 mmol), Pd(OAc)$_2$ (0.5 mol%), PCy$_3$ (0.5 mol%), and PivOH (0.15 mol%) were taken in a Schlenk tube under nitrogen atmosphere. Dry DMA (5 mL) was added to that and kept the reaction at 120 $^\circ$C temperature under the same atmosphere for 24 h. The reaction mixture was washed with 200 mL of water and extracted with 150 mL of CH_2Cl_2. Solvents

were removed under reduced pressure and purified by column chromatography by using

EtOAc and pet. ether as an eluent to give compound **9** as brown solid. Yield: 85mg, 32%. Mp

196-203 °C; FT-IR (dry film, cm^{-1}): 2957 (s), 2926 (s), 2867 (m), 1649 (s), 1600 (s), 1505 (s);

^{1}H NMR (200 MHz, CDCl$_3$) δ: 3.82 (s, 6 H), 3.83 (s, 6 H), 4.19-4.32 (m, 4H), 4.38-4.41 (m,

4 H), 6.83-6.93 (m, 11 H), 7.03-7.13 (m, 8 H), 7.56 (d, J = 12 Hz, 2 H), 8.16 (d, J = 8 Hz, 1

H), 9.91 (s, 1 H), 10.01 (s, 1 H).

D$_1$-D$_2$, **10**: A mixture of dialdehyde derivative, **9** (110 mg, 0.076 mmol), cyanoacetic acid (70

mg, 0.63 mmol), NH$_4$OAc (7 mg, 0.5 mmol) and glacial CH$_3$COOH (10 mL) was heated

under reflux for 12 h during which time the aldehyde is completely consumed as indicated by

TLC. The reaction mixture was washed with water, CH$_3$OH and Et$_2$Orepeatedly. Black

colour **D$_1$-D$_2$** was insoluble in PhMe, EtOAc, CH$_2$Cl$_2$, CHCl$_3$ and partially soluble in DMSO.

Compound was purified by washing with water, Et$_2$O and CH$_3$OH. Yield 126 mg, 48%. Mp

256-260°C; FT-IR (dry film, cm^{-1}): 3445-3432 (br), 2964-2883 (br), 2019 (s), 1659 (s), 1569

(s), 1523 (s); ^{1}H and ^{13}C NMR spectra were recorded by addition of TFA.^{1}H NMR (500

MHz, DMSO-d_6 +TFA) δ: 3.75 (s, 12 H), 4.31-4.49 (m, 8 H), 6.86-6.92 (m, 10 H), 6.97-7.04

(m, 10 H), 8.33-8.37 (m, 2 H), 8.40-8.42 (m, 2 H);^{13}C NMR (125 MHz, DMSO-d_6 +TFA) δ:

13.9, 19.7, 23.5, 29.5, 42.6, 57.7, 66.3, 79.2, 79.4, 101.8, 114.7, 115.2, 116.1, 117.3, 118.2,

127, 128.5, 131.8, 140.6, 145.7, 149.2, 153.7, 155.1, 156.8, 164.5, 181.4; MALDI-TOF m/z

for [M+K]$^+$ [C$_{61}$H$_{48}$KN$_6$O$_{12}$S$_3$] $^+$calcd for 1189.1967, found 1189.2160.

6'-(7-(Bis(4-methoxyphenyl)amino)benzo[c][1,2,5]thiadiazol-4-yl)-2H,2'H,4H,4'H-3,3'-spirobi[thieno[3,4-b][1,4]dioxepine]-6,8'-dicarbaldehyde, 11: Dioxepine dialdehyde, **1**

(150 mg, 0.43 mmol), 7-bromo-N,N-bis(4-methoxyphenyl)benzo[c][1,2,5]thiadiazol-4-amine

(190mg, 0.43 mmol), K$_2$CO$_3$ (150 mg, 1.1 mmol), Pd(OAc) $_2$ (0.5 mol%), PCy$_3$ (0.5 mol%),

and PivOH (0.15 mol%) were taken in a Schlenk tube under nitrogen atmosphere. Anhydrous DMA (5 mL) was added to that and kept the reaction at 120 °C temperature under the same atmosphere for 24 h. The reaction mixture was washed with 200 mL of water and extracted with 150 mL of CH_2Cl_2. Solvents were removed under reduced pressure and purified by column chromatography by using EtOAc and pet. ether as an eluent to give compound **11** as brown solid. Yield: 110 mg, 41%. Mp 169-178 °C; FT-IR (dry film, cm^{-1}): 2958 (s), 2923 (s), 2853 (w), 1731 (m), 1647 (s), 1535 (w), 1502 (s); ^{1}H NMR (200 MHz, CDCl$_3$) δ: 3.83 (s, 6H), 4.26-4.37 (m, 8H), 6.83-6.88 (m, 4 H), 6.96-6.97 (m, 2 H), 7.02-7.07 (m, 4 H), 8.15 (d, *J*= 8 Hz, 1H), 9.94 (d, *J*= 2 Hz, 2 H), 10 (s, 1H);^{13}C NMR (100 MHz, CDCl$_3$) δ: 55.5, 70.9, 114.6, 115.7, 124.3, 126.5, 130, 136, 161.8, 166.5, 170.7, 180.8; MALDI-TOF *m/z* calcd for[M+] $^+$[C$_{35}$H$_{27}$N$_3$O$_8$S$_3$] $^+$713.0960, found 712.9735.

6-(4-(Bis(4-((2-ethylhexyl)oxy)phenyl)amino)phenyl)-6'-(7-(bis(4-methoxyphenyl)amino)benzo[c][1,2,5]thiadiazol-4-yl)-2H,2'H,4H,4'H-3,3'-spirobi[thieno[3,4-b][1,4]dioxepine]-8,8'-dicarbaldehyde, 13: Dicarbaldehyde derivative, **11**(120 mg, 0.17 mmol), 4-bromo-N,N-bis(4-((2-ethylhexyl)oxy)phenyl)aniline (**12**) (120mg, 0.2 mmol), K$_2$CO$_3$ (58 mg, 0.42 mmol), Pd(OAc) $_2$ (0.5 mol%), PCy$_3$ (0.5 mol%), and PivOH (0.15 mol%) were taken in a Schlenk tube under nitrogen atmosphere. Anhydrous DMA (5 mL) was added to that and kept the reaction at 120 °C for 24 h. The reaction mixture was washed with 200 mL of water and extracted with 150 mL of CH_2Cl_2. Solvents were removed under reduced pressure and purified by column chromatography by using EtOAc and pet. ether as an eluent to give compound 13 as a brown solid. Yield: 98 mg, 45 %. Mp 201-206 °C; FT-IR (dry film, cm^{-1}): 2957 (w), 2919 (s), 2851 (s), 1729 (m), 1702 (m), 1600 (w), 1504 (w); ^{1}H NMR (400 MHz, CDCl$_3$) δ: 0.90-1.02 (m, 6H), 1.32-1.42 (m, 12H), 1.72-1.85 (m, 4H), 1.87-1.98 (m, 4H), 2.04-2.08 (m, 2H), 2.23-2.25 (m, 2 H), 3.84(s, 6 H), 3.39-4.02 (m, 2 H), 4.27-4.38 (m, 6 H), 4.42 (s, 4 H), 6.87 (d, *J* = 8 Hz, 9 H), 6.96 (d, *J* = 8 Hz, 2 H), 7.06

(d, J = 8 Hz, 9 H), 8.17 (d, J = 8 Hz, 2 H), 10 (s, 2H);^{13}C NMR (125 MHz, CDCl$_3$) δ: 11.2, 14.1, 15.3, 25.4, 26, 33, 49.1, 50.4, 55.5, 70.8, 70.9, 114.6, 116.8, 118.1, 120.5, 126.5, 129.4, 130.6, 140.7, 141.5, 144.6, 153.9, 154.5, 155.1, 156.6, 156.7, 167.6, 167.8, 171.7, 180.6, 184.8; MALDI-TOF *m/z* calcd for (M+H$^+$) $^+$(C$_{69}$H$_{73}$N$_4$O$_{10}$S$_3$) $^+$ 1213.4480, found 1213.4915

Synthesis of **D$_2$-D$_4$** , **14**: A mixture **13** (57 mg, 0.05 mmol), cyanoacetic acid (24 mg, 0.28 mmol), NH$_4$OAc (40 mg, 0.05 mmol) and glacial acetic acid (5 mL) was heated under reflux for 12 h during which time the aldehyde is completely consumed as indicated by TLC. After 12 h the reaction mixture was washed with water, CH$_3$OH and Et$_2$O thoroughly to give **D$_2$-D$_4$** as a brown solid. The reaction mixture was soluble in PhMe, EtOAc, CH$_2$Cl$_2$, CHCl$_3$ and DMSO. Compound was purified by washing and yield was 40 mg (62%). Mp 239-243 °C; FT-IR (dry film, cm^{-1}): 3240-3235 (br), 2957-2858 (br), 2218 (s), 1732 (s), 1615 (w), 1489 (w);^{1}H NMR (500 MHz, CDCl$_3$) δ: 0.87-0.91 (m, 6 H), 1.36-1.39 (m, 6 H), 1.40-1.49 (m, 4 H), 1.49-1.55 (m, 4 H), 1.60-1.69 (m, 4 H), 1.82- 1.87 (m, 4 H), 1.90-1.96 (m, 2 H) 3.84 (s, 6 H), 3.98-4.02 (m, 2 H), 4.22 (s, 2 H), 4.24-4.38 (m, 2 H),4.30-4.35 (m, 4 H), 4.38-4.40 (m, 2 H), 6.87 (d, J = 10 Hz, 9 H), 6.98 (d, J = 5 Hz, 2H), 7.06 (d, J = 5 Hz, 9 H), 7.46 (s, 1 H), 7.48 (s, 1 H), 8.19 (d, J = 5 Hz, 2 H); ^{13}C NMR (200 MHz, CDCl$_3$) δ: 14.1, 17.0, 25.7, 26.3, 28.2, 29.3, 29.7, 32., 38.4, 46.1, 50.54, 55.5, 86.9, 92.6, 94.1, 105.5, 106.2, 106.5, 114.6, 116.6, 118.8, 126.4, 126.7, 129.7, 145.3, 146.5, 147.1, 148.9, 156.2, 162.2, 165, 170;

3,4-Dimethoxythiophene-2-carbaldehyde, 15: 3,4-Dimethoxy thiophene (100 mg, 0.7 mmol) was dissolved in 10 mL of dry1,2-DCE. DMF (136 µL, 1.74 mmol) was added slowly under 0˚C temperature under inert atmosphere. After 15 min of addition POCl$_3$ (163 µL, 1.74 mmol) was added to that and reflux the reaction mixture for 24 h under the same atmosphere. Reaction was monitoring by TLC. After overnight reflux reaction mixture was washed with

water (100 mL) and extracted by CH_2Cl_2. The organic layer was dried by Na_2SO_4 and concentrated by reducing pressure. Reaction mixture was purified by column chromatography using pet. ether and EtOAc (20:1) as an eluent to give compound 15 as a yellow solid. Yield: 126mg, 85%. Mp 101-119 °C; FT-IR (dry film, cm^{-1}): 3097 (s), 2962 (w), 2846 (w), 1638 (s), 1488 (s) 1448 (m); ^{1}H NMR (200 MHz, CDCl$_3$) δ: 3.88 (s, 3 H), 4.13 (s, 3 H), 6.66 (d, J = 1.4 Hz, 1 H), 10.0 (d, J = 1.4 Hz, 1 H); ^{13}C NMR (200 MHz, CDCl$_3$) δ: 57.8, 61.6, 106.7, 124.1, 150.1, 153.6, 181.7; MALDI-TOF m/z calcd for [M+Na] $^+$[C$_7$H$_8$O$_3$SNa] $^+$195.0086, found 194.9541.

5-(4-(Bis(4-methoxyphenyl)amino)phenyl)-3,4-dimethoxythiophene-2-carbaldehyde, 16:
3,4-Dimethoxy-2-carboxaldehyde (150 mg, 0.87 mmol, 1 equivalent), **2** (400 mg, 1 mmol), K$_2$CO$_3$ (300 mg, 2.2 mmol), Pd(OAc)$_2$ (0.5 mol%), PCy$_3$ (0.5 mol%), and PivOH (0.15 mol%) were taken in a Schlenk tube under nitrogen atmosphere. Anhydrous DMA (5 mL) was added to that and kept the reaction at 120 °C temperature under the same atmosphere for 24 h. After 24 h TLC was checked in 10% EtOAc in pet. ether. The reaction mixture was washed with 200 mL of water and extracted with 150 mL of CH_2Cl_2. Solvents were removed under reduced pressure and purified by column chromatography by using EtOAc and pet. ether as an eluent to give compound 16 as a yellow solid. Yield was 45%. Mp 150-153 °C; FT-IR (dry film, cm^{-1}): 2953 (w), 2927 (w), 2836 (w), 1701 (w), 1644 (s), 1598 (s), 1502 (s);^{1}H NMR (200 MHz, CDCl$_3$) δ: 3.79 (s, 3H), 3.82 (s, 6H), 4.17 (s, 3H), 6.86-6.91 (m, 6H), 7.11(d, J =10 Hz, 4 H) , 7.59 (d, J = 5 Hz, 2 H), 9.99 (s, 1 H);^{13}C NMR (125 MHz, CDCl$_3$) δ: 55.5, 60.4, 61.7, 114.7, 118.7, 119.9, 122.6, 127.3, 127.9, 138, 139.8, 144.3, 149.6, 156.5, 157.6, 180.4;MALDI-TOF m/z calcd for[M+Na]$^+$[C$_{27}$H$_{25}$NO$_5$SNa]$^+$498.1351, found 498.2029.

D$_1$, 17: A mixture **16** (100 mg, 0.21 mmol), cyanoacetic acid (107 mg, 1.26 mmol), NH$_4$OAc (12 mg, 0.15 mmol) and glacial CH$_3$COOH (5 mL) was heated under reflux for 12 h during which time the aldehyde is completely consumed as indicated by TLC. After 12 h the reaction mixture was washed with water, CH$_3$OH and Et$_2$O thoroughly to afford D$_1$ as dark solid. The reaction mixture was soluble in PhMe, EtOAc, CH$_2$Cl$_2$, CHCl$_3$ and DMSO. Compound was purified by washing with Et$_2$O. Yield: 102 mg, 60%. Mp 198-206 °C; FT-IR (dry film, cm^{-1}): 3326-3330 (br), 3005-2857 (br), 2207 (s), 1695 (s), 1577 (s);^{1}H NMR (200 MHz, CDCl$_3$) δ: 3.71 (s, 3H), 3.75 (s, 6 H),3.92 (s, 1 H) 4.05 (s, 2 H), 6.78-6.83 (m, 6 H), 7.02-7.06 (m, 4 H), 7.55 (d, *J* = 12 Hz, 2H), 8.38 (s, 1H);^{13}C NMR (125 MHz, CDCl$_3$) δ: 50.4, 55.5, 70.9, 105.4, 115, 115.7, 116.8, 118.8, 122.5, 127.3, 127.9, 128.1, 131.6, 139.2, 139.8, 156.6, 157; MALDI-TOF *m/z* calcd for[M] $^+$[C$_{30}$H$_{26}$N$_2$O$_6$S]$^+$542.1512, found 542.1580.

5-(7-(Bis(4-methoxyphenyl)amino)benzo[c][1,2,5]thiadiazol-4-yl)-3,4-dimethoxythiophene-2-carbaldehyde, 18: 3,4-Dimethoxy-2-carboxaldehyde (60 mg, 0.35 mmol), **5** (0.18 g, 0.42 mmol), K$_2$CO$_3$ (120 g, 0.87 mmol), Pd(OAc)$_2$ (0.5 mol%), PCy$_3$ (0.5 mol%), and PivOH (0.15 mol%) were taken in a Schlenk tube under nitrogen atmosphere. Anhydrous DMA (5 mL) was added to that and kept the reaction at 120 °C temperature under the same atmosphere for 24 h. After 24 h TLC was checked in 10% EtOAc in pet. ether. The reaction mixture was washed with 100 mL of water and extracted with 150 mL of CH$_2$Cl$_2$. Solvents were removed under reduced pressure and purified by column chromatography by using EtOAc and pet. ether as an eluent to afford compound 18 as a brown solid. Yield: 98mg, 58 %. Mp 226-231 °C: FT-IR (dry film, cm^{-1}); 2923 (w), 2852 (w), 1642 (s), 1535 (w), 1504 (s), 1464 (w);^{1}H NMR (200 MHz, CDCl$_3$) δ: 3.82 (s, 6 H), 3.86 (s, 3 H), 4.19 (s, 3 H), 6.85 (d, *J* = 8 Hz, 4 H), 6.95 (d, *J* = 12 Hz, 1 H), 7.04 (d, *J* = 8 Hz, 4 H), 8.17 (d, *J* = 10 Hz, 1 H), 10.08 (s, 1 H);^{13}C NMR (125 MHz, CDCl$_3$) δ: 55.5, 72.1, 105.4, 114.9, 115.7, 116.8,

118.8, 127.3, 127.9, 128.1, 131.6, 139.2, 139.8, 155, 156.6, 157, 180.7; MALDI-TOF m/z calcd for $[M+H]^+[C_{27}H_{24}N_3O_5S_2]^+$534.1152, found 534.2228

D$_2$, **19**: A mixture of **18** (78 mg, 0.15 mmol), cyanoacetic acid (75 mg, 0.88mmol), NH_4OAc (8mg, 0.11 mmol) and CH_3COOH (5 mL) was heated under reflux for 12 h during which time the aldehyde is completely consumed as indicated by TLC. After 12 h the reaction mixture was washed with water, CH_3OH and Et_2O thoroughly to afford D$_2$ as a deep brown solid. The reaction mixture was insoluble in PhMe, EtOAc, CH_2Cl_2, $CHCl_3$ and soluble in DMSO. Compound was purified by washing with water, MeOH and Et_2O thoroughly. Yield 63%. Mp 265-278 °C; FT-IR (dry film, cm^{-1}): 3400-3416 (br), 2924-2855 (br), 2215 (s), 1712 (s), 1594 (s), 1535 (m); ^{1}H NMR (200 MHz, DMSO-d_6) δ: 3.76 (s, 6 H), 3.83 (s, 3 H), 3.99 (s, 3 H), 6.90-7.02 (m, 10 H), 7.68 (d, J = 6 Hz, 1 H), 8.24 (d, J = 4 Hz, 1 H). ^{13}C NMR (200 MHz, CDCl$_3$) δ 55.7, 60.5, 61.9, 92.9, 115.2, 117.3, 119.2, 119.7, 126.7, 127.0, 130, 140.9, 147.2, 147.6, 150.6, 156.5, 160 ;MALDI-TOF m/z calcd for $[M]^+[C_{30}H_{24}N_4O_6S_2]^+$600.1137, found 600.0725.

2.5 References

(1) Mishra, A.; Fischer, M. K. R.; Bäuerle, P. Metal-Free Organic Dyes for Dye-Sensitized Solar Cells: From Structure: Property Relationships to Design Rules. *Angew. Chem. Int. Ed.* **2009**, *48*, 2474–2499.

(2) O'Regan, B.; Grätzel, M. A Low-Cost, High-Efficiency Solar Cell Based on Dye-Sensitized Colloidal TiO$_2$ Films. *Nature* **1991**, *353*, 737–740.

(3) Choi, H.; Kim, J.-J.; Song, K.; Ko, J.; Nazeeruddin, M. K.; Grätzel, M. Molecular Engineering of Panchromatic Unsymmetrical Squaraines for Dye-Sensitized Solar Cell Applications. *J. Mater. Chem.* **2010**, *20*, 3280–3286.

(4)   Nazeeruddin, M. K.; Péchy, P.; Renouard, T.; Zakeeruddin, S. M.; Humphry-Baker, R.;
        Comte, P.; Liska, P.; Cevey, L.; Costa, E.; Shklover, V.; Spiccia, L.; Deacon, G. B.;
        Bignozzi, C. A.; Grätzel, M. Engineering of Efficient Panchromatic Sensitizers for
        Nanocrystalline TiO$_2$-Based Solar Cells. *J. Am. Chem. Soc.* **2001**, *123*, 1613–1624.

(5)   Bisht, R.; Kavungathodi, M. F. M.; Singh, A. K.; Nithyanandhan, J. Panchromatic
        Sensitizer for Dye-Sensitized Solar Cells: Unsymmetrical Squaraine Dyes Incorporating
        Benzodithiophene π-Spacer with Alkyl Chains to Extend Conjugation, Control the Dye
        Assembly on TiO$_2$, and Retard Charge Recombination. *J. Org. Chem.* **2017**, *82*, 1920–
        1930.

(6)   Shen, P.; Liu, Y.; Huang, X.; Zhao, B.; Xiang, N.; Fei, J.; Liu, L.; Wang, X.; Huang, H.;
        Tan, S. Efficient Triphenylamine Dyes for Solar Cells: Effects of Alkyl-Substituents
        and π-Conjugated Thiophene Unit. *Dyes Pigm.* **2009**, *83*, 187–197.

(7)   Nguyen, W. H.; Bailie, C. D.; Burschka, J.; Moehl, T.; Grätzel, M.; McGehee, M. D.;
        Sellinger, A. Molecular Engineering of Organic Dyes for Improved Recombination
        Lifetime in Solid-State Dye-Sensitized Solar Cells. *Chem. Mater.* **2013**, *25*, 1519–1525.

(8)   Pandey, S. S.; Inoue, T.; Fujikawa, N.; Yamaguchi, Y.; Hayase, S. Substituent Effect in
        Direct Ring Functionalized Squaraine Dyes on near Infra-Red Sensitization of
        Nanocrystalline TiO$_2$ for Molecular Photovoltaics. *J. Photochem. Photobiol. Chem.*
        2010, *214*, 269–275.

(9)   Chen, G.; Sasabe, H.; Sasaki, Y.; Katagiri, H.; Wang, X.-F.; Sano, T.; Hong, Z.; Yang,
        Y.; Kido, J. A Series of Squaraine Dyes: Effects of Side Chain and the Number of
        Hydroxyl Groups on Material Properties and Photovoltaic Performance. *Chem. Mater.*
        2014, *26*, 1356–1364.

(10)   Koumura, N.; Wang, Z.-S.; Mori, S.; Miyashita, M.; Suzuki, E.; Hara, K. Alkyl-
        Functionalized Organic Dyes for Efficient Molecular Photovoltaics. *J. Am. Chem. Soc.*
        2006, *128*, 14256–14257.

(11) Suzuka, M.; Hayashi, N.; Sekiguchi, T.; Sumioka, K.; Takata, M.; Hayo, N.; Ikeda, H.; Oyaizu, K.; Nishide, H. A Quasi-Solid State DSSC with 10.1% Efficiency through Molecular Design of the Charge-Separation and -Transport. *Sci. Rep.* **2016**, *6*, 28022.

(12) Listorti, A.; O'Regan, B.; Durrant, J. R. Electron Transfer Dynamics in Dye-Sensitized Solar Cells. *Chem. Mater.* **2011**, *23*, 3381–3399.

(13) Mathew, S.; Yella, A.; Gao, P.; Humphry-Baker, R.; Curchod, B. F. E.; Ashari-Astani, N.; Tavernelli, I.; Rothlisberger, U.; Nazeeruddin, M. K.; Grätzel, M. Dye-Sensitized Solar Cells with 13% Efficiency Achieved through the Molecular Engineering of Porphyrin Sensitizers. *Nat. Chem.* **2014**, *6*, 242–247.

(14) Yao, Z.; Zhang, M.; Wu, H.; Yang, L.; Li, R.; Wang, P. Donor/Acceptor Indenoperylene Dye for Highly Efficient Organic Dye-Sensitized Solar Cells. *J. Am. Chem. Soc.* **2015**, *137*, 3799–3802.

(15) Hwang, S.; Lee, J. H.; Park, C.; Lee, H.; Kim, C.; Park, C.; Lee, M.-H.; Lee, W.; Park, J.; Kim, K.; Park, N.-G.; Kim, C. A Highly Efficient Organic Sensitizer for Dye-Sensitized Solar Cells. *Chem. Commun.* **2007**, *46*, 4887–4889.

(16) Gong, J.; Liang, J.; Sumathy, K. Review on Dye-Sensitized Solar Cells (DSSCs): Fundamental Concepts and Novel Materials. *Renew. Sustain. Energy Rev.* **2012**, *16*, 5848–5860.

(17) Li, X.; Zheng, Z.; Jiang, W.; Wu, W.; Wang, Z.; Tian, H. New D–A–π–A Organic Sensitizers for Efficient Dye-Sensitized Solar Cells. *Chem. Commun.* **2015**, *51*, 3590–3592.

(18) Saccone, D.; Galliano, S.; Barbero, N.; Quagliotto, P.; Viscardi, G.; Barolo, C. Polymethine Dyes in Hybrid Photovoltaics: Structure–Properties Relationships. *Eur. J. Org. Chem.* **2016**, *2016*, 2244–2259.

(19) Yella, A.; Lee, H.-W.; Tsao, H. N.; Yi, C.; Chandiran, A. K.; Nazeeruddin, M. K.; Diau, E. W.-G.; Yeh, C.-Y.; Zakeeruddin, S. M.; Grätzel, M. Porphyrin-Sensitized Solar Cells

with Cobalt (II/III)-Based Redox Electrolyte Exceed 12 Percent Efficiency. *Science* **2011**, *334*, 629–634.

(20) Urbani, M.; Grätzel, M.; Nazeeruddin, M. K.; Torres, T. Meso-Substituted Porphyrins for Dye-Sensitized Solar Cells. *Chem. Rev.* **2014**, *114*, 12330–12396.

(21) Tang, Y.; Wang, Y.; Li, X.; Ågren, H.; Zhu, W.-H.; Xie, Y. Porphyrins Containing a Triphenylamine Donor and up to Eight Alkoxy Chains for Dye-Sensitized Solar Cells: A High Efficiency of 10.9%. *ACS Appl. Mater. Interfaces* **2015**, *7*, 27976–27985.

(22) Porphyrins as excellent dyes for dye-sensitized solar cells: recent developments and insights, Higashino, T.; Imahori, H. *Dalton Trans.***, 2015**, *44*, 448-463.

(23) Large π-Aromatic Molecules as Potential Sensitizers for Highly Efficient Dye-Sensitized Solar Cells, Imahori H.; Umeyama, T.; Ito, S. *Acc. Chem. Res.* **2009**, *42* , 1809–1818.

(24) Ince, M.; Yum, J.-H.; Kim, Y.; Mathew, S.; Grätzel, M.; Torres, T.; Nazeeruddin, M. K. Molecular Engineering of Phthalocyanine Sensitizers for Dye-Sensitized Solar Cells. *J. Phys. Chem. C* **2014**, *118*, 17166–17170.

(25) Alagumalai, A.; Kavungathodi, M. F. M.; Vellimalai, P.; Sil, M. C.; Nithyanandhan, J. Effect of Out-of-Plane Alkyl Group's Position in Dye-Sensitized Solar Cell Efficiency: A Structure–Property Relationship Utilizing Indoline-Based Unsymmetrical Squaraine Dyes. *ACS Appl. Mater. Interfaces* **2016**, *8*, 35353–35367.

(26) Kasha, M.; Rawls, H. R.; Ashraf El-Bayoumi, M. The Exciton Model in Molecular Spectroscopy. *Pure Appl. Chem.* **1965**, *11*, 371–392.

(27) Sayama, K.; Hara, K.; Mori, N.; Satsuki, M.; Suga, S.; Tsukagoshi, S.; Abe, Y.; Sugihara, H.; Arakawa, H. Photosensitization of a Porous TiO$_2$ Electrode with Merocyanine Dyes Containing a Carboxyl Group and a Long Alkyl Chain. *Chem. Commun.* **2000**, *13*, 1173–1174.

(28) Kryman, M. W.; Nasca, J. N.; Watson, D. F.; Detty, M. R. Selenorhodamine Dye-Sensitized Solar Cells: Influence of Structure and Surface-Anchoring Mode on Aggregation, Persistence, and Photoelectrochemical Performance. *Langmuir* **2016**, *32*, 1521–1532.

(29) Khazraji, A. C.; Hotchandani, S.; Das, S.; Kamat, P. V. Controlling Dye (Merocyanine-540) Aggregation on Nanostructured TiO_2 Films. An Organized Assembly Approach for Enhancing the Efficiency of Photosensitization. *J. Phys. Chem. B* **1999**, *103*, 4693–4700.

(30) Hassan, H. C.; Abidin, Z. H. Z.; Chowdhury, F. I.; Arof, A. K. A High Efficiency Chlorophyll Sensitized Solar Cell with Quasi Solid PVA Based Electrolyte. *Int. J. Photoenergy* **2016**, *2016*, 1-9.

(31) Baheti, A.; Justin Thomas, K. R.; Li, C.-T.; Lee, C.-P.; Ho, K.-C. Fluorene-Based Sensitizers with a Phenothiazine Donor: Effect of Mode of Donor Tethering on the Performance of Dye-Sensitized Solar Cells. *ACS Appl. Mater. Interfaces* **2015**, *7*, 2249–2262.

(32) Ziółek, M.; Karolczak, J.; Zalas, M.; Hao, Y.; Tian, H.; Douhal, A. Aggregation and Electrolyte Composition Effects on the Efficiency of Dye-Sensitized Solar Cells. A Case of a Near-Infrared Absorbing Dye for Tandem Cells. *J. Phys. Chem. C* **2014**, *118*, 194–205.

(33) Wang, Z.; Liang, M.; Tan, Y.; Ouyang, L.; Sun, Z.; Xue, S. Organic Dyes Containing dithieno[2,3-d:2′,3′-d′]thieno[3,2-b:3′,2′-B′]dipyrrole Core for Efficient Dye-Sensitized Solar Cells. *J. Mater. Chem. A* **2015**, *3*, 4865–4874.

(34) Paek, S.; Choi, H.; Kim, C.; Cho, N.; So, S.; Song, K.; Nazeeruddin, M. K.; Ko, J. Efficient and Stable Panchromatic Squaraine Dyes for Dye-Sensitized Solar Cells. *Chem. Commun.* **2011**, *47*, 2874–2876.

(35) Chai, Q.; Li, W.; Wu, Y.; Pei, K.; Liu, J.; Geng, Z.; Tian, H.; Zhu, W. Effect of a Long Alkyl Group on Cyclopentadithiophene as a Conjugated Bridge for D–A−π–A Organic

Sensitizers: IPCE, Electron Diffusion Length, and Charge Recombination. *ACS Appl. Mater. Interfaces* **2014**, *6*, 14621–14630.

(36) Galoppini, E.; Guo, W. Long-Distance Electron Transfer Across Molecule-Nanocrystalline Semiconductor Interfaces. *J. Am. Chem. Soc.* **2001,** *123,* 4342-4343.

(37) Galoppini, E.; Guo, W.; Zhang, W.; Hoertz, P.G.; Qu, P.; Meyer, G. J. Long-Range Electron Transfer across Molecule-Nanocrystalline Semiconductor Interfaces Using Tripodal Sensitizers. *J. Am. Chem. Soc.* **2002**, *124*, 7801-7811.

(38) Piotrowiak, P.; Galoppini, E.; Wei, Q.; Meyer, G. J.; Wiewiór, P. Subpicosecond Photoinduced Charge Injection from "Molecular Tripods" into Mesoporous TiO$_2$ Over the Distance of 24 Angstroms. *J. Am. Chem. Soc.* **2003**, *125*, 5278-5279.

(39) Clark, C. C.; Meyer, G. J.; Wei, Q.; Galoppini, E. Tuning Open Circuit Photovoltages with Tripodal Sensitizers. *J. Phys. Chem. B* **2006**, *110*, 11044.

(40) Freitag, M.; Galoppini, E. Molecular Host–guest Complexes: Shielding of Guests on Semiconductor Surfaces. *Energy Environ. Sci.* **2011**, *4*, 2482–2494.

(41) Hamann, T. W.; Farha, O. K.; Hupp, J. T. Outer-Sphere Redox Couples as Shuttles in Dye-Sensitized Solar Cells. Performance Enhancement Based on Photoelectrode Modification via Atomic Layer Deposition. *J. Phys. Chem. C* **2008**, *112*, 19756–19764.

(42) Manfredi, N.; Cecconi, B.; Abbotto, A. Multi-Branched Multi-Anchoring Metal-Free Dyes for Dye-Sensitized Solar Cells. *Eur. J. Org. Chem.* **2014**, *2014*, 7069–7086.

(43) Hagberg, D. P.; Marinado, T.; Karlsson, K. M.; Nonomura, K.; Qin, P.; Boschloo, G.; Brinck, T.; Hagfeldt, A.; Sun, L. Tuning the HOMO and LUMO Energy Levels of Organic Chromophores for Dye Sensitized Solar Cells. *J. Org. Chem.* **2007**, *72*, 9550–9556.

(44) Liu, W.-H.; Wu, I.-C.; Lai, C.-H.; Lai, C.-H.; Chou, P.-T.; Li, Y.-T.; Chen, C.-L.; Hsu, Y.-Y.; Chi, Y. Simple Organic Molecules Bearing a 3,4-Ethylenedioxythiophene Linker for Efficient Dye-Sensitized Solar Cells. *Chem. Commun.* **2008**, *41*, 5152–5154.

(45) Seo, K. D.; You, B. S.; Choi, I. T.; Ju, M. J.; You, M.; Kang, H. S.; Kim, H. K. Dual-Channel Anchorable Organic Dyes with Well-Defined Structures for Highly Efficient Dye-Sensitized Solar Cells. *J. Mater. Chem. A* **2013**, *1*, 9947–9953.

(46) Seo, K. D.; You, B. S.; Choi, I. T.; Ju, M. J.; You, M.; Kang, H. S.; Kim, H. K. Dual-Channel Anchorable Organic Dye with Triphenylamine-Based Core Bridge Unit for Dye-Sensitized Solar Cells. *Dyes Pigm.* **2013**, *99*, 599–606.

(47) Leandri, V.; Ruffo, R.; Trifiletti, V.; Abbotto, A. Asymmetric Tribranched Dyes: An Intramolecular Cosensitization Approach for Dye-Sensitized Solar Cells. *Eur. J. Org. Chem.* **2013**, *2013*, 6793–6801.

(48) Teng, C.; Yang, X.; Yang, C.; Tian, H.; Li, S.; Wang, X.; Hagfeldt, A.; Sun, L. Influence of Triple Bonds as π-Spacer Units in Metal-Free Organic Dyes for Dye-Sensitized Solar Cells. *J. Phys. Chem. C* **2010**, *114*, 11305–11313.

(49) Baheti, A.; Thomas, K. R. J.; Lee, C.-P.; Ho, K.-C. Synthesis and Characterization of Dianchoring Organic Dyes Containing 2,7-Diaminofluorene Donors as Efficient Sensitizers for Dye-Sensitized Solar Cells. *Org. Electron.* **2013**, *14*, 3267–3276.

(50) Zhang, H.; Fan, J.; Iqbal, Z.; Kuang, D.-B.; Wang, L.; Meier, H.; Cao, D. Novel dithieno[3,2-b:2′,3′-D]pyrrole-Based Organic Dyes with High Molar Extinction Coefficient for Dye-Sensitized Solar Cells. *Org. Electron.* **2013**, *14*, 2071–2081.

(51) Ren, X.; Jiang, S.; Cha, M.; Zhou, G.; Wang, Z.-S. Thiophene-Bridged Double D-π-A Dye for Efficient Dye-Sensitized Solar Cell. *Chem. Mater.* **2012**, *24*, 3493–3499.

(52) Cao, D.; Peng, J.; Hong, Y.; Fang, X.; Wang, L.; Meier, H. Enhanced Performance of the Dye-Sensitized Solar Cells with Phenothiazine-Based Dyes Containing Double D−A Branches. *Org. Lett.* **2011**, *13*, 1610–1613.

(53) Zhang, T.; Qian, X.; Zhang, P.-F.; Zhu, Y.-Z.; Zheng, J.-Y. A Meso–meso Directly Linked Porphyrin Dimer-Based Double D–π–A Sensitizer for Efficient Dye-Sensitized Solar Cells. *Chem. Commun.* **2015**, *51*, 3782–3785.

(54) Reeves, B. d.; Thompson, B. c.; Abboud, K. a.; Smart, B. e.; Reynolds, J. r. Dual Cathodically and Anodically Coloring Electrochromic Polymer Based on a Spiro Bipropylenedioxythiophene [(Poly(spiroBiProDOT)]. *Adv. Mater.* **2002**, *14*, 717–719.

(55) Pozzi, G.; Orlandi, S.; Cavazzini, M.; Minudri, D.; Macor, L.; Otero, L.; Fungo, F. Synthesis and Photovoltaic Applications of a 4,4′-Spirobi[cyclopenta[2,1-b;3,4-B′]dithiophene]-Bridged Donor/Acceptor Dye. *Org. Lett.* **2013**, *15*, 4642–4645.

(56) Ganesan, P.; Fu, K.; Gao, P.; Raabe, I.; Schenk, K.; Scopelliti, R.; Luo, J.; Wong, L. H.; Grätzel, M.; Nazeeruddin, M. K. A Simple Spiro-Type Hole Transporting Material for Efficient Perovskite Solar Cells. *Energy Environ. Sci.* **2015**, *8*, 1986–1991.

(57) Sadekar, A. G.; Mohite, D.; Mulik, S.; Chandrasekaran, N.; Sotiriou-Leventis, C.; Leventis, N. Robust PEDOT Films by Covalent Bonding to Substrates Using in Tandem Sol–gel, Surface Initiated Free-Radical and Redox Polymerization. *J. Mater. Chem.* **2011**, *22*, 100–108.

(58) Lafrance, M.; Fagnou, K. Palladium-Catalyzed Benzene Arylation: Incorporation of Catalytic Pivalic Acid as a Proton Shuttle and a Key Element in Catalyst Design. *J. Am. Chem. Soc.* **2006**, *128*, 16496–16497.

(59) Liégault, B.; Lapointe, D.; Caron, L.; Vlassova, A.; Fagnou, K. Establishment of Broadly Applicable Reaction Conditions for the Palladium-Catalyzed Direct Arylation of Heteroatom-Containing Aromatic Compounds. *J. Org. Chem.* **2009**, *74*, 1826–1834.

(60) Lu, W.; Kuwabara, J.; Kanbara, T. Polycondensation of Dibromofluorene Analogues with Tetrafluorobenzene via Direct Arylation. *Macromolecules* **2011**, *44*, 1252–1255.

(61) Ronca, E.; Marotta, G.; Pastore, M.; De Angelis, F. Effect of Sensitizer Structure and TiO_2 Protonation on Charge Generation in Dye-Sensitized Solar Cells. *J. Phys. Chem. C* **2014**, *118*, 16927–16940.

(62) Cariello, M.; Ahn, S.; Park, K.-W.; Chang, S.-K.; Hong, J.; Cooke, G. An Investigation of the Role Increasing π-Conjugation Has on the Efficiency of Dye-Sensitized Solar Cells Fabricated from Ferrocene-Based Dyes. *RSC Adv.* **2016**, *6*, 9132–9138.

(63) Pecnikaj, I.; Minudri, D.; Otero, L.; Fungo, F.; Cavazzini, M.; Orlandi, S.; Pozzi, G. Fluorous Molecules for Dye-Sensitized Solar Cells: Synthesis and Properties of Di-Branched, Di-Anchoring Organic Sensitizers Containing Fluorene Subunits. *New J. Chem.* **2017**, *41*, 7729–7738.

(64) Imahori, H.; Kang, S.; Hayashi, H.; Haruta, M.; Kurata, H.; Isoda, S.; Canton, S. E.; Infahsaeng, Y.; Kathiravan, A.; Pascher, T.; Chábera, P.; Yartsev, A. P.; Sundström, V. Photoinduced Charge Carrier Dynamics of Zn−Porphyrin−TiO$_2$ Electrodes: The Key Role of Charge Recombination for Solar Cell Performance. *J. Phys. Chem. A* **2011**, *115*, 3679–3690.

(65) Ye, S.; Kathiravan, A.; Hayashi, H.; Tong, Y.; Infahsaeng, Y.; Chabera, P.; Pascher, T.; Yartsev, A. P.; Isoda, S.; Imahori, H.; Sundström, V. Role of Adsorption Structures of Zn-Porphyrin on TiO$_2$ in Dye-Sensitized Solar Cells Studied by Sum Frequency Generation Vibrational Spectroscopy and Ultrafast Spectroscopy. *J. Phys. Chem. C* **2013**, *117*, 6066–6080.

(66) Ozawa, H.; Awa, M.; Ono, T.; Arakawa, H. Effects of Dye-Adsorption Solvent on the Performances of the Dye-Sensitized Solar Cells Based on Black Dye. *Chem. – Asian J.* **2012**, *7*, 156–162.

(67) Wang, J.; Liu, K.; Ma, L.; Zhan, X. Triarylamine: Versatile Platform for Organic, Dye-Sensitized, and Perovskite Solar Cells. *Chem. Rev.* **2016**, *116*, 14675–14725.

(68) Bisquert, J.; Fabregat-Santiago, F.; Mora-Seró, I.; Garcia-Belmonte, G.; Giménez, S. Electron Lifetime in Dye-Sensitized Solar Cells: Theory and Interpretation of Measurements. *J. Phys. Chem. C* **2009**, *113*, 17278–17290.

(69) Ji, Z.; Natu, G.; Huang, Z.; Wu, Y. Linker Effect in Organic Donor–acceptor Dyes for P-Type NiO Dye Sensitized Solar Cells. *Energy Environ. Sci.* **2011**, *4*, 2818–2821.

(70) Wu, Z.; Li, X.; Ågren, H.; Hua, J.; Tian, H. Pyrimidine-2-Carboxylic Acid as an Electron-Accepting and Anchoring Group for Dye-Sensitized Solar Cells. *ACS Appl. Mater. Interfaces* **2015**, *7*, 26355–26359.

(71) Chen, P.; Yum, J. H.; Angelis, F. D.; Mosconi, E.; Fantacci, S.; Moon, S.-J.; Baker, R. H.; Ko, J.; Nazeeruddin, M. K.; Grätzel, M. High Open-Circuit Voltage Solid-State Dye-Sensitized Solar Cells with Organic Dye. *Nano Lett.* **2009**, *9*, 2487–2492.

(72) Liang, Y.; Cheng, F.; Liang, J.; Chen, J. Triphenylamine-Based Ionic Dyes with Simple Structures: Broad Photoresponse and Limitations on Open-Circuit Voltage in Dye-Sensitized Solar Cells. *J. Phys. Chem. C* **2010**, *114*, 15842–15848.

Homo- and Hetero- Dimeric Dyes for Dye-sensitized Solar Cells: Panchromatic Light Absorption and Modulated Open Circuit Potential

3.1 Introduction

Dye sensitized solar cells (DSSCs) is one of the emerging third generation PV technologies consist of photoanode, semiconducting metal oxide, dye, electrolyte and counter electrode. Owing to the tunability of various components, low cost, high performance made this technology attracted huge interest in further development. Out of various interfaces in a DSSC device, TiO$_2$-dye/electrolyte interface plays an important role in modulating the charge separation and recombination processes.[1] Different type of dyes were designed and synthesised over the years with different absorption properties having high current conversion performance mainly based on indolines[2,3], triarylamines[4,5], squaraines[3,6–8] dyes. So far, however the best conversion efficiency of about 13% was achieved for zinc-porphyrin dye[9] and 12.5% for indenoperylene dye with cobalt (II/III) redox couple.[2] These types of metal based organic sensitizer contains expensive ruthenium metal and require more attention to synthesize and purification.[10] Non-metallic organic sensitizer have higher promising role than metallic sensitizer due to their higher molar absorptivities and absorption properties can be modulated by changing its structural units.[11] Even though, the efficiency of organic dye-sensitized solar cell cannot comparable with metallic organic dyes because of their narrow absorption spectra, shorter excited-state lifetimes and the problem of self-aggregation or self-quenching of the photoexcited state on the semiconductor surface.[11–14] To improve the intramolecular charge transfer and broad absorption spectrum from visible to NIR region dye configuration of D-π-A[12] and D-A-π-A[13] have been designed to harvest the visible light photons. Porphyrin[14–18], phthalocyanines[19] and polymethine[20] dyes have been utilized to harvest the visible and NIR regions of the solar spectrum. To get an efficient device performance of organic dye-sensitized solar cells, the sensitizer should harvest all the photons, and the dye-TiO$_2$/electrolyte interface affiliated with minimized charge injection and

dye regeneration overpotentials. Photovoltaic performance is also strongly depend on charge recombination, which can be tailored by the proper dye orientation on TiO_2 surface.[18,21–23] Further dyes with multiple anchoring groups[24,25], dimeric dyes[26–32] have been reported to enhance the electronic coupling between the dye and TiO_2 surface. It was recently reported a general strategy to install same or two different dye moieties in a single dye molecule. Several dye design with panchromatic light absorption, co-sensitization, FRET based strategy have been utilized for efficient light absorption.[33–36] For an efficient panchromatic[7,8,37–40] light harvesting process, suitable mixture of dyes with complementary absorption properties were utilized. However the method of co-sensitization usually faced some major difficulty associated recombination with kinetics of different dyes, which may lead to decrease the efficiency of the solar cell. Co-sensitization of two different dyes in a same solvent may fascinate unwanted reaction between dyes, as well as increase the chances of unfavourable charge recombination.[41–43] Recently, broadening absorption spectra of organic dyes by molecular plasmon-like excitation have been proposed.[44] There were specific anchoring groups that promote the interfacial charge transfer from dye to TiO_2 that avoids the charge injection overpotential.[45–49] Further V_{oc} can be increased by the uplifted shift of TiO_2 conduction band, which is generated by sensitizer by developing its intrinsic electrostatic potential or dipole moment.[50–55] Aggregation of dyes on the TiO_2 surface is another important factor that diminish the device performance.[56] However controlled aggregation of dyes leads to often enhance the DSSC device performance.[3]

In this chapter, two new spiro-linker based dyes constituted with homo dimeric $\mathbf{D_{sq}}$-$\mathbf{D_{sq}}$ and hetero dimeric $\mathbf{D_1}$-$\mathbf{D_{sq}}$, in which two same monomeric dye ($\mathbf{D_{sq}}$) and different types of dye ($\mathbf{D_1}$ and $\mathbf{D_{sq}}$) molecules are connected by spiro linker were synthesized and characterized. Herein in an effort to broaden the absorption spectrum of dye molecules by controlled interaction between them is targeted, hence dimeric squaraine dye ($\mathbf{D_{sq}}$-$\mathbf{D_{sq}}$) and

imparting complementary absorbing dye D_1 and D_{sq} through spiro-spacer[44] for panchromatic light absorption were synthesized. Generally D-π-A (D_1), D-A-D (D_{sq}), based dyes have been utilized to harvest the visible and NIR regions of the solar spectrum, respectively. Excitation energy transfer from of donor dyes (D_1-D_1 and D_1) with acceptor dyes (D_{sq}-D_{sq} and D_{sq}) in solution. Donor dyes (D_1-D_1 and D_1) are D-π-A containing organic sensitizer that has a strong absorption in the visible region of the solar absorption spectrum. On the other hand acceptor dyes were (D_{sq}-D_{sq} and D_{sq}) showing prominent absorption at far red region. Device study of D_1-D_1 and D_1 and their application as a sensitizer were reported.[57] From UV-Vis and fluorescence spectroscopy, the spectral overlap between the absorption of acceptor (D_{sq}-D_{sq} and D_{sq}) dyes and emission of donor (D_1-D_1 and D_1) dyes established the resonance energy transfer process in solution state. IPCE profile showed that D_1-D_{sq} dye showed panchromatic power conversion efficiency with the device performance of 3.9%, $V_{oc} = 0.652$ V, $J_{sc} = 8.89$ mA/cm^2 and $ff = 69\%$.

3.2 Results and discussion

3.2.1. Dye design and synthesis. In order to study the combined effects of panchromatic absorption and controlled dye-dye interaction to broaden the absorption spectrum, two different squaraine based homo- and hetero dimeric dyes were synthesised and characterized. Owing to the sharp and intense absorptions properties of organic dyes, mixture of complementary dyes have been used for panchromatic light absorption, besides few single panchromatic light absorbing dyes reported in the literature for DSSC devices.[58] In this chapter, a D-π-A and a D-A-D based squaraine dye (D_{sq}) were covalently connected through a spiro spacer to have homo- (D_{sq}-D_{sq}) and hetero dimeric (D_1-D_{sq}) squaraine dyes. It is well known that squaraine dyes aggregate in solution and in solid states. In one hand, aggregation of dye helps to broaden the absorption spectrum, however the charge injection efficiency

from aggregated structure has been observed to be very poor, that suppress the device performance. On the other hand, controlled aggregation of dyes lead to charge injection from aggregated state that helps to design a single dye that can form an aggregated structure to broaden the spectrum with panchromatic light to current conversion efficiency. The presence of spiro moiety helps to passivate the TiO_2 surface effectively to reduce the recombination of electrons in TiO_2 to the electrolyte. Presences of two anchoring groups help enhancing electronic communication between LUMO of the dye, and conduction band of TiO_2. The targeted structures of symmetric and asymmetric squaraine dyes are presented in **Figure 1**.
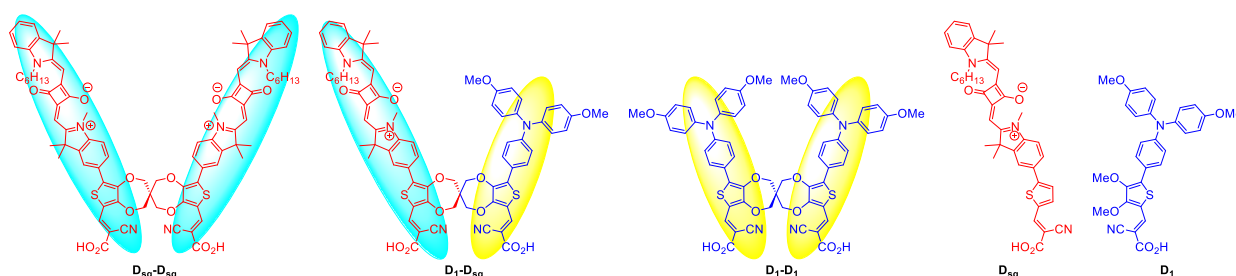
Figure 1. Structures of homo-dimeric (**D$_{sq}$-D$_{sq}$**, **D$_1$-D$_1$**), hetero-dimeric (**D$_1$-D$_{sq}$**) and model dyes (**D$_1$** and **D$_{sq}$**).

SpiroBiProDOT (2H,2'H,4H,4'H-3,3'-spirobi[thieno[3,4-b][1,4]dioxepine]) was judiciously selected as a π-spacer for synthesizing the targeted dimeric dyes containing two anchoring groups. Solid state studies inferred that SpiroBiProDOT derivatives showed different conformations depending upon the substitution present in the moiety which helps to provide different orientation between the dyes that were functionalized with this spacer.[59] SpiroBiProDOT was synthesized from *trans*-etherification of 3,4-dimethoxythiophene.[60] Vilsmeier-Haack formylation of spiroBiProDOT afforded the symmetric mono-formylated dialdehyde, **6** in good yield.[57] Synthesis of semi squaric acid derivative **2** was carried out by following reported procedure.[61]
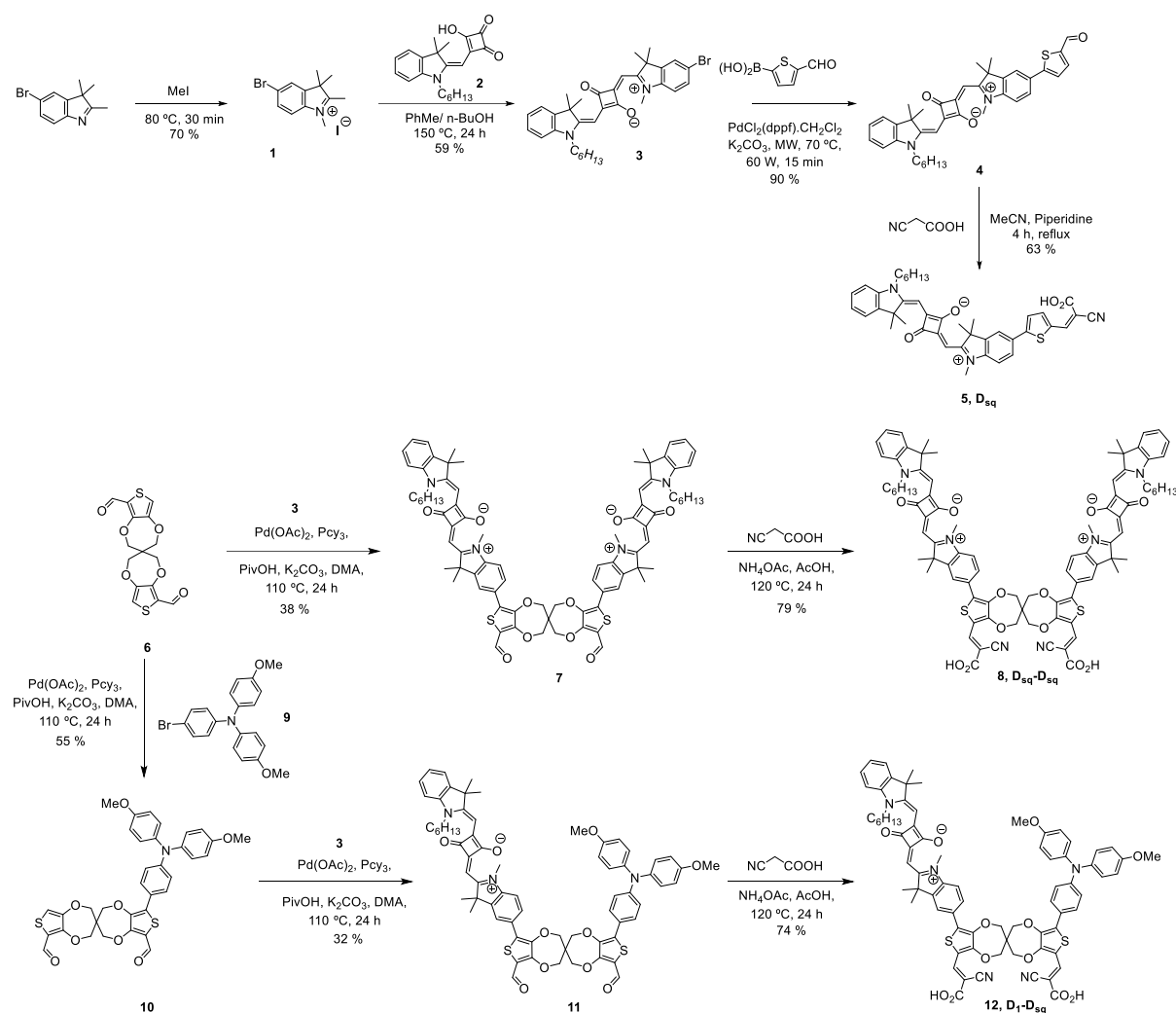
Scheme 1. Synthesis of model monomeric dye **D$_{sq}$**, homo-dimeric **D$_{sq}$-D$_{sq}$** and hetero-dimeric **D$_1$- D$_{sq}$** dyes.

The bromoindolium derivative, **1** was condensed with the semisquaric acid, **2** by azeotropic distillation of water employing Dean−Stark apparatus to afford bromo-functionalized squaraine precursor **3** in moderate yield as a blue colour solid (**Scheme 1**). Homodimeric **D$_{sq}$-D$_{sq}$** dye has been synthesized by Pd^{2+}catalyzed direct arylation reaction of bromosquaraine derivative, **3** with dialdehyde dioxepine derivative, **6** to afford the corresponding aldehyde derivative, **7** of 38% yield and further Knoevenagel condensation with cyanoaceticacid afforded the required dimeric dye of 79% yield. However, to synthesize

hetero dimeric dye, the required dialdehyde derivative **11** was achieved by sequential Pd-catalyzed direct arylation of dialdehyde, **6** with **9** and **3**, further Knoevenagel condensation of **11** with a cyanoacetic acid afforded the required hetero dimeric dye **D₁-D_{sq}** with moderate yield (74 %). For the synthesis of homodimeric dye, the precursor spiro-dialdehyde requires stoichiometric equivalents of bromo-functionalized squaraine precursor, **3**.

3.2.2 Photophysical properties. The molecular structures of the homo- and hetero dimeric and model monomeric dyes were shown in **Figure 1**. The absorption and emission spectra for the three dyes in solution were shown in **Figure 2**. Dye **D_{sq}-D_{sq}** showed a slightly broader absorption centred at 661 nm besides a broad absorption at visible region centred at 419-450 nm compared to monomeric **D_{sq}**. Also the charge transfer peak at 661 nm is blue shifted compared to the model monomeric dye **D_{sq}**. Dye **D₁-D_{sq}**, showed peaks centred at 464 nm and 660 nm corresponds to the respecting λ_{max} of **D₁** and **D_{sq}**, in **D₁-D_{sq}**. The absorption spectra of both **D_{sq}-D_{sq}**, **D₁-D_{sq}** are broader than the monomeric **D_{sq}** dye (**Figure 2a** and **2b**) and it is due to the dye-dye interactions. In the present case of **D_{sq}-D_{sq}**, **D₁-D_{sq}** dyes, two, same or different, dipole possessing dye molecules have been merely separate by pentaerythritol based spiro linker which may enforce the dye-dye interaction in solution. Both **D_{sq}-D_{sq}**, **D₁-D_{sq}** showed an intense charge transfer band at 660 nm and 661 nm, respectively for the squaraine part. Furthermore, the corresponding absorption coefficient of **D_{sq}-D_{sq}**, **D₁-D_{sq}** and **D_{sq}** were $6.32 \times 10^5 M^{-1} cm^{-1}$ (661 nm), $2.37 \times 10^5 M^{-1} cm^{-1}$ (660 nm) and $3.43 \times 10^5 M^{-1} cm^{-1}$, respectively. Excitation at 540 nm, a sharp peak was obtained at 667 nm (for **D_{sq}-D_{sq}**) and 668 nm (for **D₁-D_{sq}**). By investigating the absorption and emission profile of **D₁**, and **D_{sq}** (**Figure 2a**) a good spectral overlap between emission profile of **D₁** and absorption spectrum of squaraine dye is observed, such factor helps in transferring the excitation energy between the pair of dyes. Exciting of **D₁-D_{sq}** at 540 nm, where **D_{sq}-D_{sq}** absorb the light weakly and

observation of strong emission peak at 665 nm indicates the excitation energy transfer from

D_1 to D_{sq} unit of D_1-D_{sq} (**Figure 2d**).
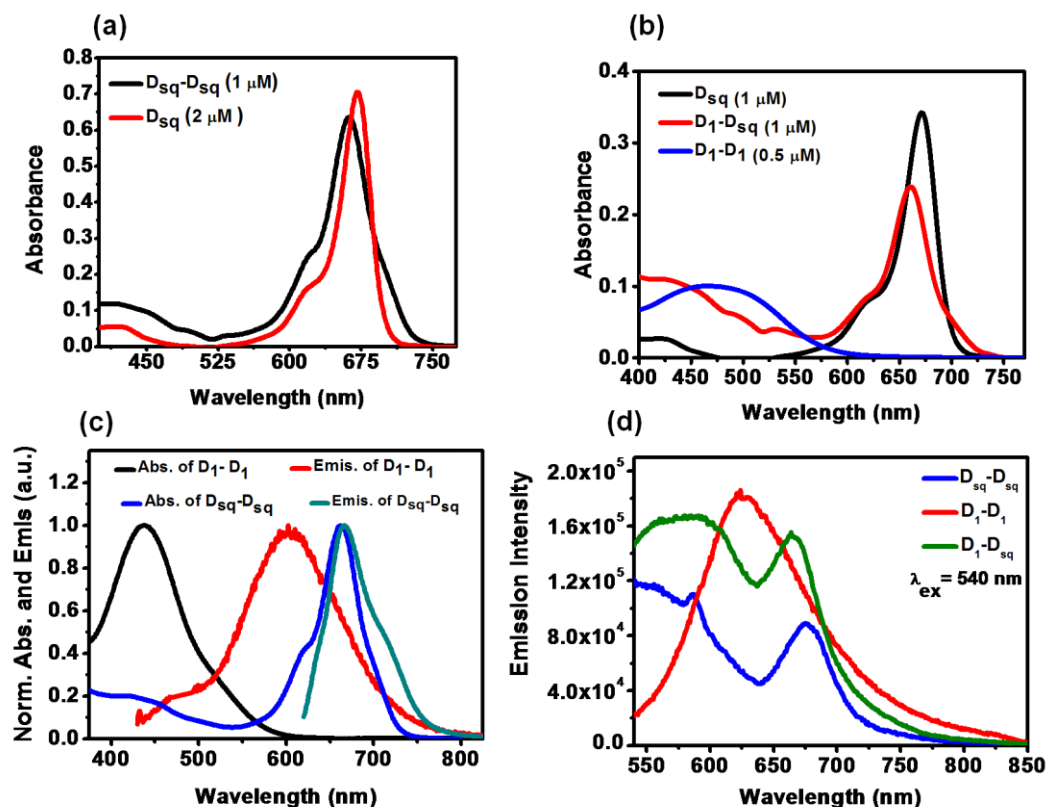
Figure 2. (a) Absorption spectra of D_{sq}-D_{sq} (1 μM) and D_{sq} (2 μM) in CHCl$_3$ (b) absorption

spectra of D_1-D_{sq} (1 μM), D_{sq} (1 μM) and D_1-D_1 (0.5 μM) in CHCl$_3$ (c) absorption and

emission spectra of D_1-D_1 (excitation wavelength 430 nm) and D_{sq}-D_{sq} (excitation wavelength

660 nm) and (d) emission spectra of optically matched solutions of D_{sq}-D_{sq}, D_1-D_{sq}, and D_1-

D_1 (excitation wavelength 540 nm).

Careful analysis indicates that the absorption peaks for D_{sq}-D_{sq} are 614 nm, and

661nm and broadening the peak (**Figure 3a**) in the far red region, whereas D_{sq} is having

transition at 604 nm and 671 nm. It has been seen that λ_{max} of D_{sq}-D_{sq} was 6 nm blue shifted

and broadened compared to D_{sq} due to the formation of dye aggregates.[62,63] It is very clear

from the Uv-Vis spectra of both D_{sq}-D_{sq} and D_{sq} is that dimer having wide and broad spectra compared to monomer D_{sq}. Binding upon TiO$_2$, two peaks at 616 nm and 658 nm were observed for D_{sq} which is a result of H-type aggregation. In case of D_{sq}-D_{sq} two monomeric D_{sq} are in a constrained by spiro moiety, leads to the reduction of H-aggregates, a definite interaction between the two D_{sq} monomeric moieties was the reason for the broad absorption spectrum from 613 nm to 663 nm (**Figure 3a**). In the case of D_1-D_{sq}, the peak was moderately narrow in compared to D_{sq} or D_{sq}-D_{sq} as reduced the interaction between D$_1$ and D$_{sq}$ (in D_1-D_{sq})
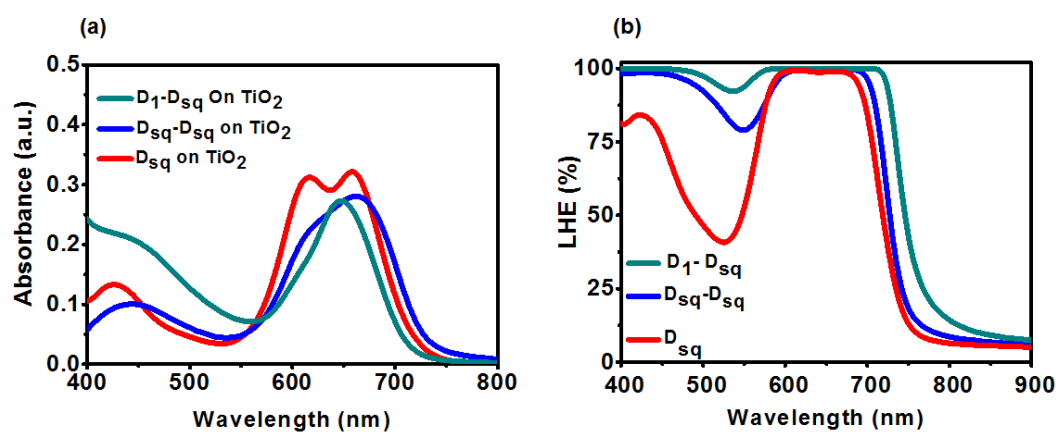
Figure 3. (a) UV-vis spectra of D_1-D_{sq}, D_{sq}-D_{sq} and D_{sq} on TiO$_2$ surface and (b) LHE of D_1-D_{sq}, D_{sq}-D_{sq} and D_{sq} (LHE=1−10^{-A}, A = absorbance).

The fraction of photons absorbed by the dye at certain wavelength is provided by light harvesting efficiency (LHE = 1-10^{-A}). LHE of D_{sq}-D_{sq}, D_1-D_{sq} and D_{sq} (**Figure 3b**) provide the details about the presence of dye aggregation which can be controlled in the presence of dimeric spiro D_{sq}-D_{sq} monomeric D_{sq} and D_1-D_{sq}. The TiO$_2$ electrodes were dipped in to the 0.2 mM dye solution in CHCl$_3$ for 12 h and the LHE experiments was carried out. For example, the monomeric D_{sq} possess the spectral broadening with $\Delta\lambda$ = 118 nm (at 90% of LHE) at the CT transition and aggregation regions. However, $\Delta\lambda$ (128 nm at 90 %) was

increased upon introducing spiro-dioxepine linkage in between two monomeric D_{sq} dye in

D_{sq}-D_{sq} due to the dye-dye interaction. Further in the case of hetero dimeric D_1-D_{sq} dye, the

peak broadening was extended to NIR region with panchromatic effect in the visible region

due to the D_1 dye. In order to understand the dye loading on TiO_2, dyes from TiO_2 electrodes

were desorbed in the presence of aqueous HCl (0.1 M, $EtOH/H_2O$, 1:1). The extend of dye

loading for D_{sq}, D_{sq}-D_{sq} and D_1-D_{sq} were found to be 5.24×10^{-8} mol/cm^2, 2.48×10^{-8} mol/cm^2

and 8.09×10^{-8} mol/cm^2, respectively (**Figure 4** and **Table 1**).
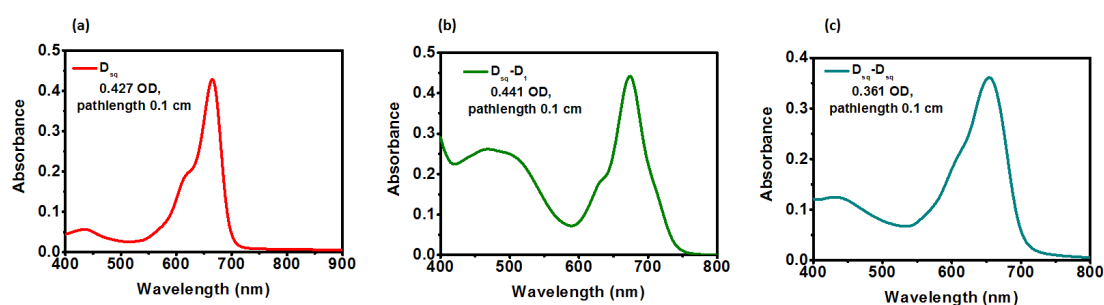
Figure 4. UV-Vis spectra after desorption of (a) D_{sq}, (b) D_1-D_{sq} and (c) D_{sq}-D_{sq} from TiO_2 electrode (each dye solution was 1 mL).

Table 1. Calculation of dye concentration on TiO_2 by desorbing the dyes.

Dye	Absorbance (OD)	$\mathcal{E}$ (10^5 M^{-1}cm^{-1})	Path length (cm)	Area of dye absorbed on TiO_2 (cm^2)	Conc. (mmol/cm^2)
D_{sq}-D_{sq}	0.361	6.32 (661 nm)	0.1	0.23	2.48×10^{-8}
D_1-D_{sq}	0.441	2.37 (660 nm)	0.1	0.23	8.09×10^{-8}
D_{sq}	0.427	3.54 (671 nm)	0.1	0.23	5.24×10^{-8}

3.2.3 Electrochemical studies. Differential pulse voltammetry (DPV) were performed by solubilizing dyes in anhydrous DMSO by using 0.1 M tetra butyl ammonium perchlorate as supporting electrolyte (**Figure 5a**). The highest occupied molecular orbital (HOMO) of **D$_{sq}$-D$_{sq}$** and **D$_1$-D$_{sq}$** were -4.97 eV and -5.15 eV respectively and evaluated from the peak potential of that DPV graph (**Figure 5b**). The zero-zero excitation (E_{0-0}) calculated from the onset of UV-vis absorption spectrum. E_{LUMO} energy level was calculated by subtracting the value of optical band gap (E_{0-0}) from E_{HOMO}. Based upon DPV experiment it has seen that LUMO of the oxidised **D$_{sq}$-D$_{sq}$** and **D$_1$-D$_{sq}$** are -3.23 eV and -3.44 eV respectively and situated on the above of Fermi level of TiO$_2$ (-4.2 V). Therefore, E_{LUMO} of **D$_{sq}$-D$_{sq}$** and **D$_1$-D$_{sq}$** facilitates efficiently electron injection from towards the conduction band of TiO$_2$. On the other hand, calculated values of E_{HOMO} of **D$_{sq}$-D$_{sq}$** (-4.97 eV) and **D$_1$-D$_{sq}$** (-5.15 eV) dyes were below the energy level of I$_3$/I$_3^-$ (-4.9 eV) electrolyte, which facilities the regeneration of oxidized dyes. These two squaraine dye were showing a significant potential loss (around 200-300 mV) for the LUMO to conduction band edge electron transfer which has overcome minimum over potentials required for electron injection (around 100-150 mV). Electrochemical and photophysical properties of all dyes are described in **Table2**.
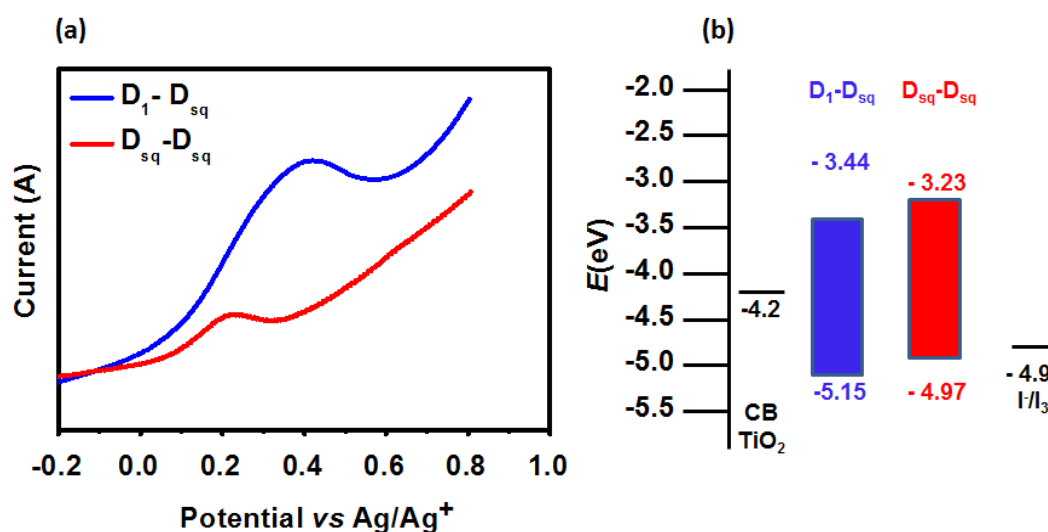
Figure 5. Electrochemical properties of three D_{sq}-D_{sq} and D_1-D_{sq}. (a) DPV of homo and heterodimeric dyes and (b) schematic energy level representation of spiro-based dye cell with various DSSC device components.

Table 2.Photophysical and electrochemical properties of the dyes

Dye	λ_{max} (nm)[a]	$\mathcal{E}$ (10^5 $M^{-1}cm^{-1}$)	λ_{em} (nm)[b]	$\lambda_{em (nm)}$ on TiO$_2$[c]	E_{HOMO}[d] (eV)	E_{LUMO}[e] (eV)	ΔE_{0-0}[f] (eV)
D_{sq}-D_{sq}	661, 450	6.32 (661 nm) 0.97 (450 nm)	667	442, 663	-4.97	- 3.44	1.53
D_1-D_{sq}	660, 450	2.37 (660 nm) 0.99 (450 nm)	668	423, 645	-5.15	- 3.23	1.92
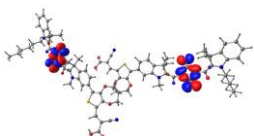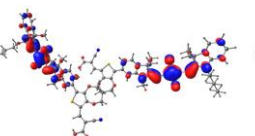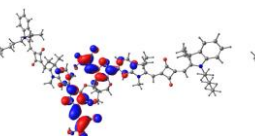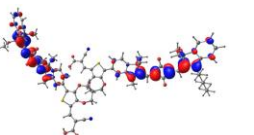
[a]Absorption maxima of dye in CHCl$_3$.[b]Emission maxima of dye in CHCl$_3$ (excitation, for D_{sq}-D_{sq} and D_1-D_{sq} are 620 and 645 nm respectively. [c] Absorption maxima of absorbed dye on TiO$_2$ (thickness 6 μm, dye concentration 0.1 mM in CHCl$_3$, dipping time 60 min). [d]The oxidation potentials were measured in CHCl$_3$ with 0.1 M TBAP as supporting electrolyte, Fc$^+$/Fc as an internal standard. HOMO energy level was calculated from ($E_{HOMO}= -\{E_p$ [Dye] $-E_{1/2}$ [Fc$^+$/Fc]$\}$ + 4.8). [e]E_{LUMO} was calculated from E_{HOMO} and E_{0-0}. [f]Experimental band gap.

3.2.4 Computational analysis of dyes and functionalized electron distribution.
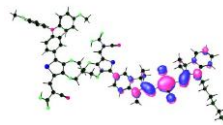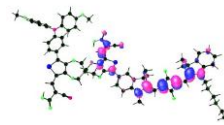
Density functional theory (DFT) in gas phase were performed with Gaussian 09 programme using B3LYP/6-31G (d, p) level to understand the electron distribution of squaraine dyes. On careful investigation it has seen that electron density localization is maximum on squaraine moiety in HOMO whereas, LUMO is localised on the cyanoacrylic acid units (**Table 3**). Thus, it was expected that efficient photo-induced charge separation and the relatively

stronger anchoring effect would enhance the degree of electron injection to the TiO_2 electrode. The HOMO and LUMO energy level of D_{sq}-D_{sq} calculated from DFT -4.66 eV and -3.07 eV respectively. The isosurface plots and theoretical energy levels for D_1-D_{sq} and D_{sq} were provided in **Table 4** and **Table 5** respectively.
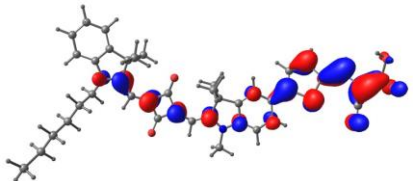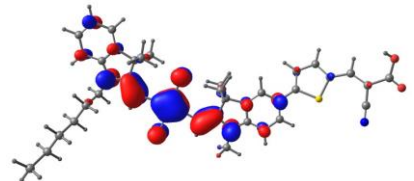
Table 3. DFT calculation of D_{sq}-D_{sq} dye

Description	HOMO-1	HOMO	LUMO	LUMO + 1
Molecular orbital				
Energy (eV)	-5.52	-4.66	-3.07	-2.45

Table 4. DFT calculation of D_1-D_{sq} dye
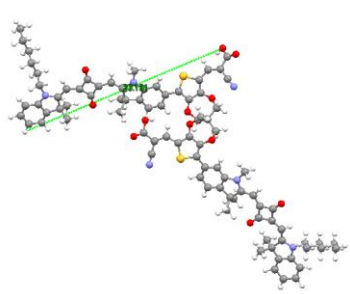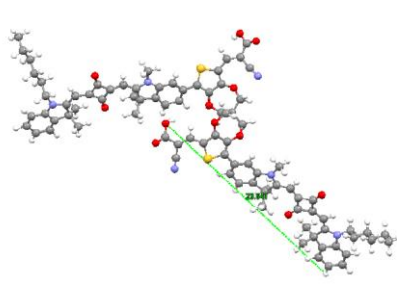
Description	HOMO-1 of D_1 in D_1-D_{sq}	HOMO of D_{sq} in D_1-D_{sq}	LUMO of D_{sq} in D_1-D_{sq}	LUMO + 1 of D_1 in D_1-D_{sq}
Molecular orbital				
Energy (eV)	-4.93	-4.73	-2.79	-2.71

Table 5. DFT calculation of monomeric D_{sq} dye

Dye	Molecular orbital of LUMO	Molecular orbital of HOMO	E_{LUMO}	E_{HOMO}
D_{sq}			-2.81	-4.79

Dipole length of each D_{sq} unit, the bond distance of two oxygen atom of –COH anchoring groups and dihedral angle of spiroBiProDOT in D_{sq}-D_{sq} dyes were calculated and given in **Table 6**.

**Table 6.** Geometrical studies of optimized structure of D_{sq}-D_{sq} dye (DFT method)

Dipole length of left side D_{sq} unit (23.1 Å)	Dipole length of right side D_{sq} unit (23.64 Å)	Bond distance[a]	Dihedral angle[b]
		11.680 Å	143.56°

[a]Bond distance was calculated between two oxygen atom of –COH anchoring group. [b]Dihedral angle calculated from sp^3 spiro carbon, adjacent two carbon atoms and one oxygen atom of spiroBiProDOT unit.

3.2.5 Photovoltaic performance. The photovoltaic device performances of **D$_{sq}$-D$_{sq}$**, **D$_1$-D$_{sq}$** and **D$_{sq}$** dyes under standard conditions (AM 1.5 G, 100 mW/cm^2) were measured using iodine/triiodide (I$^-$/I$_3$$^-$) liquid electrolyte, and the device parameters are summarized in **Table 7** (**Figure 6**). The solvent for preparing the dye both bath plays an important role in various device performance.[64] Dye bath was optimized to MeOH: CH$_2$Cl$_2$ (3:2) as **D$_{sq}$-D$_{sq}$** and **D$_1$-D$_{sq}$** were not completely soluble in MeOH. DSSC device fabricated **D$_{sq}$-D$_{sq}$** and **D$_1$-D$_{sq}$** dyes were showed the efficiencies of 2.16 % (V_{oc} of 0.54 V, J_{sc} of 5.81 mA/cm^2, *ff* of 68.7 %) and 3.37 % (V_{oc} of 0.64 V, J_{sc} of 7.14 mA/cm^2, *ff* of 72.2 %) without co-absorbing with optically transparent molecules. However, the device performances have increased to 2.78 % and 3.9 % in the presence of 3 mM CDCA with concomitantal increase from both V_{oc} and J_{sc} for **D$_{sq}$-D$_{sq}$** and **D$_1$-D$_{sq}$** dyes, respectively. It is interesting to note that the monomeric **D$_{sq}$** dye showed the device efficiency of 1.6 % (V_{oc} of 0.54 V, J_{sc} of 4.2 mA/cm^2, *ff* of 71.5 %) under the similar experimental condition. Though the structural backbone of monomeric dye (**D$_{sq}$**) is similar to reported **YR6** dye,[40] the device performance have been changed significantly in the presence of different alkyl groups.[65]
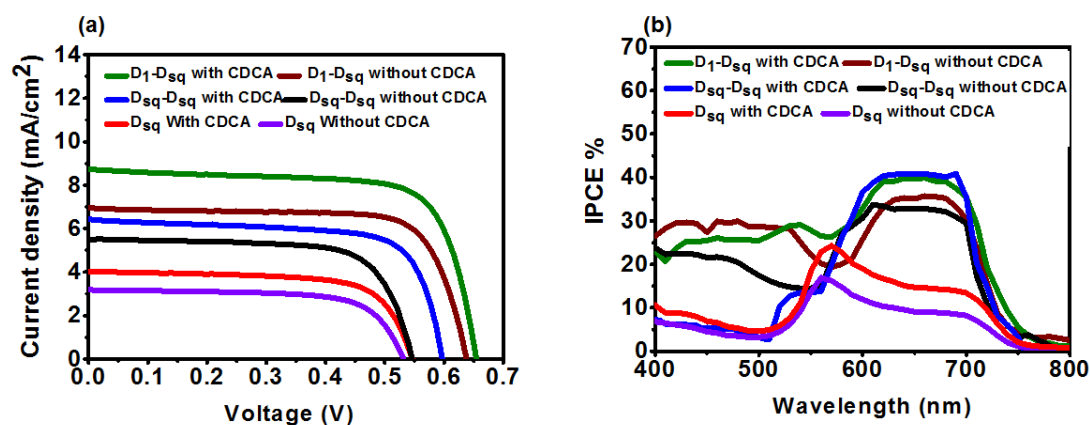
Figure 6. (a) Current density-voltage curve (dye dipping solvent mentioned in Table 2), and (b) IPCE of D_1-D_{sq} and D_{sq}-D_{sq} with and without 3 mM of CDCA in MeOH: CH_2Cl_2 (3:2).

Table 7. Photovoltaic parameters of D_{sq}-D_{sq}, D_1-D_{sq} and D_{sq} dyes[a]

Dye (0.3 mM)	Solvent mixture	Conc. of CDCA	J_{sc} (mA/cm^2)	V_{oc} (V)	ff (%)	η (%)
D_1-D_{sq}	MeOH: CH_2Cl_2 (3:2)	-	7.01±0.13	0.64±0.002	72±1.2	3.2± 0.17
D_1-D_{sq}	MeOH: CH_2Cl_2 (3:2)	3mM	8.74±0.15	0.65±0.002	68±0.8	3.8± 0.19
D_{sq}-D_{sq}	MeOH: CH_2Cl_2 (3:2)	-	5.70±0.11	0.54±0.002	68±0.7	2.1± 0.06
D_{sq}-D_{sq}	MeOH:CH_2Cl_2 (3:2)	3mM	6.46±0.16	0.60±0.007	69±0.3	2.4± 0.38
D_{sq}	MeOH: CH_2Cl_2 (3:2)	-	3.2±0.23	0.52±0.015	69±0.9	1.1± 0.19

|						
D_{sq}	MeOH: CH_2Cl_2 (3:2)	3mM	4.01±0.19	0.54±0.01	71±0.5	1.5± 0.12
D_{sq}-D_{sq} and D_1-D_1[b]	MeOH: CH_2Cl_2 (3:2)	-	8.41± 0.12	0.63±0.02	71±0.6	3.76±0.1
D_{sq}-D_{sq} and D_1-D_1[b]	MeOH: CH_2Cl_2 (3:2)	3 mM	9.31± 0.15	0.67±0.04	70±0.9	4.36±0.16
D_{sq} and D_1[b]	MeOH: CH_2Cl_2 (3:2)	-	5.6± 0.13	0.61±0.01	73±1.1	2.49±0.14
D_{sq} and D_1[b]	MeOH: CH_2Cl_2 (3:2)	3 mM	7.42± 0.08	0.63±0.05	67±0.5	3.13±0.08

[a]TiO_2 thickness 8+5 µm and 0.235 cm^2, [dye] = 0.2 mM under AM 1.5 illumination (100 mW/cm^2). Dye dipping time 16 h. [b]Mixture of two dyes with 0.2 mM concentration

The V_{oc} obtained for the devices were in the order of D_{sq} (0.52 V) < D_{sq}-D_{sq} (0.54 V) < D_1-D_{sq} (0.64 V), in the absence of CDCA. However, enhancement in V_{oc} has been observed in the presence of 3 mM CDCA (dye:CDCA=1:15) in the order of D_{sq} (0.54 V) < D_{sq}-D_{sq} (0.60 V) < D_1-D_{sq} (0.65 V).

This can be explained by the presence of inter molecular π-π interaction and intra molecular dipole-dipole interaction, between the dye molecules, which strongly influence the V_{oc}.[66] Suppression of inter molecular π-π interaction, the V_{oc} increases significantly, which were affected by the presence of 3 mM of CDCA. Further suppression of intramolecular dipole-dipole interaction can be explained by comparing the V_{oc} of D_{sq}-D_{sq} and D_1-D_{sq}. Due to the presence of long dipole D_{sq} unit in D_{sq}-D_{sq}, predominant intramolecular dipole-dipole

interactions leads to decrease the V_{oc}. However, V_{oc} increasing due to the effective passivation by the presence of spiro-linker that decreases the charge recombination process. In the case of **D$_1$-D$_{sq}$,** the intermolecular $\pi-\pi$ interaction is decreased by the addition of CDCA and the intramolecular dipole-dipole interaction is reduced by the presence of two different dipoles. Dipole moment and dipole length of two different monomeric dyes **D$_1$** and **D$_{sq}$** were calculated from fully optimized molecular structures at B3LYP/6-31G (d, p) level (**Table 9**). Further the effective dipole moment also significantly alter the position of CB$_{TiO2}$ to increase the V_{oc}.[50–55]

To get the panchromatic light absorption, device fabrication was carried out by mixing **D$_{sq}$-D$_{sq}$, D$_{sq}$** with **D$_1$-D$_1$** and **D$_1$** respectively (**Figure 7**). Without using of CDCA, **D$_{sq}$-D$_{sq}$** and **D$_1$-D$_1$** mixture affored to get 3.86 % of PCE (J_{sc} of 8.53 mA/cm^2 and V_{oc} of 0.63 V). An improvement of PCE of 4.5 % (J_{sc} of 9.46 mA/cm^2 and V_{oc} of 0.674 V) was observed by using 3 mM of CDCA on **D$_{sq}$-D$_{sq}$** and **D$_1$-D$_1$** mixture. In contrast, the mixture of **D$_{sq}$** and **D$_1$** dyes showed 2.6 % of PCE (J_{sc} of 5.73 mA/cm^2 and V_{oc} of 0.61 V) without CDCA. After addition of 3 mM of CDCA the efficiency was increased up to 3.2 % with J_{sc} of 7.5 mA/cm^2 and V_{oc} of 0.635 V. Further, the IPCE profile of both **D$_1$-D$_{sq}$,** and the mixture of **D$_{sq}$-D$_{sq}$, D$_1$-D$_1$** and **D$_{sq}$, D$_1$** were looking almost with same feature. This indicates that the excitation transfer from excited D$_1$ to D$_{sq}$ moiety in **D$_1$-D$_{sq}$** is negligible in device. Further, it has been observed that the V_{oc} of dye mixture of **D$_1$-D$_1$** and **D$_{sq}$-D$_{sq}$** is 0.674 V, which is very close to the independent V_{oc} of **D$_1$-D$_1$** (0.673 V)[57] and 74 mV higher than that of **D$_{sq}$-D$_{sq}$**. Similar trends also have been observed for mixture of **D$_1$** and **D$_{sq}$** dyes.
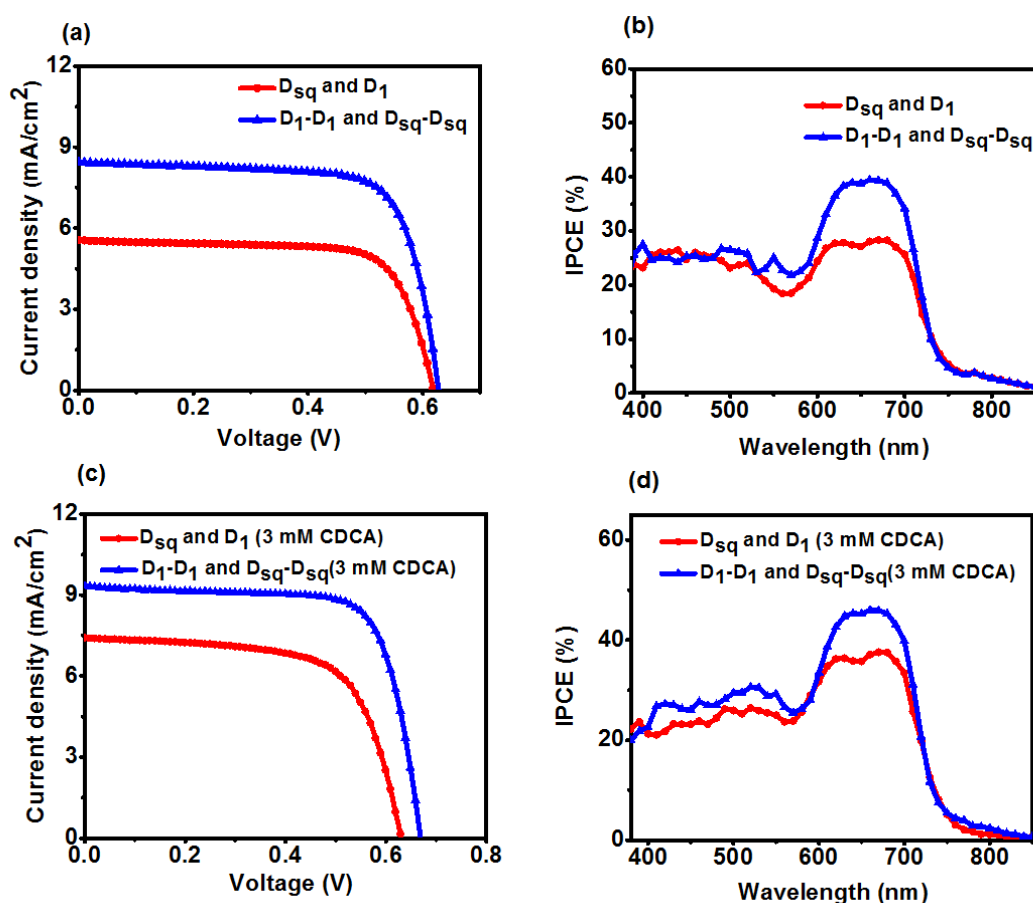
Figure 7. (a) Current density-voltage curve (dye dipping solvent mentioned in **Table 7**), and (b) IPCE of mixture of dye D_1-D_1 with D_{sq}-D_{sq} and D_1 with D_{sq} without CDCA. (c) Current density-voltage curve and (d) IPCE of mixture of dye D_1-D_1 with D_{sq}-D_{sq} and D_1 with D_{sq} (with 3 mM CDCA in MeOH: CH_2Cl_2 as a solvent mixture at 3:2 ratios).

The V_{oc} for the mixture of D_1 and D_{sq} dyes was 0.635 V, which is 15 mV and 95 mV higher than that of individually observed V_{oc} of D_1 (0.62 V) and D_{sq} (0.54 V), respectively. Therefore the V_{oc} observed for the D_1-D_{sq} (0.65 V) dye is higher than that of the dye mixture of D_1 and D_{sq} (0.635 V) and lower than that the mixture of D_1-D_1 and D_{sq}-D_{sq} (0.674 V) dyes. Hence the modulated Voc for the D_1-D_{sq} device is the combined effects of effective dipole moment, dye-dye interaction and surface passivation spiro linker. The J_{sc} of D_1-D_{sq} (7.14 mA/cm^2) was higher than that of D_{sq}-D_{sq} (5.8 mA/cm^2) without any CDCA concentration due

to the panchromatic absorbing nature of this dye. By addition of 3 mM of CDCA further help to increase the J_{sc} of **D$_1$-D$_{sq}$** (8.89 mA/cm^2) and **D$_{sq}$-D$_{sq}$** (6.5 mA/cm^2). With the increased J_{sc} and V_{oc} value **D$_1$-D$_{sq}$** reached upto highest 4 % of PCE compared to **D$_{sq}$-D$_{sq}$** dye by using 3 mM of CDCA.

The increased value of J_{sc} of can be explained by IPCE integration of both homo- and hetero dimeric squaraine dyes. In **D$_{sq}$-D$_{sq}$** an intense IPCE response found in far red (600-700 nm). In contrast the IPCE responses of **D$_1$-D$_{sq}$** were found in UV (400-500 nm) and NIR (600-710 nm) regions, by which the J_{sc} became higher than **D$_{sq}$-D$_{sq}$**. The IPCE % was increasing for all devices by using 3 mM of CDCA which reduces the intermolecular interaction.

3.2.6 Electrochemical Impedance Spectroscopy. The charge recombination dynamics between the injected electrons in TiO$_2$ conduction band (CB$_{TiO2}$) and I$_3^-$ ions in electrolyte at the interface of TiO$_2$-dye/electrolyte competes with the charge collection process and controls the V_{oc} and J_{sc}. Electrochemical impedance spectroscopy (EIS) has been used to probe the correlation of dye structure and photovoltage by measuring the current response to the application of small ac perturbation as a function of the frequency. EIS analysis data were acquired under 1 sun illumination (100 mW/cm^2). The second semicircle at the intermediate frequency region of Nyquist plot in (**Figure 8**), ascribed to charge recombination resistance between CB$_{TiO2}$ and electrolyte. Here, the major semicircle is related to the charge transport process at the interfaces between TiO$_2$ and the electrolyte because of the experiment carried out in dark. The charge transfer resistance (R_{ct}) on the TiO$_2$ surface denoted the charge recombination between the electrons resides on TiO$_2$ at forward bias and electrolyte which is measured by the large semicircle area.
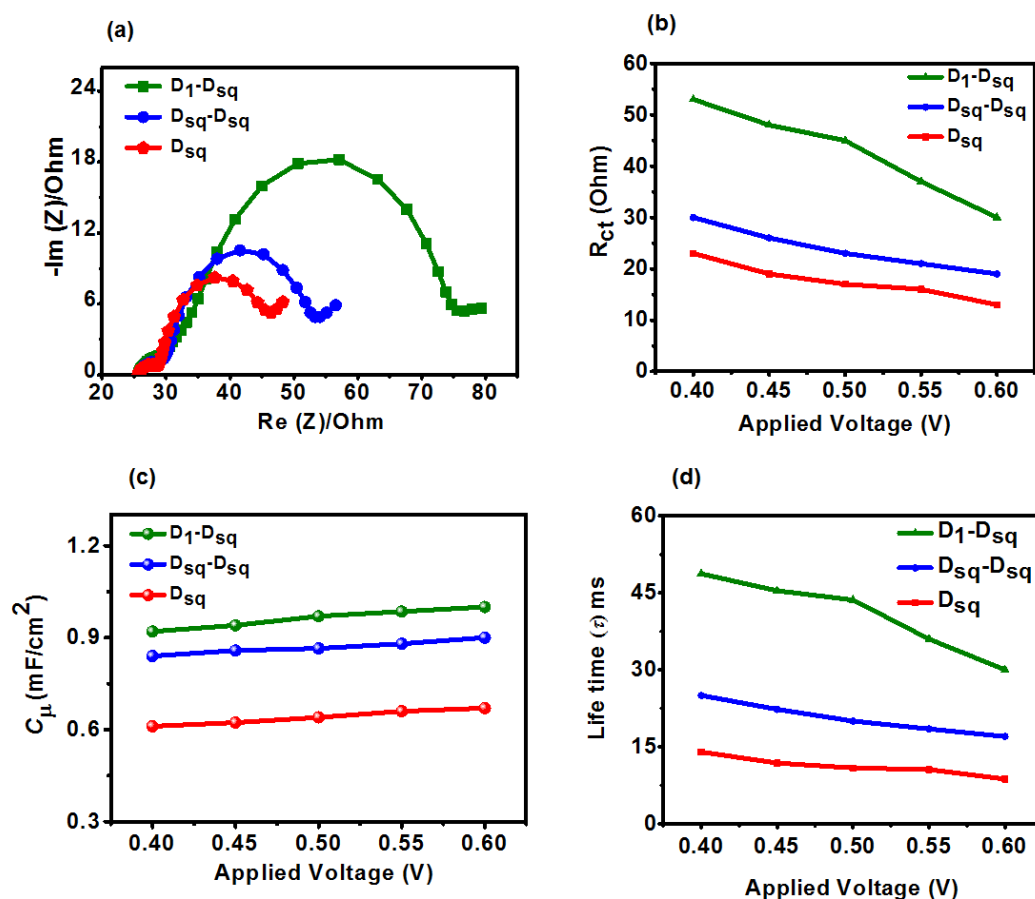
Figure 8. Impedance analysis of D_1-D_{sq}, D_{sq}-D_{sq} and D_{sq} dyes. (a) Nyquist plot, (b) charge transfer resistance (c) capacitance, and (d) electron lifetime *vs* applied potential.

[a]TiO$_2$thickness 8+5 μm and 0.235 cm^2, [dye] = 0.2 mM, [CDCA] = 3 mM in MeOH: CH$_2$Cl$_2$ (3:2)

A large R_{ct} indicates the slow charge recombination process and vice versa. The R_{ct} values for D_{sq}-D_{sq}, D_{sq}, and D_1-D_{sq} are 23 ohm, 17 ohm and 45 ohm respectively were calculated and presented in **Table 8** at 0.5 V. Among the series D_1-D_{sq} showed high impedance of 45 ohm whereas, in dimeric D_{sq}-D_{sq} was higher (23 ohm) compared to its monomeric analogue D_{sq} dye (17 ohm). It is reported that under illumination, V_{OC} is

determined by the potential difference between redox potential of electrolyte (E_{red}) and Fermi

level of photo electrode (E_{Fn}). Although Fermi level of photo electrode is constant, but the

conduction band may varied with the function of absolute temperature, free electron density

and accessible states on the conduction band.

Table 8. Electrochemical impedance parameters[a] of spiro dyes at applied bias of 0.5 V (only

for R_{ct})

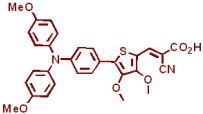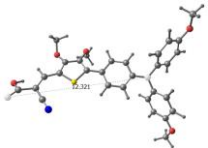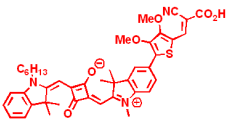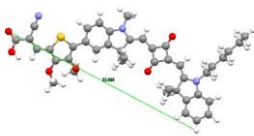| Dyes[a](CDCA)	R_{ct} (ohm)	C_μ (mF/cm^2)	τ_n(ms)[b]
D_1-D_{sq}	45	0.97	43.7
D_{sq}-D_{sq}	23	0.87	20
D_{sq}	17	0.64	10.9
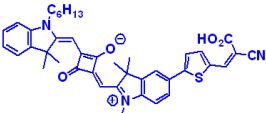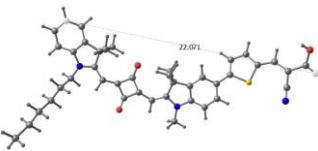
[a]Dye:CDCA (1:15), [dye]= 0.2 mM. [b]Electron lifetime was calculated from capacitance and

charge transfer resistance: Life time (τ) = $R_{ct}\times C_\mu$

The chemical capacitance (C_μ) has been extrapolated from fitting the experimental

data with an equivalent circuit model. High capacitance of dimeric D_{sq}-D_{sq} (0.87 mF/cm^2)

compared to monomeric D_{sq} dye (0.64 mF/cm^2) indicates that long lifetime of electron of D_{sq}-

D_{sq} (23 ms) and more number of electrons present the conduction band. Out of these three

dyes D_1-D_{sq} was showing highest capacitance (0.97 mF/cm^2) and life time of electron (43.7

ms). Dipole moment for the D_{sq} and D_1 evaluated from DFT studies were 12.8 D and 12.1 D

respectively. The model squaraine dye with two-methoxy groups in thiophene π-spacer is

13.1 D (**Table 9**). Further the V_{oc} of the DSSC device is increased by the direction of

resultant dipole moment as the position of the CB$_{TiO2}$ shifted upward and decreased by the extent of dipole-dipole interaction.

Table 9. Dipole moment calculation of dyes by DFT method (field-independent basis).

Dye	Structure	Dipole moment (Debye)	Molecular orbital	Dipole length
D$_{sq}$		12.8		22.07 Å
D$_1$		12.1		12.32 Å
D$_{sq1}$		13.1		22.09 Å
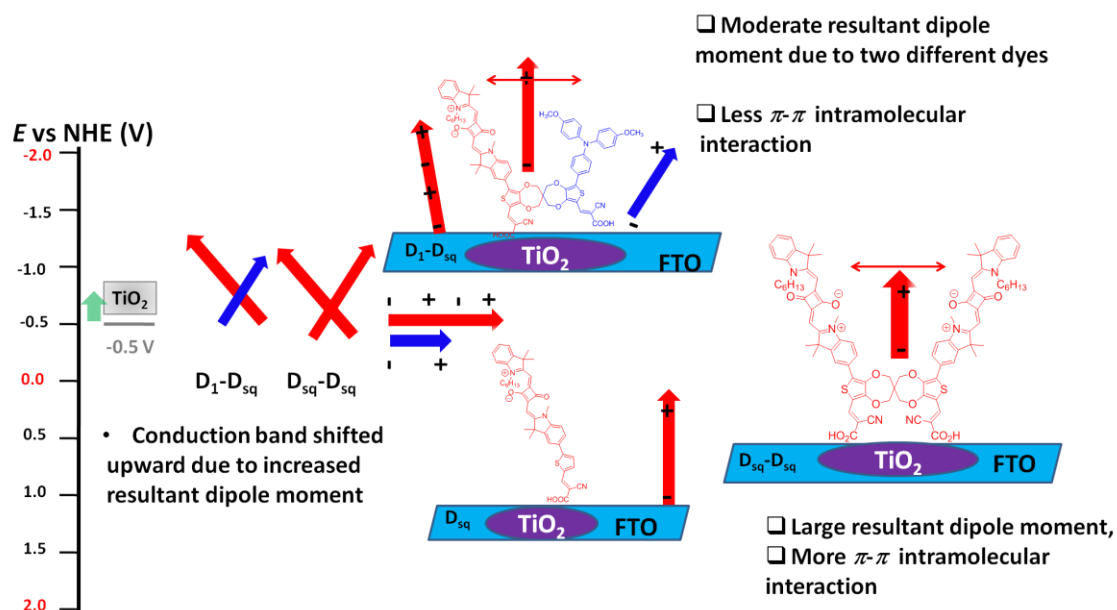
Figure 9. Postulated diagram of uplifted conduction band of **D₁-D$_{sq}$** absorbed TiO₂ compared to **D$_{sq}$** and **D₁-D$_{sq}$** absorbed on TiO₂ due to less $\pi-\pi$ intramolecular interaction and high resultant dipole moment. Dipole length of **D₁** = 12.32 Å (estimated from carbonyl carbon of –COOH group to nitrogen atom of triarylamine). Dipole length of **D$_{sq}$** = 22.07 Å (estimated from carbonyl carbon of –COOH group to para carbon atom of indoline –N). Dipole moment of **D₁** and **D$_{sq}$** are 12.1 D and 12.8 D, respectively. Dipole moment and dipole length of monomeric dyes (**D₁** and **D$_{sq}$**) were calculated from DFT method (**Table 7**).

Hence a resultant strong dipole moment of **D₁-D$_{sq}$** can be influence the V_{oc} by exerting an upward shift in position of conduction band of TiO₂; **Figure 9** shows a schematic representation of effect of dye structure on conduction band. Electron lifetime was increased same as the observed trend in R_{ct} and C_μ and which are linearly increased with the applied potential, upward shift of capacitance and high charge transfer resistance improved the V_{oc}. This trend appears to be consistent with the values of device V_{oc}. The R_{ct}, C_μ and τ_n data were also suggested the possibility (i) efficient passivation of TiO₂ surface in case of **D$_{sq}$-D$_{sq}$**

compared to $\mathbf{D_{sq}}$ besides strong dipole-dipole interaction. (ii) The increased V_{oc} of $\mathbf{D_1}$-$\mathbf{D_{sq}}$ device due to the resultant dipole moment and reduced dipole-dipole interaction.

3.3 Conclusion

Two homo- ($\mathbf{D_{sq}}$-$\mathbf{D_{sq}}$) and hetero- ($\mathbf{D_1}$-$\mathbf{D_{sq}}$) dimeric dyes which absorb in the NIR and visible-NIR regions were synthesized by direct arylation method, respectively. Broadening UV-Vis absorption transitions in solution indicated the presence of dipole-dipole interaction in compared to the individual dye systems. Further excitation energy transfer from D_1^* to squaraine unit was also established. Electrochemical studies inferred the feasibility of efficient charge injection avoid charge recombination and dye aggregation. The photovoltaic performances of the homo- and hetero-dimeric dyes, $\mathbf{D_1}$-$\mathbf{D_1}$ and $\mathbf{D_1}$-$\mathbf{D_{sq}}$ were better than the model monomeric squaraine dye, $\mathbf{D_{sq}}$. A systematic comparison of V_{oc} and J_{sc} for $\mathbf{D_1}$-$\mathbf{D_{sq}}$ with mixture of spiro dyes, $\mathbf{D_{sq}}$-$\mathbf{D_{sq}}$ and $\mathbf{D_1}$-$\mathbf{D_1}$ and monomer pairs ($\mathbf{D_{sq}}$ and $\mathbf{D_1}$) were carried out. Though the increased Jsc for the $\mathbf{D_1}$-$\mathbf{D_{sq}}$ dyes can be explained on the basis of panchromatic nature of the modulated V_{oc} can be explained on the basis of (i) modulated dipole-dipole interaction, which depends on the length of the dye dipole (intra molecular interaction), (ii) the effective dipole moment that shifts the conduction band of the TiO_2 (iii) avoiding the intermolecular interaction by the addition of CDCA and (iv) Further passivation of TiO_2 surface by the spiro linker. The DSSC device based on $\mathbf{D_1}$-$\mathbf{D_{sq}}$ performed with the highest efficiency of 3.9% owing to its highest J_{SC} value of 8.9 mA cm^{-2}, which was attributed to the broadening of the absorption spectra and its highest V_{OC} value of 0.65 V.

3.4 Experimental section

3.4.1 Materials and instruments. All the reagents and solvents were purchased from Aldrich and TCI chemicals and used without further purification. Required 2H,2'H,4H,4'H-3,3'-spirobi[thieno[3,4-b][1,4]dioxepine]-6,6'-dicarbaldehyde, **6** was synthesized by following our previous publication.[57] All oxygen- and moisture-sensitive reactions were performed under nitrogen atmosphere. The other materials were of the common commerciallevel and used as received. PhMe was dried over Na/benzophenoneketyl and freshly distilled prior to use.

3.4.2 Characterization. All the instruments for characterization (^{1}H NMR, ^{13}C NMR, MALDI-TOF-MS, UV-vis spectra, differential pulse voltammetry, electrochemical impedance spectra, solar simulator) of organic dyes are same as presented in **Chapter 2**, section 2.4.2.

3.4.3 Fabrication of dye sensitized solar cells. The methods of preparation of solar cell with synthesized dyes were same as presented in **Chapter 2**, section 2.4.3.

3.4.4 Characterization of synthetic compound

5-Bromo-1,2,3,3-tetramethyl-3H-indol-1-ium iodide, 1: To a mixture of iodomethane (0.715 g, 5.04 mmol) and 5-bromo-2,3,3-trimethyl-3H-indole (1 g, 4.2 mmol) in a 50 mL round bottom flask and heated at 80 ^{o}C for 30 minutes. The reaction mixture was cooled to room temperature and dissolved in minimum amount of CH_2Cl_2 and poured into stirring Et_2O and was washed with Et_2O (2 × 40 mL) to afford the required compound as a pink-colour solid. The product was not purified further. Yield: 1.12 g, 70 %. ^{1}H NMR (CDCl$_3$, 200 MHz) δ: 8.18 (b s, 1H), 7.87 (b s, 2H), 3.95 (s, 3H), 2.75 (s, 3H), 1.54 (s, 6H).

3-((1-Hexyl-3,3-dimethylindolin-2-ylidene)methyl)-4-hydroxycyclobut-3-ene-1,2-dione,

2: Precursor **2** was synthesis from the reported procedure.[61]

(E)-4-((5-Bromo-1,3,3-trimethyl-3H-indol-1-ium-2-yl)methylene)-2-(((E)-1-hexyl-3,3-dimethylindolin-2-ylidene)methyl)-3-oxocyclobut-1-en-1-olate, 3: A mixture of **1** (0.403 g, 1.06 mmol), and **2** (0.3 g, 0.884 mmol) were dissolved in 1-butanol and dry toluene (1:1, 8 mL each) in a 50 mL two necked round bottom flask, and charged with Dean-Stark apparatus. The reaction mixture was refluxed under inert atmosphere for 24 h. The reaction mixture was cooled to room temperature and the solvents were removed under reduced pressure. The reaction mixture was subjected to column chromatography (SiO_2, 100-200 mesh, 1.3 % methanol and 98.7 % CH_2Cl_2) to afford the required dye as golden blue coloured solid. Yield: 300 mg, 59 %. ^1H NMR (CDCl$_3$, 400 MHz): δ 7.42-7.31 (m, 4H), 7.18 (m, 1H), 7.03 (d, J = 8 Hz, 1H), 6.83 (d, J = 8 Hz, 1H), 6.01(s, 1H), 5.89 (s, 1H), 4.03 (b, 2H), 3.47 (s, 3H), 1.79 (s, 12H), 1.46-1.28 (m, 8H), 0.91-0.87 (m, 3H); ^{13}C NMR (CDCl$_3$, 100 MHz) δ: 14, 22.6, 27, 27.2, 27.3, 30, 30.5, 31.5, 44, 49, 49.7, 87.1, 109.8, 110.1, 116.1, 122.4, 124.3, 125.7, 127.9, 130.7, 142.3, 142.5, 144, 168.9, 171.5, 178.4, 181.73.

(E)-4-((5-(5-Formylthiophen-2-yl)-1,3,3-trimethyl-3H-indol-1-ium-2-yl)methylene)-2-(((E)-1-hexyl-3,3-dimethylindolin-2-ylidene)methyl)-3-oxocyclobut-1-en-1-olate, 4: Started with precursor **3** (20 mg, 0.035 mmol) and 5-formylthiophen-2-ylboronic acid (20 mg, 0.12 mmol), PdCl$_2$(dppf)·CH$_2$Cl$_2$ (3 mg, 0.035 mmol), and potassium carbonate (30 mg, 0.21 mmol) were added to a dry microwave tube. It was flushed with nitrogen in a glove box for 30 min and, under nitrogen, toluene (2 mL) and methanol (2 mL) were added and the tube was capped. The microwave reactor (CEM, Discover) was set to standard mode: T = 70 °C, Power = 60 watt, hold time = 15 min. The reaction mixture was subjected to column chromatography (SiO_2, 100-200 mesh, 30% ethyl acetate and 70% CH_2Cl_2) to afford the

required dye as golden blue coloured solid. Yield: 18 mg, 90%. ^{1}H NMR (400 MHz, CDCl$_3$) 0.83-0.95 (m, 3 H), 1.23-1.36 (m, 8 H), 1.85 (s, 12 H), 3.5 (s, 3 H), 4.03 (t, J = 12 Hz, 2 H), 5.96 (s, 1 H), 6.06 (s, 1 H), 6.97-7.17 (m, 2 H), 7.20-7.39 (m, 4 H), 7.41-7.66 (m, 2 H), 7.75 (d, J = 8 Hz, 1 H), 9.88 (s, 1 H). ^{13}C NMR (125 MHz, CDCl$_3$) δ: 14, 14.1, 22.5, 26.7, 26.8, 27.2, 27.3, 29.7, 31.5, 44, 48.6, 49.8, 87.4, 87.6, 109.2, 110, 120.2, 122.4, 123.5, 124.5, 126.6, 127.9, 128.2, 137.6, 141.8, 142.2, 142.5, 143, 153.9, 168.4, 171.8, 171.9, 173.7, 177.2, 182.6.

D$_{sq}$, 5: A mixture of **4** (18 mg, 0.03 mmol) and cyanoacetic acid (6 mg, 0.06 mmol) were added to a dry round-bottomed flask, which was then evacuated and filled with nitrogen 3 times. Anhydrous acetonitrile (5 mL) was added to dissolve the reactants. The reaction mixture was heated up to reflux for 4 h after the addition of piperidine (10 μL). The crude product, obtained from the major fraction, was dissolved in CH$_2$Cl$_2$ and washed with aqueous acetic acid and water. The organic layer was dried over Na$_2$SO$_4$ and evaporated and purified by column chromatography using methanol and CH$_2$Cl$_2$. Yield: 90 mg, 63%. Mp 182-186 °C; FT-IR (dry film, cm^{-1}): 2955-2850 (br), 2213 (s), 1706 (s), 1639 (s), 1542 (m); ^{1}H NMR (400 MHz, CDCl$_3$) δ: 0.89-0.92 (m, 3 H), 1.46-1.49 (m, 4 H), 1.50-1.61 (m, 4 H), 1.82 (s, 12 H), 3.63 (d, J = 2 Hz, 3 H), 4.18 (t, J = 8 Hz, 2 H), 5.92 (s, 1 H), 6.04 (s, 1 H), 7.28- 7.31 (m, 2 H), 7.39-7.41 (m, 1 H), 7.48- 7.50 (m, 1 H), 7.59 (d, J = 4 Hz, 1 H), 7.75-7.80 (m, 3 H), 7.92 (s, 1 H), 8.30 (s, 1 H). ^{13}C NMR (125 MHz, CDCl$_3$) δ: 12.9, 22.1, 24.7, 25.7, 25.9, 26, 29, 29.3, 31.2, 66.7, 47, 62.8, 86.3, 91.7, 110, 110.4, 119.6, 122, 123.7, 124, 124.5, 126.3, 128, 135, 140.7, 144, 144.2, 148.4, 150.2, 153.4.

6'-Acetyl-2H,2'H,4H,4'H-3,3'-spirobi[thieno[3,4-b][1,4]dioxepine]-6-carbaldehyde , 6: Compound **6** was synthesized from the reported procedure.[57]

(4E,4'E)-2,2'-(((2Z,2'Z)-(6,6'-Diformyl-2H,2'H,4H,4'H-3,3'-spirobi[thieno[3,4-b][1,4]dioxepine]-8,8'-diyl)bis(1,3,3-trimethylindoline-5-yl-ylidene))bis(methanylylidene))bis(4-((1-hexyl-3,3-dimethyl-3H-indol-1-ium-2-yl)methylene)-3-oxocyclobut-1-en-1-olate), 7: Started with dialdehyde derivative, **6** (0.170 mmol, 120 mg), indolium derivative, **3** (0.196 g, 0.341 mmol), K_2CO_3 (60 mg, 0.620 mmol), Pd(OAc)$_2$ (0.5 mol%), PCy$_3$ (0.5 mol%), and PivOH (0.15 mol%) were taken in a Schlenk tube under nitrogen atmosphere. Dry DMA (5 mL) was added to that and kept the reaction at 120 $^\circ$C temperature under the same atmosphere for 24 h. The reaction mixture was washed with 150 mL of water and extracted with 100 mL of CH_2Cl_2. Solvents were removed under reduced pressure and purified by column chromatography. Yield: 138 mg, 38 %. ^{1}H NMR (200 MHz, CDCl$_3$) δ: 0.89 – 0.92 (m, 6 H), 1.35 – 1.46 (m, 16 H),1.81-1.95 (m, 26 H), 3.54 (s, 3 H), 3.57 (s, 3 H), 4.04-4.07 (m, 4 H), 4.29 -4.44 (m, 8 H), 6.01 (t, J = 25 Hz, 4 H), 7.01 – 7.07 (m, 4 H), 7.18 – 7.21 (m, 3 H), 7.32 – 7.35 (m, 2 H), 7.39 (d, J = 5Hz, 2 H), 7.41 (s, 2H), 7.6 (d, J = 10 Hz, 2 H) 10.00 (s, 1 H), 10.06 (s, 1 H) . ^{13}C NMR (125 MHz, CDCl$_3$) δ: 14.3, 22.4, 26.1, 27, 31.3, 34.6, 35.4, 43.8, 49, 49.2, 49.7, 70.6, 71.1, 86.5, 87.3, 108.5, 108.7, 109.3, 120.9, 122.3, 123.6, 126.9, 127.7, 142, 146.6, 168, 169.6, 178.9, 180.2.

D$_{sq}$-D$_{sq}$, 8: A mixture of **7** (0.1g, 0.074 mmol), cyanoacetic acid (0.040 g, 0.449 mmol), ammonium acetate (0.010 g, 0.438 mmol) and glacial acetic acid (12 mL) was heated under reflux for 12 h during which time the aldehyde is completely consumed as indicated by TLC. After 12 h the reaction mixture was washed with water and Et$_2$O thoroughly. Yield: 125 mg, 79%. Mp 227-230 $^{\circ}$C; FT-IR (dry film, cm^{-1}): 2954-2852 (br), 2211 (s), 1712 (s), 1582 (s), 1491 (w); ^{1}H NMR (500 MHz, CDCl$_3$) δ : 0.85 – 0.92 (m, 6 H), 1.67 - 1.79 (m, 38 H), 3.60 (s, 6 H), 4.07 – 4.12 (m, 4 H), 4.35 – 4.44 (m, 8 H), 5.78- 5.87 (m, 4 H), 7.03 - 7.20 (m, 4 H), 7.30 - 7.37 (m, 6 H), 7.54 (s, 2 H) 7.75 - 7.83 (m, 2 H), 8.22 (s, 2 H).^{13}C NMR (125 MHz, DMSO-d_6): 14.3, 21.5, 22.7, 28.9, 29.3, 30, 31.7, 33.5, 35.2, 37.6, 47.7, 48.5, 55.8, 61, 62.5,

72.2, 72.5, 104.6, 114.4, 114.8, 115.5, 119, 123.1, 126.2, 127.2, 127.9, 134.9, 138.8, 141.6, 149.3, 153.1, 170.5. MALDI-TOF m/z calcd for $[M]^+$ $[C_{87}H_{86}N_6O_{12}S_2]^+$ 1471.7950, found 1471.4498

6'-(4-(Bis(4-methoxyphenyl)amino)phenyl)-2H,2'H,4H,4'H-3,3'-spirobi[thieno[3,4-b][1,4]dioxepine]-6,8'-dicarbaldehyde, 10: Compound 10 was synthesized from the reported procedure.[57]

(E)-2-(((Z)-5-(6'-(4-(Bis(4-methoxyphenyl)amino)phenyl)-6,8'-diformyl-2H,2'H,4H,4'H-3,3'-spirobi[thieno[3,4-b][1,4]dioxepin]-8-yl)-1,3,3-trimethylindolin-2-ylidene)methyl)-4-((1-hexyl-3,3-dimethyl-3H-indol-1-ium-2-yl)methylene)-3-oxocyclobut-1-en-1-olate, 11: A mixture of **10** (70 mg, 0.091 mmol), **3** (0.052 g, 0.091 mmol), K_2CO_3 (0.031 g, 0.223 mmol), Pd(OAc)$_2$ (0.5 mol%), PCy$_3$ (0.5 mol%), and PivOH (0.15 mol%) were taken in a Schlenk tube under nitrogen atmosphere. Dry DMA (5 mL) was added to that and kept the reaction at 120 °C temperature under the same atmosphere for 24 h. The reaction mixture was washed with 150 mL of water and extracted with 100 mL of CH_2Cl_2. Solvents were removed under reduced pressure and purified by column chromatography by using ethyl acetate and pet. ether as an eluent. Yield: 58 mg, 32%. ^{1}H NMR (400 MHz, CDCl$_3$) δ: 0.85-0.91 (m, 3 H), 1.27 – 1.39 (m, 8 H), 1.82 (s, 12 H), 3.54 (s, 3 H), 3.83 (s, 6 H), 4.01 – 4.12 (m, 2 H), 4.25 – 4.43 (m, 8 H), 5.93 -6.06 (m, 2 H), 6.88 – 6.95 (m, 4 H), 7.02- 7.05 (m, 2 H), 7.07 - 7.14 (m, 4 H), 7.36 – 7.41 (m, 4 H), 7.54- 7.66 (m, 3 H), 7.54 – 7.63 (m, 2 H) , 9.96 (t, $J=4$ Hz, 1 H), 10.05 (d, $J=4$ Hz, 1 H).^{13}C NMR (125 MHz, CDCl$_3$) δ: 13.9, 22.5, 26.1, 26.3, 26.8, 26.9, 27.3, 29.7, 31.5, 35.4, 43.8, 44.1, 48.5, 49.1, 49.5, 49.8, 50.5, 70.7, 71.2, 71.4, 76.6, 76.9, 77.3, 86.9, 87.1, 87.3, 87.7, 108.8, 109.3, 109.6, 109.7, 121.1, 122.4, 124.5, 126.5, 126.6, 127.5, 133.3, 136.6, 141.6, 148.2, 142.4, 168.5, 169.7, 170.7, 178.8, 180.0, 182.3. MALDI-TOF m/z calcd for $[M + K]^+$ $[C_{68}H_{65}N_3O_{10}S_2+K]$ 1186.3748, found 1186.8379.

D$_1$-D$_{sq}$, 12: A mixture of **11** (80mg, 0.04 mmol), cyanoacetic acid (0.022g, 0.262 mmol), ammonium acetate (0.05g, 0.0304 mmol) and glacial acetic acid (10 mL) was heated under reflux for 12 h during which time the aldehyde is completely consumed as indicated by TLC. Reaction mixture was washed with water and Et$_2$O thoroughly. Yield: 126 mg, 48%. Mp 201-207 °C; FT-IR (dry film, cm^{-1}): 2960-2852 (br), 2313 (w), 2203 (w), 1678 (s), 1588 (s), 1491 (m); ^{1}H NMR (500 MHz, DMSO-d_6) 0.79-0.84 (m, 3 H), 1.23-1.29 (m, 10 H), 1.74 (s, 12 H), 3.65 (s, 3 H), 3.75 (s, 6 H), 4.07- 4.41 (m, 8 H), 5.77-5.87 (m, 2 H), 6.93- 6.97 (m, 2 H), 7.13 - 7.18 (m, 6 H), 7.25 -7.28 (m, 5 H), 7.34- 7.41 (m, 4 H), 7.52 - 7.56 (m, 2 H), 8.08 - 8.16 (m, 2 H). δ: ^{13}C NMR (125 MHz, DMSO-d_6) δ: 19.0, 26.2, 27.3, 31.0, 32, 33.8, 34.2, 36.1, 36.4, 40, 50, 50.2, 60.4, 76.6, 76.8, 76.9, 77.3, 84.2, 84.4, 91.8, 98.3, 120.3, 120.4, 122.9, 127.5, 127.6, 131, 132.1, 132.5, 132.7, 132.8, 133.6, 146.8, 147.0, 147.3, 150.6, 151, 152.5, 161.4, 169.7, 177.3, 185.9.

3.5 References

(1) O'Regan, B.; Grätzel, M. A Low-Cost, High-Efficiency Solar Cell Based on Dye-Sensitized Colloidal TiO$_2$ Films. *Nature* **1991**, *353*, 737–740.

(2) Yao, Z.; Zhang, M.; Wu, H.; Yang, L.; Li, R.; Wang, P. Donor/Acceptor Indenoperylene Dye for Highly Efficient Organic Dye-Sensitized Solar Cells. *J. Am. Chem. Soc.* **2015**, *137*, 3799–3802.

(3) Alagumalai, A.; Kavungathodi, M. F. M.;Vellimalai, P.; Sil, M. C.; Nithyanandhan, J. Effect of Out-of-Plane Alkyl Group's Position in Dye-Sensitized Solar Cell Efficiency: A Structure–Property Relationship Utilizing Indoline-Based Unsymmetrical Squaraine Dyes. *ACS Appl. Mater. Interfaces* **2016**, *8*, 35353–35367.

(4)   Liang, M.; Chen, J. Arylamine Organic Dyes for Dye-Sensitized Solar Cells. *Chem. Soc. Rev.* **2013**, *42*, 3453–3488.

(5)   Liang, M.; Xu, W.; Cai, F.; Chen, P.; Peng, B.; Chen, J.; Li, Z. New Triphenylamine-Based Organic Dyes for Efficient Dye-Sensitized Solar Cells. *J. Phys. Chem. C* **2007**, *111*, 4465–4472.

(6)   Treibs, A.; Jacob, K. Cyclotrimethine Dyes Derived from Squaric Acid. *Angew. Chem. Int. Ed. Engl.* **1965**, *4*, 694–694.

(7)   Beverina, L.; Ruffo, R.; Mari, C. M.; Pagani, G. A.; Sassi, M.; De Angelis, F.; Fantacci, S.; Yum, J.-H.; Grätzel, M.; Nazeeruddin, M. K. Panchromatic Cross-Substituted Squaraines for Dye-Sensitized Solar Cell Applications. *ChemSusChem* **2009**, *2*, 621–624.

(8)   Park, J.; Barbero, N.; Yoon, J.; Del′Orto, E.; Galliano, S.; Borrelli, R.; Yum, J.-H.; Censo, D. D.; Grätzel, M.; Nazeeruddin, M. K.; et al. Panchromatic Symmetrical Squaraines: A Step Forward in the Molecular Engineering of Low Cost Blue-Greenish Sensitizers for Dye-Sensitized Solar Cells. *Phys. Chem. Chem. Phys.* **2014**, *16*, 24173–24177.

(9)   Mathew, S.; Yella, A.; Gao, P.; Humphry-Baker, R.; Curchod, B. F. E.; Ashari-Astani, N.; Tavernelli, I.; Rothlisberger, U.; Nazeeruddin, M. K.; Grätzel, M. Dye-Sensitized Solar Cells with 13% Efficiency Achieved through the Molecular Engineering of Porphyrin Sensitizers. *Nat. Chem.* **2014**, *6*, 242–247.

(10) Connell, A.; Holliman, P. J.; Davies, M. L.; Gwenin, C. D.; Weiss, S.; Pitak, M. B.; Horton, P. N.; Coles, S. J.; Cooke, G. A Study of Dye Anchoring Points in Half-Squarylium Dyes for Dye-Sensitized Solar Cells. *J. Mater. Chem. A* **2014**, *2*, 4055–4066.

(11) Mishra, A.; Fischer, M. K. R.; Bäuerle, P. Metal-Free Organic Dyes for Dye-Sensitized Solar Cells: From Structure: Property Relationships to Design Rules. *Angew. Chem. Int. Ed.* **2009**, *48*, 2474–2499.

(12) Gong, J.; Liang, J.; Sumathy, K. Review on Dye-Sensitized Solar Cells (DSSCs): Fundamental Concepts and Novel Materials. *Renew. Sustain. Energy Rev.* **2012**, *16*, 5848–5860.

(13) Li, X.; Zheng, Z.; Jiang, W.; Wu, W.; Wang, Z.; Tian, H. New D–A–π–A Organic Sensitizers for Efficient Dye-Sensitized Solar Cells. *Chem. Commun.* **2015**, *51*, 3590–3592.

(14) Yella, A.; Lee, H.-W.; Tsao, H. N.; Yi, C.; Chandiran, A. K.; Nazeeruddin, M. K.; Diau, E. W.-G.; Yeh, C.-Y.; Zakeeruddin, S. M.; Grätzel, M. Porphyrin-Sensitized Solar Cells with Cobalt (II/III)-Based Redox Electrolyte Exceed 12 Percent Efficiency. *Science* **2011**, *334*, 629–634.

(15) Urbani, M.; Grätzel, M.; Nazeeruddin, M. K.; Torres, T. Meso-Substituted Porphyrins for Dye-Sensitized Solar Cells. *Chem. Rev.* **2014**, *114*, 12330–12396.

(16) Tang, Y.; Wang, Y.; Li, X.; Ågren, H.; Zhu, W.-H.; Xie, Y. Porphyrins Containing a Triphenylamine Donor and up to Eight Alkoxy Chains for Dye-Sensitized Solar Cells: A High Efficiency of 10.9%. *ACS Appl. Mater. Interfaces* **2015**, *7*, 27976–27985.

(17) Imahori, H.; Umeyama, T.; Ito, S. Large π-Aromatic Molecules as Potential Sensitizers for Highly Efficient Dye-Sensitized Solar Cells. *Acc. Chem. Res.* **2009**, *42*, 1809–1818.

(18) Higashino, T.; Imahori, H. Porphyrins as Excellent Dyes for Dye-Sensitized Solar Cells: Recent Developments and Insights. *Dalton Trans.* **2014**, *44*, 448–463.

(19) Ince, M.; Yum, J.-H.; Kim, Y.; Mathew, S.; Grätzel, M.; Torres, T.; Nazeeruddin, M. K. Molecular Engineering of Phthalocyanine Sensitizers for Dye-Sensitized Solar Cells. *J. Phys. Chem. C* **2014**, *118*, 17166–17170.

(20) Saccone, D.; Galliano, S.; Barbero, N.; Quagliotto, P.; Viscardi, G.; Barolo, C. Polymethine Dyes in Hybrid Photovoltaics: Structure–Properties Relationships. *Eur. J. Org. Chem.* **2016**, *2016*, 2244–2259.

(21) Imahori, H.; Umeyama, T.; Ito, S. Large π-Aromatic Molecules as Potential Sensitizers for Highly Efficient Dye-Sensitized Solar Cells. *Acc. Chem. Res.* **2009**, *42*, 1809–1818.

(22) Imahori, H.; Kang, S.; Hayashi, H.; Haruta, M.; Kurata, H.; Isoda, S.; Canton, S. E.; Infahsaeng, Y.; Kathiravan, A.; Pascher, T.; et al. Photoinduced Charge Carrier Dynamics of Zn−Porphyrin−TiO$_2$ Electrodes: The Key Role of Charge Recombination for Solar Cell Performance. *J. Phys. Chem. A* **2011**, *115*, 3679–3690.

(23) Higashino, T.; Imahori, H. Porphyrins as Excellent Dyes for Dye-Sensitized Solar Cells: Recent Developments and Insights. *Dalton Trans.* **2014**, *44*, 448–463.

(24) Galoppini, E.; Guo, W.; Zhang, W.; Hoertz, P. G.; Qu, P.; Meyer, G. J. Long-Range Electron Transfer across Molecule−Nanocrystalline Semiconductor Interfaces Using Tripodal Sensitizers. *J. Am. Chem. Soc.* **2002**, *124*, 7801–7811.

(25) Piotrowiak, P.; Galoppini, E.; Wei, Q.; Meyer, G. J.; Wiewiór, P. Subpicosecond Photoinduced Charge Injection from "Molecular Tripods" into Mesoporous TiO_2 Over the Distance of 24 Angstroms. *J. Am. Chem. Soc.* **2003**, *125*, 5278–5279.

(26) Hagberg, D. P.; Marinado, T.; Karlsson, K. M.; Nonomura, K.; Qin, P.; Boschloo, G.; Brinck, T.; Hagfeldt, A.; Sun, L. Tuning the HOMO and LUMO Energy Levels of Organic Chromophores for Dye Sensitized Solar Cells. *J. Org. Chem.* **2007**, *72*, 9550–9556.

(27) Liu, W.-H.; Wu, I.-C.; Lai, C.-H.; Lai, C.-H.; Chou, P.-T.; Li, Y.-T.; Chen, C.-L.; Hsu, Y.-Y.; Chi, Y. Simple Organic Molecules Bearing a 3,4-Ethylenedioxythiophene Linker for Efficient Dye-Sensitized Solar Cells. *Chem. Commun.* **2008**, *0*, 5152–5154.

(28) Seo, K. D.; You, B. S.; Choi, I. T.; Ju, M. J.; You, M.; Kang, H. S.; Kim, H. K. Dual-Channel Anchorable Organic Dyes with Well-Defined Structures for Highly Efficient Dye-Sensitized Solar Cells. *J. Mater. Chem. A* **2013**, *1*, 9947–9953.

(29) Leandri, V.; Ruffo, R.; Trifiletti, V.; Abbotto, A. Asymmetric Tribranched Dyes: An Intramolecular Cosensitization Approach for Dye-Sensitized Solar Cells. *Eur. J. Org. Chem.* **2013**, *2013*, 6793–6801.

(30) Baheti, A.; Thomas, K. R. J.; Lee, C.-P.; Ho, K.-C. Synthesis and Characterization of Dianchoring Organic Dyes Containing 2,7-Diaminofluorene Donors as Efficient Sensitizers for Dye-Sensitized Solar Cells. *Org. Electron.* **2013**, *14*, 3267–3276.

(31) Zhang, H.; Fan, J.; Iqbal, Z.; Kuang, D.-B.; Wang, L.; Meier, H.; Cao, D. Novel Dithieno[3,2-b:2′,3′-d]Pyrrole-Based Organic Dyes with High Molar Extinction Coefficient for Dye-Sensitized Solar Cells. *Org. Electron.* **2013**, *14*, 2071–2081.

(32) Ren, X.; Jiang, S.; Cha, M.; Zhou, G.; Wang, Z.-S. Thiophene-Bridged Double D-π-A Dye for Efficient Dye-Sensitized Solar Cell. *Chem. Mater.* **2012**, *24*, 3493–3499.

(33) Shiu, J.-W.; Chang, Y.-C.; Chan, C.-Y.; Wu, H.-P.; Hsu, H.-Y.; Wang, C.-L.; Lin, C.-Y.; Diau, E. W.-G. Panchromatic Co-Sensitization of Porphyrin-Sensitized Solar Cells to Harvest near-Infrared Light beyond 900 Nm. *J. Mater. Chem. A* **2014**, *3*, 1417–1420.

(34) Holliman, P. J.; Mohsen, M.; Connell, A.; Davies, M. L.; Al-Salihi, K.; Pitak, M. B.; Tizzard, G. J.; Coles, S. J.; Harrington, R. W.; Clegg, W.; Serpa, C.; Fontes, O. H.; Charbonneau, C.; Carnie, M. J. Ultra-Fast Co-Sensitization and Tri-Sensitization of Dye-Sensitized Solar Cells with N719, SQ1 and Triarylamine Dyes. *J. Mater. Chem.* **2012**, *22*, 13318–13327.

(35) Han, L.; Islam, A.; Chen, H.; Malapaka, C.; Chiranjeevi, B.; Zhang, S.; Yang, X.; Yanagida, M. High-Efficiency Dye-Sensitized Solar Cell with a Novel Co-Adsorbent. *Energy Environ. Sci.* **2012**, *5*, 6057–6060.

(36) Kimura, M.; Nomoto, H.; Masaki, N.; Mori, S. Dye Molecules for Simple Co-Sensitization Process: Fabrication of Mixed-Dye-Sensitized Solar Cells. *Angew. Chem. Int. Ed.* **2012**, *51*, 4371–4374.

(37) Cid, J.-J.; Yum, J.-H.; Jang, S.-R.; Nazeeruddin, M. K.; Martínez-Ferrero, E.; Palomares, E.; Ko, J.; Grätzel, M.; Torres, T. Molecular Cosensitization for Efficient Panchromatic Dye-Sensitized Solar Cells. *Angew. Chem.* **2007**, *119*, 8510–8514.

(38) Islam, A.; Chowdhury, T. H.; Qin, C.; Han, L.; Lee, J.-J.; Bedja, I. M.; Akhtaruzzaman, M.; Sopian, K.; Mirloup, A.; Leclerc, N. Panchromatic Absorption of Dye Sensitized Solar Cells by Co-Sensitization of Triple Organic Dyes. *Sustain. Energy Fuels* **2017**, *2*, 209–214.

(39) Kolemen, S.; Altan Bozdemir, O.; Cakmak, Y.; Barin, G.; Erten-Ela, S.; Marszalek, M.; Yum, J.-H.; M. Zakeeruddin, S.; K. Nazeeruddin, M.; Grätzel, M.; et al. Optimization of Distyryl-Bodipy Chromophores for Efficient Panchromatic Sensitization in Dye Sensitized Solar Cells. *Chem. Sci.* **2011**, *2*, 949–954.

(40) Shi, Y.; Hill, R. B. M.; Yum, J.-H.; Dualeh, A.; Barlow, S.; Grätzel, M.; Marder, S. R.; Nazeeruddin, M. K. A High-Efficiency Panchromatic Squaraine Sensitizer for Dye-Sensitized Solar Cells. *Angew. Chem.* **2011**, *123*, 6749–6751.

(41) Holliman, P. J.; Davies, M. L.; Connell, A.; Velasco, B. V.; Watson, T. M. Ultra-Fast Dye Sensitisation and Co-Sensitisation for Dye Sensitized Solar Cells. *Chem. Commun.* **2010**, *46*, 7256–7258.

(42) Xue, Z.; Wang, L.; Liu, B. Facile Fabrication of Co-Sensitized Plastic Dye-Sensitized Solar Cells Using Multiple Electrophoretic Deposition. *Nanoscale* **2013**, *5*, 2269–2273.

(43) Hardin, B. E.; Sellinger, A.; Moehl, T.; Humphry-Baker, R.; Moser, J.-E.; Wang, P.; Zakeeruddin, S. M.; Grätzel, M.; McGehee, M. D. Energy and Hole Transfer between Dyes Attached to Titania in Cosensitized Dye-Sensitized Solar Cells. *J. Am. Chem. Soc.* **2011**, *133*, 10662–10667.

(44) Li, J.-H.; Gryn′ova, G.; Prlj, A.; Corminboeuf, C. Enhancing the Power Conversion Efficiency of Dye-Sensitized Solar Cells via Molecular Plasmon-like Excitations. *Chem. Commun.* **2017**, *53*, 2423–2426.

(45) Fujisawa, J. Large Impact of Reorganization Energy on Photovoltaic Conversion Due to Interfacial Charge-Transfer Transitions. *Phys. Chem. Chem. Phys.* **2015**, *17*, 12228–12237.

(46) Fujisawa, J.; Hanaya, M. Light Harvesting and Direct Electron Injection by Interfacial Charge-Transfer Transitions between TiO_2 and Carboxy-Anchor Dye LEG4 in Dye-Sensitized Solar Cells. *J. Phys. Chem. C* **2018**, *122*, 8–15.

(47) Fujisawa, J.; Nagata, M.; Hanaya, M. Charge-Transfer Complex versus σ-Complex Formed between TiO_2 and Bis(Dicyanomethylene) Electron Acceptors. *Phys. Chem. Chem. Phys.* **2015**, *17*, 27343–27356.

(48) Fujisawa, J.; Muroga, R.; Hanaya, M. Interfacial Charge-Transfer Transitions in a TiO_2-Benzenedithiol Complex with Ti–S–C Linkages. *Phys. Chem. Chem. Phys.* **2015**, *17*, 29867–29873.

(49) Jono, R.; Fujisawa, J.; Segawa, H.; Yamashita, K. Theoretical Study of the Surface Complex between TiO_2 and TCNQ Showing Interfacial Charge-Transfer Transitions. *J. Phys. Chem. Lett.* **2011**, *2*, 1167–1170.

(50) Nieto-Pescador, J.; Abraham, B.; Li, J.; Batarseh, A.; Bartynski, R. A.; Galoppini, E.; Gundlach, L. Heterogeneous Electron-Transfer Dynamics through Dipole-Bridge Groups. *J. Phys. Chem. C* **2016**, *120*, 48–55.

(51) Ngo, K. T.; Rochford, J.; Fan, H.; Batarseh, A.; Chitre, K.; Rangan, S.; Bartynski, R. A.; Galoppini, E. Photoelectrochemical Properties of Porphyrin Dyes with a Molecular Dipole in the Linker. *Faraday Discuss.* **2015**, *185*, 497–506.

(52) Rangan, S.; Batarseh, A.; Chitre, K. P.; Kopecky, A.; Galoppini, E.; Bartynski, R. A. Tuning Energy Level Alignment At Organic/Semiconductor Interfaces Using a Built-In Dipole in Chromophore–Bridge–Anchor Compounds. *J. Phys. Chem. C* **2014**, *118*, 12923–12928.

(53) Chitre, K.; Batarseh, A.; Kopecky, A.; Fan, H.; Tang, H.; Lalancette, R.; Bartynski, R. A.; Galoppini, E. Synthesis of Zinc Tetraphenylporphyrin Rigid Rods with a Built-In Dipole. *J. Phys. Chem. B* **2015**, *119*, 7522–7530.

(54) Ronca, E.; Pastore, M.; Belpassi, L.; Tarantelli, F.; Angelis, F. D. Influence of the Dye Molecular Structure on the TiO_2 Conduction Band in Dye-Sensitized Solar Cells: Disentangling Charge Transfer and Electrostatic Effects. *Energy Environ. Sci.* **2012**, *6*, 183–193.

(55) Cheng, M.; Yang, X.; Zhao, J.; Chen, C.; Tan, Q.; Zhang, F.; Sun, L. Efficient Organic Dye-Sensitized Solar Cells: Molecular Engineering of Donor–Acceptor–Acceptor Cationic Dyes. *ChemSusChem* **2013**, *6*, 2322–2329.

(56) Yum, J.-H.; Walter, P.; Huber, S.; Rentsch, D.; Geiger, T.; Nüesch, F.; De Angelis, F.; Grätzel, M.; Nazeeruddin, M. K. Efficient Far Red Sensitization of Nanocrystalline TiO$_2$ Films by an Unsymmetrical Squaraine Dye. *J. Am. Chem. Soc.* **2007**, *129*, 10320–10321.

(57) Sil, M. C.; Sudhakar, V.; Kavungathodi, M. F. M.; Punitharasu, V.; Nithyanandhan, J. Orthogonally Functionalized Donor/Acceptor Homo- and Heterodimeric Dyes for Dye-Sensitized Solar Cells: An Approach to Introduce Panchromaticity and Control the Charge Recombination. *ACS Appl. Mater. Interfaces* **2017**, *9*, 34875–34890.

(58) Jradi, F. M.; O′Neil, D.; Kang, X.; Wong, J.; Szymanski, P.; Parker, T. C.; Anderson, H. L.; El-Sayed, M. A.; Marder, S. R. A Step Toward Efficient Panchromatic Multi-Chromophoric Sensitizers for Dye Sensitized Solar Cells. *Chem. Mater.* **2015**, *27*, 6305–6313.

(59) Jiang, J.-X.; Laybourn, A.; Clowes, R.; Khimyak, Y. Z.; Bacsa, J.; Higgins, S. J.; Adams, D. J.; Cooper, A. I. High Surface Area Contorted Conjugated Microporous Polymers Based on Spiro-Bipropylenedioxythiophene. *Macromolecules* **2010**, *43*, 7577–7582.

(60) Reeves, B. d.; Thompson, B. c.; Abboud, K. a.; Smart, B. e.; Reynolds, J. r. Dual Cathodically and Anodically Coloring Electrochromic Polymer Based on a Spiro Bipropylenedioxythiophene [(Poly(SpiroBiProDOT)]. *Adv. Mater.* **2002**, *14*, 717–719.

(61) Bisht, R.; Kavungathodi, M. F. M.; Singh, A. K.; Nithyanandhan, J. Panchromatic Sensitizer for Dye-Sensitized Solar Cells: Unsymmetrical Squaraine Dyes Incorporating Benzodithiophene π-Spacer with Alkyl Chains to Extend Conjugation, Control the Dye Assembly on TiO$_2$, and Retard Charge Recombination. *J. Org. Chem.* **2017**, *82*, 1920–1930.

(62) Liang, K.; Farahat, M. S.; Perlstein, J.; Law, K.-Y.; Whitten, D. G. Exciton Interactions in Nonconjugated Squaraine Dimers. Mechanisms for Coupling and Consequences for Photophysics and Photochemistry. *J. Am. Chem. Soc.* **1997**, *119*, 830–831.

(63) Sissa, C.; Terenziani, F.; Painelli, A.; Abbotto, A.; Bellotto, L.; Marinzi, C.; Garbin, E.; Ferrante, C.; Bozio, R. Dimers of Quadrupolar Chromophores in Solution: Electrostatic Interactions and Optical Spectra. *J. Phys. Chem. B.* **2010**, *114*, 882–893.

(64) Ozawa, H.; Awa, M.; Ono, T.; Arakawa, H. Effects of Dye-Adsorption Solvent on the Performances of the Dye-Sensitized Solar Cells Based on Black Dye. *Chem. – Asian J.* **2012**, *7*, 156–162.

(65) Shivashimpi, G. M.; Pandey, S. S.; Watanabe, R.; Fujikawa, N.; Ogomi, Y.; Yamaguchi, Y.; Hayase, S. Effect of Nature of Anchoring Groups on Photosensitization Behavior in Unsymmetrical Squaraine Dyes. *J. Photochem. Photobiol. Chem.* **2014**, *273*, 1–7.

(66) Cui, Y.; Wu, Y.; Lu, X.; Zhang, X.; Zhou, G.; Miapeh, F. B.; Zhu, W.; Wang, Z.-S. Incorporating Benzotriazole Moiety to Construct D–A−π–A Organic Sensitizers for Solar Cells: Significant Enhancement of Open-Circuit Photovoltage with Long Alkyl Group. *Chem. Mater.* **2011**, *23*, 4394–4401.

Effect and Position of Spiro-Bipropylenedioxythiophene π-Spacer in Donor/Acceptor Dyes for Dye-Sensitized Solar Cell

4.1 Introduction

Photovoltaic technology (PV) is an optimistic and explored area that has accomplished with most successive growth in the last few years. Dye sensitized solar cell is one of the most important branch of emerging photovoltaic technology that has been extended into a most inexpensive energy generator and due to development of cheap and efficient components.[1] The discovery of a laboratory scale device in which homoleptic metallated ruthenium based inorganic dye was used as energy harvesting component became the first master device optimized by O'Regan and Grätzel in 1991.[2,3] A DSSC devices consists of components such as sensitizer, metal oxide semiconductor (TiO_2) coated in transparent conducting oxide, redox electrolyte, and counter electrode (fluorine doped tin oxide). First highest 7.12 % device efficiency was discovered by using ruthenium based dye and last more than two and half decades research was enriched to understand the basic mechanism of functional materials, interfacial charge transfer and recombination processes. Molecular engineering for designing the light absorbing sensitizers with panchromatic light absorption,[4–6] reduced charge recombination[7,8] and controlled dye aggregation to achieve high device efficiency have been attempted besides minimizing the charge injection and dye regeneration overpotentials.[9] The best power conversion efficiency has been achieved in zinc-porphyrin (13%)[10] and indenoperylene dye (12.5%)[11] with cobalt (II/III) redox couple electrolyte so far. High molar absorptivity, strong intramolecular charge transfer (ICT)[12] and tuneable optical and electrochemical properties are enhancing the priority of metal free dye into interesting research materials. Core structure of organic dyes is playing an important role in their photo-physical properties. For example dyes having D-π-A[13] and D-A-π-A[14] configuration showed better harvesting efficiency in visible and far-red region of the solar spectrum, on the other hand dyes consisted with polymethine,[15] porphyrin[16–20] and phthalocyanine[21] showing photo-

current efficiency in far red and near infrared regions. Intermolecular interaction in the vicinity of dye surface provoked them to aggregate which broadens the absorption spectrum.[22] The head-to-head and head-to-tail arrangements of dipoles of the dyes form H-type and J-type aggregated structure which causes blue and red shift respectively compared to monomer in the absorption spectrum.[23,24] The uncertainty has been also observed in charge injection from aggregated dye structure by which the photovoltaic parameters are also varied in different type of aggregation. It is reported to control the aggregation of dyes by using transparent CDCA with co-adsorbing dye on TiO_2.[25–27] Yet it has become a challenging task for researchers to design a light harvesting sensitizer having desired optimistic optical band gap and administrate dye aggregation, recombination and regeneration. Different type of methodology has established to increase the efficiency of dye by reducing dye aggregation and charge recombination. One of the most efficient methodologies is functionalization of dyes with bulky and linear alkyl group in spacer or donor site.[28,29] Supramolecular chemistry approach and atomic layer deposition method have been explored in controlling the dye aggregation process.[30–34] Dyes with two same or different anchoring groups were reported to control the above mentioned aggregation issues, resist charge recombination which in turn increase both the short circuit current density (J_{sc}) and open circuit photo-voltage (V_{oc}). The light harvesting efficiencies of di-anchoring dyes is remarkably greater than that of mono-anchoring dye and it can passivates the TiO_2 surface effectively to reduce the charge recombination of electrons from TiO_2 to oxidized electrolyte.[35–38] An efficient charge transfer from dye to TiO_2 through anchoring unit is essential for better device efficiency. One more important thing is that distance between two anchoring group has to close with each other and the same direction so that two groups can bind to TiO_2 simultaneously to get better open circuit photovoltage.[39] It is necessary to maintain a definite spacer length and anchoring group's position of a sensitizer for better efficiency of a cell.[40] Further dye orientation on the

surface of the TiO$_2$ plays an important role in DSSC device performance as more perpendicular orientation of the dye on the surface increases the electron life time on the conduction band.[19,20,38] In a two anchoring group containing dyes, distance between the anchoring group is important for an efficient electronic communication between dye and TiO$_2$.

In the present chapter, this critical aggregation problem was modulated by connecting two D-π-A dyes are connected through spiro-linkage and tuning the distance of two anchoring group. Hence **TT$_1$**, **T$_1$T** and **TT$_1$T** dyes have been synthesized. In these homodimeric dyes two monomeric motifs are attached orthogonally through spiro-based π-spacer. Distance between two anchoring group was tailored by changing the position of spiroBiProDOT branching unit. SpiroBiProDOT (2H,2'H,4H,4'H-3,3'-spirobi[thieno[3,4-b][1,4]dioxepine]) was selected based π-spacer where monomeric dye motif were connected and four additional sp^3-C atoms at the branching unit increase the flexibility, decrease the dye aggregation of dyes and giving better passivation of surface. There is a development of modified approach for synthesizing spiro bridged thiophene (branching unit), in which it position was shifted from nearby (**TT$_1$**) to far away (**T$_1$T**) from its anchoring group. Out of these two isomeric dyes **T$_1$T** was giving better efficiency (2.8 %) than that of **TT$_1$** (1.8 %), under simulated AM 1.5G illumination (100 mW/cm^2) without any co-adsorbent. Further a thiophene unit was incorporated in the both monomeric strand of **T$_1$T** moiety to afford **TT$_1$T**, which exhibits highest efficiency of 2.9 % out of these three dyes (V_{oc} of 0.566 V, J_{sc} of 7.20 mA/cm^2) without any co-adsorbent. After addition with 5 equivalents of CDCA with all three dyes, **TT$_1$T** was giving highest efficiency of 4.29 % (V_{oc} of 0.589 V, J_{sc} of 9.8 mA/cm^2) than that of two isomeric dyes **TT$_1$** of 2.6 % (V_{oc} of 0.568 V, J_{sc} of 6.3 mA/cm^2) and **T$_1$T** of 3.9 % (V_{oc} of 0.593 V, J_{sc} of 9.1 mA/cm^2).

4.2 Results and discussion

4.2.1. Dye design and synthesis. To understand the effect of position of branched spacer unit in a series of dimeric dyes in controlling the orientation, aggregation on TiO_2 surface **TT$_1$**, **T$_1$T** and **TT$_1$T** were designed. SpiroBiProDOT spacer showed the various conformations with respect to different substitution at the thiophene units.[42,43] The distance between two same monomeric dye strands can be modulated by changing the position of spiroBiProDOT branching unit in **TT$_1$** and **T$_1$T** (**Figure 1**). The flexibility of spiro units encourages the binding ability of both monomeric dye strands and at the same time dye molecules passivates the TiO_2 surface by which charge recombination process can be reduced. Binding of two anchoring group enhance the stability of charge on the conduction band in TiO_2 as well as charge injection process. The targeted dimeric dyes are presented in **Figure 1**.
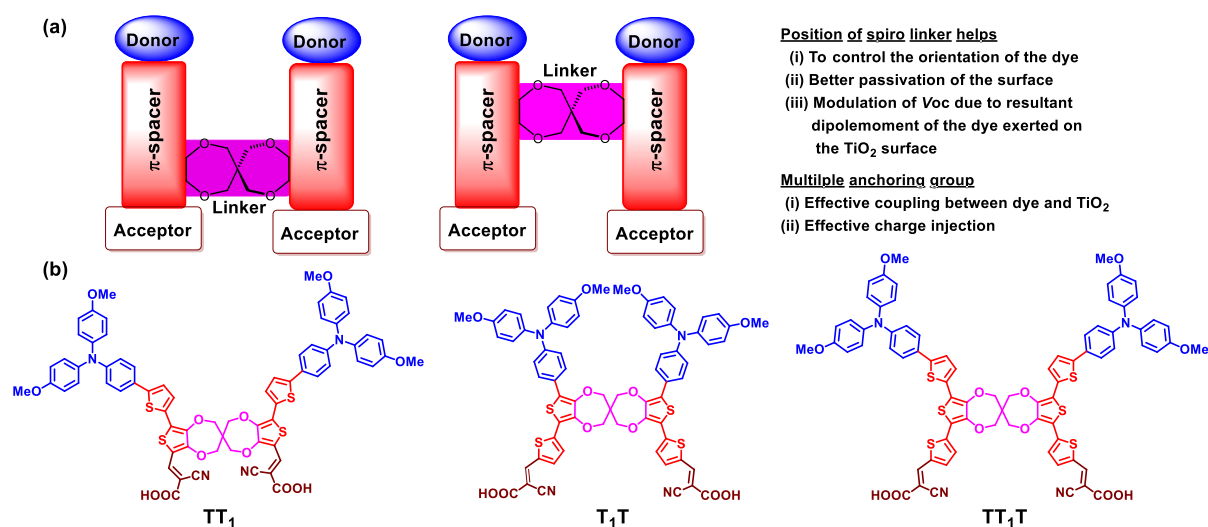
Figure 1. (a) Design of spiro- dyes and (b) molecular structures of **TT$_1$**, **T$_1$T** and **TT$_1$T**spiro dyes.

SpiroBiProDOT was synthesized from *trans*-etherification of 3, 4-dimethoxythiophene with pentaerythritol. Selective bromination and Vilsmeier-Haack formylation of spiroBiProDOT, **5** afforded the symmetric di-brominated spiroBiProDOT, **6** and mono-formylated dialdehyde, **8**, respectively. Suzuki coupling was carried out with **6** with 5-formyl 2-thienyl boronic acid with 65 % yield to afforded bithiophene dialdehyde, **7**. Precursor **2** was synthesised by literature procedure and further Suzuki coupling was done by using 2-bromo thiophene followed by bromination, precursor **4** was afforded. Symmetric homomeric **T₁T** and **TT₁T** dyes have synthesized by Pd²⁺catalyzed direct arylation reaction of suitable triaryl halide **1** and **4** with bithiophene dialdehyde, **7** to afford the corresponding aldehyde and further Knoevenagel condensation with cyanoaceticacid. Homodimeric **TT₁** was synthesized by Pd²⁺catalyzed direct arylation reaction of suitable triaryl halide, **4** with dialdehyde, **8** to afford corresponding aldehyde and further Knoevenagel condensation with cyanoaceticacid. The donor triaryl amines are attached to the aldehyde derivative of spiroBiProDOT moiety by direct arylation method using catalytic amount of Pd(OAc) ₂, PCy₃, PivOH. Yield for the synthesis dialdehyde derivative, **11** was 52%. Finally, **11** dialdehyde was condensed with cyanoaceticacid in the presence of NH₄OAc to afford the target spiro dye **T₁T** in 73% yield via a Knoevenagel reaction. Dyes **TT₁** and **TT₁T** were synthesized in moderate yields (**Scheme 1**).
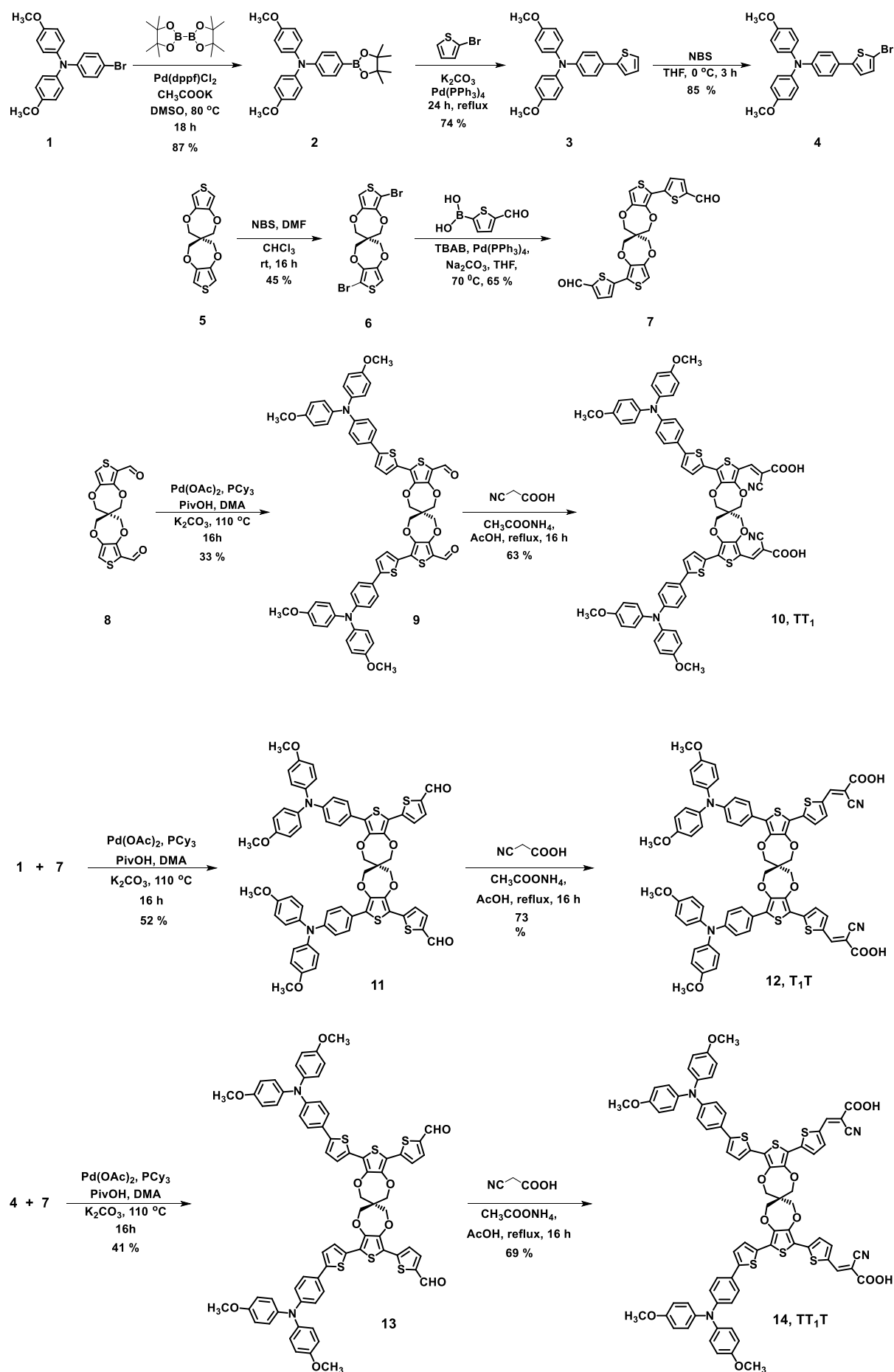
Scheme 1. Synthesis of bithiophene and terthiophene containing spiro dimeric dyes **TT₁**, **T₁T**, and **TT₁T**.

4.2.2 Photophysical properties. Optical properties of **TT₁**, **T₁T**, and **TT₁T** were recorded in solution (DMSO) and on thin mesoporous TiO_2 film. **Figure 2a** showed the absorption spectra of all the dimeric spiro-dyes (**TT₁**, **T₁T** and **TT₁T**) and the corresponding data were summarized in **Table 1**.
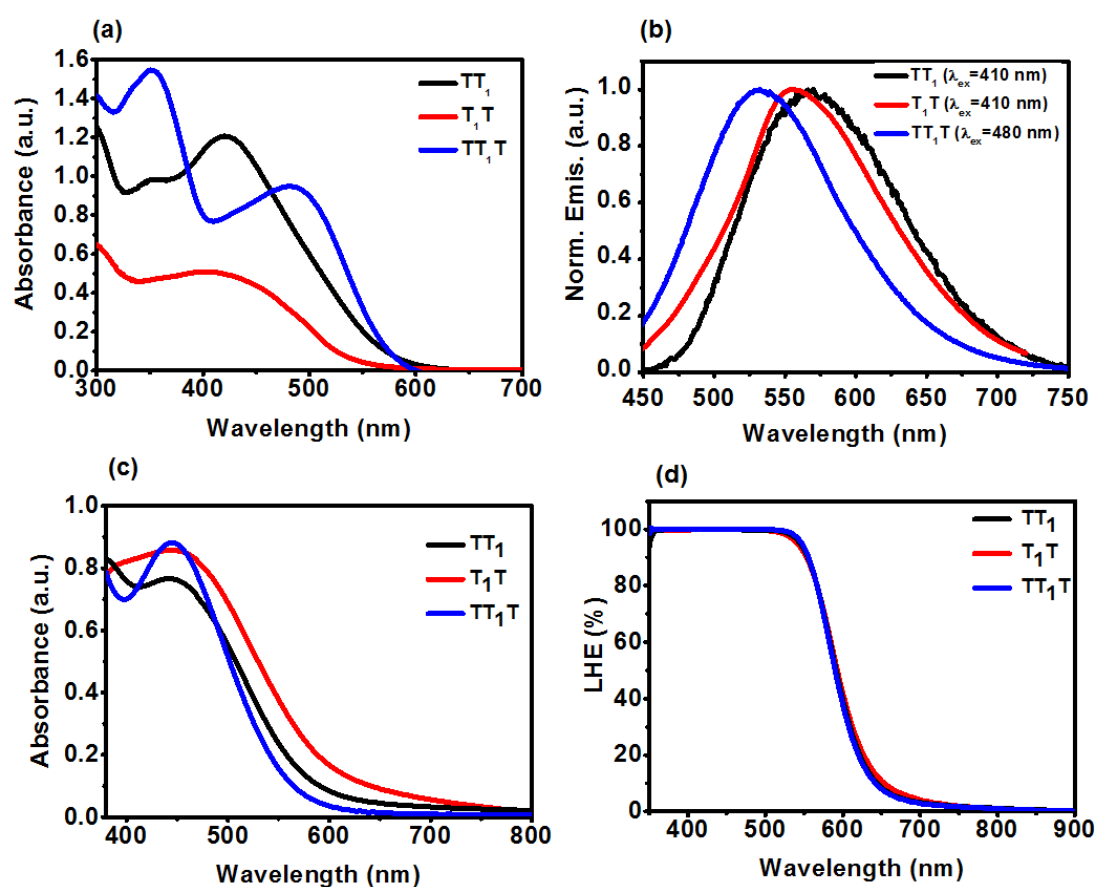
Figure 2. (a) Normalized UV-Vis absorption spectra, (b) emission spectra (c) absorption spectra on TiO_2 and (d) LHE (LHE=1−10⁻ᴬ, A = absorbance) of **TT₁**, **T₁T**, **TT₁T**.

The dye **TT₁** showed the absorption maxima of 348 nm and 421 nm are corresponding to the π-$\pi*$ transition of triarylamine group and intramolecular charge transfer (ICT) transition from

donor to acceptor respectively. While changing the position of the branching unit spiroBiProDOT away from the anchoring group, as in T_1T broad absorption spectra has been seen of absorption maxima 405 has seen due to ICT. Similar results like TT_1 has also confirmed in case of TT_1T. Here also two absorption maxima were seen at 351 and 482 nm due to same reason as explained for TT_1 (**Figure 2a**). Bathochromic shift ($\Delta\lambda = 77$ nm) was observed in TT_1T than that of TT_1 due to increase the conjugation by inserting thiophene unit in between the acceptor and spiroBiProDOT branching unit.

At the same time it is also true that inserting a thiophene unit in between the acceptor and spiroBiProDOT unit may also destroy the planarity of the molecule and hence blue shift is observed in T_1T ($\Delta\lambda = 16$ nm) compared to TT_1. Calculated molar extinction co-efficient of TT_1 is 1.4×10^4 M^{-1} cm^{-1} and 3.3×10^4 M^{-1} cm^{-1} with respect to 348 and 421 nm. Extinction co-efficient of 1.68×10^4 M^{-1} cm^{-1} was calculated for T_1T at 405 nm. Highest molar extinction co-efficient was observed ($\varepsilon = 4.7 \times10^4$ M^{-1} cm^{-1} for 482 nm and ($\varepsilon = 5.3 \times10^4$ M^{-1} cm^{-1} for 351 nm) in TT_1T. Emission spectra of TT_1, T_1T and TT_1T were found 568 nm, 554 nm and 530 nm upon excitation wavelength 410 nm, 410 nm and 480 nm respectively (**Figure 2b**).

To understand the aggregation property of spiro dyes, UV-Vis spectra of all sensitizers adsorbed on to a transparent nanocrystalline TiO_2 film was carried out (**Figure 2c**). Generally, two types of aggregation is possible upon binding with TiO_2 namely H-type and J-type, which usually results in absorption band blue shifted relative to the corresponding free monomer in solution, or edge-edge π-aggregates (J-aggregates) giving red shifted absorption band, besides deprotonation of dyes on TiO_2 surface. The ICT band of TT_1T was blue shifted ($\Delta\lambda = 37$ nm) upon binding with TiO_2, whereas both T_1T ($\Delta\lambda = 38$ nm), TT_1 ($\Delta\lambda = 23$ nm) showed red shifted transitions. Therefore it may be concluded that in T_1T and TT_1

were formed J-aggregation, whereas H-type of aggregation was observed in **TT₁T** upon

binding with TiO₂

4.2.3 Electrochemical studies. Differential pulse voltammetry (DPV) experiments on **TT₁**,

T₁T and **TT₁T** dyes were studied to understand the electron injection from the specified dye

to conduction band of TiO₂ and the efficiency of dye regeneration, which is performed in

DMSO by using 0.1 M tetra butyl ammonium perchlorate as supporting electrolyte (**Figure**

3a).
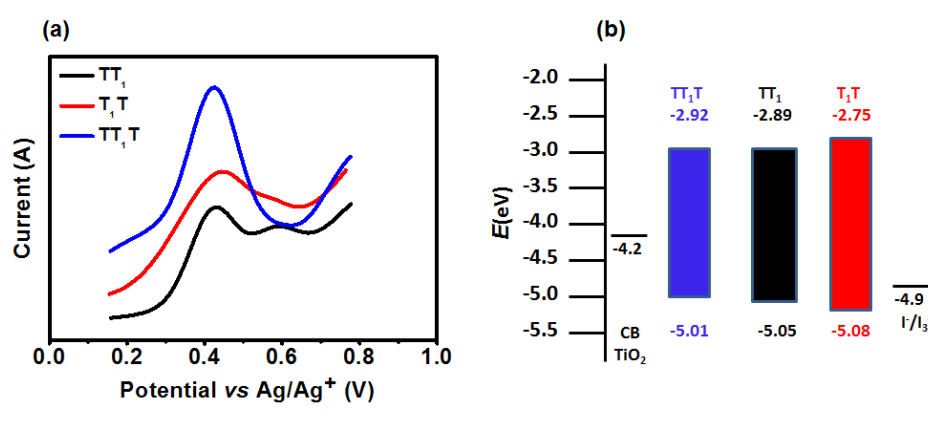
Figure 3. Electrochemical properties of three different spiro dyes. (a) differential pulse

voltammetry (DPV) and (b) schematic energy level representation of spiro-based dye cell

with various DSSC device components.

The highest occupied molecular orbital (HOMO) of all these dyes (-5.01 eV to -5.08 eV) are

lying below the energy level of I^-/I_3^- redox couple (-4.9 eV), so that the oxidized dye formed

after electron injection into the conduction band of TiO₂ can be effectively regenerated by

accepting electrons from the I^-/I_3^- redox couple. Furthermore the LUMO of the dyes (-2.75

eV to -2.92 eV) were situated above to the Fermi level of TiO₂ (- 4.2 eV) which facilitates the

efficient electron injection from the LUMO of dyes (**Figure 3b**). The zero-zero excitation (E_{0-}

0) estimated from the onset of UV-Vis absorption spectrum. E_{LUMO} energy level was calculated by subtraction of E_{0-0} from E_{HOMO}. Instead minimum overpotentials required for electron injection, around 100-150 mV, these dyes showed a significant potential loss (around 1 eV) for the LUMO to conduction band edge electron transfer.

Table 1.Photophysical and electrochemical properties of the dyes

Dye	λ_{max} (nm)[a]	λ_{max} (nm)[b] On TiO$_2$	λ_{em} (nm)[c]	$\mathcal{E}$ (10^4 $M^{-1}cm^{-1}$)	E_{HOMO}[d] (eV)	E_{LUMO}[e] (eV)	ΔE_{0-0}[f] (eV)	E_{HOMO}[g] (eV)	E_{LUMO}[g] (eV)
TT_1	348, 421	445	568	1.4, 3.3	-5.05	-2.89	2.16	-4.82	-2.91
T_1T	405	443	554	1.68	-5.08	-2.75	2.33	-4.73	-2.74
TT_1T	351, 482	445	530	5.3, 4.7	-5.01	-2.92	2.09	-4.53	-2.97

[a]Absorption maxima of dye in DMSO. [b]Absorption maxima of absorbed dye on TiO$_2$ (thickness 8 μm, dye concentration 0.3 mM in DMSO, dipping time 30 min. [c]Emission maxima of dye in DMSO (excitation wavelength TT_1, 410 nm, T_1T, 410 nm and TT_1T, 480 nm). [d]The oxidation potentials were measured by DPV in DMSO with 0.1 M TBAP as supporting electrolyte, Fc$^+$/Fc as an internal standard, scan rate 200 mV/s, potential window −0.05 to 0.55 V and supporting electrolyte is tetrabutylammonium perchlorate. HOMO energy level was calculated from ($E_{HOMO} = -\{E_p$ [Dye] $- E_{1/2}$ [Fc+/Fc]$\} + 4.8$). [e]The excited-state oxidation potentials (E_{LUMO}) for the dyes were calculated from the equation $E_{LUMO} =$

$-\{E_{\text{HOMO}} - E_{\text{g/opt}}\}$. ^{f}Experimental band gap. $^g E_{\text{HOMO}}$ and E_{LUMO} by DFT calculation (B3LYP, 6-31 G (d,p) level).

4.2.4 Computational approach. To gain a better in-depth insight in the electron distribution of spiro dye, DFT calculations were performed with Gaussian 09 programme using B3LYP/6-31 G (d,p) level. From the frontier molecular orbital calculation supported that HOMO of all the three spiro dyes, probability of electron density is maximum on amino phenyl groups whereas, in LUMO state electron density is maximum on the cyanoacrylic acid units. Thus, from this above calculation also manifesting that the LUMO consist of efficient charge transfer. The efficient photo-induced electron transfer can also be predicted from that above distribution of electron density in different optimum states. The HOMO and LUMO energy level of **TT$_1$, T$_1$T** and **TT$_1$T** are calculated from DFT (**Table 1**), which is closely related to the result obtained from DPV and UV-vis study. In **T$_1$T** and **TT$_1$**, the angle in between two monomeric dyes through sp^3- C and the distance in between allylic carbon of cyanoacetic acid were calculated from this study. It has seen that the angle between two monomeric dyes was nearly same but the distance between two allylic carbon of cyanoacetic acid in **T$_1$T** (17 Å) is higher than that of **TT$_1$** (10.1 Å) which should make an impact on binding with TiO$_2$ surface (**Figure 4**). Optimized structure of **TT$_1$T** (**Table 2**), dipole moment and dipole length of monomeric units of spiro dyes (**TT$_1$, T$_1$T, TT$_1$T**) (**Table 3**) were also calculated from DFT studies.
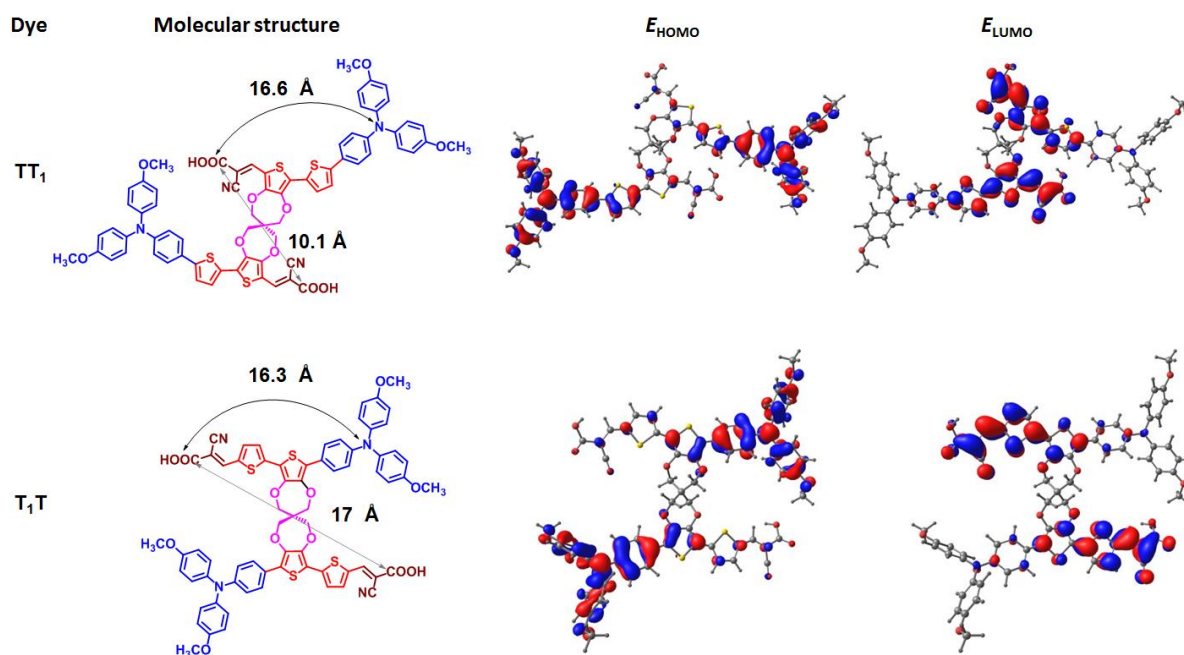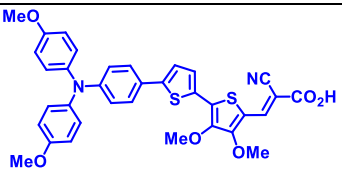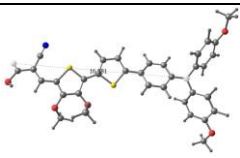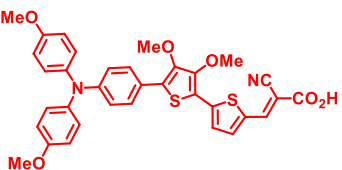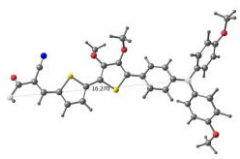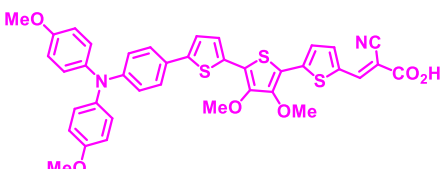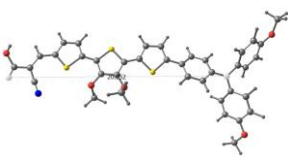
Figure 4. Dipole length of monomeric units and the distance between the carbon atom of the carboxylic group of the optimized structures of **TT$_1$** and **T$_1$T** were calculated using DFT method. E_{HOMO} (**TT$_1$**) = -4.82 eV, E_{LUMO} (**TT$_1$**) = -2.91 eV; E_{HOMO} (**T$_1$T**) = -4.73 eV, E_{LUMO} (**T$_1$T**) = -2.74 eV.

Table 2. Optimized structure of **TT$_1$T** was calculated using DFT method

Dye	Molecular orbital of HOMO	Molecular orbital of LUMO	E_{HOMO}	E_{LUMO}
TT$_1$T			-4.53	-2.97

Table 3. Dipole moment calculation of monomeric dyes by DFT method (field-independent basis).

Structure	Dipole moment (Debye)	Molecular orbital	Dipole length
	12.91		16.58 Å
	12.14		16.27 Å
	12.07		20.25 Å

Dipole length of each monomeric unit was estimated from carbonyl oxygen of –COOH group to nitrogen atom of triaryl amine).

4.2.5 Photovoltaic performance. The photocurrent density-voltage (*J-V*) measurements of the cells were carried out under an irradiance of 100 mW/cm^2 simulated AM 1.5G sunlight. Commercially available I$^-$/I$_3^-$ based electrolyte from Solaronix was used as an electrolyte. Dyes were freely soluble only in DMSO, so all the dye solution was prepared in DMSO and corresponding *J-V* characteristics are showed in **Figure 5** and **Table 4**. In comparison between two geometrically isomeric dye **T$_1$T** and **TT$_1$**, it has seen that CDCA **T$_1$T** was showed better efficiency of 2.76 % (*J*$_{sc}$= 7.21 mA/cm^2 and *V*$_{oc}$ = 0.557 V) than that of **TT$_1$** (*J*$_{sc}$= 4.77 mA/cm^2, *V*$_{oc}$ = 0.564 V and *η* =1.8 %) without CDCA. Although both having two

anchoring group but the distance between two monomeric strands are quite different because of its shifted branching (spiroBiProDOT) unit.
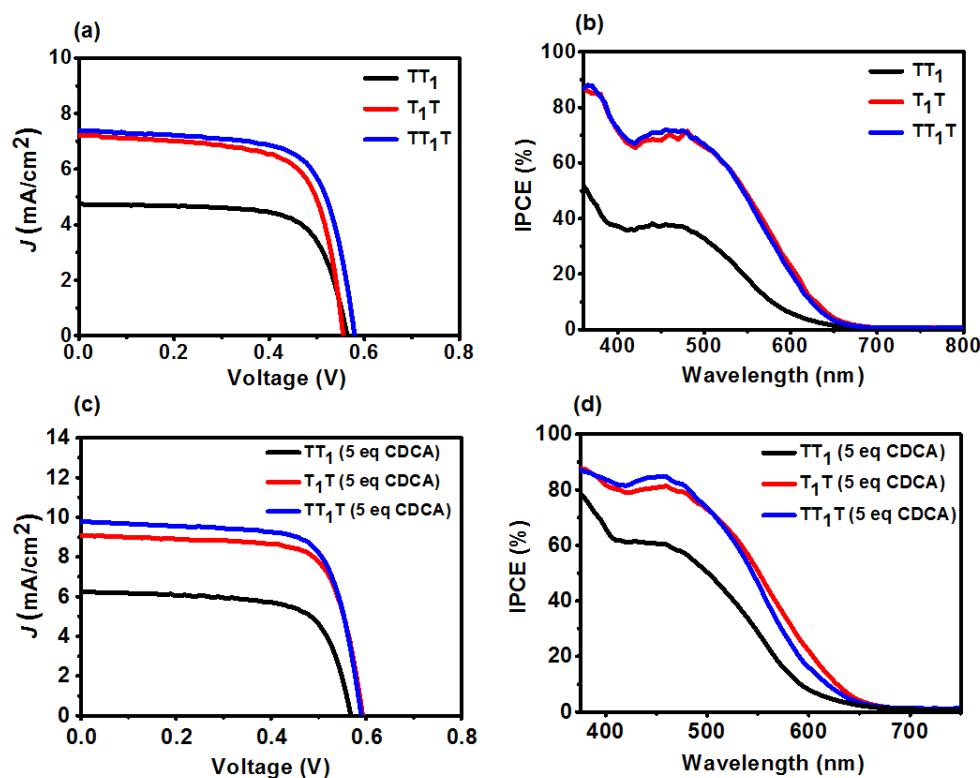
Figure 5. (a) Current density-voltage curve (dye dipping solvent mentioned in **Table 4**), and (b) IPCE of **TT₁**, **T₁T**, **TT₁T** without CDCA, (c) Current density-voltage curve of spiro dyes with 1 mM of CDCA and (d) and IPCE of **TT₁**, **T₁T**, **TT₁T** with 1 mM of CDCA in DMSO (Dye: CDCA= 1:5).

Although, inserting a thiophene unit in between acceptor and branching unit (**T₁T**) made a steric hindrance and increase the angle in between two monomeric strands and therefore increase the distance of two anchoring unit. V_{oc} of two isomeric dyes (**T₁T** and **TT₁**) are relatively same but J_{sc} is 1.5 times higher in **T₁T** than that of **TT₁** (**Figure 5a**). In **TT₁T**, where conjugation was increased by inserting another thiophene unit in between donor and branching unit showing gradually increased photovoltaic parameters of **TT₁T** (J_{sc}= 7.37

mA/cm^2, V_{oc} = 0.581 V and η = 2.96%). Results of the above discussed data indicate that the distance between two anchoring group of monomeric strands make an impact on their photovoltaic parameters.

Table 4. Photovoltaic parameters of dimeric and monomeric dyes

Dyes	J_{sc} (mA/cm^2)	V_{oc} (V)	ff (%)	PCE (%)
TT$_1$	4.69 ± 0.08	0.544 ± 0.020	70.1 ± 0.20	1.79 ± 0.10
TT$_1$/CDCA/5 eqv	6.25 ± 0.15	0.568 ± 0.023	69.1 ± 0.30	2.45 ± 0.17
TT$_1$/CDCA/10 eqv	4.65 ± 0.06	0.533 ± 0.030	69.1 ± 0.20	1.71 ± 0.12
TT$_1$/CDCA/20 eqv	3.60 ± 0.03	0.553 ± 0.015	69.5 ± 0.30	1.38 ± 0.06
T$_1$T	7.11 ± 0.10	0.547 ± 0.010	68.0 ± 0.70	2.76 ± 0.12
T$_1$T /CDCA/5 eqv	9.09 ± 0.02	0.593 ± 0.012	72.4 ± 0.10	3.92 ± 0.07
T$_1$T /CDCA/10 eqv	5.9 ± 0.04	0.565 ± 0.070	70.4 ± 0.02	2.38 ± 0.02
T$_1$T /CDCA/20 eqv	4.43 ± 0.11	0.571 ± 0.008	71.2 ± 0.50	1.80 ± 0.08
TT$_1$T	7.20 ± 0.17	0.566 ± 0.015	69.2 ± 0.30	2.82 ± 0.14
TT$_1$T/CDCA/5 eqv	9.79 ± 0.12	0.589 ± 0.010	72.1 ± 0.20	4.16 ± 0.13
TT$_1$T/CDCA/10 eqv	7.32 ± 0.15	0.571 ± 0.011	72.0 ± 0.20	3.01 ± 0.12
TT$_1$T /CDCA/20 eqv	4.41 ± 0.20	0.561 ± 0.020	71.5 ± 0.30	1.92 ± 0.15

TiO$_2$ thickness 8+5 μm and 0.235 cm^2, [dye] = 0.2 mM, dipping solvent DMSO, dipping time 12 h, under AM 1.5 illumination (100 mW/cm^2)

By using 5 equivalent of CDCA as a co-absorbent on **TT$_1$**, the J_{sc} (6.25 mA/cm^2), V_{oc} (0.568 V) are increased and giving 2.45 % cell efficiency. Similar observation also has seen in **T$_1$T** where J_{sc}, V_{oc} are increased up to 9.09 mA/cm^2 and 0.593 V respectively and giving 3.92 % cell efficiency (**Figure 5c**). Maximum cell efficiency were standardised in **TT$_1$T** of 4.16 % (J_{sc}= 9.79 mA/cm^2 and V_{oc} = 0.589 V). With increasing CDCA equivalent of CDCA the V_{oc} comparatively remained same but J_{sc} and PCE were gradually decreased for three dyes (**Table 4**, **Figure 5b**), due to competitive binding of CDCA over the dyes. Better orientation of **T$_1$T** may be the reason for enhanced V_{oc} and J_{sc}.[20,41,44,45] Photo-current density and IPCE curve of all spiro dyes by using 10 equivalents and 20 equivalents of CDCA has shown in **Figure 6**.
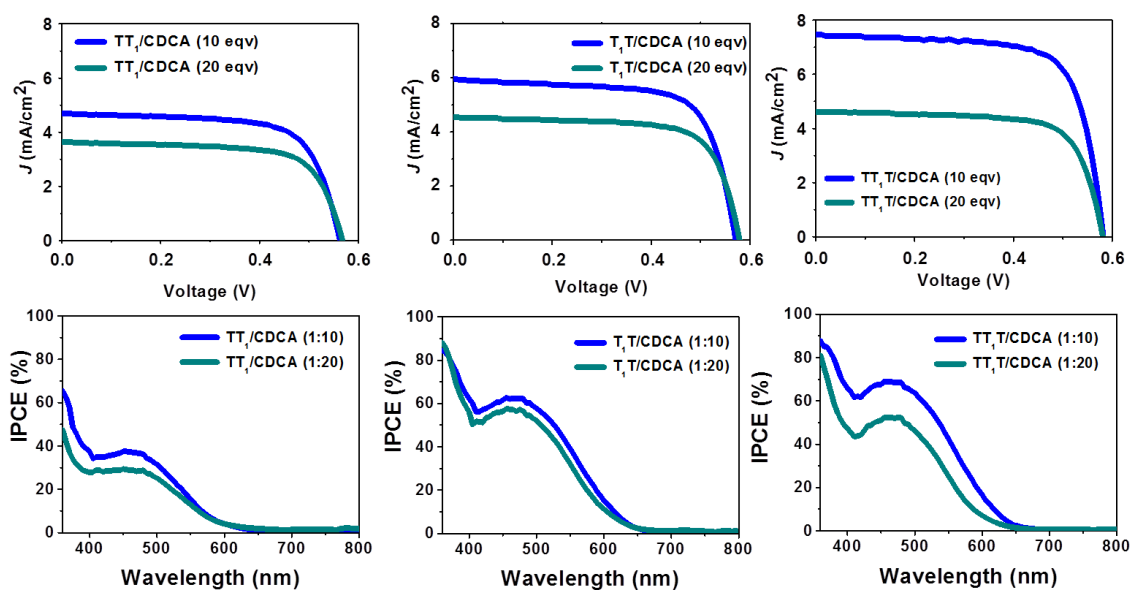
Figure 6. Current density-voltage curve (dye dipping solvent mentioned in **Table 4**), and IPCE of **TT$_1$**, **T$_1$T**, **TT$_1$T** with 10 and 20 equivalents of CDCA.

The change in V_{oc} can be explained on the basis of (i) reduced charge recombination and (ii) resultant dipole moment of the dimeric dye on the TiO$_2$ surface that upshift the conduction band of TiO$_2$.[46–51] Considering the similar passivating property of spiro-spacer,

the increased V_{oc} can be explained on the basis of resultant dipole moment of the dye exerted on the TiO_2 surface. In a D-π-A dye, the negative pole of dye is located near to TiO_2 surface upon anchoring, which leads to a positive dipole moment (pole pointing from negative to positive direction). This positive dipole normal to the surface can induce upshift in the conduction-band potential of the TiO_2 electrode to increase the V_{oc} of a DSSC device (**Equation 1**).[52–58] In the case of **TT₁** and **T₁T**, the degree of freedom for anchoring for the later dye is more. Depending on the available anchoring site at the anatase 101 facet, **T₁T** dye can have either **Figure 7b** or **Figure 7c** mode of anchoring.
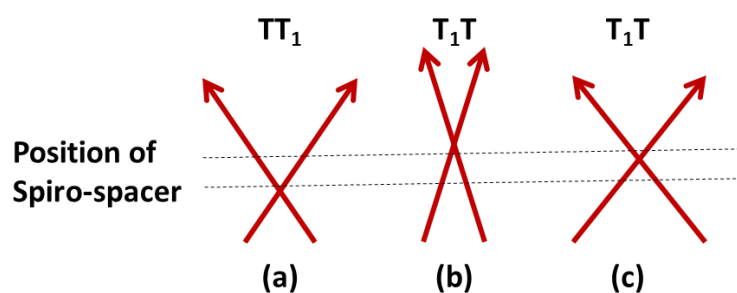
Figure 7. General proposed mechanism of binding affinity of **T₁T** and **TT₁** dyes on TiO_2 surface (DFT calculated dipole moment of monomeric unit of **TT₁**, **T₁T** and **TT₁T** dyes are 12.91 D, 12.14 D and 12.07 D, respectively).

However for **TT₁** dye, due to the close proximity of branching unit and TiO_2 surface, it can have one specific mode of anchoring. Hence the resultant dipole moment exerted by the **T₁T** dye may increase in the case of **Figure 7b** or similar to **TT₁** in the case of **Figure 7c**. As the dipole moment of the sensitizers modulates the V_{oc} of a DSSC device, the photovoltaic results can be correlated with the resultant dipole moment exerted by the **T₁T**, **TT₁** and **TT₁T** dyes on the surface. Further, in a dimeric dye, the inter- and intramolecular interactions plays an important role in defining the V_{oc} of the device, the intermolecular interactions can be

diminished by the addition of co-adsorbents and the intramolecular interactions can be modulated by the changing the dye with different dipole lengths. The V_{oc} for the **T₁T** and **TT₁** devices were 557 mV and 564 mV, respectively in the absence of CDCA, and significantly increased (48 mV for **T₁T** and 27 mV for **TT₁**) in the presence of 5 equivalent of CDCA.

$$\Delta CB = - q\mu_{normal}\gamma/\varepsilon_o\varepsilon \qquad\qquad (1)$$

Where, q is the electron charge, γ measures the dye's surface concentration, and μ_{normal} is the component of the dipole moment of the individual molecule perpendicular to the TiO₂ surface. ε_o and ε are the dielectric constant of the monolayer and the permittivity of the vacuum, respectively. The maximum V_{oc} was obtained in **TT₁T**, which is 24 mV and 15 mV is higher than that of **T₁T** and **TT₁**, respectively. The long dipole of each monomeric strand of **TT₁T** makes high resultant dipole moment (μ_{normal}) on TiO₂ surface. This is the reason of upward shifting of conduction band and consequently giving high V_{oc} in case of **TT₁T** dye.

Incident photon-to-electron conversion efficiencies (IPCE) of isomeric dyes (**TT₁** and **T₁T**) and **TT₁T** were recorded to understand the conversion efficiency of spiro dyes on TiO₂; corresponding profiles are shown in **Figure 5d**. **TT₁** show IPCE of 39% at 442 nm, whereas **T₁T** was optimized at 70 % at 481 nm. Maximum enhancement of IPCE was observed in **TT₁T** (72% at 462 nm). The origin of 1.5 fold higher J_{sc} of **T₁T** can be correlates with this significant enhancement of photon-to-electron conversion, where PCE of **TT₁T** and **T₁T** are 58 and 54 % higher than that of **TT₁** (**Table 4**) without using any co-adsorbent (CDCA). Addition of 5 equivalent of CDCA enhances both V_{oc} and J_{sc} due to diminished intermolecular π-π interactions. The increment in IPCE response was more for **T₁T** (81% at 450 nm) and **TT₁T** dyes (85% at 450 nm) than **TT₁** dye (60% at 450 nm). Further addition of CDCA resulted decrease J_{sc} due to the reduction of dye concentration on the surface.

4.2.6 Electrochemical Impedance Spectroscopy. Impedance analysis was carried out to justify the significant improvement in V_{oc} and J_{sc} of **TT$_1$T** which results in 1.6 and 1.5 fold increases in PCE than **TT$_1$** and **T$_1$T** respectively. The Nyquist plots of three dyes at 0.47 V are shown in **Figure 8a**.
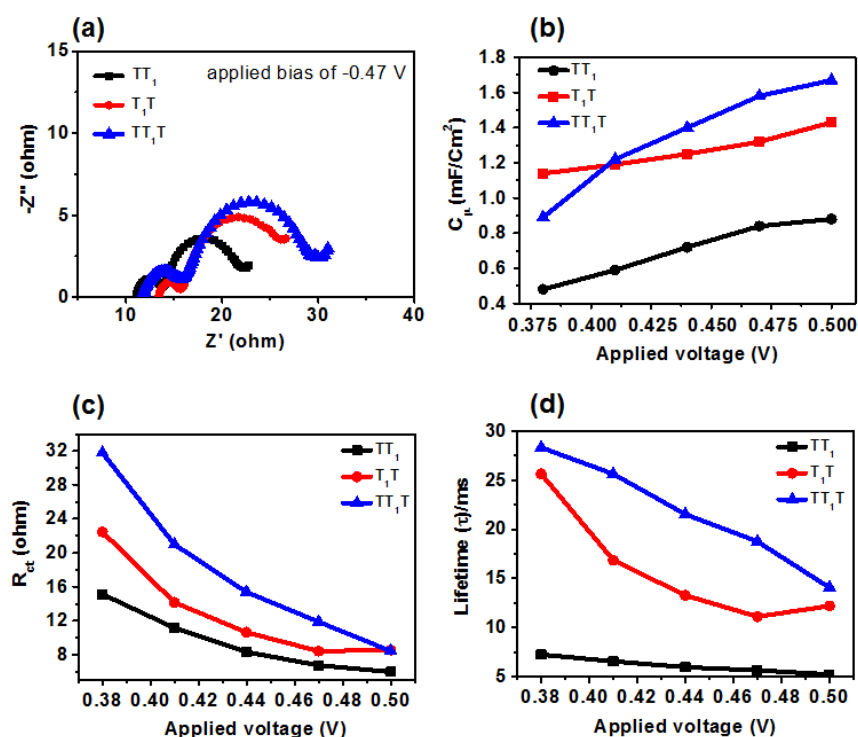
Figure 8. Impedance analysis of D/A dyes. (a) Nyquist plot, (b) capacitance, (c) charge transfer resistance and (d) electron lifetime *vs* applied potential.

The charge transfer resistance (R_{ct}) on the TiO$_2$ surface denoted the charge recombination between the electrons resides on TiO$_2$ at forward bias and electrolyte which is measured by the large semicircle area. A large R_{ct} is indicated by a slow charge recombination process. The R_{ct} values for **T$_1$T**, **TT$_1$** and **TT$_1$T** dyes-based DSSCs were calculated and presented in **Table 5** at 0.47 V. Among three dyes **TT$_1$T** showed high charge transfer resistance of 11.87 ohm and for **TT$_1$** and **T$_1$T** R_{ct} were reduced to 6.75 ohm and 8.42 ohm, respectively. The plot

of fitted capacititive response *vs* bias potential provides the information about the position of conduction band of TiO$_2$ (**Figure 8b**).[29] Among the isomeric dyes, the chemical capacitance (Cμ) of **T$_1$T** (1.32 mF) is higher than that of **TT$_1$** (0.84 mF) at the bias potential of 0.47 V.

Table 5. Electrochemical impedance parameters of spiro dyes at applied bias of 0.47 V[a]

[a]Dye:CDCA	R_{ct} (ohm)	C_μ (mF)	τ_n (ms)[b]
TT$_1$	6.75	0.84	5.67
T$_1$T	8.42	1.32	11.1
TT$_1$T	11.87	1.58	18.8

[a]Dye:CDCA (1:5), [dye]= 0.2 mM. [b]Electron lifetime was calculated from capacitance and charge transfer resistance: Lifetime (τ) = $R_{ct} \times C_\mu$

This observation is in agreement with the increased resultant dipole moment of **T$_1$T** dye compared to **TT$_1$** on the surface that upshift the conduction band level of TiO$_2$.[55–58] Evidently, the electron lifetime in TiO$_2$ for the **T$_1$T** dye (11.1 ms) is higher than that of the isomeric **TT$_1$** (5.67 ms). Comparatively less interaction of two monomeric strands in **T$_1$T** and **TT$_1$T** will decrease the charge recombination and increase the stability of electron on conduction band of TiO$_2$ which in turns increase the charge injection. Electron lifetime was calculated from charge transfer resistance and capacitance. The long electron lifetime and better passivation of surface infers the high J_{sc} of **TT$_1$T** (18.8 ms) than **TT$_1$** and **T$_1$T**. The electrochemical impedance spectra of spiro-dyes are recorded for the DSSC devices under a forward bias of 0.38, 0.41, 0.44, 0.47 and 0.5 V in the dark (**Figure 9**).
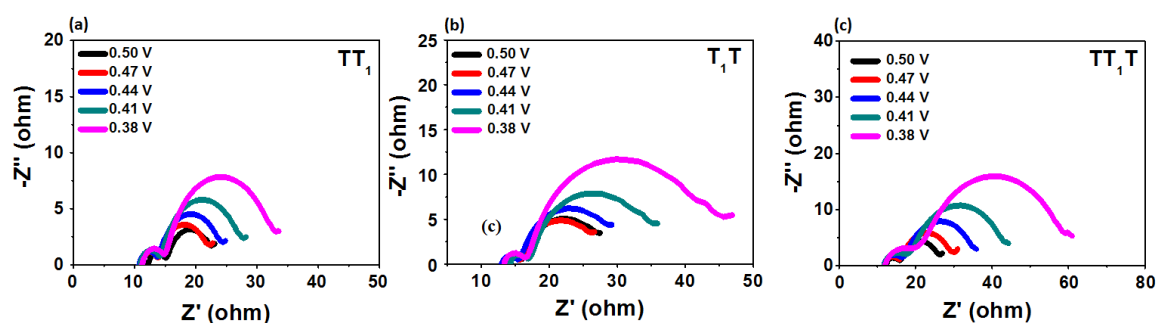
Figure 9. Impedance spectra of (a) **TT$_1$**, (b) **T$_1$T** and (c) **TT$_1$T** at different applied bias.

4.3 Conclusion

Homo-dimeric spiro dyes were synthesised by using Suzuki coupling followed by direct arylation method. Structural isomeric **TT$_1$**, **T$_1$T** and **TT$_1$T** were synthesized by coupling in between different donor moiety with different formylated spiroBiProDOT. Dye aggregation and recombination were reduced by increasing the flexibility of linker connecting two monomeric dye strands. J_{sc} of dimeric dyes **TT$_1$T** (9.79 mA/cm^2) and **T$_1$T** (9.09 mA/cm^2) are near about 1.5 times higher than that of **TT$_1$** (6.25 mA/cm^2) which implies that of charge injection on TiO$_2$ conduction band will also be high in case of **TT$_1$T** and **TT$_1$**. The V_{oc} of the dimeric spiro-dyes **TT$_1$T** (0.589 V) and **T$_1$T** (0.593 V) are also higher than that of **TT$_1$** (0.568 V) may be result of increased resultant dipole moment of **T$_1$T** due to increase the angle in between two monomeric dye strands. The two anchoring groups of these dimeric dyes facilitate strong binding with TiO$_2$ surface which renders controlled orientation and reduced the self-aggregation. This study shows a new molecular approach to increasing the photovoltaic parameters by changing the angle and increasing additional acceptor units in homo-dimeric dyes.

4.4 Experimental section

4.4.1 Materials and instruments. All the reagents and solvents were purchased from Aldrich and TCI chemicals and used without further purification. Required precursors **1**,[62] **2**,[61] **5**,[60] **8**,[6] 3, 4-dimethoxy thiophene[59] was synthesised from thiophene and converted into 2H,2'H,4H,4'H-3,3'-spirobi[thieno[3,4-b][1,4]dioxepine][60] according to the reported literature procedure. All oxygen- and moisture-sensitive reactions were performed under nitrogen atmosphere. The other materials were of the common commercial level and used as received. PhMe was dried over Na/benzophenone ketyl and freshly distilled prior to use. Details of spectrometers for characterization and evaluating the photophysical, electrochemical, photovoltaic parameters, and electron impedance spectroscopy were providing in supporting information.

4.4.2 Characterization. All the instruments for characterization (^{1}H NMR, ^{13}C NMR, MALDI-TOF-MS, UV-vis spectra, differential pulse voltammetry, electrochemical impedance spectra, solar simulator) of organic dyes are same as presented in **Chapter 2**, section 2.4.2.

4.4.3 Fabrication of dye sensitized solar cells. The methods of preparation of solar cell with synthesized dyes were same as presented in **Chapter 2**, section 2.4.3.

4.4.4 Synthesis of dyes

4-Methoxy-N-(4-methoxyphenyl)-N-(4-(thiophen-2-yl) phenyl) aniline, 3: Compound **2** and 2-bromo-thiophene were solubilised in 20 mL mixture of THF in H_2O (9:1) solvent. The solution is purged with nitrogen for 10 min. To this solution were added K_2CO_3 and Pd(PPh$_3$)$_4$ and the reaction mixture was refluxed for 18 h under N_2 atmosphere. The reaction mixture was cooled to rt and then poured into water. The product was extracted with 200 mL EtOAc and washed with 50 mL of H_2O. The organic layer was concentrated under reduced

pressure and purified by column chromatography using CH_2Cl_2 and pet. ether as an eluent. Yield 345 mg (78%). ^{1}H-NMR (200 MHz, $CDCl_3$) δ: 3.80 (s, 6 H), 6.81-6.83 (m, 4 H), 6.85-6.86 (m, 2 H), 7.03-7.06 (m, 5 H), 7.1-7.18 (m, 2 H), 7.38-7.43 (m, 2 H). ^{13}C NMR (100 MHz, $CDCl_3$) δ: 55.8, 114.9, 115.2, 119.2, 123.4, 124.6, 126.4, 127.6, 129.7, 133.8, 140.5, 149.5, 156.7.

(4-(5-Bromothiophen-2-yl)-N,N-bis(4-methoxyphenyl)aniline, 4: N-Bromo bromosuccinimide (150 mg, 0.8 mmol) was solubilised in 5 mL of dry THF in a 25 mL single neck round bottom flask. **3** (320 mg, 0.8 mmol) was dissolved in 5 mL of dry THF in a double neck round bottomed flask followed by the addition of NBS in THF solution drop wise and stirred at 0 °C under nitrogen atmosphere for 3 h. The reaction mixture was quenched by addition of water (50 mL) and extracted with CH_2Cl_2 (150 mL). The organic layer was concentrated under reduced pressure and purified by column chromatography using CH_2Cl_2 and pet. ether as an eluent. Yield 370 mg (83%). ^{1}H NMR (200 MHz, $CDCl_3$) δ: 3.80 (s, 6 H), 6.83-6.87 (m, 6 H), 6.91- 6.97 (m, 2 H), 7.08-7.12 (m, 4 H), 7.34-7.38 (m, 2 H). ^{13}C NMR (100 MHz, $CDCl_3$) δ: 55.8, 112.7, 115.1, 116, 122.3, 126.9, 128.1, 132.1, 140.9, 148.3, 148.7, 156.4.

6,6'-Dibromo-2H,2'H,4H,4'H-3,3'-spirobi[thieno[3,4-b][1,4]dioxepine], 6: N-Bromosuccinimide (570 mg, 3.2 mmol) was dissolved in 20 mL of DMF in a 50 mL single neck round bottomed flask. Compound **5** (500 mg, 1.7 mmol) was solubilised in dry $CHCl_3$ in a 100 mL double neck round bottom flask under nitrogen atmosphere followed by the addition of NBS in DMF solution dropwise and stirred at 0 °C for 3 h and further stirred at rt for 15 h. The reaction mixture was washed with brine solution and extracted with CH_2Cl_2. The organic layer was concentrated under reduced pressure and purified by column chromatography using PhMe and pet. ether as an eluent. Yield 280 mg (40%). ^{1}H NMR (500

MHz, CDCl$_3$) δ: 4.07 (d, J = 5 Hz, 4 H), 4.14 (d, J = 5 Hz, 4 H), 6.49 (d, J = 5 Hz, 2 H). ^{13}C NMR (125 MHz, CDCl$_3$) δ: 50.7, 70.8, 71.1, 71.5, 104.8, 105.4, 146.2, 146.7, 147.9, 148.7. MALDI-TOF m/z calcd for [M+ Na]$^+$ [C$_{13}$H$_{10}$Br$_2$O$_4$S$_2$+Na]$^+$ 477.1368, found 477.3457.

5,5'-(2H,2'H,4H,4'H-3,3'-Spirobi[thieno[3,4-b][1,4]dioxepine]-6,6'-diyl)bis(thiophene-2-carbaldehyde), 7: **6** (250 mg, 0.55 mmol), 5-formyl-2-thiopheneboronicacid (200 mg, 1.3 mmol), tetra-n-butylammoniumbromide (50 mg, 0.17 mmol) and Pd(PPh$_3$)$_4$ (10 mg, 0.005 mmol) were taken in a 100 mL 2 neck round bottomed flask followed by 50 mL of dry THF under nitrogen atmosphere. Saturated aqueous solution of Na$_2$CO$_3$ was added dropwise to that reactant solution and stirred it for 16 h at 70 °C under the same atmospheric condition. The reaction mixture was washed with brine solution and extracted by CH$_2$Cl$_2$ (100 mL). Organic layer was concentrated by reducing pressure and purified by column chromatography using pet. ether and EtOAc an eluent. Yield 150 mg (52%). ^{1}H NMR (400 MHz, CDCl$_3$) δ: 4.16 (d, J = 12 Hz, 4 H), 4.31 (d, J = 20 Hz, 4 H), 6.54 (d, J = 8 Hz, 2 H), 7.29-7.32 (m, 2 H), 7.60 (s, 1 H), 7.79 (t, J = 4 Hz, 1 H), 9.91 (d, J = 4 Hz, 2 H). ^{13}C NMR (100 MHz, CDCl$_3$) δ: 50.6, 50.7, 70.8, 71, 71.5, 105, 105.6, 123.4, 124.1, 128, 130, 134.7, 136.4, 136.5, 141.5, 142.3, 143, 144.4, 146.3, 146.5, 148.6, 149, 182.8, 182.9. MALDI-TOF m/z calcd for [M+ Na]$^+$ [C$_{23}$H$_{16}$O$_6$S$_4$Na+Na]$^+$ 539.6048, found 539.7344.

General for palladium catalyzed direct arylation reactions:

The dialdehyde derivative **7** or **8** and triarylhalide **1** or **4**, K$_2$CO$_3$, Pd(OAc)$_2$ (0.5 mol%), PCy$_3$ (0.5 mol%), and PivOH (0.15 mol%) were taken in a Schlenk tube under nitrogen atmosphere. 5 mL of dry DMA was added to that and kept the reaction at 120 $^{°}$C under inert atmosphere for 24 h. The reaction mixture was washed with 200 mL of water and extracted

with 150 mL of CH_2Cl_2. Solvents were removed under reduced pressure and purified by column chromatography.

5,5'-(6,6'-Bis(5-(4-(bis(4-methoxyphenyl)amino)phenyl)thiophen-2-yl)-2H,2'H,4H,4'H-3,3'-spirobi[thieno[3,4-b][1,4]dioxepine]-8,8'-diyl)bis(thiophene-2-carbaldehyde), 13: Started with **7** (200 mg, 0.39 mmol), **4** (450 mg, 0.97 mmol), K_2CO_3 (40 mg, 0.290 mmol). Column chromatography was done by using EtOAc and pet. ether. Yield 190 mg (38 %). ^{1}H NMR (500 MHz, DMSO-d_6) δ: 3.82-4.04 (m, 12 H), 4.18-4.31 (m, 6 H), 6.87-7.12 (m, 14 H), 7.33-7.37 (m, 14 H), 7.42-7.48 (m, 4 H), 9.73-9.91 (m, 2H). ^{13}C NMR (125 MHz, CDCl$_3$) δ: 21.8, 30.3, 31.1, 54.9, 55.7, 70.6, 71.1, 114.2, 114.5, 114.8, 117.0, 119, 120.4, 124.2, 124.6, 124.8, 125.6, 126, 127.4, 128.5, 128.8, 129.4, 129.9, 131.5, 139.6, 140.2, 141.1, 154.8, 155.3, 156.4, 158.1.

6,6'-Bis(5-(4-(bis(4-methoxyphenyl)amino)phenyl)thiophen-2-yl)-2H,2'H,4H,4'H-3,3'-spirobi[thieno[3,4-b][1,4]dioxepine]-8,8'-dicarbaldehyde, 9: Started with **8** (120 mg, 0.34 mmol), **4** (320 mg, 0.68 mmol), K_2CO_3 (150 mg, 1.07 mmol). Column chromatography was done by using CH_2Cl_2 and pet. ether. Yield 195 mg (51 %). ^{1}H NMR (500 MHz, CDCl$_3$) δ: 3.74 (s, 12 H), 3.83-4.44 (m, 8 H), 6.89 (d, $J = 4$ Hz, 10 H), 6.95 (d, $J = 8$ Hz, 4 H), 7.10-7.14 (m, 10 H), 7.38 (s, 2H), 7.51-7.54 (m, 2 H), 9.97 (s, 2H). ^{13}C NMR (125 MHz, CDCl$_3$) δ: 22.5, 29.1, 31.5, 55.5, 70.9, 71.1, 107, 114.6, 114.9, 118.5, 118.9, 123.1, 127.3, 129.4, 130.2, 132.1, 140.1, 140.5, 140.6, 143.3, 149.3, 154.5, 156.4, 180. . MALDI-TOF m/z calcd for [M]$^+$ [$C_{63}H_{50}N_2O_{10}S_4$]$^+$ 1123.3370, found 1123.6525.

5,5'-(6,6'-Bis(4-(bis(4-methoxyphenyl)amino)phenyl)-2H,2'H,4H,4'H-3,3'-spirobi[thieno[3,4-b][1,4]dioxepine]-8,8'-diyl)bis(thiophene-2-carbaldehyde), 11: Started with **7** (160 mg, 0.31 mmol), **1** (220 mg, 0.77 mmol), K_2CO_3 (110 mg, 0.77 mmol). Column

chromatography by using EtOAc and CH_2Cl_2. Yield 105 mg (43%). ^1H NMR (500 MHz, $CDCl_3$) δ: 3.83-3.84 (m, 12 H), 4.11-4.44 (m, 8 H), 6.88-6.90 (m, 10 H), 6.96-7.02 (m, 4 H), 7.08-7.15 (m, 10 H), 7.57-7.59 (m, 2 H), 7.69-7.76 (m, 2 H), 9.9-9.94 (m, 2 H). ^{13}C NMR (125 MHz, DMSO-d_6) δ: 22.6, 29.3, 29.4, 29.8, 55.5, 70, 71.3, 72.4, 114.6, 114.8, 114.9, 115, 115.2, 117, 119.3, 120.1, 126.8, 127.7, 129.1, 130.1, 131.6, 134.3, 139.3, 140.2, 142.4, 156.0, 156.3, 156.3, 156.8,182.2, 182.9, 183.2. MALDI-TOF m/z calcd for $[M]^+$ $[C_{63}H_{50}N_2O_{10}S_4]^+$ 1123.3370, found 1123.6528.

General procedure for the Knoevenagel condensation:

A mixture of dialdehyde derivative **9** or **11** or **13** cyanoacetic acid, NH_4OAc (10 mg) and glacial aceticacid (10 mL) was heated under reflux for 12 h. The reaction mixture was washed with water and Et_2O thoroughly.

TT$_1$T Dye, 14: Started with **13** (80 mg, 0.062 mmol), cyanoacetic acid (32 mg, 0.37 mmol). Yield 65 mg (74%). ^1H-NMR (400 MHz, DMSO-d_6) δ: 3.71 (s, 12 H), 3.87-4.14 (m, 4 H), 4.24-4.36 (m, 4 H), 6.57-6.62 (m, 10 H), 7.06-7.16 (m, 18 H), 7.35-7.54 (m, 4 H), 8.03-8.11 (m, 2 H). ^{13}C-NMR (100 MHz, DMSO-d_6) δ: 21.8, 29.5, 31.9, 35, 43.5, 55.4, 55.9, 70.1, 71.9, 73, 113.1, 113.8, 114.1, 115.4, 115.9, 116.2, 119.3, 122.9, 123.7, 124.7, 128.9, 129.9, 134.5, 135.6, 136.1, 136.6, 138.3, 138.7, 138.9, 139.4, 153.8, 155.5, 155.9, 156.2, 157.3, 170.1. MALDI-TOF m/z calcd for $[M-2H]^+$ $[C_{63}H_{50}N_2O_{10}S_4]^+$ 1419.6710, found 1419.6537.

TT$_1$ dye, 10: Started with 9 (70 mg, 0.064 mmol), cyanoacetic acid (32 mg, 0.37 mmol). Yield 61 mg (78%). ^1H NMR (400 MHz, DMSO-d_6) δ: 3.73 (s, 12 H), 4.18-4.52 (m, 8 H), 6.61 (s, 2 H), 6.75 (s, 4 H), 6.93 (s, 8 H), 7.08 (d, J = 8 Hz, 8 H), 7.44 (s, 6 H), 8.14 (s, 2H). ^{13}C NMR (100 MHz, DMSO-d_6) δ: 20.5, 21.2, 28.6, 55.6, 56.3, 72.1, 72.2, 72.4, 105.8, 107, 107.0, 113.8, 115.1, 115.2, 115.3, 115.5, 115.6, 119.2, 120.1, 127.9, 128, 129.7, 139.6, 139.7,

149.4, 156.8, 172.3, 172.6. MALDI-TOF *m/z* calcd for [M+Na]⁺ [C$_{69}$H$_{52}$N$_4$O$_{12}$S$_4$ + Na]⁺ 1280.4208, found 1280.6603.

T$_1$T dye, 12: Started with 11 (100 mg, 0.09 mmol), cyanoacetic acid (45 mg, 0.53 mmol). Yield 88 mg (%). ¹H NMR (400 MHz, DMSO-*d₆*) δ: 3.70-3.87 (m, 12 H), 4.28-4.40 (m, 8 H), 6.78-7.18 (m, 26 H), 7.41-7.68 (m, 2 H), 8.12 (s, 1 H), 8.32 (s, 1 H). ¹³C NMR (100 MHz, DMSO-*d₆*) δ: 24.7, 56.1, 71.5, 72, 88.6, 89.8, 94.5, 101.7, 102.2, 103.1, 115.3, 115.5, 115.7, 115.8, 127.2, 127.5, 127.6, 127.9, 128.6, 140.2, 140.3, 165.6. MALDI-TOF *m/z* calcd for [M+Na]⁺ [C$_{69}$H$_{52}$N$_4$O$_{12}$S$_4$ + Na]⁺ 1280.4208, found 1280.6603.

4.5 References

(1)   Mishra, A.; Fischer, M. K. R.; Bäuerle, P. Metal-Free Organic Dyes for Dye-Sensitized Solar Cells: From Structure: Property Relationships to Design Rules. *Angew. Chem. Int. Ed.* **2009**, *48*, 2474–2499.

(2)   O'Regan, B.; Grätzel, M. A Low-Cost, High-Efficiency Solar Cell Based on Dye-Sensitized Colloidal TiO$_2$ Films. *Nature* **1991**, *353*, 737–740.

(3)   Ning, Z.; Fu, Y.; Tian, H. Improvement of Dye-Sensitized Solar Cells: What We Know and What We Need to Know. *Energy Environ. Sci.* **2010**, *3*, 1170–1181.

(4)   Nazeeruddin, M. K.; Péchy, P.; Renouard, T.; Zakeeruddin, S. M.; Humphry-Baker, R.; Comte, P.; Liska, P.; Cevey, L.; Costa, E.; Shklover, V.; et al. Engineering of Efficient Panchromatic Sensitizers for Nanocrystalline TiO$_2$-Based Solar Cells. *J. Am. Chem. Soc.* **2001**, *123*, 1613–1624.

(5)   Bisht, R.; Kavungathodi, M. F. M.; Singh, A. K.; Nithyanandhan, J. Panchromatic Sensitizer for Dye-Sensitized Solar Cells: Unsymmetrical Squaraine Dyes Incorporating Benzodithiophene π-Spacer with Alkyl Chains to Extend Conjugation, Control the Dye Assembly on TiO$_2$, and Retard Charge Recombination. *J. Org. Chem.* **2017**, *82*, 1920–1930.

(6)   Sil, M. C.; Sudhakar, V.; Kavungathodi, M. F. M.; Punitharasu, V.; Nithyanandhan, J. Orthogonally Functionalized Donor/Acceptor Homo- and Heterodimeric Dyes for Dye-Sensitized Solar Cells: An Approach to Introduce Panchromaticity and Control the Charge Recombination. *ACS Appl. Mater. Interfaces* **2017**, *9*, 34875–34890.

(7)   Nguyen, W. H.; Bailie, C. D.; Burschka, J.; Moehl, T.; Grätzel, M.; McGehee, M. D.; Sellinger, A. Molecular Engineering of Organic Dyes for Improved Recombination Lifetime in Solid-State Dye-Sensitized Solar Cells. *Chem. Mater.* **2013**, *25*, 1519–1525.

(8)   Koumura, N.; Wang, Z.-S.; Mori, S.; Miyashita, M.; Suzuki, E.; Hara, K. Alkyl-Functionalized Organic Dyes for Efficient Molecular Photovoltaics. *J. Am. Chem. Soc.* **2006**, *128*, 14256–14257.

(9)   Listorti, A.; O'Regan, B.; Durrant, J. R. Electron Transfer Dynamics in Dye-Sensitized Solar Cells. *Chem. Mater.* **2011**, *23*, 3381–3399.

(10) Mathew, S.; Yella, A.; Gao, P.; Humphry-Baker, R.; Curchod, B. F. E.; Ashari-Astani, N.; Tavernelli, I.; Rothlisberger, U.; Nazeeruddin, M. K.; Grätzel, M. Dye-Sensitized Solar Cells with 13% Efficiency Achieved through the Molecular Engineering of Porphyrin Sensitizers. *Nat. Chem.* **2014**, *6*, 242–247.

(11) Yao, Z.; Zhang, M.; Wu, H.; Yang, L.; Li, R.; Wang, P. Donor/Acceptor Indenoperylene Dye for Highly Efficient Organic Dye-Sensitized Solar Cells. *J. Am. Chem. Soc.* **2015**, *137*, 3799–3802.

(12) Hwang, S.; Lee, J. H.; Park, C.; Lee, H.; Kim, C.; Park, C.; Lee, M.-H.; Lee, W.; Park, J.; Kim, K.; et al. A Highly Efficient Organic Sensitizer for Dye-Sensitized Solar Cells. *Chem. Commun.* **2007**, *0*, 4887–4889.

(13) Gong, J.; Liang, J.; Sumathy, K. Review on Dye-Sensitized Solar Cells (DSSCs): Fundamental Concepts and Novel Materials. *Renew. Sustain. Energy Rev.* **2012**, *16*, 5848–5860.

(14) Li, X.; Zheng, Z.; Jiang, W.; Wu, W.; Wang, Z.; Tian, H. New D–A–π–A Organic Sensitizers for Efficient Dye-Sensitized Solar Cells. *Chem. Commun.* **2015**, *51*, 3590–3592.

(15) Saccone, D.; Galliano, S.; Barbero, N.; Quagliotto, P.; Viscardi, G.; Barolo, C. Polymethine Dyes in Hybrid Photovoltaics: Structure–Properties Relationships. *Eur. J. Org. Chem.* **2016**, *2016*, 2244–2259.

(16) Yella, A.; Lee, H.-W.; Tsao, H. N.; Yi, C.; Chandiran, A. K.; Nazeeruddin, M. K.; Diau, E. W.-G.; Yeh, C.-Y.; Zakeeruddin, S. M.; Grätzel, M. Porphyrin-Sensitized Solar Cells with Cobalt (II/III)-Based Redox Electrolyte Exceed 12 Percent Efficiency. *Science* **2011**, *334*, 629–634.

(17) Urbani, M.; Grätzel, M.; Nazeeruddin, M. K.; Torres, T. Meso-Substituted Porphyrins for Dye-Sensitized Solar Cells. *Chem. Rev.* **2014**, *114*, 12330–12396.

(18) Tang, Y.; Wang, Y.; Li, X.; Ågren, H.; Zhu, W.-H.; Xie, Y. Porphyrins Containing a Triphenylamine Donor and up to Eight Alkoxy Chains for Dye-Sensitized Solar Cells: A High Efficiency of 10.9%. *ACS Appl. Mater. Interfaces* **2015**, *7*, 27976–27985.

(19) Higashino, T.; Imahori, H. Porphyrins as Excellent Dyes for Dye-Sensitized Solar Cells: Recent Developments and Insights. *Dalton Trans.* **2014**, *44*, 448–463.

(20) Imahori, H.; Umeyama, T.; Ito, S. Large π-Aromatic Molecules as Potential Sensitizers for Highly Efficient Dye-Sensitized Solar Cells. *Acc. Chem. Res.* **2009**, *42*, 1809–1818.

(21) Ince, M.; Yum, J.-H.; Kim, Y.; Mathew, S.; Grätzel, M.; Torres, T.; Nazeeruddin, M. K. Molecular Engineering of Phthalocyanine Sensitizers for Dye-Sensitized Solar Cells. *J. Phys. Chem. C* **2014**, *118*, 17166–17170.

(22) Alagumalai, A.; Kavungathodi, M. F. M.; Vellimalai, P.; Sil, M. C.; Nithyanandhan, J. Effect of Out-of-Plane Alkyl Group's Position in Dye-Sensitized Solar Cell Efficiency: A Structure–Property Relationship Utilizing Indoline-Based Unsymmetrical Squaraine Dyes. *ACS Appl. Mater. Interfaces* **2016**, *8*, 35353–35367.

(23) Lee, Y. H.; Kang, J. Y.; Kim, D. W.; Kim, J. S.; Kim, J. H.; Suresh, T. Aggregation Property and Photovoltaic Performance Optimization of Symmetrical Squaraine Dye Containing Bis-Anchoring Groups for Dye-Sensitized Solar Cell. *Mol. Cryst. Liq. Cryst.* **2016**, *635*, 148–157.

(24) Zhang, L.; M. Cole, J. Dye Aggregation in Dye-Sensitized Solar Cells. *J. Mater. Chem. A* **2017**, *5*, 19541–19559.

(25) Salvatori, P.; Marotta, G.; Cinti, A.; Anselmi, C.; Mosconi, E.; De Angelis, F. Supramolecular Interactions of Chenodeoxycholic Acid Increase the Efficiency of Dye-Sensitized Solar Cells Based on a Cobalt Electrolyte. *J. Phys. Chem. C* **2013**, *117*, 3874–3887.

(26) Baheti, A.; Justin Thomas, K. R.; Li, C.-T.; Lee, C.-P.; Ho, K.-C. Fluorene-Based Sensitizers with a Phenothiazine Donor: Effect of Mode of Donor Tethering on the Performance of Dye-Sensitized Solar Cells. *ACS Appl. Mater. Interfaces* **2015**, *7*, 2249–2262.

(27) Ziółek, M.; Karolczak, J.; Zalas, M.; Hao, Y.; Tian, H.; Douhal, A. Aggregation and Electrolyte Composition Effects on the Efficiency of Dye-Sensitized Solar Cells. A Case of a Near-Infrared Absorbing Dye for Tandem Cells. *J. Phys. Chem. C* **2014**, *118*, 194–205.

(28) Wang, Z.; Liang, M.; Tan, Y.; Ouyang, L.; Sun, Z.; Xue, S. Organic Dyes Containing Dithieno[2,3-d:2′,3′-D′]Thieno[3,2-b:3′,2′-B′]Dipyrrole Core for Efficient Dye-Sensitized Solar Cells. *J. Mater. Chem. A* **2015**, *3*, 4865–4874.

(29) Chai, Q.; Li, W.; Wu, Y.; Pei, K.; Liu, J.; Geng, Z.; Tian, H.; Zhu, W. Effect of a Long Alkyl Group on Cyclopentadithiophene as a Conjugated Bridge for D–A−π–A Organic Sensitizers: IPCE, Electron Diffusion Length, and Charge Recombination. *ACS Appl. Mater. Interfaces* **2014**, *6*, 14621–14630.

(30) Freitag, M.; Galoppini, E. Molecular Host–guest Complexes: Shielding of Guests on Semiconductor Surfaces. *Energy Environ. Sci.* **2011**, *4*, 2482–2494.

(31) Hamann, T. W.; Farha, O. K.; Hupp, J. T. Outer-Sphere Redox Couples as Shuttles in Dye-Sensitized Solar Cells. Performance Enhancement Based on Photoelectrode Modification via Atomic Layer Deposition. *J. Phys. Chem. C* **2008**, *112*, 19756–19764.

(32) Li, T. C.; Góes, M. S.; Fabregat-Santiago, F.; Bisquert, J.; Bueno, P. R.; Prasittichai, C.; Hupp, J. T.; Marks, T. J. Surface Passivation of Nanoporous TiO_2 via Atomic Layer Deposition of ZrO_2 for Solid-State Dye-Sensitized Solar Cell Applications. *J. Phys. Chem. C* **2009**, *113*, 18385–18390.

(33) Liu, L.; Karuturi, S. K.; Su, L. T.; Tok, A. L. Y. TiO_2 Inverse-Opal Electrode Fabricated by Atomic Layer Deposition for Dye -Sensitized Solar Cell Applications. *Energy Environ. Sci.* **2011**, *4*, 209–215.

(34) Ganapathy, V.; Karunagaran, B.; Rhee, S.-W. Improved Performance of Dye-Sensitized Solar Cells with TiO_2/Alumina Core–shell Formation Using Atomic Layer Deposition. *J. Power Sources* **2010**, *195*, 5138–5143.

(35) Pozzi, G.; Orlandi, S.; Cavazzini, M.; Minudri, D.; Macor, L.; Otero, L.; Fungo, F. Synthesis and Photovoltaic Applications of a 4,4′-Spirobi[Cyclopenta[2,1-b;3,4-B′]Dithiophene]-Bridged Donor/Acceptor Dye. *Org. Lett.* **2013**, *15*, 4642–4645.

(36) Manfredi, N.; Cecconi, B.; Abbotto, A. Multi-Branched Multi-Anchoring Metal-Free Dyes for Dye-Sensitized Solar Cells. *Eur. J. Org. Chem.* **2014**, *2014*, 7069–7086.

(37) Zhang, F.; Fan, J.; Yu, H.; Ke, Z.; Nie, C.; Kuang, D.; Shao, G.; Su, C. Nonplanar Organic Sensitizers Featuring a Tetraphenylethene Structure and Double Electron-Withdrawing Anchoring Groups. *J. Org. Chem.* **2015**, *80*, 9034–9040.

(38) Lo, C.-Y.; Kumar, D.; Chou, S.-H.; Chen, C.-H.; Tsai, C.-H.; Liu, S.-H.; Chou, P.-T.; Wong, K.-T. Highly Twisted Dianchoring D−π–A Sensitizers for Efficient Dye-Sensitized Solar Cells. *ACS Appl. Mater. Interfaces* **2016**, *8*, 27832–27842.

(39) Clark, C.C.; Meyer, G. J.; Wei, Q.; Galoppini, E. Tuning Open Circuit Photovoltages with Tripodal Sensitizers. *J. Phy. Chem. B*. **2006**, *110*, 11044-11046.

(40) Galoppini, E.; Guo, W.; Qu, P.; Meyer, G. J. Long-Distance Electron Transfer Across Molecule−Nanocrystalline Semiconductor Interfaces. *J. Am. Chem. Soc.* **2001**, *123*, 4342–4343.

(41) Imahori, H.; Kang, S.; Hayashi, H.; Haruta, M.; Kurata, H.; Isoda, S.; Canton, S. E.; Infahsaeng, Y.; Kathiravan, A.; Pascher, T.; et al. Photoinduced Charge Carrier Dynamics of Zn−Porphyrin−TiO$_2$ Electrodes: The Key Role of Charge Recombination for Solar Cell Performance. *J. Phys. Chem. A* **2011**, *115*, 3679–3690.

(42) Reeves, B. d.; Thompson, B. c.; Abboud, K. a.; Smart, B. e.; Reynolds, J. r. Dual Cathodically and Anodically Coloring Electrochromic Polymer Based on a Spiro Bipropylenedioxythiophene [(Poly(SpiroBiProDOT)]. *Adv. Mater.* **2002**, *14*, 717–719.

(43) Cooper, T.; Novak, A.; Humphreys, L. D.; Walker, M. D.; Woodward, S. User-Friendly Methylation of Aryl and Vinyl Halides and Pseudohalides with DABAL-Me$_3$. *Adv. Synth. Catal.* **2006**, *348*, 686–690.

(44) Higashino, T.; Imahori, H. Porphyrins as Excellent Dyes for Dye-Sensitized Solar Cells: Recent Developments and Insights. *Dalton Trans.* **2015**, *44*, 448–463.

(45) Imahori, H.; Hayashi, S.; Hayashi, H.; Oguro, A.; Eu, S.; Umeyama, T.; Matano, Y. Effects of Porphyrin Substituents and Adsorption Conditions on Photovoltaic Properties of Porphyrin-Sensitized TiO₂ Cells. *J. Phys. Chem. C* **2009**, *113*, 18406–18413.

(46) Nieto-Pescador, J.; Abraham, B.; Li, J.; Batarseh, A.; Bartynski, R. A.; Galoppini, E.; Gundlach, L. Heterogeneous Electron-Transfer Dynamics through Dipole-Bridge Groups. *J. Phys. Chem. C* **2016**, *120*, 48–55.

(47) Ngo, K. T.; Rochford, J.; Fan, H.; Batarseh, A.; Chitre, K.; Rangan, S.; Bartynski, R. A.; Galoppini, E. Photoelectrochemical Properties of Porphyrin Dyes with a Molecular Dipole in the Linker. *Faraday Discuss.* **2015**, *185*, 497–506.

(48) Rangan, S.; Batarseh, A.; Chitre, K. P.; Kopecky, A.; Galoppini, E.; Bartynski, R. A. Tuning Energy Level Alignment At Organic/Semiconductor Interfaces Using a Built-In Dipole in Chromophore–Bridge–Anchor Compounds. *J. Phys. Chem. C* **2014**, *118*, 12923–12928.

(49) Chitre, K.; Batarseh, A.; Kopecky, A.; Fan, H.; Tang, H.; Lalancette, R.; Bartynski, R. A.; Galoppini, E. Synthesis of Zinc Tetraphenylporphyrin Rigid Rods with a Built-In Dipole. *J. Phys. Chem. B* **2015**, *119*, 7522–7530.

(50) Ronca, E.; Pastore, M.; Belpassi, L.; Tarantelli, F.; Angelis, F. D. Influence of the Dye Molecular Structure on the TiO₂ Conduction Band in Dye-Sensitized Solar Cells: Disentangling Charge Transfer and Electrostatic Effects. *Energy Environ. Sci.* **2012**, *6*, 183–193.

(51) Cheng, M.; Yang, X.; Zhao, J.; Chen, C.; Tan, Q.; Zhang, F.; Sun, L. Efficient Organic Dye-Sensitized Solar Cells: Molecular Engineering of Donor–Acceptor–Acceptor Cationic Dyes. *ChemSusChem* **2013**, *6*, 2322–2329.

(52) Preat, J.; Jacquemin, D.; Perpète, E. A. Towards New Efficient Dye-Sensitised Solar Cells. *Energy Environ. Sci.* **2010**, *3*, 891–904.

(53) Rühle, S.; Greenshtein, M.; Chen, S.-G.; Merson, A.; Pizem, H.; Sukenik, C. S.; Cahen, D.; Zaban, A. Molecular Adjustment of the Electronic Properties of Nanoporous Electrodes in Dye-Sensitized Solar Cells. *J. Phys. Chem. B* **2005**, *109*, 18907–18913.

(54) Sfez, R.; Peor, N.; Yitzchaik, S. Experimental Evidence of Molecular Cooperative Effect in a Mixed Parallel and Antiparallel Dipole Monolayer. *J. Phys. Chem. C* **2010**, *114*, 20531–20538.

(55) Lee, M.-W.; Kim, J.-Y.; Son, H. J.; Kim, J. Y.; Kim, B.; Kim, H.; Lee, D.-K.; Kim, K.; Lee, D.-H.; Ko, M. J. Tailoring of Energy Levels in D-π-A Organic Dyes via Fluorination of Acceptor Units for Efficient Dye-Sensitized Solar Cells. *Sci. Rep.* **2015**, *5*, 7711.

(56) Fabregat-Santiago, F.; Bisquert, J.; Palomares, E.; Otero, L.; Kuang, D.; Zakeeruddin, S. M.; Grätzel, M. Correlation between Photovoltaic Performance and Impedance Spectroscopy of Dye-Sensitized Solar Cells Based on Ionic Liquids. *J. Phys. Chem. C* **2007**, *111*, 6550–6560.

(57) Kim, J.-Y.; Kim, J. Y.; Lee, D.-K.; Kim, B.; Kim, H.; Ko, M. J. Importance of 4-Tert-Butylpyridine in Electrolyte for Dye-Sensitized Solar Cells Employing SnO2 Electrode. *J. Phys. Chem. C* **2012**, *116*, 22759–22766.

(58) Ronca, E.; Pastore, M.; Belpassi, L.; Tarantelli, F.; Angelis, F. D. Influence of the Dye Molecular Structure on the TiO$_2$ Conduction Band in Dye-Sensitized Solar Cells: Disentangling Charge Transfer and Electrostatic Effects. *Energy Environ. Sci.* **2012**, *6*, 183–193.

(59) Sadekar, A. G.; Mohite, D.; Mulik, S.; Chandrasekaran, N.; Sotiriou-Leventis, C.; Leventis, N. Robust PEDOT Films by Covalent Bonding to Substrates Using in Tandem Sol–gel, Surface Initiated Free-Radical and Redox Polymerization. *J. Mater. Chem.* **2011**, *22*, 100–108.

(60) Reeves, B. d.; Thompson, B. c.; Abboud, K. a.; Smart, B. e.; Reynolds, J. r. Dual Cathodically and Anodically Coloring Electrochromic Polymer Based on a Spiro Bipropylenedioxythiophene [(Poly(SpiroBiProDOT)]. *Adv. Mater.* **2002**, *14*, 717–719.

(61) Koldemir, U.; Tinkham, J. S.; Johnson, R.; Lim, B.; Yemam, H. A.; Gagnon, K. J.; Parkin, S.; Sellinger, A. Orthogonal 4,10 and 6,12 Substitution of Dibenzo Polycyclic Aromatic Small Molecules. *J. Mater. Chem. C* **2017**, *5*, 8723–8733.

(62) Cunha, M. P. da; Do, T. T.; Yambem, S. D.; Pham, H. D.; Chang, S.; Manzhos, S.; Katoh, R.; Sonar, P. A Triphenylamine Substituted Quinacridone Derivative for

Solution Processed Organic Light Emitting Diodes. *Mater. Chem. Phys.* **2018**, *206*, 56–63.

Orthogonally Functionalized Molecular Dyad Containing D-π-A Dye and Hole Transport Moiety for Dye-Sensitized Solar Cell

5.1 Introduction

The development of renewable energy sources became the greater challenge to make the world better civilized society as well as to surmount the energy demands in this era. The usage of fossil fuels is not the permanent solution to develop this planet in terms of energy and it has to be replaced by adjustable renewable energy resources.[1,2] Solar energy becomes a good option because the earth is getting abundant resources of solar power to door to door.[3] The high cost of solar panels by using silicon base semiconductors materials is the main disadvantage of this technology. Therefore it is required to replace silicon based semiconductor to make cheapest solar device. Dye sensitized solar cell became an optimistic important photovoltaic technology,[4–12] which is rapidly developing technology under intensive studies by researchers. In 1991, Grätzel and co-workers introduced a new dye solar cell based upon ruthenium metal complex as a light absorbing sensitizer and nanocrystalline TiO_2 as semiconductor.[13] The great advantage of mesopourous structures formed by TiO_2 nanocrystals is that it can provide a large surface area for dye adsorption which is an important factor better light harvesting process. Photo-excitation upon sensitizers promotes an electron from HOMO level to LUMO level. The excited electron in LUMO is injected to the conduction band of TiO_2. The oxidized dye is then regenerated by getting an electron from hole transporting material/electrolyte. The electron in TiO_2 transferred to the redox couple electrolyte (hole transporting material) through external circuit. Finally oxidized electrolyte is regenerated by electrochemical reaction on Pt surface.[14–16] This system contains redox electrolyte in solution or solid for the hole transporting process. Dye-sensitized solar cells (DSSCs) have emerged as a potential device architecture to harvest the solar energy due to ease in device fabrication and modular choice of its components such as anode, dyes, electrolytes and cathode. The maximum efficiency was achieved 11 % by using ruthenium based dyes in DSSC cell[17,18] and last two and half decades research on this area enlightened

better understanding of device mechanism associated with interfacial charge transfer and recombination process.[19–21] Based on structure and its material properties various organometallic and metal-free organic dyes have been reported so far. The best current conversion efficiency of about 13%, 12.5% were achieved for zinc-phorphyrin and indenoperylene dyes respectively by using cobalt (II/III) as a redox electrolyte.[22,23] Till date, highly efficient DSSC cell of 14.3% was achieved by co-sensitization of ADEKA-1 (silyl anchor) and LEG-4 (carboxy anchor).[24] Organic dyes with D-π-A and D-A-π-A configuration have several advantages than metal based dye regarding intermolecular charge transfer (ICT), optical and electrochemical properties.[23,25] However such cells suffer from potential leakage problems associated with the corrosive and volatile nature of the liquid electrolyte and, thus, may be impractical for large-scale applications.[26] More importantly, the overpotential required for dye regeneration by I^-/I_3^- redox couple limits the maximum obtainable voltage from the DSSC device. The triiodide ion absorbs a significant part of the visible light when employed in high concentrations. A number of alternate redox electrolytes have replaced I^-/I_3^- electrolyte. Many of these redox couples investigated, such as Br^-/Br_3^-,[27] $SCN^-/(SCN)_3^-$,[28] $SeCN^-/(SeCN)_3^-$,[29] and thiolate/disulphide,[30–32] redox couples, involves the interchange of 2 electrons. The one-electron-transfer redox mediator $[Co(dbbip)_2](ClO_4)_2$ (dbbip=2,6-bis(1-butylbenzimidazol-2$^/$-yl) pyridine)[33] performed best among the compounds investigated. But it is observed a lower efficiency than that of using I^-/I_3^- electrolyte due to reduced hole mobility, low electron-transfer kinetics, and inefficient contact at the dye and HTM interface. Recombination or back electron transfer from the conduction band of TiO_2 to the oxidized dye (inner path recombination) or electrolyte (outer path recombination) used to make a significant loss which is known as the dark current.[34] This mechanism of recombination can be prohibited by using hydrophobic chain attached on that dye. **N719** dye is a suitable example which itself acts to suppress the dark current by forming a bulky layer on the TiO_2

surface.[35,36] To control the charge recombination of electrons in the TiO_2 and oxidised electrolyte species (I_3^-), an additional electron donor unit was integrated with the dye structure in the literature with or without a linker. The additional electron donor unit not only serve as a barrier layer for back electron transfer process but also faster dye regeneration step.[37–41] In this chapter, a hole transporting conjugated triarylamine unit[42] was orthogonally functionalized with a D-π-A dye, **D$_1$-HTM**, through a spiro non-conjugated spiro-spacer to enhance the dye regeneration process. The HOMO/LUMO of this **D$_1$-HTM** was calculated with the help of cyclic voltammetry and band gap which is nicely adjustable with photo-induced electron transfer and dye regeneration via additional HTM attached to the dye (**D$_1$**) directly. To understand the electron transfer mechanism in between the HTM unit and photoexcited dye, photoluminescence quenching studies were carried out by quenching the emission intensity of dyes **D$_1$-D$_1$** and **D$_1$** by the addition of hole-transporting material **PTS1** and **HTM-1,** respectively. **D$_1$-D$_1$** and **D$_1$** were synthesized by following the reported article.[43] Device fabrication were carried out by using **D$_1$-HTM** as a sensitizer and the best efficiency of 2.24 % (V_{oc} of 0.59 V, J_{sc} of 5.27 mA/cm^2) was calculated.

5.2 Results and discussion

Synthesis of a molecular dyad containing 4, 4'-(3, 4-dimethoxythiophene-2, 5-diyl) bis(N,N-bis(4-methoxyphenyl)aniline) unit (HTM part) and D-π-A unit connected were connected through flexible spiroBiProDOT spacer (**Figure 1a**) to control dye aggregation. This spiro linkage helps not only control the dye aggregation but also due to the presence of HTM unit, the dye moiety (**D$_1$**) is well separated from the surface of I^-/I_3^- (**Figure 1b**). This facilitates a uniform electron transfer from I^-/I_3^- to dye (**D$_1$**) part via HTM unit, which is connected to dye through sp^3 carbon. This uniform electron transfer leads to minimize the charge

recombination from CB_{TiO2} to I^-/I_3^- system. The possible photo-induced electron transfer mechanism of targeted **D_1-HTM** dye is presented in **Figure 1c**.

5.2.1 Design and synthesis of dyes

SpiroBiProDOT was utilized as a π-spacer (2H,2'H,4H,4'H-3,3'-spirobi[thieno[3,4-b][1,4]dioxepine]) for synthesizing the dyad containing a D-π-A based dye and HTM moiety. SpiroBiProDOT was synthesized from *trans*-etherification of 3,4-dimethoxythiophene.[45] Selectively Vilsmeier-Haack formylation of spiroBiProDOT afforded the asymmetric mono-formylated dioxepine derivative, **1**.
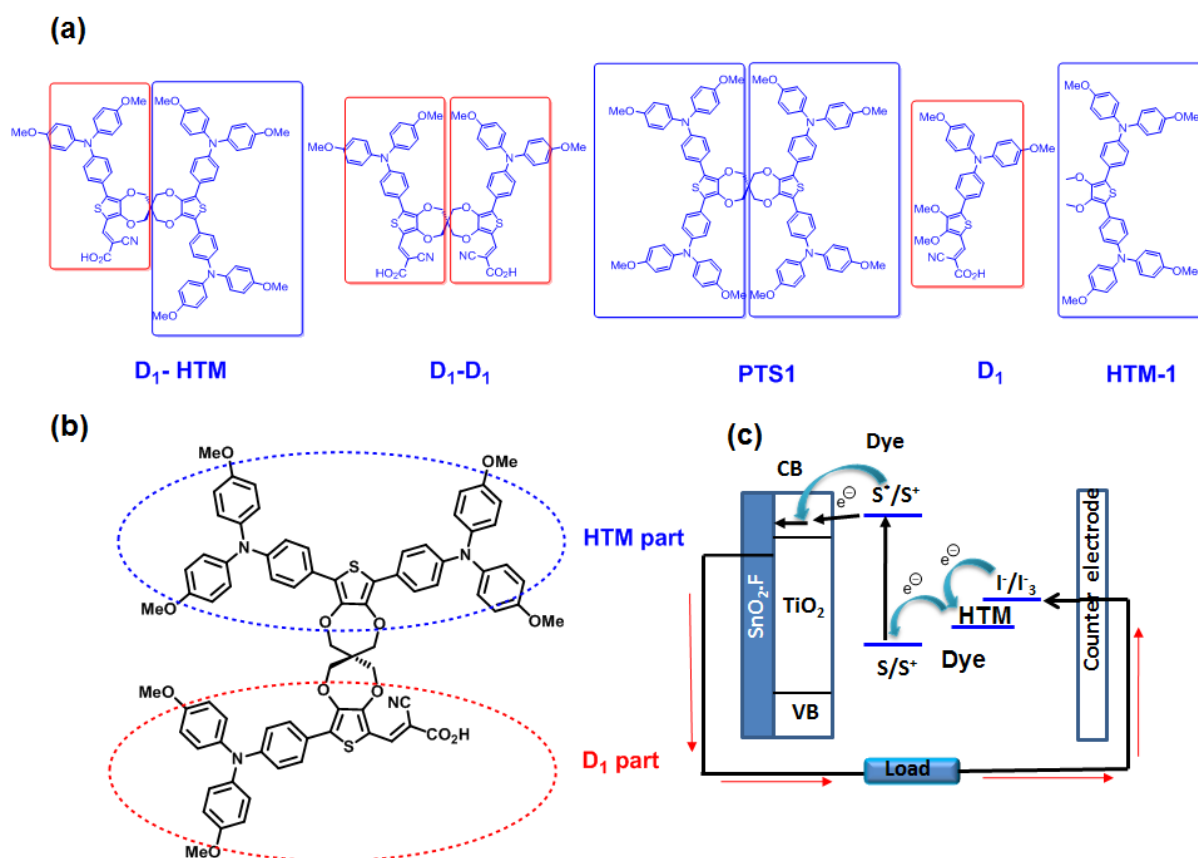
Figure 1. Structures of (a) **D_1-HTM**, **D_1-D_1**, **PTS1**, **D_1**, **HTM-1**. (b) Separation of dye and HTM parts in **D_1-HTM**. (c) Possible mechanism dye regeneration and electron injection.

Direct arylation of **1** with bromotriarylamine **2**[50] afforded to get aldehyde derivative **3** with 46% of yield. Knoevenagel condensation with of aldehyde derivative, **3** with cyanoaceticacid afforded **D₁-HTM** (**Scheme 1a**) with moderate yield (79%). The bromotriarylamine also attached to 2H,2'H,4H,4'H-3,3'-spirobi[thieno[3,4-b][1,4]dioxepine]-6-carbaldehyde as well as 3,4-dimethoxythiophene to afford **PTS1** and **HTM-1** respectively (**Scheme 1b**) by Pd-catalyzed direct arylation reaction.

(a)

(b)
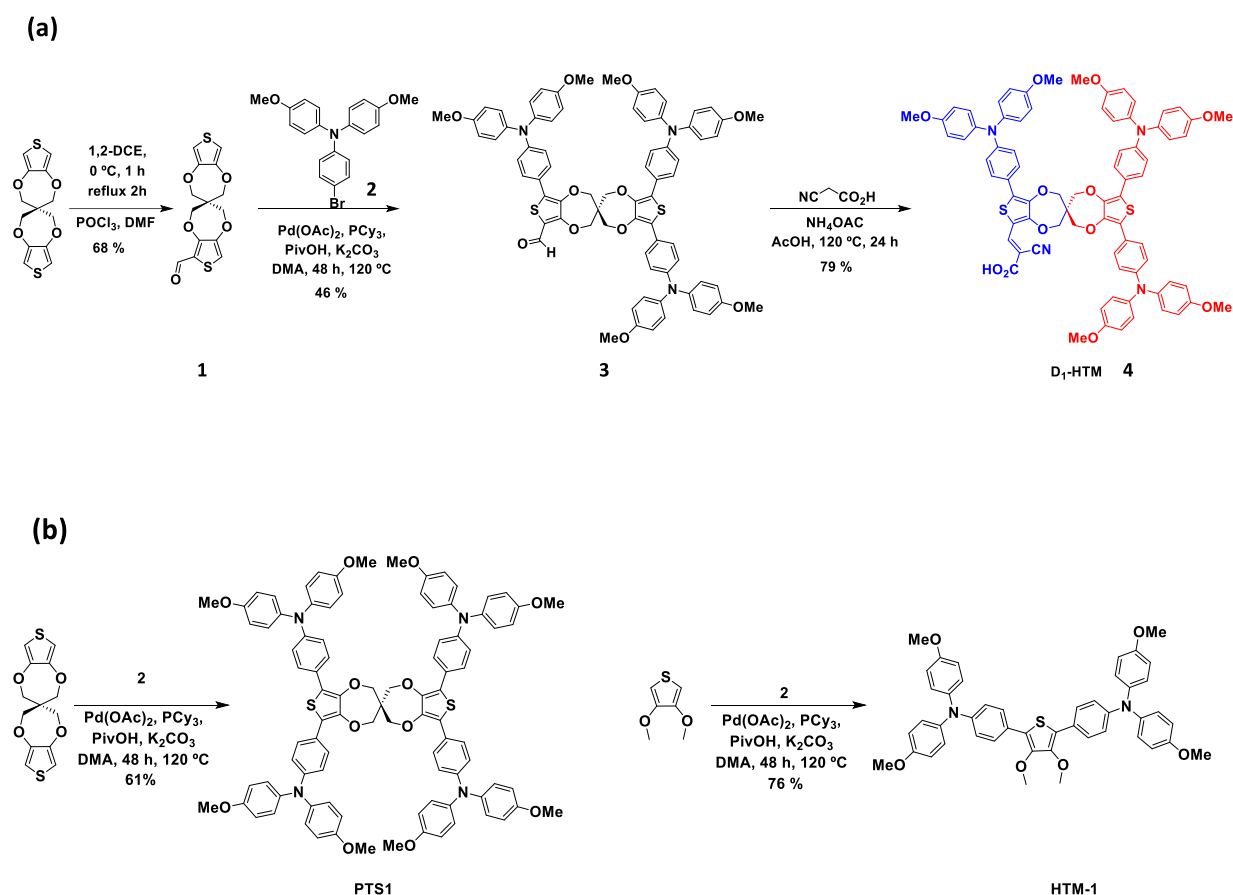
Scheme 1. (a) Synthesis of **D₁-HTM** dye by direct arylation method. (b) Synthesis of **PTS1** and **HTM-1** by direct arylation method.

5.2.2 Photophysical Properties

Optical properties of **D₁-HTM** was carried out both halogenated (CH₂Cl₂ and CHCl₃) and non-halogenated (CH₃CN and CH₃OH) solvent.
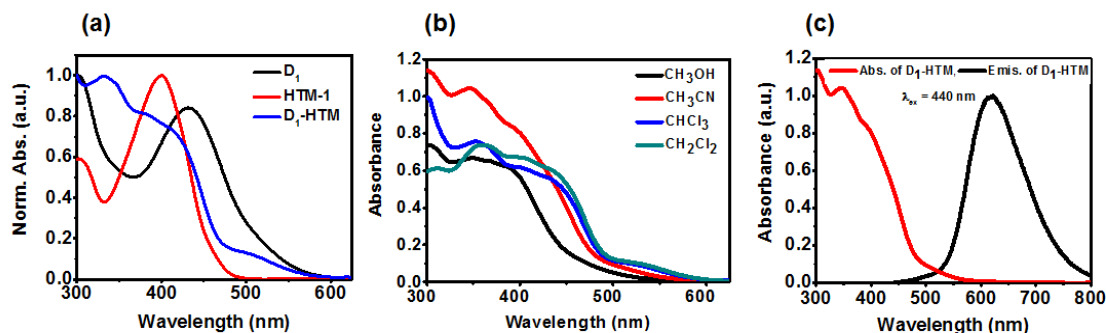
Figure 2. (a) Normalized absorption spectra of **D₁-HTM**, **D₁**, and **HTM-1**. (b) Absorption spectra of D₁-HTM in different solvent. (c) Normalized UV-Vis absorption and emission spectra of D₁-HTM in CHCl₃.

The characteristic peak at 352 nm and 428 nm (**Figure 2a**) is due to π-$\pi*$ and ICT transition from the donor triarylamine unit, donor to acceptor in **D₁** respectively. It was observed that at halogenated solvent the **D₁-HTM** was showing another peak at 517 nm. This peak is may be due to the interaction between dye and HTM part which leads to observe the broadened spectrum (**Figure 2c**). Such broadening of spectrum by plasmon type excitation is proposed recently.[47] Further, the λ_{max} of the D₁-HTM were blue shifted in compared to model chromophores **D₁** and **HTM-1**.
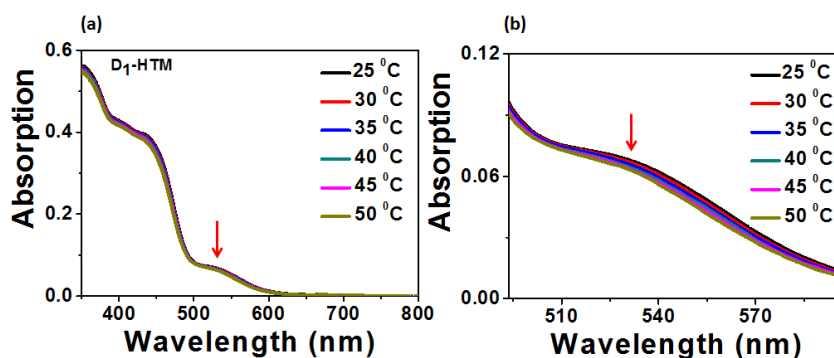
Figure 3. (a) UV-Vis spectra of **D₁-HTM** at various temperatures and (b) the zoomed version of the same spectra in the temperature range from 510 nm to 580 nm.

To understand the nature of possible interaction between dye and HTM units (at 517 nm) temperature dependent UV-Vis study was carried out to understand the nature of broad peak centred at 517 nm..

Table 1. Photophysical and electrochemical properties of **D₁-D₁** and **D₁-HTM**

Dye	$\lambda_{max\ (nm)}$[a]	$\lambda_{max\ (nm)}$[b]	$\lambda_{em\ (nm)}$[c]	$\varepsilon\ (10^4\ M^{-1}cm^{-1})$	E_{HOMO}[d] (eV)	E_{LUMO}[e] (eV)	ΔE_{0-0}[f] (eV)
D₁-D₁	437	464	606	4.37 (427nm)	- 5.06	- 2.96	2.10
D₁-HTM	352, 428, 517	-	621	1.17 (352nm), 1.00 (428nm), 0.23 (517 nm)	-5.14	- 2.81	2.33
PTS1	392	-	525	6.03 (392 nm)	- 4.93	-2.40	2.53

[a]Absorption maxima of dye in CH_2Cl_2. [b]Absorption maxima of absorbed dye on TiO_2 (thickness 6 μm, dye concentration 0.1 mM in CH_2Cl_2, dipping time 60 min. [c]Emission maxima of dye in CH_2Cl_2 (excitation, for **D₁-D₁** = 420 nm, for **D₁-HTM** = 440 nm. [d]The oxidation potentials were measured in CH_2Cl_2 with 0.1 M TBAP as supporting electrolyte, Fc^+/Fc as an internal standard. HOMO energy level was calculated from ($E_{HOMO}= - \{E_{ox}$ [Dye] $- E_{1/2}$ [Fc^+/Fc]$\} + 4.8$). [e]E_{LUMO} was calculated from E_{HOMO} and E_{0-0}. [f]Experimental band gap.

It has seen that with increasing the temperature from 25 to 50 °C the intensity of the peak observed at 517 nm was gradually decreased as showed in **Figure 3**, which indicates that the interaction between D₁ and HTM units can be modulated due to

change in orientation. From that above results signified that an intramolecular electron transfer from HTM part to dye unit is possible[48] upon photo excitation. Excitation of **D₁-HTM** at 440 nm showed the emission at 680 nm (**Figure 2a, Table 1**). The absorption and emission wavelength of **D₁-D₁**, **PTS1** and **D₁-HTM** respectively are summarized in **Table 1**. The extinction coefficient belongs to 352, 428 and 517 are 1.17×10^4 M^{-1} cm^{-1} and 1.10×10^4 M^{-1} cm^{-1} and 0.23×10^4 M^{-1}cm^{-1} respectively, which make **D₁-HTM** a better light harvesting sensitizer
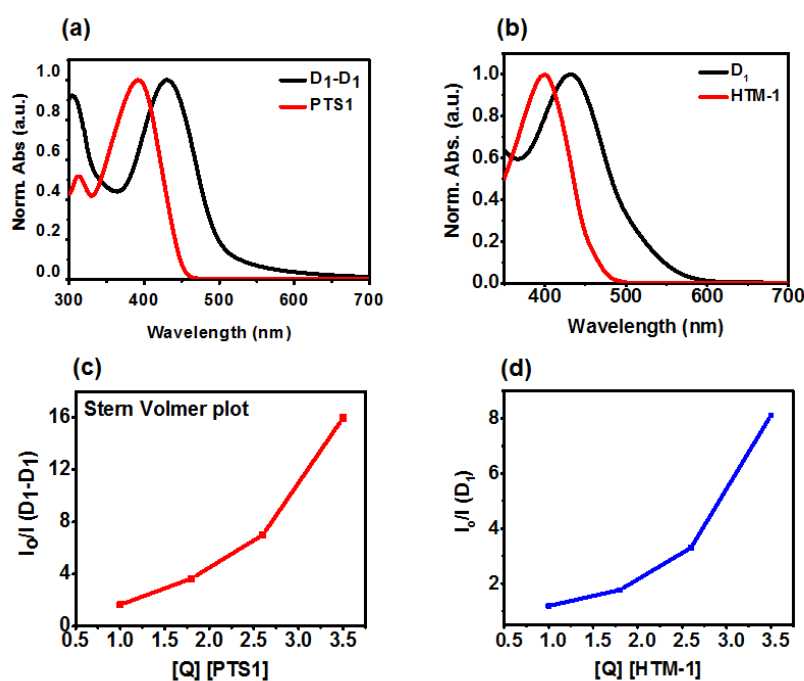
Figure 4. (a) UV-vis absorption spectra of **D₁-D₁** and **PTS1**. (b) UV-vis absorption spectra of **D₁** and **HTM-1**. (c) Stern-Volmer plot were carried out from fluorescence quenching of **D₁-D₁** and **D₁** by addition of quencher **PTS1** and (d) **HTM-1**. λ_{ex} for **D₁-D₁**, **D₁** are 437nm and 433 nm respectively.

For better understanding the photo-induced electron transfer from HTM moiety to **D₁** dye part in **D₁-HTM** careful photoluminescence quenching studies were carried out. The

intensity of **D$_1$-D$_1$** and **D$_1$** were quenched by addition of specified concentration of **PTS1** and **HTM-1** respectively (**Figure 4a** and **Figure 4b**). The excitation wavelength of 560 nm was selected for **D$_1$-D$_1$** so that the **PTS1** was not excited directly (λ_{max} = 437 nm). A similar experiment of quenching of excited state of **D$_1$** by **HTM-1** was also carried out. On these above experiment it has seen that the intensity of both **D$_1$-D$_1$** and **D$_1$** were reduced gradually. Therefore a clear electron transfer mechanism was established from **PTS1** and **HTM-1** to **D$_1$-D$_1$** and **D$_1$** respectively upon excitation. This result gave a specific idea about the photo-induced electron transfer from **D$_1$** moiety to HTM part in **D$_1$-HTM** molecule.

5.2.3 Electrochemical Studies

Cyclic voltammetry (CV) were studied to understand the electron injection from the **D$_1$-HTM** to conduction band of TiO$_2$ and the efficiency of dye regeneration, which is performed in CH$_2$Cl$_2$ by using 0.1 M tetra butyl ammonium perchlorate as supporting electrolyte. The electrochemical properties of dyes were investigated by cyclic voltammetry (**Figure 5**). The highest occupied molecular orbital (HOMO) of **D$_1$-HTM** (–5.14 eV) are lying below the energy level of I$^-$/I$_3^-$ redox couple (−4.6 eV), so that the oxidized dye formed after electron injection into the conduction band of TiO$_2$ can be effectively regenerated by accepting electrons from the redox couple.

Furthermore the LUMO of the oxidised dyes (−2.81 eV) is situated on the above of Fermi level of TiO$_2$ (− 4.0 eV) which facilitates the electron injection from the LUMO of dye. The zero-zero excitation (E_{0-0}) estimated from the onset of UV-vis absorption spectrum. E_{LUMO} energy level was calculated by subtraction of E_{0-0} from E_{HOMO}.
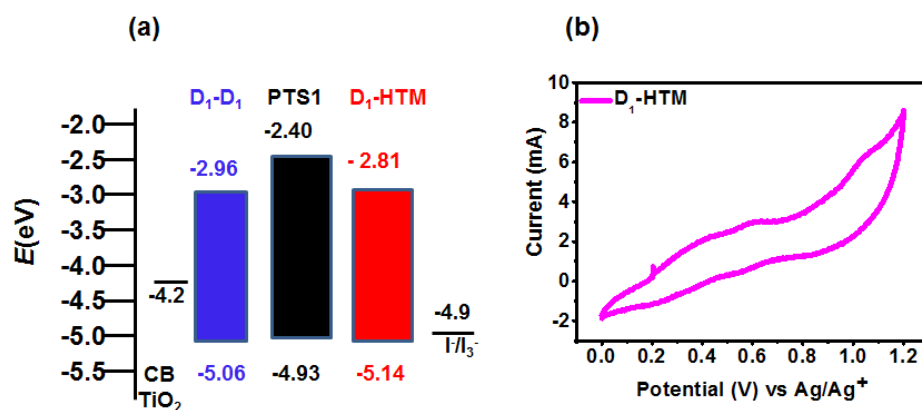
Figure 5. (a)Energy level diagram of **D₁-HTM**, **D₁-D₁** and **PTS1**. (b) Cyclic voltammetry of **D₁-HTM**.

Instead minimum over potentials required for electron injection, around 100-150mV, these dyes showed a significant potential loss (around 1.2 eV) for the LUMO to conduction band edge electron transfer. On careful observation it has seen the HOMO (–5.14 eV) and LUMO (–2.81 eV) of **D₁-HTM** were close to HOMO of **PTS1** (–4.93 eV) and LUMO of **D₁-D₁**. This observation also support the photo-induced electron transfer from donor HTM part to excited **D₁** dye moiety in **D₁-HTM**.

5.2.4 Density Functional Theory Calculations

To understand the electron distribution of **D₁-HTM**, DFT calculations were performed with Gaussian 09 programme using B3LYP/6-31 G (d,p) level (**Table 2a** and **Table 2b**). From the frontier molecular orbital calculation it has seen that HOMO and HOMO−1 of **D₁-HTM** are localized mostly on HTM unit and HOMO−2 electron densities is maximum on donor part of **D₁** unit. Electron density of LUMO and LUMO+2 are maximum on the anchoring unit of **D₁** part whereas, electron localization is maximum on HTM part in LUMO+1.
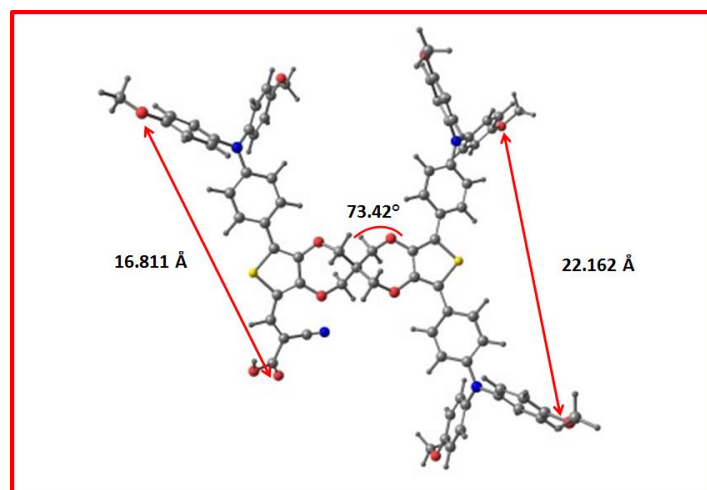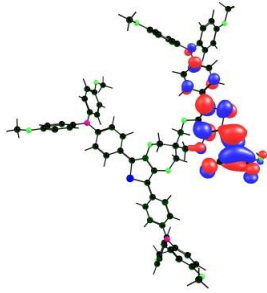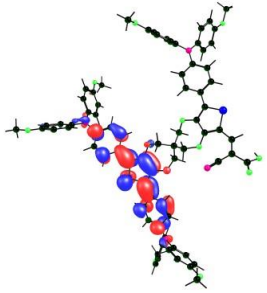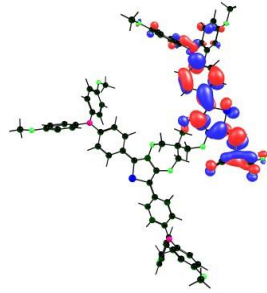
Figure 6. The calculated distance between two oxygen atoms of opposite sides methoxy group (HTM part, right side of dioxepine) and distance between oxygen atom of methoxy group to carbonyl oxygen of dye part (left side of dioxepine).

The energy level of HOMO–2 (–4.95 eV) and LUMO (–2.48 eV) calculated from DFT studied of **D₁-HTM** is nicely closed to result calculated from cyclic voltammetry. Dipole length of HTM, dye and dihedral angle of spiroBiProDOT in that **D₁-HTM** were calculated from the optimized structure (**Figure 6**).

Table 2a. DFT studies of **D₁- HTM**.

Description	HOMO of HTM in D_1-HTM	HOMO - 1 of HTM in D_1-HTM	HOMO of dye in D_1-HTM
Molecular orbital			
Energy (eV)	-4.29	-4.66	-4.95

Table 2b. DFT studies of **D₁- HTM**.

Description	LUMO of D₁ in **D₁-HTM**	LUMO of HTM in **D₁-HTM**	LUMO + 1 of D₁ in **D₁-HTM**
Molecular orbital			
Energy (eV)	-2.48	-1.08	-0.84

5.2.5 Photovoltaic Studies

The photocurrent density-voltage (*J-V*) measurements of the cells were carried out under an irradiance of 100 mW/cm^2 simulated AM 1.5G sunlight. Dye is completely soluble in CH$_2$Cl$_2$, so dye solution was prepared in CH$_2$Cl$_2$ and corresponding *J-V* characteristics are showed in **Table 3**. In comparison the best efficiency of 2.24 % (J_{sc}= 5.27 mA/cm^2 and V_{oc} = 0.590 V) was obtained by using 5 equivalent CDCA. But addition of 10 equivalent of CDCA the efficiency is decreased up to 1.84 % (J_{sc}= 4.38 mA/cm^2 and V_{oc} = 0.587 V). Here CDCA played an important rule for increasing all the photovoltaic parameters. By using 5 equivalent of CDCA the J_{sc} is increased more than 100 % but, V_{oc} increased up to 30 mV. On addition of 10 equivalent of CDCA the 17 % of J_{sc} is decreased whereas, the V_{oc} remains almost same (**Figure 7a**). The reason could be reduced amount of dye on TiO$_2$ surface. Incident photon-to-current

conversion efficiency (IPCE) of **D$_1$-HTM** was recorded to understand the current conversion efficiency on TiO$_2$; corresponding profiles are shown in **Figure 7b**.
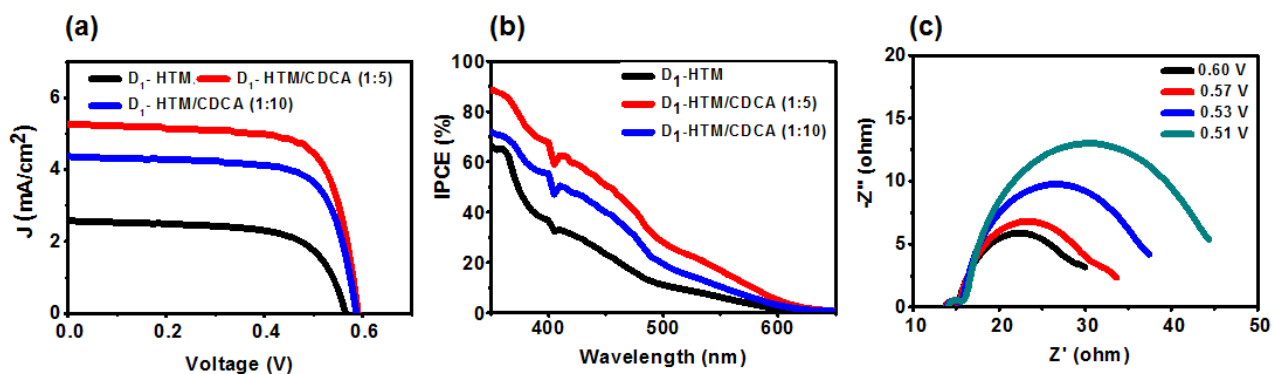
Figure 7. (a) IV and (b) IPCE curve of **D$_1$-HTM** at without CDCA, 5 equivalents and 10 equivalents of CDCA. (c) Impedance spectra of **D$_1$-HTM** at different applied bias (0.6 to 0.51 V).

D$_1$-HTM generally was showing three types of peak in IPCE spectra. Among them highest intensity was shown by using 5 equivalent of CDCA as a co-adsorbent. Without of any co-adsorbent IPCE of 30 % at 440 nm and 8 % at 520 nm which is increased to IPCE of 60 % at 442 nm and 21 % at 517 nm after using 5 equivalent of CDCA. This result also supports the *J-V* curve of **D$_1$-HTM** at 5 equivalent of CDCA. Again the IPCE is also decreased after addition of 10 equivalent of CDCA. Photovoltaic device data of this dye with 5% and 10% equivalent of CDCA was given in **Table 3**.

Table 3. Photovoltaic parameters of **D₁-HTM** dye.

Dyes	J_{sc} (mA/cm^2)	V_{oc} (V)	ff (%)	PCE (%)
D₁-HTM	2.58	0.566	66.1	0.96
D₁-HTM/CDCA (1:5)	5.27	0.590	72.1	2.24
D₁-HTM/CDCA (1:10)	4.38	0.587	71.7	1.84

TiO$_2$ thickness 8+5 μm and 0.235 cm^2, [dye] = 0.3 mM, dipping solvent CH$_2$Cl$_2$, dipping time 12 h, under AM 1.5 illumination (100 mW/cm^2). [CDCA] = 1.5 mM and 3 mM.

5.2.6 Electrochemical Impedance Spectroscopy

The impedance of electrons in the photo electrochemical cell at the forward bias was analysed by electrochemical impedance spectroscopy (EIS). The electrochemical impedance spectra of spiro-dyes are recorded for the DSSC devices under a forward bias of 0.51, 0.54, 0.57 and 0.6 V in the dark (**Table 4**).

Table 4. Electrochemical impedance parameters of spiro dyes at different applied bias

DSSC	Applied Bias (V)	R_{ct} (ohm)	C_μ (mF)	τ_n (ms)	R_s (ohm)
D₁-HTM/CDCA (1:5)	0.60	10.51	1.37	14.39	13.79
D₁-HTM/CDCA (1:5)	0.57	13.42	1.19	15.96	13.89
D₁-HTM/CDCA (1:5)	0.54	17.77	0.92	16.35	14.04
D₁-HTM/CDCA (1:5)	0.51	23.63	0.71	16.78	14.19

Electron lifetime was calculated from capacitance and charge transfer resistance: Lifetime $(\tau) = R_{ct} \times C_\mu$

The Nyquist plots of three dyes are shown in **Figure 7c**. In a typical DSSC Nyquist spectrum there are three semicircles associated with the charge transfer processes , first the high frequency region associated with the counter electrode / electrolyte interface, the mid

frequency large semicircle for the charge transfer at the TiO_2-dye / electrolyte interface and the third at low frequency part indicates ion diffusion resistance or Warburg diffusion coefficient in the electrolyte. Here, the major semicircles of three dyes are associated with the charge transport process at the interfaces between TiO_2 and the electrolyte because of the experiment carried out in dark.[48,49] The charge transfer resistance (R_{ct}) on the TiO_2 surface denoted the charge recombination between the electrons resides on TiO_2 at forward bias and electrolyte which is measured by the large semicircle area. A large R_{ct} is indicated by a small charge recombination. The best efficiency cell using 5 equivalent of CDCA was used to measure Charge transfer resistance, capacitance and life time. Among different applied bias at 0.51 V **D_1-HTM** showed high impedance of 23.63 ohm, whereas the capacitance was relatively low of 0.71 mF. The chemical capacitance (C_μ) has been, thus, extrapolated from fitting the experimental data with an equivalent circuit model showed in **Figure 7c**. High capacitance of **D_1-HTM** (1.19 mF) at 0.57 applied bias indicates more number of electrons present the conduction band. Electron life time on TiO_2 of 15.96 ms at the bias potential was calculated by multiplication of charge transfer resistance with corresponding fitted capacitance. The long electron lifetime and better passivation of surface due to the spiro-linker lead to high J_{sc} of **D_1-HTM** at 0.51 V (**Table 4**).

5.3 Conclusion

Orthogonally functionalized dye and HTM in a same dioxepine moiety was synthesized and characterized. The absorption spectrum was blue shifted and broadened compared to the individual counterparts, due to dye and HTM interactions. Photoluminescence quenching studies were carried out for **D_1-D_1** and **D_1** by using the quencher **PTS1** and **HTM-1** respectively in solution process to understand the Photo-induced electron transfer mechanism. Electrochemical and photo-physical studies of **D_1-HTM** were carried out to

optimize the charge injection and dye regeneration processes. Liquid DSSC with iodolyte electrolyte, **D₁-HTM** showed a device efficiency of 2.24 % with a V_{oc} and J_{sc} of 0.590 V and 5.27 mA/cm^2. The IPCE spectrum of **D₁-HTM** increases upto 600 nm due to incorporating dye and hole transporting material linked by spiro moiety.

5.4 Experimental section

5.4.1 Materials and instrument

All the reagents and solvents were purchased from Aldrich and TCI chemicals and used without further purification. Required precursor 3,4-dimethoxythiophene[44] was synthesised from thiophene and converted into 2H,2'H,4H,4'H-3,3'-spirobi[thieno[3,4-b][1,4]dioxepine][45] according to the reported literature procedure. Precursor **2**[50] was synthesized from reported literature procedure.[46] All oxygen- and moisture-sensitive reactions were performed under nitrogen atmosphere. The other materials were of the common commercial level and used as received. PhMe was dried over Na/benzophenone ketyl and freshly distilled prior to use.

5.4.2 Characterization. All the instruments for characterization (^{1}H NMR, ^{13}C NMR, MALDI-TOF-MS, UV-vis spectra, differential pulse voltammetry, electrochemical impedance spectra, solar simulator) of organic dyes are same as presented in **Chapter 2**, section 2.4.2.

5.4.3 Characterization of synthetic compound

2H,2'H,4H,4'H-3,3'-Spirobi[thieno[3,4-b][1,4]dioxepine]-6-carbaldehyde, 1: To an ice cooled solution of dioxepine (300 mg, 1.01 mmol) in dry dichloroethane (20 mL),

DMF (100 μL, 1.1 mmol) and POCl₃ (110 μL, 1.01 mmol) were added by syringe under nitrogen atmosphere. The solution was stirred for 1 h at 0 °C then allowed to warm to room temperature and left an additional hour before heating to reflux for 2 h. The reaction mixture was cooled to rt, aqueous 1M NaOAc was added and refluxed for 4 h. The mixture was washed with water (50 mL) and extracted with CH_2Cl_2 (50 mL). Solvents were removed under reduced pressure and purified by column chromatography by using ethyl acetate and pet ether as an eluent. Yield 230 mg, 68%. ^{1}H NMR (400 MHz, CDCl₃) δ: 4.04 – 4.13 (m, 6 H), 4.29 (s, 2 H), 6.48 (s, 2 H), 6.90 (s, 1 H), 9.95 (s, 1 H). ^{13}CNMR (100 MHz, CDCl₃) δ: 50.1, 70.9, 71.4, 105.2, 115.8, 122.9, 148.6, 154.6, 180.9.

6,6',8'-Tris(4-(bis(4-methoxyphenyl)amino)phenyl)-2H,2'H,4H,4'H-3,3'-spirobi[thieno[3,4-b][1,4]dioxepine]-8-carbaldehyde, 3: A mixture of **1** (0.46 mmol, 150 mg), **2** (1.0 g, 2.8 mmol), K₂CO₃ (160 mg g, 1.2mmol), Pd(OAc)₂ (0.5 mol%), PCy₃ (0.5 mol%), and PivOH (0.15 mol%) were taken in a Schlenk tube under nitrogen atmosphere. 5 mL of dry DMA was added and kept the reaction at 120 °C temperature under the argon atmosphere for 24 h. The reaction mixture was washed with 100 mL of water and extracted with 100 mL of CH_2Cl_2. Solvents were removed under reduced pressure and purified by column chromatography by using pet ether, EtOAc and pet. ether as an eluent. Yield: 260 mg, 46 %. ^{1}H NMR (400 MHz, CDCl₃) δ: 3.81 (s, 6 H), 3.83 (s, 12 H), 4.19 (d, J = 8 Hz, 8H), 6.80-6.92 (m, 20 H), 6.97-7.06 (m, 2 H), 7.06-7.14(m,10 H), 7.60 (d, J = 8 Hz, 4 H), 10 (s, 1 H). ^{13}C NMR (100MHz, CDCl₃) δ: 55.5, 55.6, 70.5, 71, 71.3, 114.1, 114.3, 114.6, 114.8, 120.2, 121.9, 124, 125.4, 126.4, 126.5, 127.3, 127.9, 128.9, 131.2, 138, 139.7, 140.6, 143.5, 144, 156, 156.6, 158.8, 160.2, 180.2.

2-Cyano-3-(6,6',8'-tris(4-(bis(4-methoxyphenyl)amino)phenyl)-2H,2'H,4H,4'H-3,3'-spirobi[thieno[3,4-b][1,4]dioxepin]-8-yl)acrylic acid (D₁- HTM), 4: A mixture of **3** (150 mg, 0.12 mmol), cyanoacetic acid (10 mg, 0.12 mmol), NH₄OAc (10 mg, 0.12mmol) and glacial AcOH (10 mL) was refluxed for 12 h. After 12 h the reaction mixture was washed with water and Et₂O thoroughly. Compound was purified by washing and yield was 124 mg, 79 %. ^{1}H NMR (500 MHz, CDCl₃) δ : 3.83 (s, 12 H), 3.87 (s, 6 H), 4.21- 4.37 (m, 8 H), 6.87-6.95 (m, 18 H), 7.11 (d, J = 5 Hz, 8 H), 7.54 (t, J = 10 Hz, 4 H), 7.67 (t, J = 5 Hz, 5 H), 7.79 (d, J = 5 Hz, 1 H), 8.45 (s, 1 H). ^{13}C NMR (125 MHz, CDCl₃): 55.4, 55.5, 65.9, 70.4, 70.5, 71, 114, 114.1, 114.2, 114.7, 114.9, 119.3, 120, 120.3, 126.5, 126.7, 127.1, 127.2, 127.4, 127.9, 128, 140.4, 140.7, 144.2, 144.3, 156, 156.8, 158.6.MALDI-TOF m/z calcd for [M+K]$^+$ [C₇₇H₆₄N₄O₁₂S₂K]$^+$ 1340.5993, found 1340.2365.

4, 4'-(3,4-Dimethoxythiophene-2,5-diyl)bis(N,N-bis(4-methoxyphenyl)aniline), HTM-1: 3,4-Dimethoxythiophene (100 mg, 0.694 mmol), **2** (650 mg, 0.650 mmol), K₂CO₃ (240 mg, 1.74mmol), Pd(OAc)₂ (0.5 mol%), PCy₃ (0.5 mol%), and PivOH (0.15 mol%) were taken in a Schlenk tube under nitrogen atmosphere. 5 mL of dry DMA was added to that and kept the reaction at 120 °C temperature under the same atmosphere for 24 h. After 24 h, the reaction mixture was washed with 200 mL of water and extracted with 150 mL of CH₂Cl₂. Solvents were removed under reduced pressure and purified by column chromatography by using EtOAc and pet ether as an eluent. Yield: 506 mg, 97 %. ^{1}H NMR (200 MHz, CDCl₃) δ: 3.79 (s, 12 H), 3.86 (s, 6 H), 6.88 (q, J = 8 Hz, 8 H), 6.92 (d, J = 8 Hz, 4 H), 7.07 (q, J = 6 Hz, 8 H), 7.52 (d, J = 8 Hz, 4 H). ^{13}C NMR (125 MHz, CDCl₃): 55.5, 59.9, 112.4, 113.5, 114.5, 120.4, 125.6, 126.3, 127.1, 128, 145.9, 155.5.

4,4',4'',4'''-(2H,2'H,4H,4'H-3,3'-Spirobi[thieno[3,4-b][1,4]dioxepine]-6,6',8,8'-tetrayl)tetrakis(N,N-bis(4-methoxyphenyl)aniline), PTS1: In a schlenk tube 2H,2'H,4H,4'H-3,3'-spirobi[thieno[3,4-b][1,4]dioxepine] (100 mg, 0.33 mmol), compound 2 (1 g, 2.7 mmol), K_2CO_3 (120 mg, 0.84 mmol), Pd(OAc)$_2$ (0.5 mol%), PCy$_3$ (0.5 mol%), and PivOH (0.15 mol%) were taken under nitrogen atmosphere. 5 mL of dry DMA was added to that and kept the reaction at 115 °C to 120 °C temperature under innert atmosphere for 24 h. After 24 h, the reaction mixture was washed with 150 mL of water and extracted with 100 mL of CH_2Cl_2. Solvents were removed under reduced pressure and purified by column chromatography by using CH_2Cl_2 and pet ether as an eluent. Yield: 310 mg (51 %). ^{1}H NMR (200 MHz, CDCl$_3$) δ: 3.80 (s, 24 H), 3.86 (s, 8 H), 6.81-6.93 (m, 24 H), 7.01-7.14 (m, 18 H), 7.50-7.64 (m, 6 H). ^{13}C NMR (125 MHz, CDCl$_3$): 52.6, 55.3, 104.7, 113.2, 114.5, 119.9, 124.7, 125.7, 125.9, 130, 132.4, 140.9, 141.3, 149.8, 156.2.3.

5.4.4 Fabrication of dye sensitized solar cells. The methods of preparation of solar cell with synthesized dyes were same as presented in **Chapter 2**, section 2.4.3.

5.5 References

(1)   Gong, J.; Liang, J.; Sumathy, K. Review on Dye-Sensitized Solar Cells (DSSCs): Fundamental Concepts and Novel Materials. *Renew. Sustain. Energy Rev.* **2012**, *16*, 5848–5860.

(2)   Panwar, N. L.; Kaushik, S. C.; Kothari, S. Role of Renewable Energy Sources in Environmental Protection: A Review. *Renew. Sustain. Energy Rev.* **2011**, *15*, 1513–1524.

(3)   Lewis, N. S.; Nocera, D. G. Powering the Planet: Chemical Challenges in Solar Energy Utilization. *Proc. Natl. Acad. Sci.* **2006**, *103*, 15729–15735.

(4)   Chow, T. T. A Review on Photovoltaic/Thermal Hybrid Solar Technology. *Appl. Energy* **2010**, *87*, 365–379.

(5)   Gloeckler, M.; Sankin, I.; Zhao, Z. CdTe Solar Cells at the Threshold Efficiency. *IEEE J. Photovolt.* **2013**, *3*, 1389–1393.

(6)   Jackson, P.; Hariskos, D.; Lotter, E.; Paetel, S.; Wuerz, R.; Menner, R.; Wischmann, W.; Powalla, M. New World Record Efficiency for Cu(In,Ga)Se$_2$ Thin-Film Solar Cells beyond 20%. *Prog. Photovolt. Res. Appl.* **2011**, *19*, 894–897.

(7)   Li-Kao, Z. J.; Naghavi, N.; Erfurth, F.; Guillemoles, J. F.; Gérard, I.; Etcheberry, A.; Pelouard, J. L.; Collin, S.; Voorwinden, G.; Lincot, D. Towards Ultrathin Copper Indium Gallium Diselenide Solar Cells: Proof of Concept Study by Chemical Etching and Gold Back Contact Engineering. *Prog. Photovolt. Res. Appl.* **2012**, *20*, 582–587.

(8)   Saccone, D.; Galliano, S.; Barbero, N.; Quagliotto, P.; Viscardi, G.; Barolo, C. Polymethine Dyes in Hybrid Photovoltaics: Structure–Properties Relationships. *Eur. J. Org. Chem.* **2016**, *2016*, 2244–2259.

(9)   Shah, A.; Torres, P.; Tscharner, R.; Wyrsch, N.; Keppner, H. Photovoltaic Technology: The Case for Thin-Film Solar Cells. *Science* **1999**, *285*, 692–698.

(10)   Yoon, J.; Jo, S.; Chun, I. S.; Jung, I.; Kim, H.-S.; Meitl, M.; Menard, E.; Li, X.; Coleman, J. J.; Paik, U.; et al. GaAs Photovoltaics and Optoelectronics Using Releasable Multilayer Epitaxial Assemblies. *Nature* **2010**, *465*, 329–333.

(11)   Grätzel, M. Dye-Sensitized Solar Cells. *J. Photochem. Photobiol. C Photochem. Rev.* **2003**, *4*, 145–153.

(12)   Nazeeruddin, M. K. Michael Graetzel Festschrift, a Tribute for His 60th Birthday. *Coord. Chem. Rev.* **2004**, *248*, 1161–1164.

(13)   O'Regan, B.; Grätzel, M. A Low-Cost, High-Efficiency Solar Cell Based on Dye-Sensitized Colloidal TiO_2 Films. *Nature* **1991**, *353*, 737–740.

(14)   Hwang, S.; Lee, J. H.; Park, C.; Lee, H.; Kim, C.; Park, C.; Lee, M.-H.; Lee, W.; Park, J.; Kim, K.; Park, N.G.; Kim, S. A Highly Efficient Organic Sensitizer for Dye-Sensitized Solar Cells. *Chem. Commun.* **2007**, *0*, 4887–4889.

(15)   Bach, U.; Lupo, D.; Comte, P.; Moser, J. E.; Weissörtel, F.; Salbeck, J.; Spreitzer, H.; Grätzel, M. Solid-State Dye-Sensitized Mesoporous TiO_2 Solar Cells with High Photon-to-Electron Conversion Efficiencies. *Nature* **1998**, *395*, 583–585.

(16)   Hagberg, D. P.; Yum, J.-H.; Lee, H.; De Angelis, F.; Marinado, T.; Karlsson, K. M.; Humphry-Baker, R.; Sun, L.; Hagfeldt, A.; Grätzel, M.; et al. Molecular Engineering of Organic Sensitizers for Dye-Sensitized Solar Cell Applications. *J. Am. Chem. Soc.* **2008**, *130*, 6259–6266.

(17)   Grätzel, M. Conversion of Sunlight to Electric Power by Nanocrystalline Dye-Sensitized Solar Cells. *J. Photochem. Photobiol. Chem.* **2004**, *164*, 3–14.

(18)   Chiba, Y.; Islam, A.; Watanabe, Y.; Komiya, R.; Koide, N.; Han, L. Dye-Sensitized Solar Cells with Conversion Efficiency of 11.1%. *Jpn. J. Appl. Phys.* **2006**, *45*, L638.

(19)   Nguyen, W. H.; Bailie, C. D.; Burschka, J.; Moehl, T.; Grätzel, M.; McGehee, M. D.; Sellinger, A. Molecular Engineering of Organic Dyes for Improved Recombination Lifetime in Solid-State Dye-Sensitized Solar Cells. *Chem. Mater.* **2013**, *25*, 1519–1525.

(20)   Koumura, N.; Wang, Z.-S.; Mori, S.; Miyashita, M.; Suzuki, E.; Hara, K. Alkyl-Functionalized Organic Dyes for Efficient Molecular Photovoltaics. *J. Am. Chem. Soc.* **2006**, *128*, 14256–14257.

(21)   Listorti, A.; O'Regan, B.; Durrant, J. R. Electron Transfer Dynamics in Dye-Sensitized Solar Cells. *Chem. Mater.* **2011**, *23*, 3381–3399.

(22)   Mathew, S.; Yella, A.; Gao, P.; Humphry-Baker, R.; Curchod, B. F. E.; Ashari-Astani, N.; Tavernelli, I.; Rothlisberger, U.; Nazeeruddin, M. K.; Grätzel, M. Dye-Sensitized Solar Cells with 13% Efficiency Achieved through the Molecular Engineering of Porphyrin Sensitizers. *Nat. Chem.* **2014**, *6*, 242–247.

(23)   Yao, Z.; Zhang, M.; Wu, H.; Yang, L.; Li, R.; Wang, P. Donor/Acceptor Indenoperylene Dye for Highly Efficient Organic Dye-Sensitized Solar Cells. *J. Am. Chem. Soc.* **2015**, *137*, 3799–3802.

(24)   Kakiage, K.; Aoyama, Y.; Yano, T.; Oya, K.; Fujisawa, J.; Hanaya, M. Highly-Efficient Dye-Sensitized Solar Cells with Collaborative Sensitization by Silyl-Anchor and Carboxy-Anchor Dyes. *Chem. Commun.* **2015**, *51*, 15894–15897.

(25) Li, X.; Zheng, Z.; Jiang, W.; Wu, W.; Wang, Z.; Tian, H. New D–A–π–A Organic Sensitizers for Efficient Dye-Sensitized Solar Cells. *Chem. Commun.* **2015**, *51*, 3590–3592.

(26) Wang, P.; Zakeeruddin, S. M.; Moser, J. E.; Nazeeruddin, M. K.; Sekiguchi, T.; Grätzel, M. A Stable Quasi-Solid-State Dye-Sensitized Solar Cell with an Amphiphilic Ruthenium Sensitizer and Polymer Gel Electrolyte. *Nat. Mater.* **2003**, *2*, 402–407.

(27) Wang, Z.-S.; Sayama, K.; Sugihara, H. Efficient Eosin Y Dye-Sensitized Solar Cell Containing Br-/Br$_3^-$ Electrolyte. *J. Phys. Chem. B* **2005**, *109*, 22449–22455.

(28) Oskam, G.; Bergeron, B. V.; Meyer, G. J.; Searson, P. C. Pseudohalogens for Dye-Sensitized TiO$_2$ Photoelectrochemical Cells. *J. Phys. Chem. B* **2001**, *105*, 6867–6873.

(29) Wang, P.; Zakeeruddin, S. M.; Moser, J.-E.; Humphry-Baker, R.; Grätzel, M. A Solvent-Free, SeCN-/(SeCN)3- Based Ionic Liquid Electrolyte for High-Efficiency Dye-Sensitized Nanocrystalline Solar Cells. *J. Am. Chem. Soc.* **2004**, *126*, 7164–7165.

(30) Burschka, J.; Pellet, N.; Moon, S.-J.; Humphry-Baker, R.; Gao, P.; Nazeeruddin, M. K.; Grätzel, M. Sequential Deposition as a Route to High-Performance Perovskite-Sensitized Solar Cells. *Nature* **2013**, *499*, 316–319.

(31) Wang, M.; Grätzel, C.; M. Zakeeruddin, S.; Grätzel, M. Recent Developments in Redox Electrolytes for Dye -Sensitized Solar Cells. *Energy Environ. Sci.* **2012**, *5*, 9394–9405.

(32)   Tian, H.; Gabrielsson, E.; Yu, Z.; Hagfeldt, A.; Kloo, L.; Sun, L. A Thiolate/ Disulfide Ionic Liquid Electrolyte for Organic Dye -Sensitized Solar Cells Based on Pt-Free Counter Electrodes. *Chem. Commun.* **2011**, *47*, 10124–10126.

(33)   Nusbaumer, H.; Zakeeruddin, S. M.; Moser, J.-E.; Grätzel, M. An Alternative Efficient Redox Couple for the Dye-Sensitized Solar Cell System. *Chem. Weinh. Bergstr. Ger.* **2003**, *9*, 3756–3763.

(34)   Kim, B.-G.; Chung, K.; Kim, J. Molecular Design Principle of All-Organic Dyes for Dye-Sensitized Solar Cells. *Chem. – Eur. J.* **2013**, *19*, 5220–5230.

(35)   Geary, E. A. M.; Yellowlees, L. J.; Jack, L. A.; Oswald, I. D. H.; Parsons, S.; Hirata, N.; Durrant, J. R.; Robertson, N. Synthesis, Structure, and Properties of [Pt(II)(Diimine)(Dithiolate)] Dyes with 3,3'-, 4,4'-, and 5,5'-Disubstituted Bipyridyl: Applications in Dye-Sensitized Solar Cells. *Inorg. Chem.* **2005**, *44*, 242–250.

(36)   Ito, S.; Liska, P.; Comte, P.; Charvet, R.; Péchy, P.; Bach, U.; Schmidt-Mende, L.; Zakeeruddin, S. M.; Kay, A.; Nazeeruddin, M. K.; et al. Control of Dark Current in Photoelectrochemical ($TiO_2/I^- – I_3^-$) and Dye-Sensitized Solar Cells. *Chem. Commun.* **2005**, *0*, 4351–4353.

(37)   Hao, Y.; Tian, H.; Cong, J.; Yang, W.; Bora, I.; Sun, L.; Boschloo, G.; Hagfeldt, A. Triphenylamine Groups Improve Blocking Behavior of Phenoxazine Dyes in Cobalt-Electrolyte-Based Dye-Sensitized Solar Cells. *ChemPhysChem 15*, 3476–3483.

(38)   Hao, Y.; Gabrielsson, E.; Lohse, P. W.; Yang, W.; Johansson, E. M. J.; Hagfeldt, A.; Sun, L.; Boschloo, G. Peripheral Hole Acceptor Moieties on an Organic Dye Improve Dye-Sensitized Solar Cell Performance. *Adv. Sci.* 2015, *0*, 174-176.

(39)   Scholz, M.; Flender, O.; Boschloo, G.; Oum, K.; Lenzer, T. Ultrafast Electron and Hole Transfer Dynamics of a Solar Cell Dye Containing Hole Acceptors on Mesoporous TiO2 and Al2O3. *Phys. Chem. Chem. Phys.* **2017**, *19*, 7158–7166.

(40)   Hagberg, D. P.; Jiang, X.; Gabrielsson, E.; Linder, M.; Marinado, T.; Brinck, T.; Hagfeldt, A.; Sun, L. Symmetric and Unsymmetric Donor Functionalization. Comparing Structural and Spectral Benefits of Chromophores for Dye-Sensitized Solar Cells. *J. Mater. Chem.* **2009**, *19*, 7232–7238.

(41)   Feldt, S. M.; Gibson, E. A.; Gabrielsson, E.; Sun, L.; Boschloo, G.; Hagfeldt, A. Design of Organic Dyes and Cobalt Polypyridine Redox Mediators for High-Efficiency Dye-Sensitized Solar Cells. *J. Am. Chem. Soc.* **2010**, *132*, 16714–16724.

(42)   Li, H.; Fu, K.; Hagfeldt, A.; Grätzel, M.; Mhaisalkar, S. G.; Grimsdale, A. C. A Simple 3,4-Ethylenedioxythiophene Based Hole-Transporting Material for Perovskite Solar Cells. *Angew. Chem. Int. Ed. 53*, 4085–4088.

(43)   Sil, M. C.; Sudhakar, V.; Kavungathodi, M. F. M.; Punitharasu, V.; Nithyanandhan, J. Orthogonally Functionalized Donor/Acceptor Homo- and Heterodimeric Dyes for Dye-Sensitized Solar Cells: An Approach to Introduce Panchromaticity and Control the Charge Recombination. *ACS Appl. Mater. Interfaces* **2017**, *9*, 34875–34890.

(44) Sadekar, A. G.; Mohite, D.; Mulik, S.; Chandrasekaran, N.; Sotiriou-Leventis, C.; Leventis, N. Robust PEDOT Films by Covalent Bonding to Substrates Using in Tandem Sol–gel, Surface Initiated Free-Radical and Redox Polymerization. *J. Mater. Chem.* **2011**, *22*, 100–108.

(45) Reeves, B. d.; Thompson, B. c.; Abboud, K. a.; Smart, B. e.; Reynolds, J. r. Dual Cathodically and Anodically Coloring Electrochromic Polymer Based on a Spiro Bipropylenedioxythiophene [(Poly(SpiroBiProDOT)]. *Adv. Mater.* **2002**, *14*, 717–719.

(46) Li, T.-Y.; Su, C.; Akula, S. B.; Sun, W.-G.; Chien, H.-M.; Li, W.-R. New Pyridinium Ylide Dyes for Dye Sensitized Solar Cell Applications. *Org. Lett.* **2016**, *18*, 3386–3389.

(47) Li, J.-H.; Gryn'ova, G.; Prlj, A.; Corminboeuf, C. Enhancing the Power Conversion Efficiency of Dye-Sensitized Solar Cells via Molecular Plasmon-like Excitations. *Chem. Commun.* **2017**, *53*, 2423–2426.

(48) Bisquert, J.; Fabregat-Santiago, F.; Mora-Seró, I.; Garcia-Belmonte, G.; Giménez, S. Electron Lifetime in Dye-Sensitized Solar Cells: Theory and Interpretation of Measurements. *J. Phys. Chem. C* **2009**, *113*, 17278–17290.

(49) Wang, J.; Liu, K.; Ma, L.; Zhan, X. Triarylamine: Versatile Platform for Organic, Dye-Sensitized, and Perovskite Solar Cells. *Chem. Rev.* **2016**, *116*, 14675–14725.

(50) Cunha, M. P. da; Do, T. T.; Yambem, S. D.; Pham, H. D.; Chang, S.; Manzhos, S.; Katoh, R.; Sonar, P. A Triphenylamine Substituted Quinacridone Derivative for

Solution Processed Organic Light Emitting Diodes. *Mater. Chem. Phys.* **2018**, *206*, 56–63.

6.1 Summary

In **chapter 1**, more attention was given to solar energy and more conveniently narrowed down to dye sensitized solar cell research. Dye sensitized solar cell is one of the most important up growing technologies due to the low cost, and non-hazardous nature of the components. Out of two types of sensitizers non-metal or organic sensitizer were emerging due to low purification cost and superior absorption properties than the metal based one.

Statement of Problem: Out of various interfaces in DSSC device, dye-TiO$_2$ interface plays an important role for charge injection and dye regeneration besides aggregation of dye on the TiO$_2$ surface. Charge injection from aggregated structure that contributes to the device performance is varied and which can be modulated by co-adsorbing the dyes with optically transparent CDCA. Hence, controlling the dye-dye interaction on the TiO$_2$ surface has become one of the challenging tasks for synthetic chemists besides having desired optical band gap of dyes. Dimeric dyes that are connected through spiro-π-spacer showed better device efficiency than corresponding monomeric units. Generally, for panchromatic absorption, two or more dyes with complementary absorption properties were adsorbed to enhance the light harvesting properties over solar spectrum. In the present approach, this critical problem is solved by connecting two structurally different dyes through spiro-linkage. Spiro-based π-spacer spiroBiProDOT has been explored to synthesize dimeric dyes with orthogonal dye orientation.

In **2nd chapter**, spiro-configured symmetric and un-symmetric dyes were synthesised and characterised by using direct arylation method to avoid traditional Suzuki and Stille coupling. Due to congested structure of the spiro dyes, the molecules can avoid dye aggregation and the spiro-spacer may passivate the TiO$_2$ surface better to avoid the charge

recombination. The two anchoring groups of these dimeric dyes facilitate a strong binding with TiO$_2$ surface. In the context sequential direct arylation reactions have been utilized to synthesize un-symmetrical spiro-dyes by which two different D-π-A dyes can be stitched by spiro-spiroBiProDOT unit. This method is very effective in synthesizing dyes with panchromatic light absorption by judicious choice of dyes that possess complementary absorption properties. Spiro-configured symmetric and un-symmetric dyes were synthesised and characterised by using direct arylation method. This method is very effective in synthesizing dyes with panchromatic light absorption by judicious choice of dyes that possess complementary absorption properties. Dyes **D$_1$-D$_1$**, **D$_2$-D$_2$**, **D$_1$-D$_2$**, and **D$_2$-D$_4$** have been synthesized. Dye **D$_1$-D$_1$** showed the device efficiency of 7.6% (V_{oc} 0.672 V, J_{sc} 16.16 mA/cm^2, ff 70%).

In the **3rd chapter**, dimeric derivatives of symmetric (**D$_{sq}$-D$_{sq}$**), unsymmetric (**D$_1$-D$_{sq}$**) spiro-squaraine dyes and model squaraine dye **D$_{sq}$** were synthesized by using Pd catalysed direct arylation method. These dyes were designed to understand the importance of intermolecular dye-dye interaction which helps to broaden the absorption propertied of the sensitizer, and further the resulting dipole moment exerted by the dyes on the TiO$_2$ surface helps to modulate the V_{oc} of the device. . On the basis of above those points **D$_1$-D$_{sq}$** dye was synthesized in which two different dyes namely **D$_{sq}$** (squaraine unit) and **D$_1$** (donor-π-acceptor) unit connected through spiro-spacer. In this way, a broad spectrum through UV region to NIR region incorporating two different types of dye core through spiro-sp^3 linkage besides intermolecular dyad-dye interactions. In **D$_{sq}$-D$_{sq}$** dye, two **D$_{sq}$** monomeric units were attached through spiroBiProDOT unit to control the aggregation of squaraine dye as well as charge recombination. Out of symmetrical (**D$_{sq}$- D$_{sq}$**) and un-symmetrical squaraine dyes (**D$_1$-D$_{sq}$**) unsymmetrical spiro-squaraine dye (**D$_1$- D$_{sq}$**) is more efficient in terms of circuit voltage V_{oc} of 0.612 V, J_{sc} = 9 mA/cm^2, ff = 71% and η = 3.9%. Whereas, symmetrical dye was

showing V_{oc} of 0.607 V, short-circuit current $J_{sc} = 6.6$ mA/cm^2 and power conversion efficiency (η) = 2.8 % under 1 sun.

In **4th chapter** two dimeric D-π-A dyes (**TT$_1$**, **T$_1$T**) were design, synthesized and characterized to examine the effect in their photovoltaic properties due to the change in the position of spiro-π-spacer. It was observed that the dimeric spiro-dye **T$_1$T,** in which the spiro-spacer was far away from the anchoring unit, showed higher power conversion efficiency (PCE), with 3.9 % (V_{oc} of 0.593 V and J_{sc} of 9.09 mA/cm^2) under 1 sun. On the other hand the positional isomeric dye **TT$_1$**, where the branching spiro-spacer was close to anchoring unit showing maximum 2.5% efficiency (V_{oc} of 0.58 V and J_{sc} of 6.4 mA/cm^2) under simulated AM 1.5G illumination (100 mW/cm^2). On the basis of above experiments, a new dye **TT$_1$T,** where an extra thiophene unit was inserted in between the donor and π-spacer was synthesized and characterized. This dye was also showing general trends of increasing V_{oc} of 0.589 V, J_{sc} of 9.79 mA/cm^2 and maximum PCE of 4.16 %. It was concluded based upon these above studies that the branching unit will be helpful to increase the photovoltaic parameters of the device, when they are away from the anchoring group. The charge transfer resistance (R_{ct} of 11.87 ohm), electron life time (τ_n of 18.8 ms) were maximum in **TT$_1$T** than that of other dyes **TT$_1$** (R_{ct} of 6.75 ohm and τ_n of 5.67 ms) and **T$_1$T** (R_{ct} of 8.42 ohm and τ_n of 11.1 ms).

In **5th chapter**, spiro-configured dye connected with hole-transporting material (**D$_1$-HTM**) was synthesized and characterised by using direct arylation method. Spiro-configured hole-transporting material (**PTS1**) and its monomeric unit (**HTM-1**) were also synthesized by using Pd-catalyzed direct arylation method. Photo-induced electron transfer method was established by photoluminescence quenching studies of spiro-dye, **D$_1$-D$_1$** and **D$_1$** (reported in 2nd chapter) by **PTS1** and **HTM-1** respectively. Due to congested structure of the **D$_1$-HTM**,

this can avoid dye aggregation and charge recombination at the same time. The steric impediment originate from its spiro configuration and covalently connected dye with HTM make **D₁-HTM** a promising candidate for use in efficient DSSCs. Adequate number of devices have been fabricated and provided the details in this chapter. A DSSC device fabricated with **D₁-HTM** showed the PCE of 2.24 % with the V_{oc} and J_{sc} of 0.59 V, and 5.27 mAcm^{-2}, respectively in the presence of 5 equiv. of CDCA.

6.2 Future outlook

The main limitations in solid state dye sensitized solar cell are the pore filling of hole transporting material in TiO₂ layer. This can be overcome in pore filling of the mesoporus by D₁-HTM to make a better dye-HTM interface. Since **D₁-D₁** was giving highest efficiency, therefore it will tried to mixed with other squaraine dye to get panchromatic absorption and better efficiency in future in liquid dye sensitized solar cell.

List of Publications

1. <u>**Sil, M. C.**</u>; Sudhakar, V.; Kavungathodi, M. F. M.; Vellimalai, P.; Nithyanandhan, J*. Orthogonally Functionalized Donor/Acceptor Homo- and Heterodimeric Dyes for Dye-Sensitized Solar Cells: An Approach to Introduce Panchromaticity and Control the Charge Recombination. *ACS Appl. Mater. Interfaces*, **2017**, *9*, 34875-34890.

2. Alagumalai, A.; Kavungathodi, M. F. M.; Vellimalai, P.; <u>**Sil, M. C.**</u>; Nithyanandhan, J*. Effect of   Out-of-Plane Alkyl Group's Position in Dye-Sensitized Solar Cell Efficiency: A   Structure−Property   Relationship   Utilizing   Indoline-Based Unsymmetrical Squaraine Dyes. *ACS Appl. Mater. Interfaces*, **2016**, *8*, 35353−35367.

3. <u>**Sil, M. C.**</u>; Sudhakar, V.; Kavungathodi, M. F. M.; Nithyanandhan, J*. Homo- and Hetero- Dimeric Dyes for Dye-sensitized Solar Cells: Panchromatic Light Absorption and Modulated Open Circuit Potential (communicated).

4. <u>**Sil, M. C.**</u>; Kavungathodi, M. F. M.; Nithyanandhan, J*. Effect and Position of Spiro-Bipropylenedioxythiophene π-Spacer in Donor/Acceptor Dyes for Dye-Sensitized Solar Cell (communicated).

5. <u>**Sil, M. C.**</u>; Kavungathodi, M. F. M.; Nithyanandhan, J*. Orthogonally Functionalized Molecular Dyad Containing D-π-A Dye and Hole Transport Moiety for Dye-Sensitized Solar Cell (communicated).

Proton and 13 C NMR chapter 2
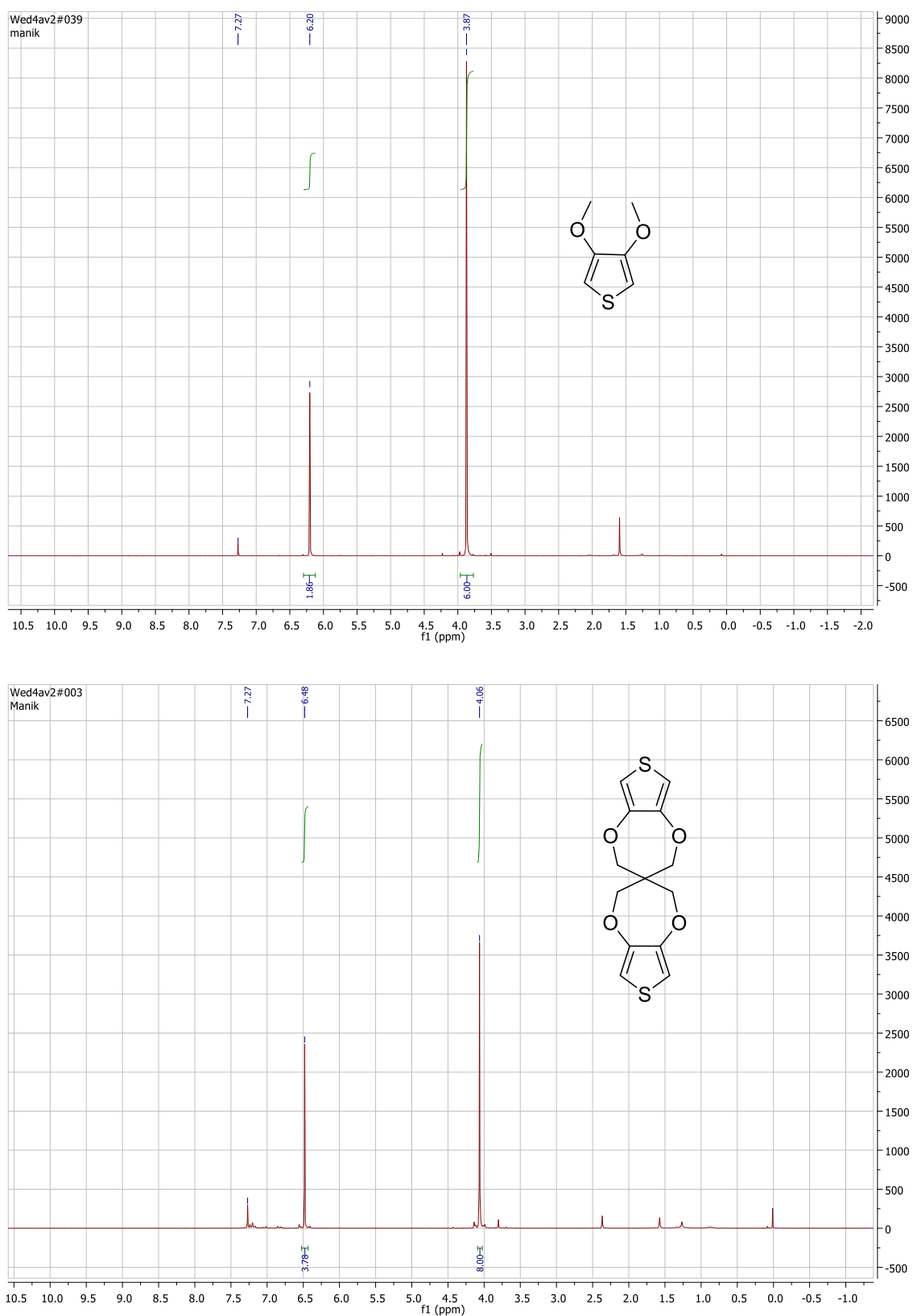
Figure 1. ^{1}H NMR (CDCl$_3$) of 3,4-dimethoxythiophene (**c**)   and 2H,2'H,4H,4'H-3,3'-spirobi[thieno[3,4-b][1,4]dioxepine] (**d**).
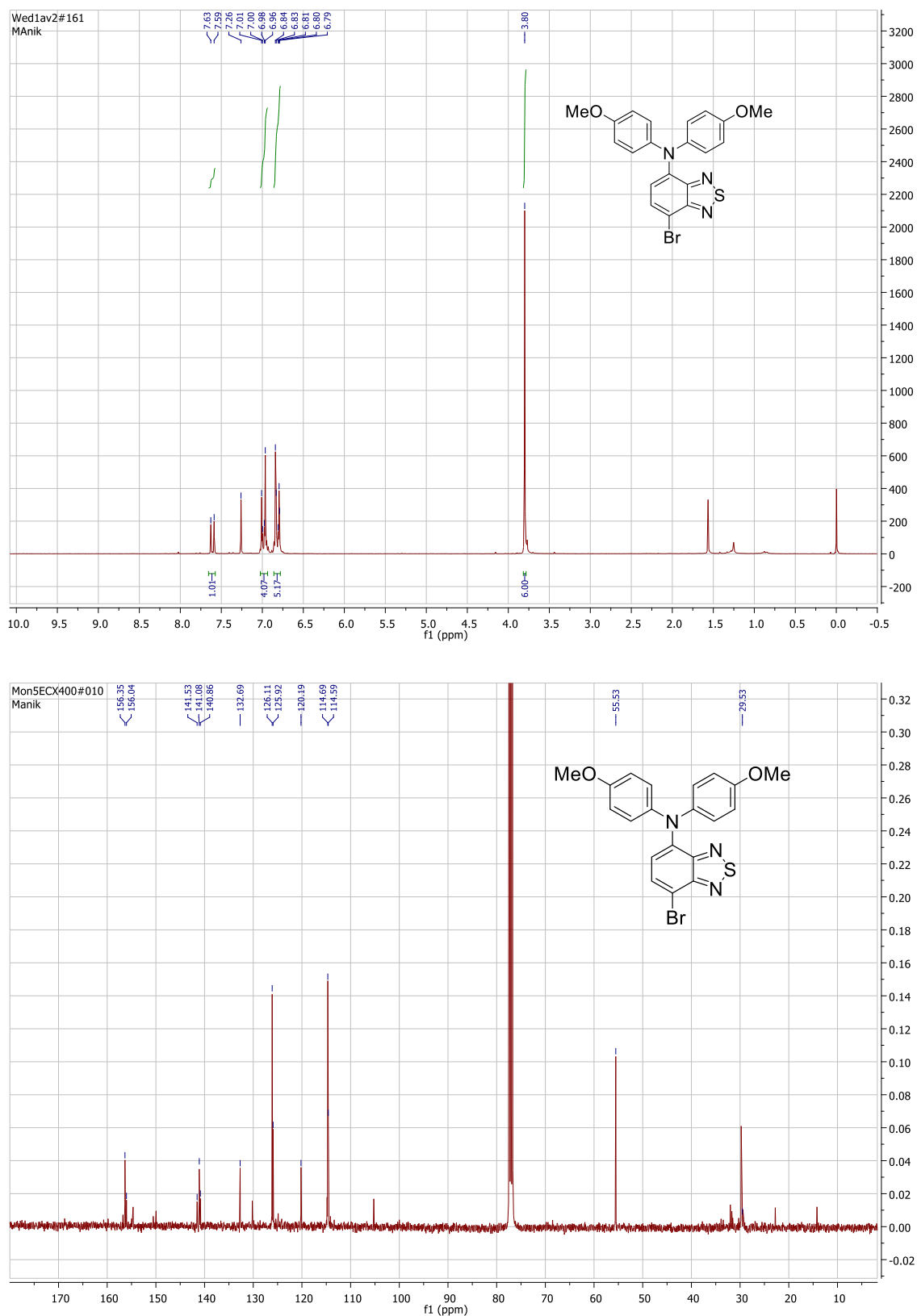
Figure 2. ^{1}H and ^{13}C NMR (CDCl$_3$) spectra of Synthesis of 7-bromo-N, N-bis(4-methoxyphenyl)benzo[c][1,2,5]thiadiazol-4-amine (**5**).
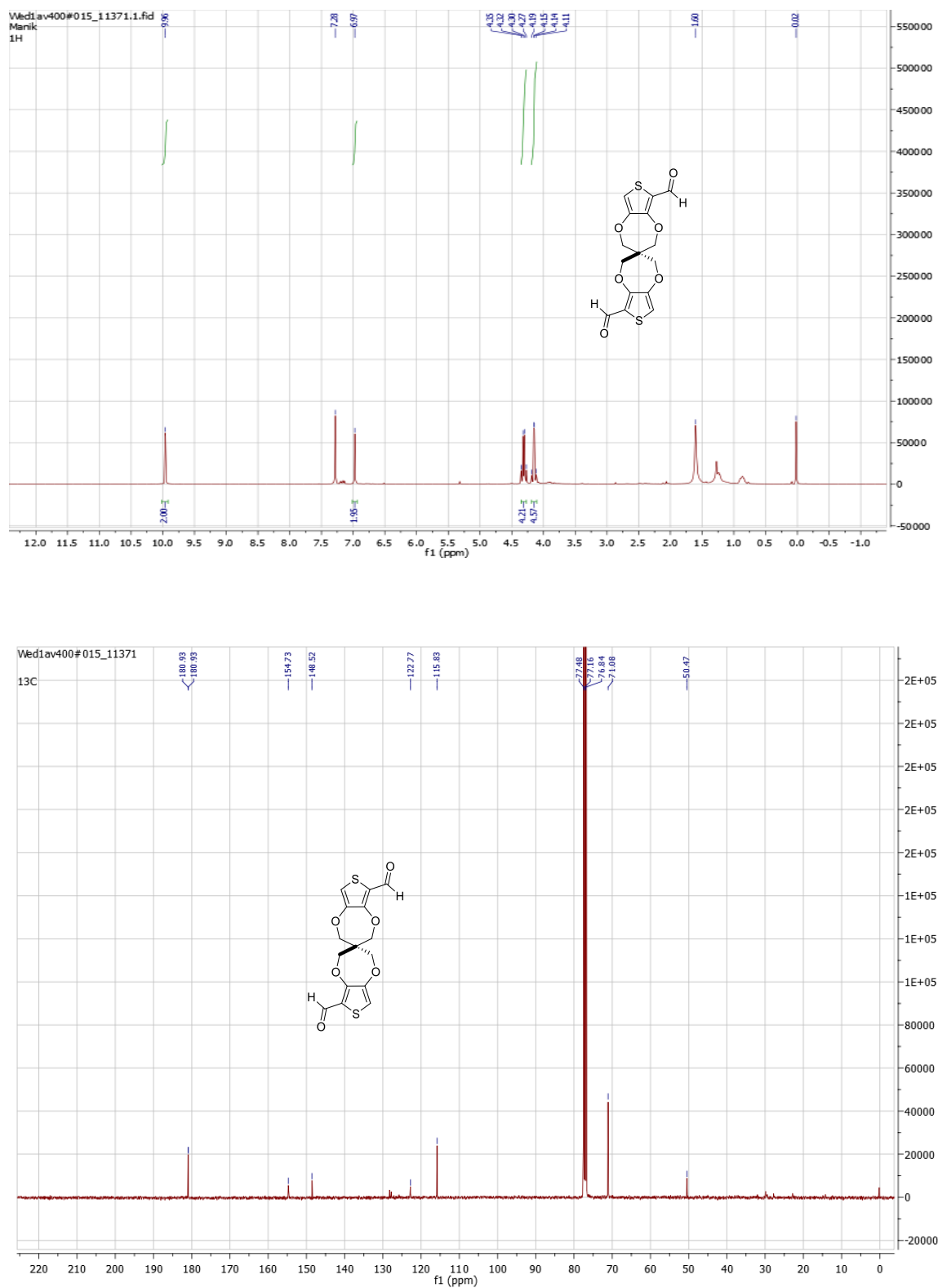
Figure S3. ^{1}H and ^{13}C NMR (CDCl₃) spectra of 2H,2'H,4H,4'H-3,3'-spirobi[thieno[3,4-b][1,4]dioxepine]-6,6'-dicarbaldehyde (**1**).

Figure S4. ^{1}H and ^{13}C NMR (CDCl$_3$)spectra of 6,6'-bis(4-(bis(4-methoxyphenyl)amino)phenyl)-2H,2'H,4H,4'H-3,3'-spirobi[thieno[3,4-b][1,4]dioxepine]-8,8'-dicarbaldehyde (**3**).
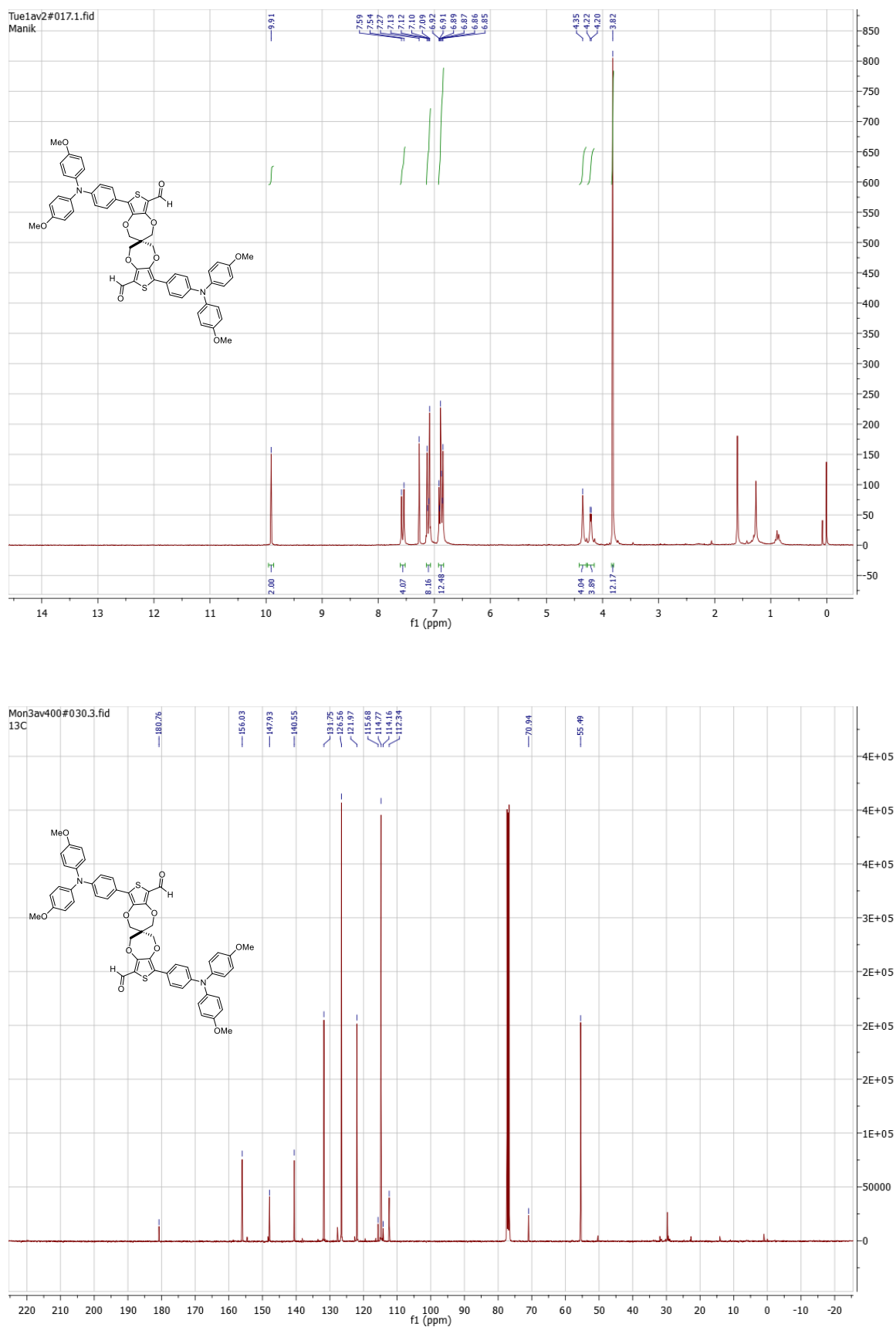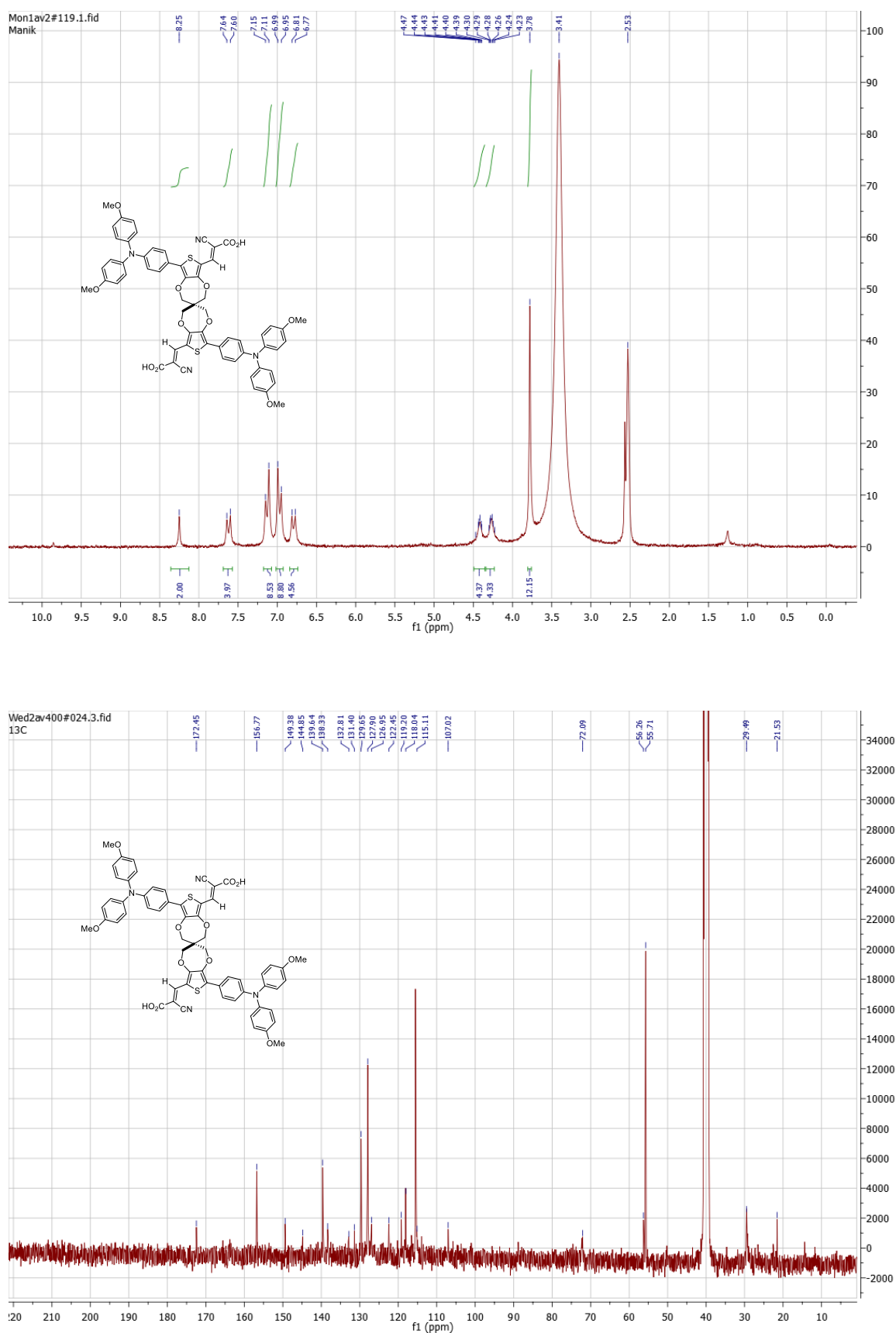
Figure 5. ^{1}H and ^{13}C NMR (DMSO-d6) spectra **D₁-D₁**, **4**.
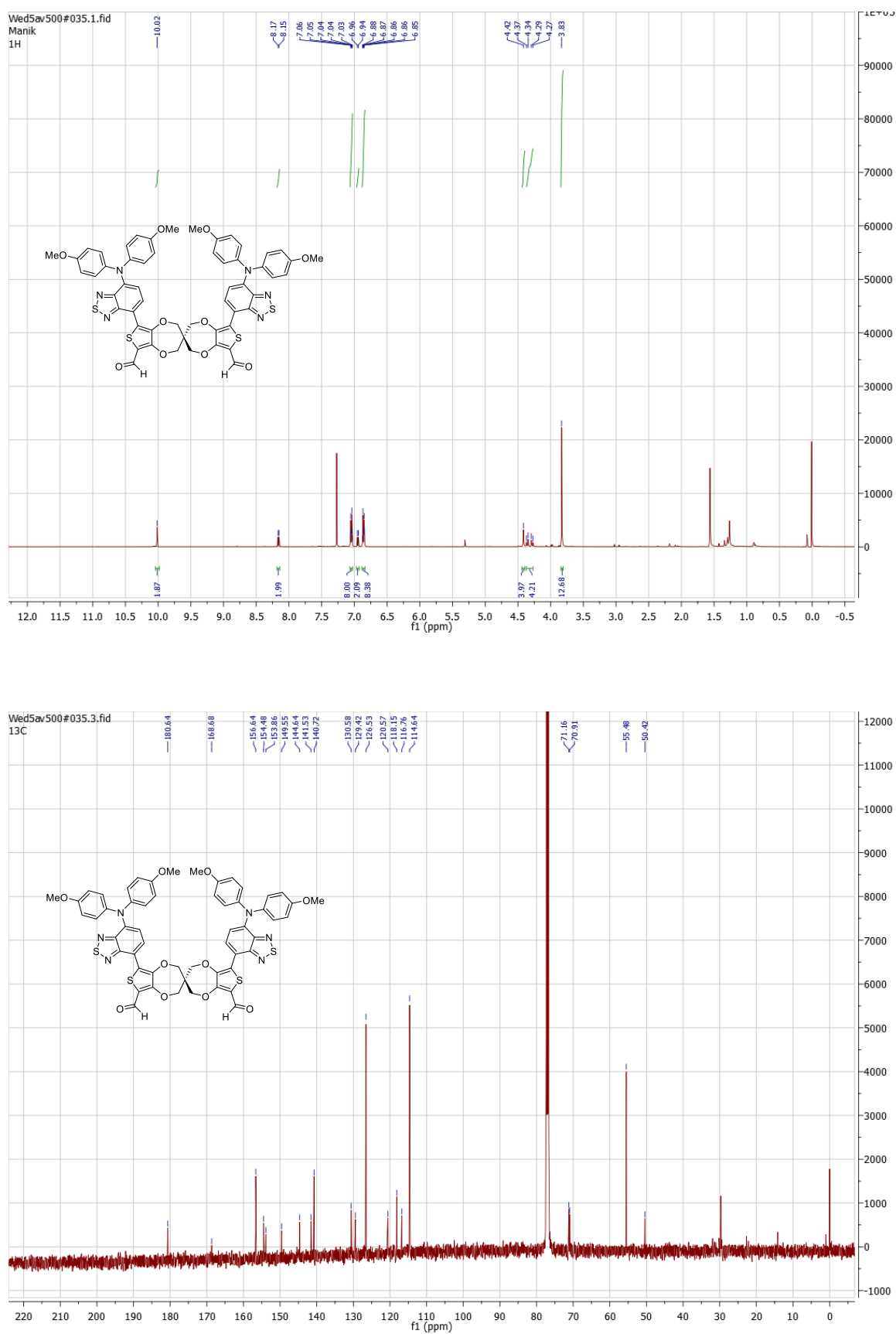
Figure 6. ^{1}H and ^{13}C NMR (CDCl$_3$) spectra of 6,6'-bis(7-(bis(4-methoxyphenyl)amino)benzo[c][1,2,5]thiadiazol-4-yl)-2H,2'H,4H,4'H-3,3'-spirobi[thieno[3,4-b][1,4]dioxepine]-8,8'-dicarbaldehyde (**6**).
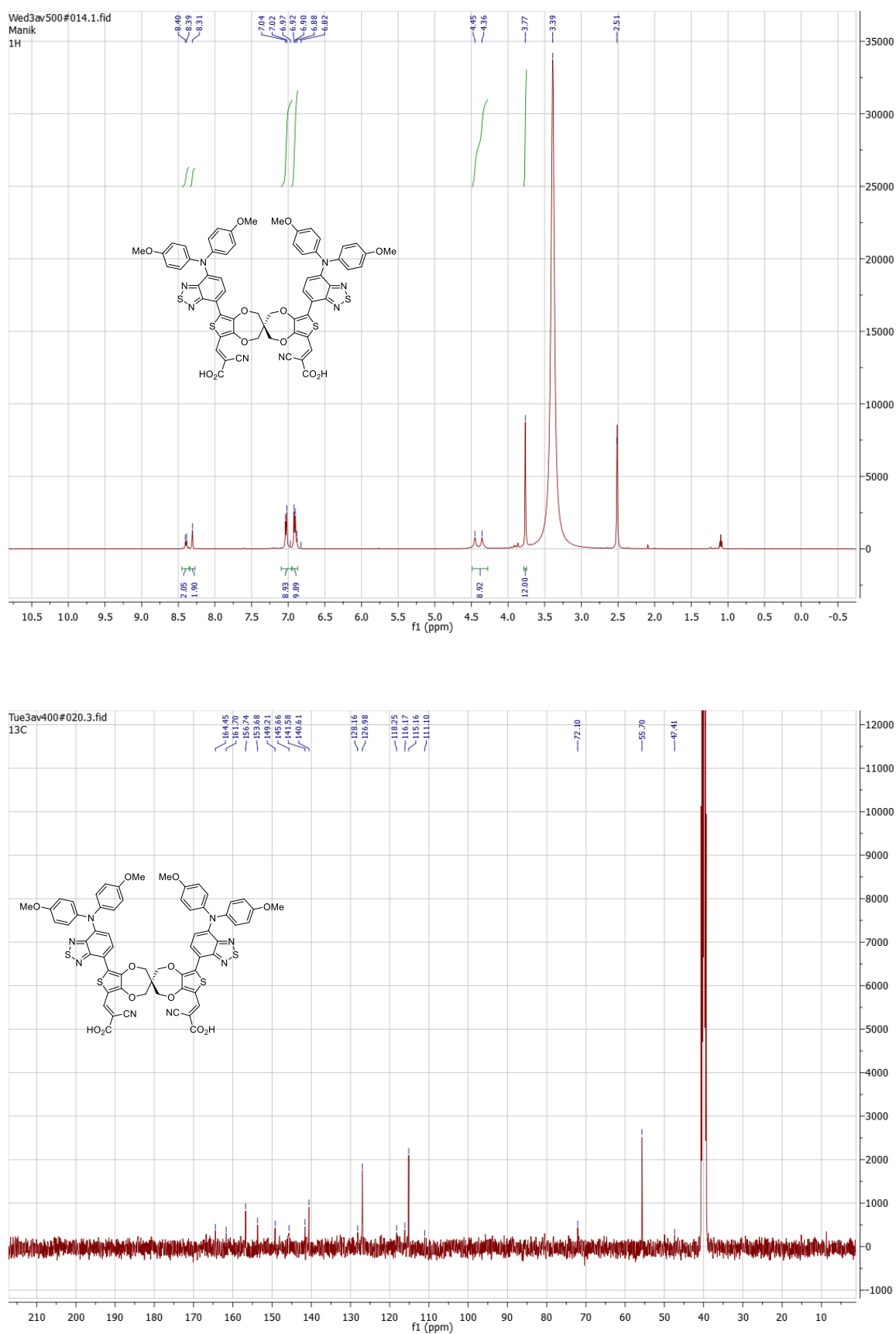
Figure 7. ^{1}H and ^{13}C NMR (DMSO-d6) spectra of **D$_2$-D$_2$**, **7**.
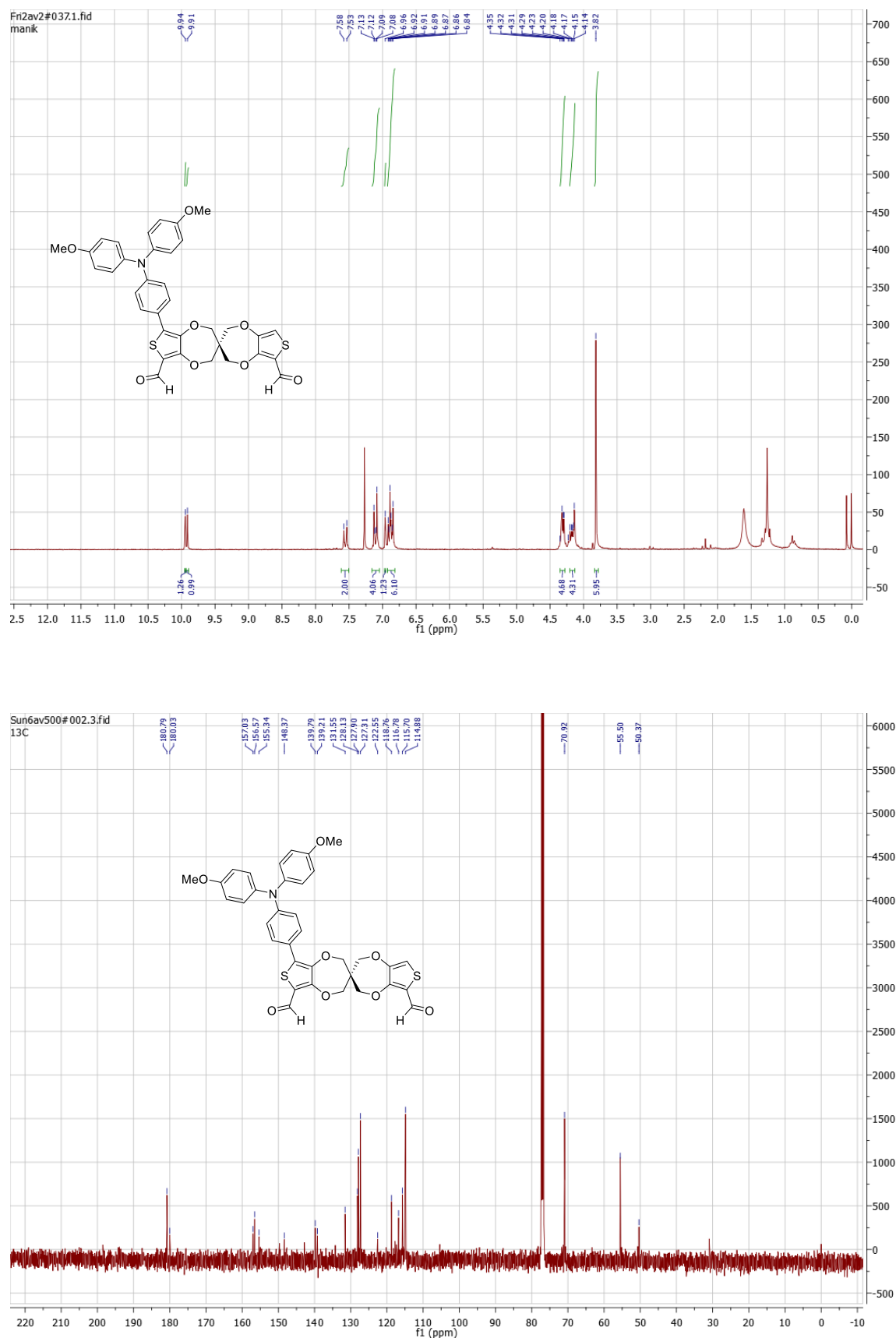
Figure 8. ^{1}H and ^{13}C NMR (CDCl₃)spectra of 6'-(4-(bis(4-methoxyphenyl)amino)phenyl)-2H,2'H,4H,4'H-3,3'-spirobi[thieno[3,4-b][1,4]dioxepine]-6,8'-dicarbaldehyde (**8**).
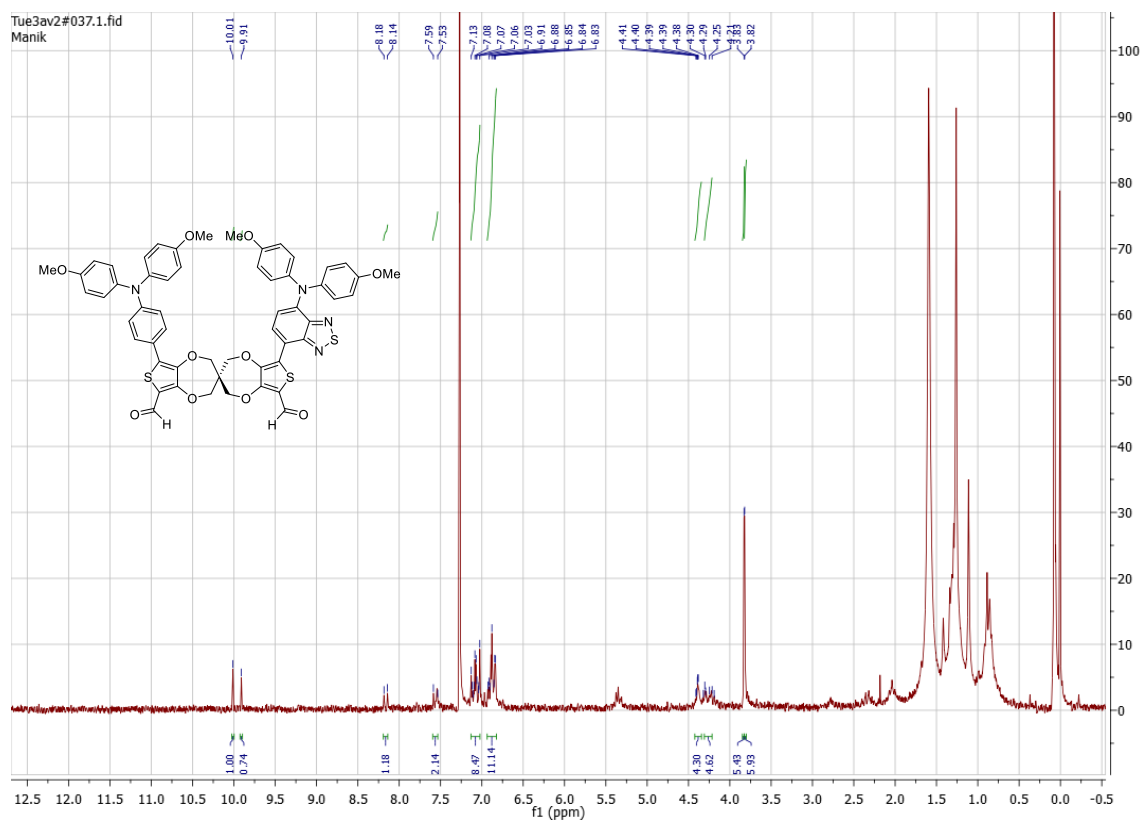
Figure 9. ^{1}H-NMR spectrum of 6-(7-(bis(4 methoxyphenyl)amino)benzo[c][1,2,5]thiadiazol-4-yl)-6'-(4-(bis(4 methoxyphenyl)amino)phenyl)-2H,2'H,4H,4'H-3,3'-spirobi[thieno[3,4-b][1,4]dioxepine]-8,8'-dicarbaldehyde (**9**).
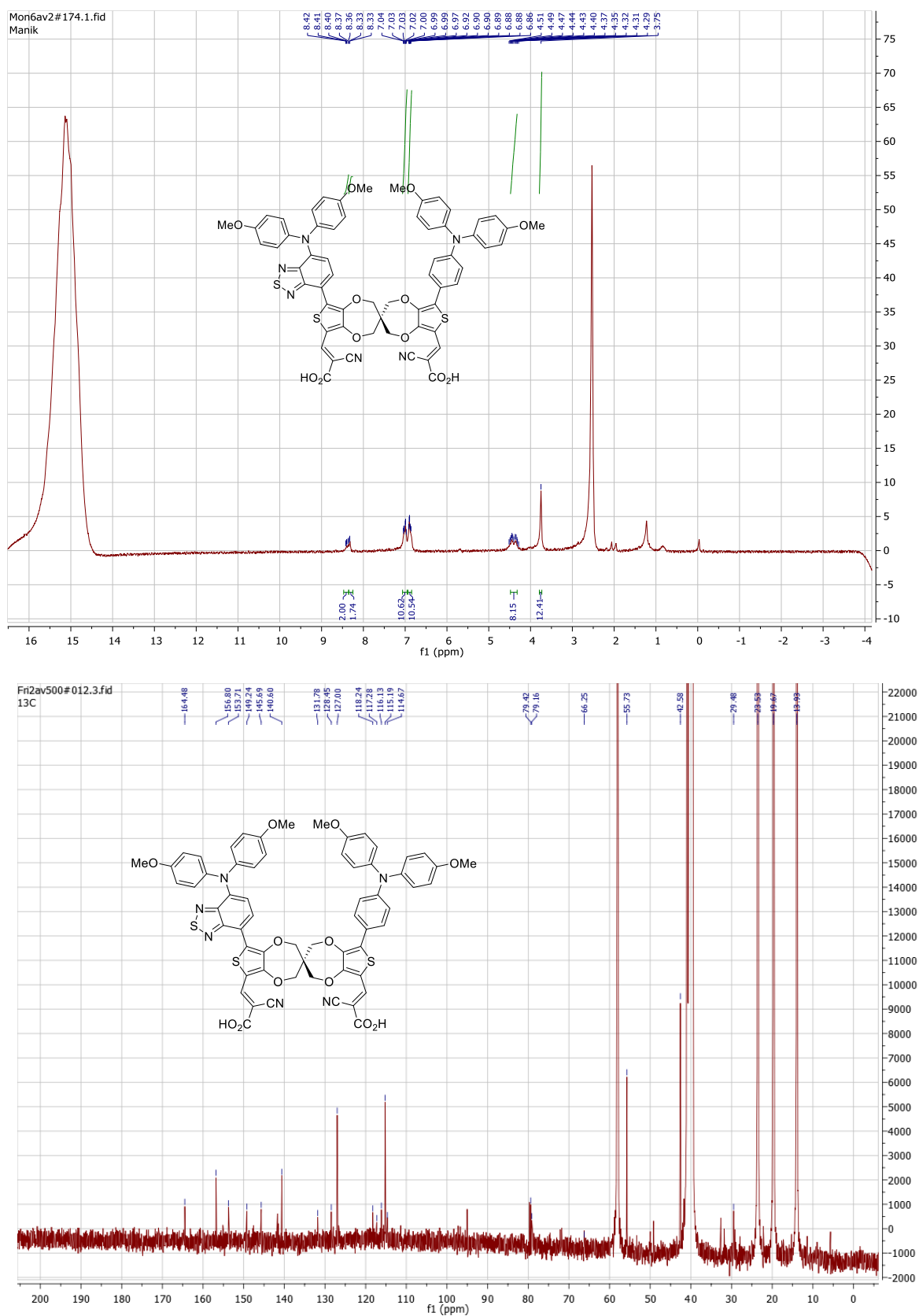
Figure 10. ^{1}H- and ^{13}C- NMR (DMSO-d$_6$ + TFA) spectra of **D$_1$-D$_2$, 10**.
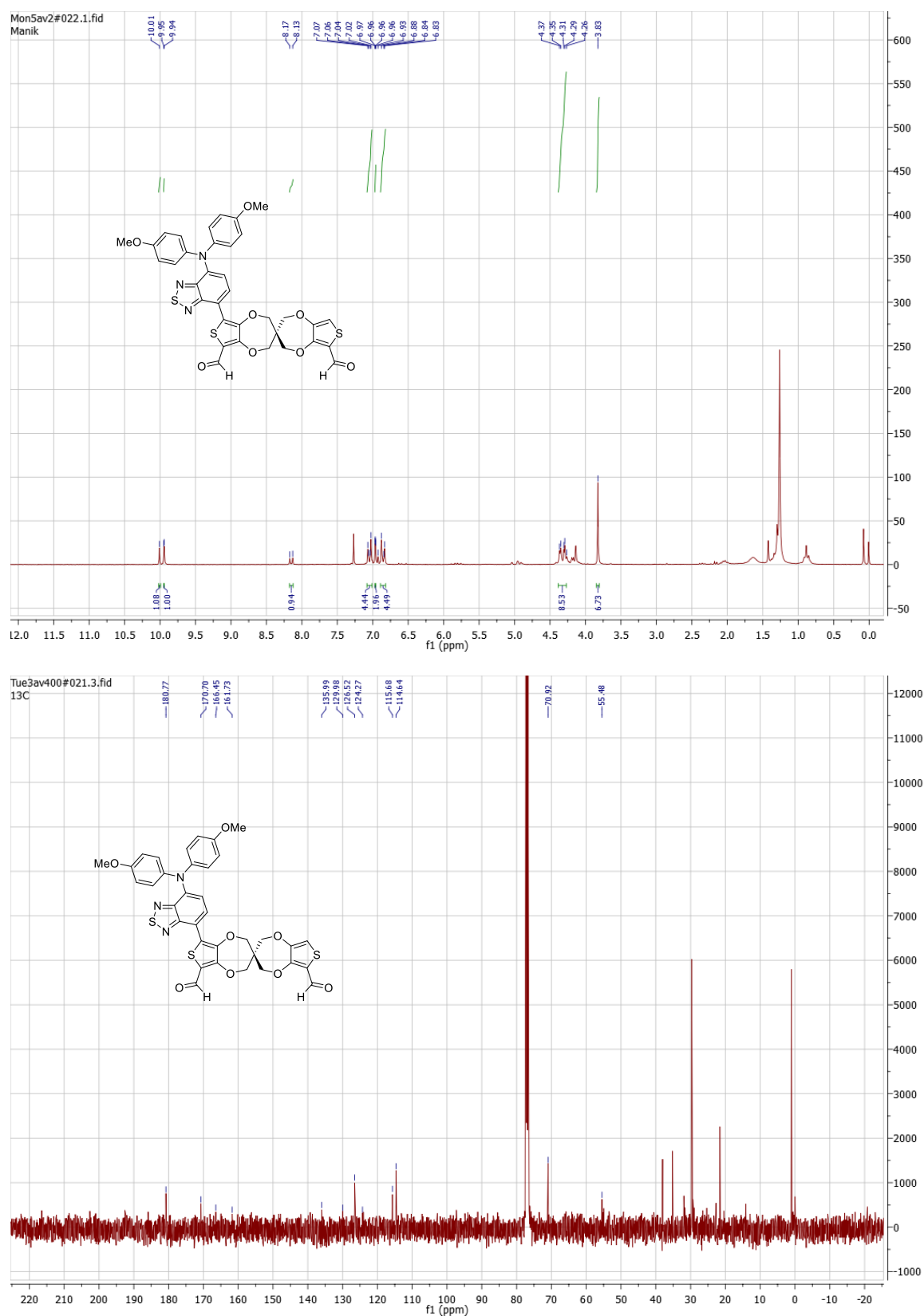
Figure 11. ^{1}H and ^{13}C NMR (CDCl$_3$)spectra of 6'-(7-(bis(4-methoxyphenyl)amino)benzo[c][1,2,5]thiadiazol-4-yl)-2H,2'H,4H,4'H-3,3'-spirobi[thieno[3,4-b][1,4]dioxepine]-6,8'-dicarbaldehyde (**11**).
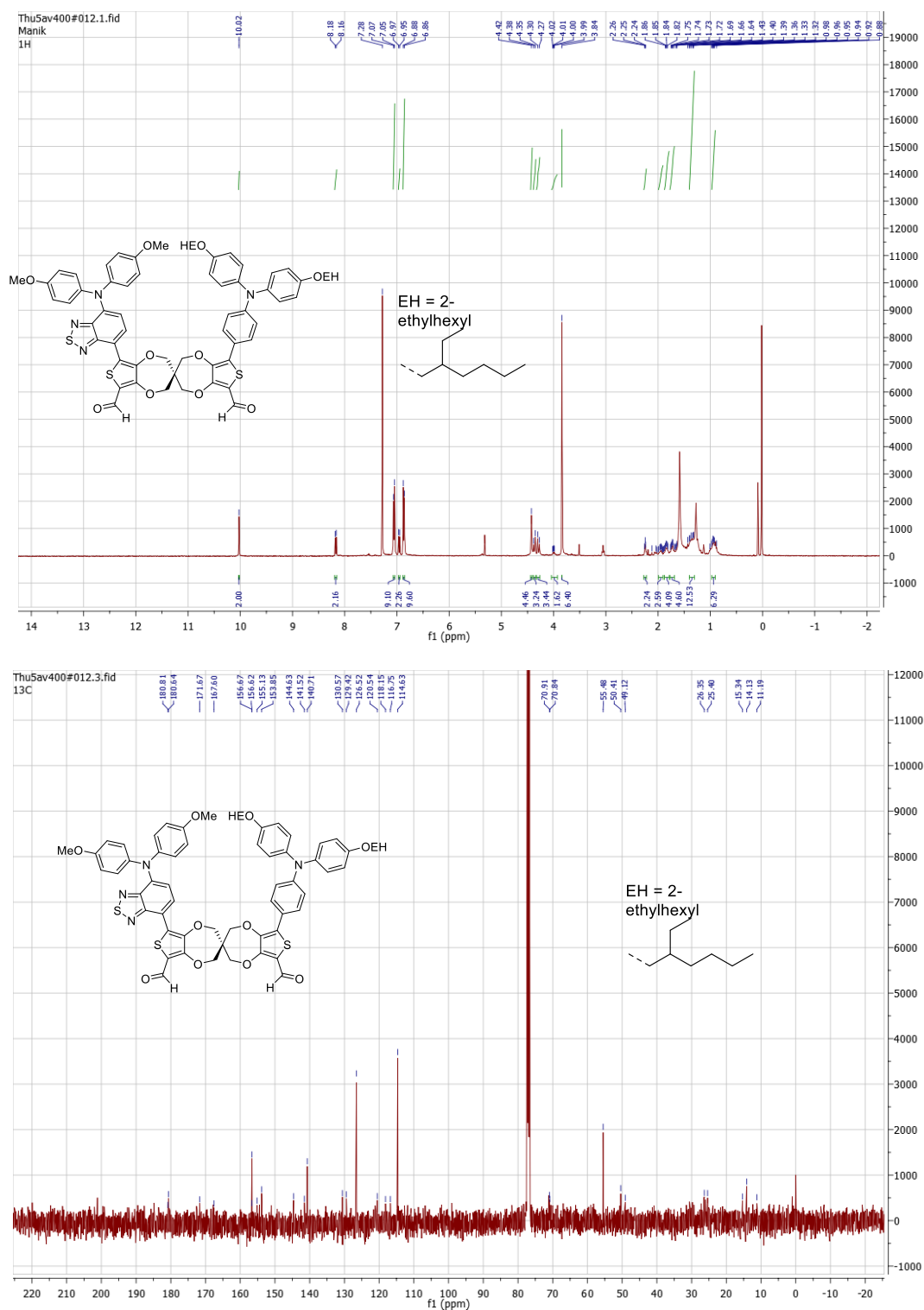
Figure 12. ^{1}H and ^{13}C NMR (CDCl$_3$)spectra of 6-(4-(bis(4-((2-ethylhexyl)oxy)phenyl)amino)phenyl)-6'-(7-(bis(4-methoxyphenyl)amino)benzo[c][1,2,5]thiadiazol-4-yl)-2H,2'H,4H,4'H-3,3'-spirobi[thieno[3,4-b][1,4]dioxepine]-8,8'-dicarbaldehyde (**13**).
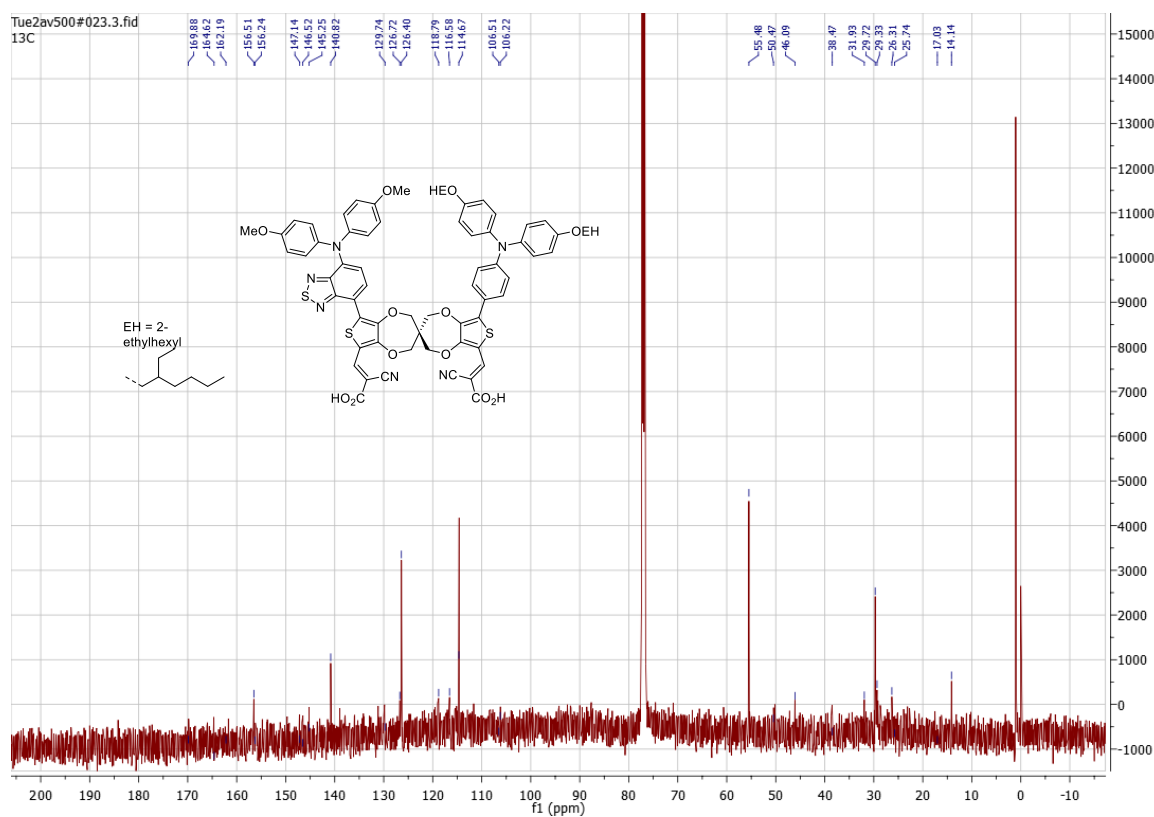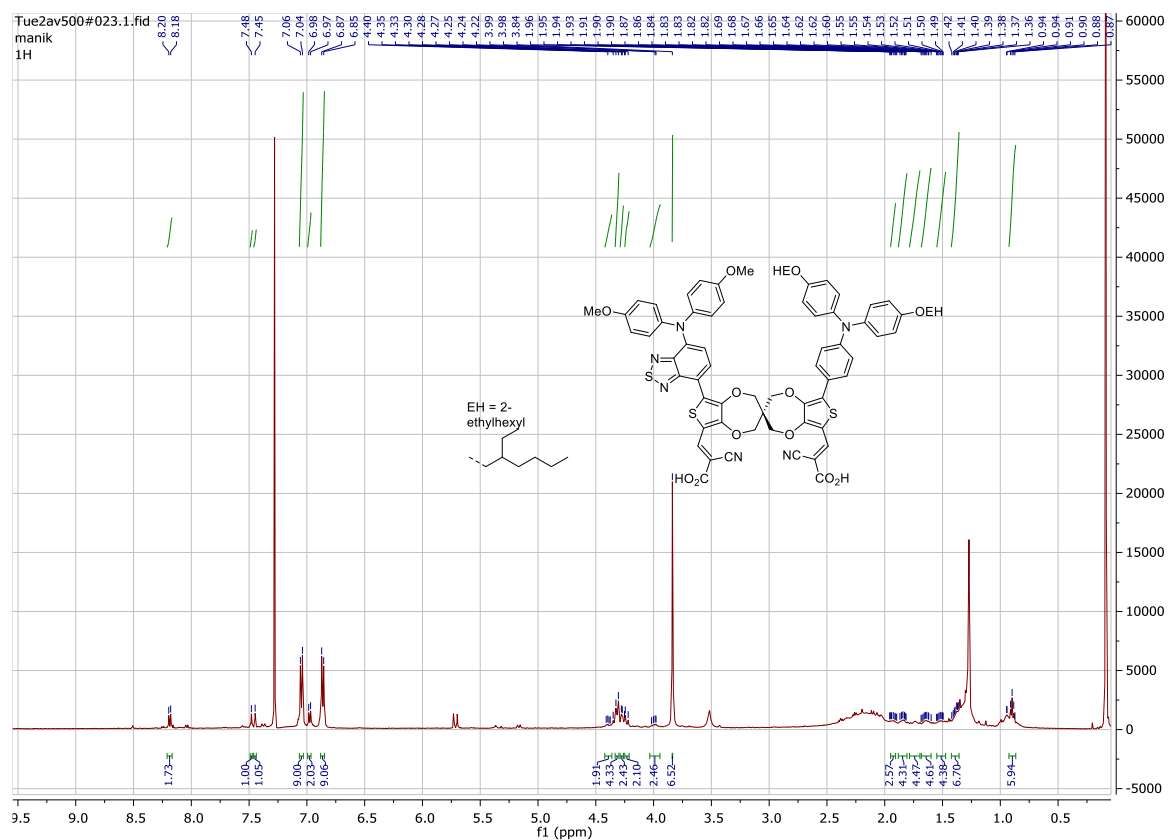
Figure 13. ^{1}H and ^{13}C NMR (CDCl$_3$) spectra of **D$_2$-D$_4$, 14**.
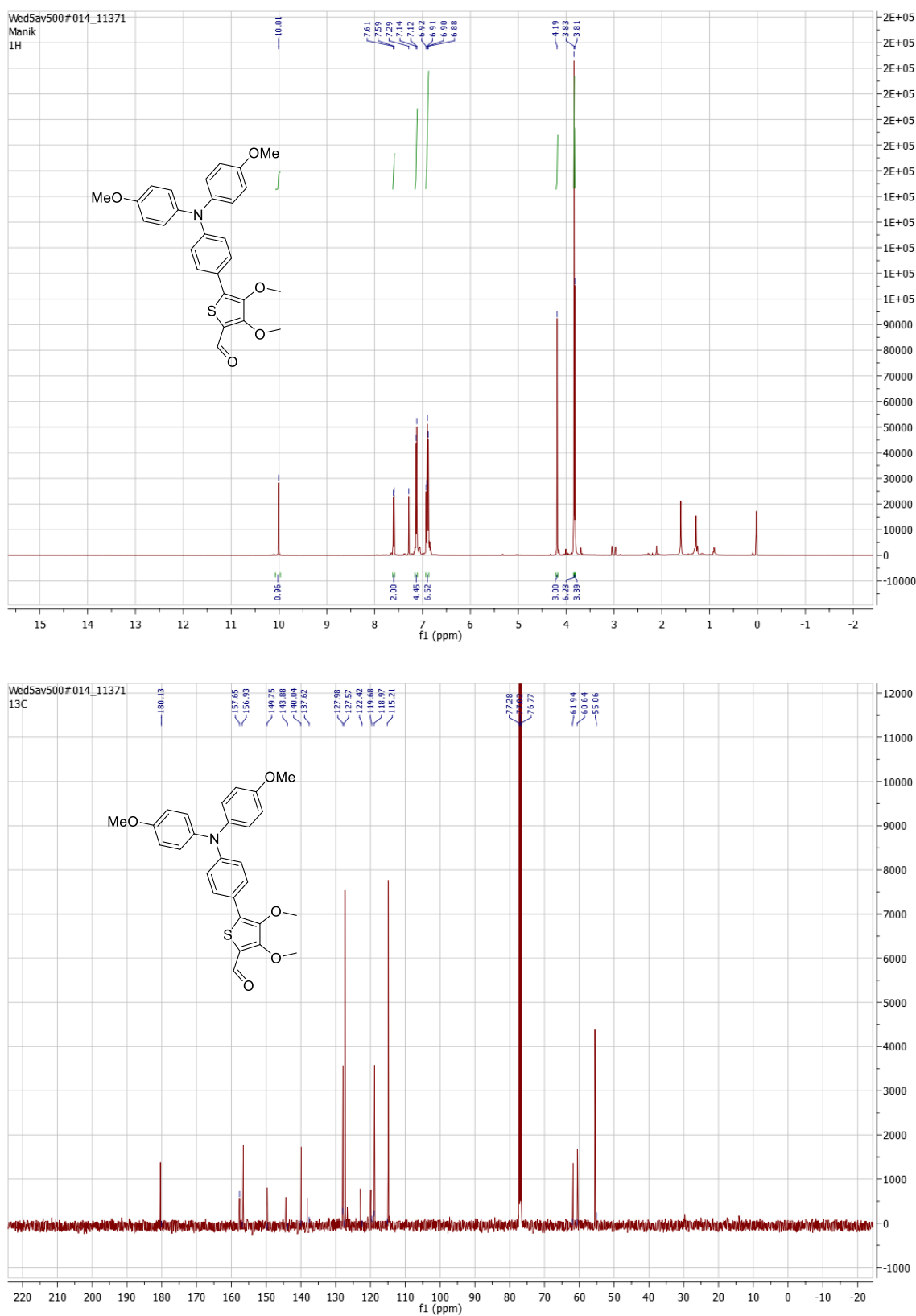
Figure 14. ^{1}H and ^{13}C NMR (CDCl$_3$) spectrum of 5-(4-(bis(4-methoxyphenyl)amino)phenyl)-3,4-dimethoxythiophene-2-carbaldehyde (**16**).
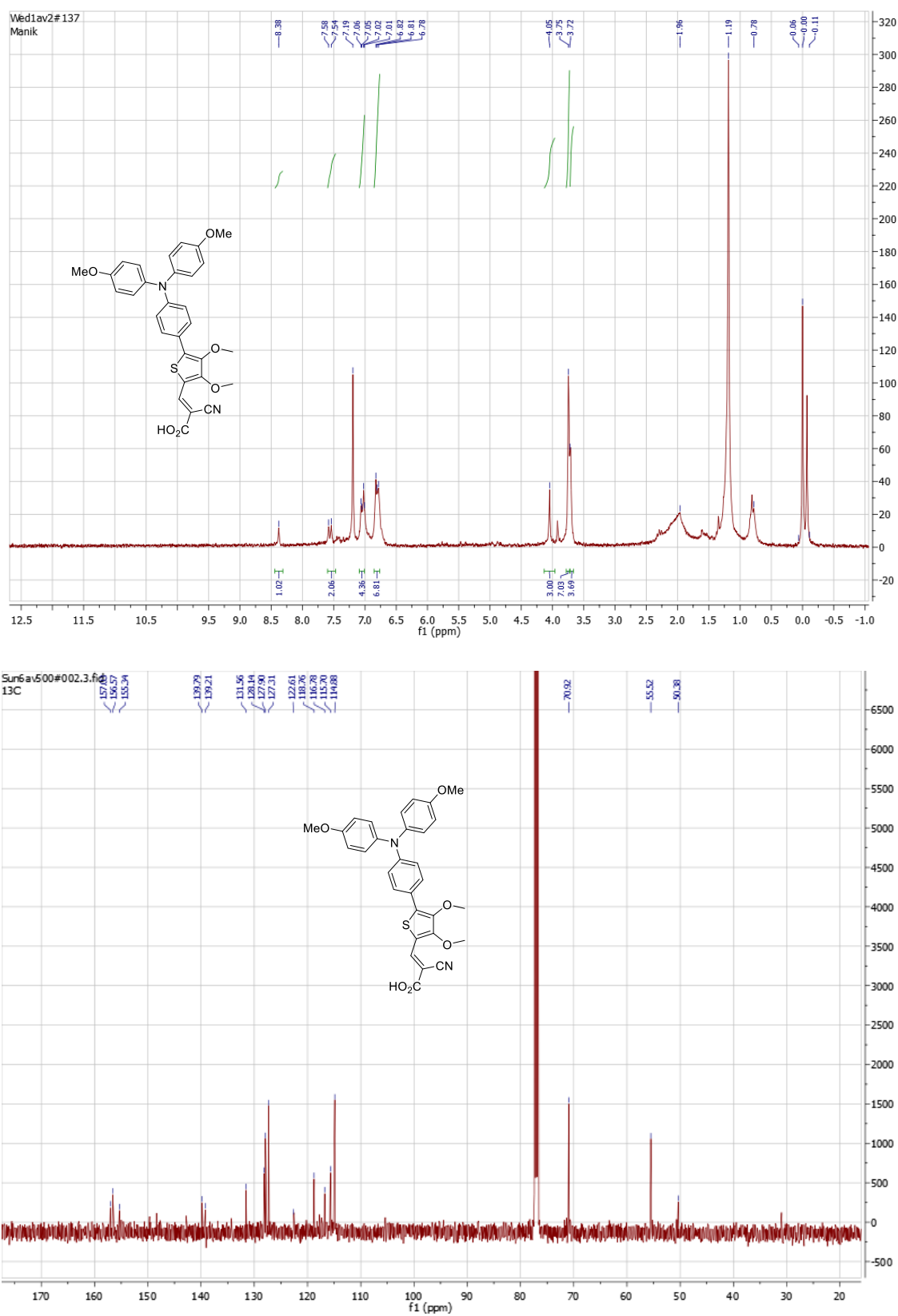
Figure 15. ^{1}H and ^{13}C NMR (CDCl$_3$) spectra **D$_1$**, **17**.
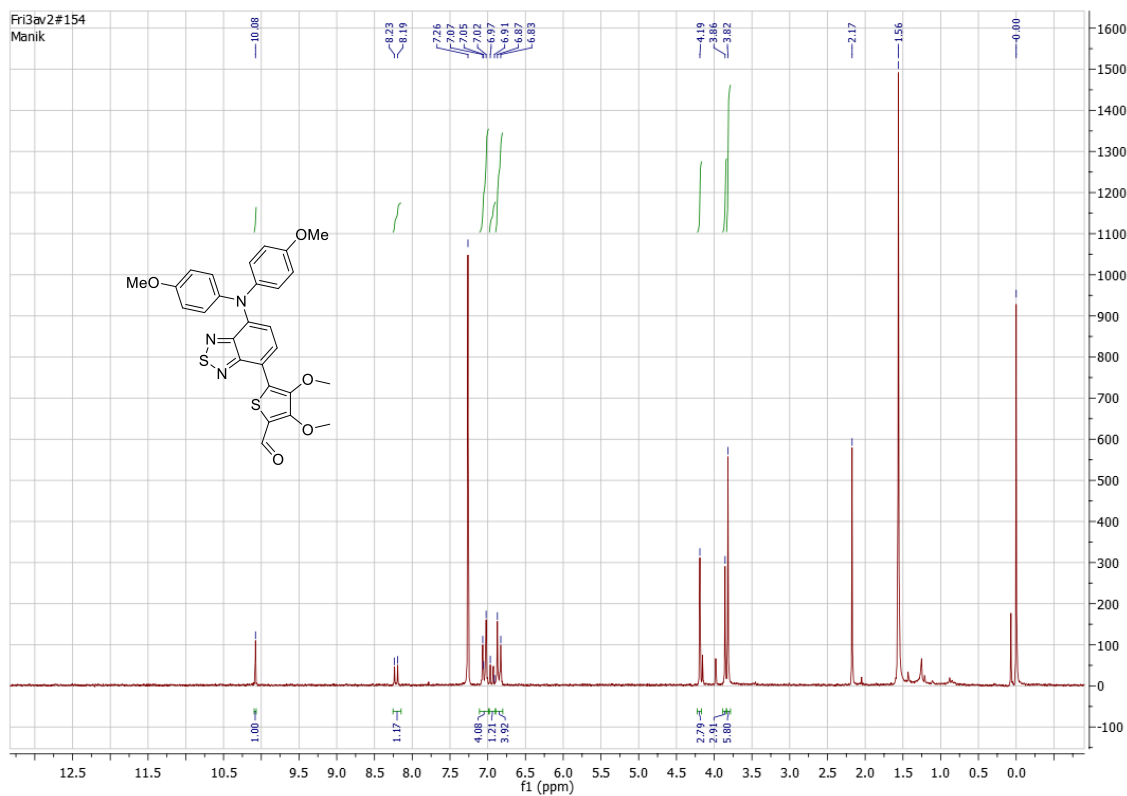
Figure 16. [^1]H spectrum (CDCl₃) of 5-(7-(bis(4-methoxyphenyl)amino)benzo[c][1,2,5]thiadiazol-4-yl)-3,4-dimethoxythiophene-2-carbaldehyde (**18**).
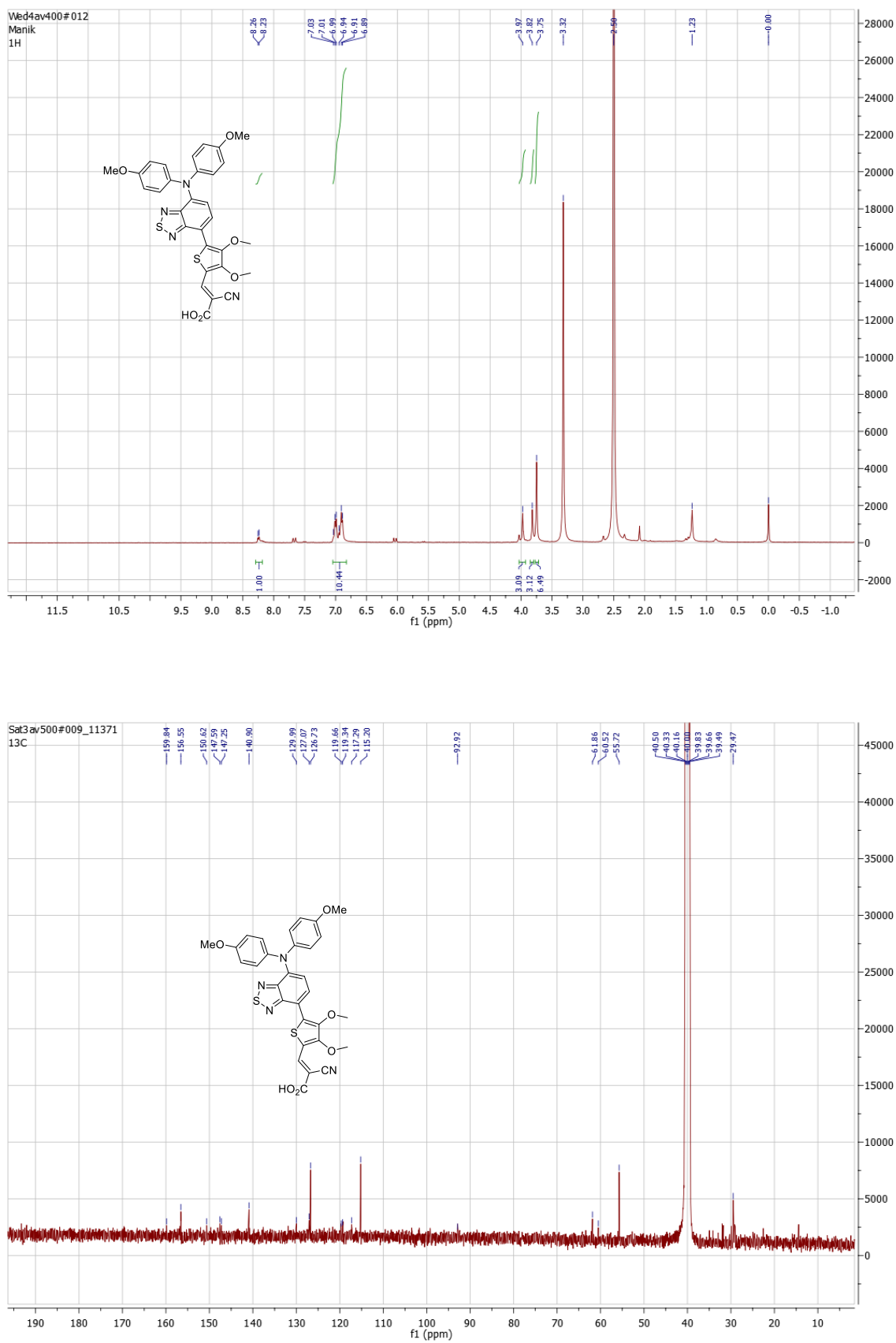
Figure 17. ^{1}H and 13C NMR (DMSO-d6) spectra of D$_2$, **19**.

Proton and 13 C NMR chapter 3
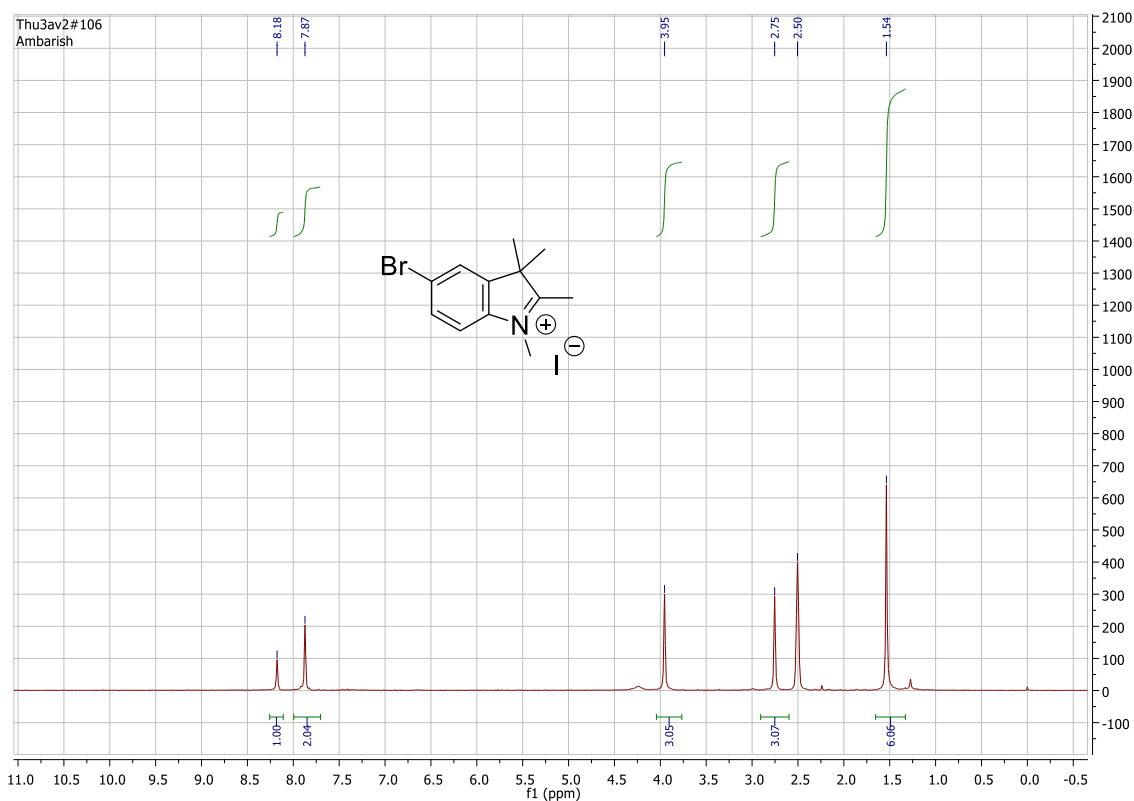
Figure 1. ^{1}H NMR spectrum of (DMSO-d_6) of 5-bromo-1,2,3,3-tetramethyl-3H-indol-1-ium (**1**).
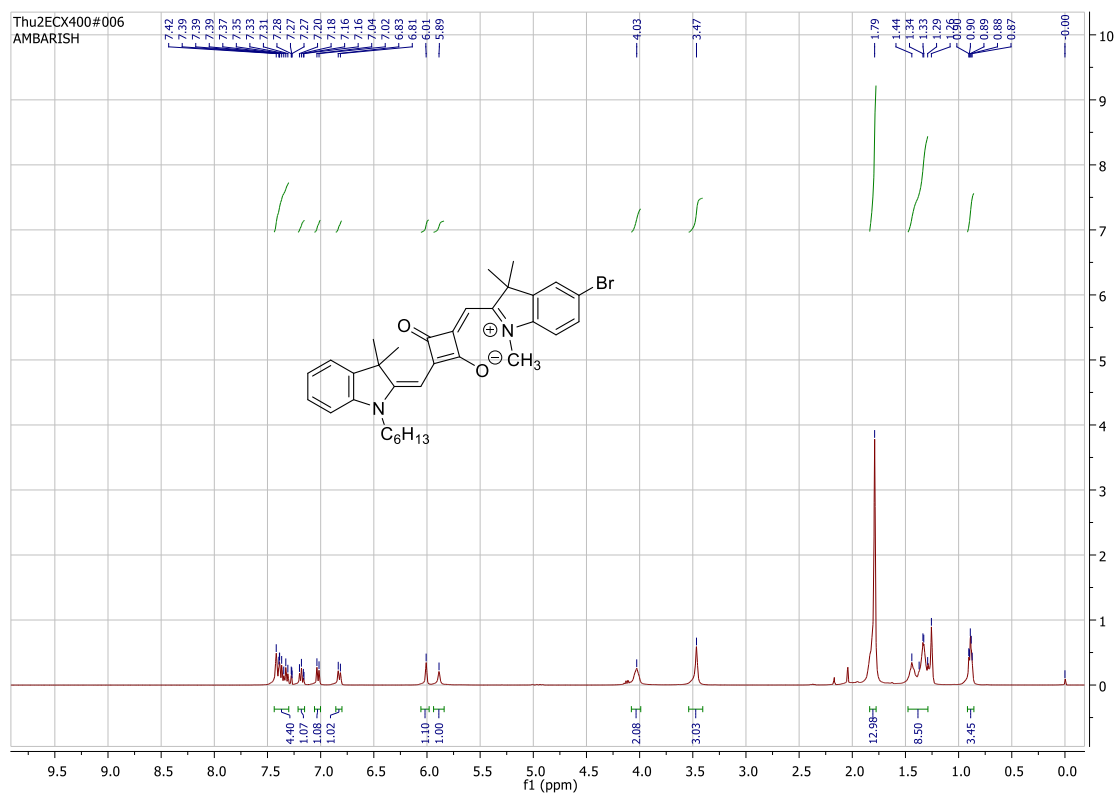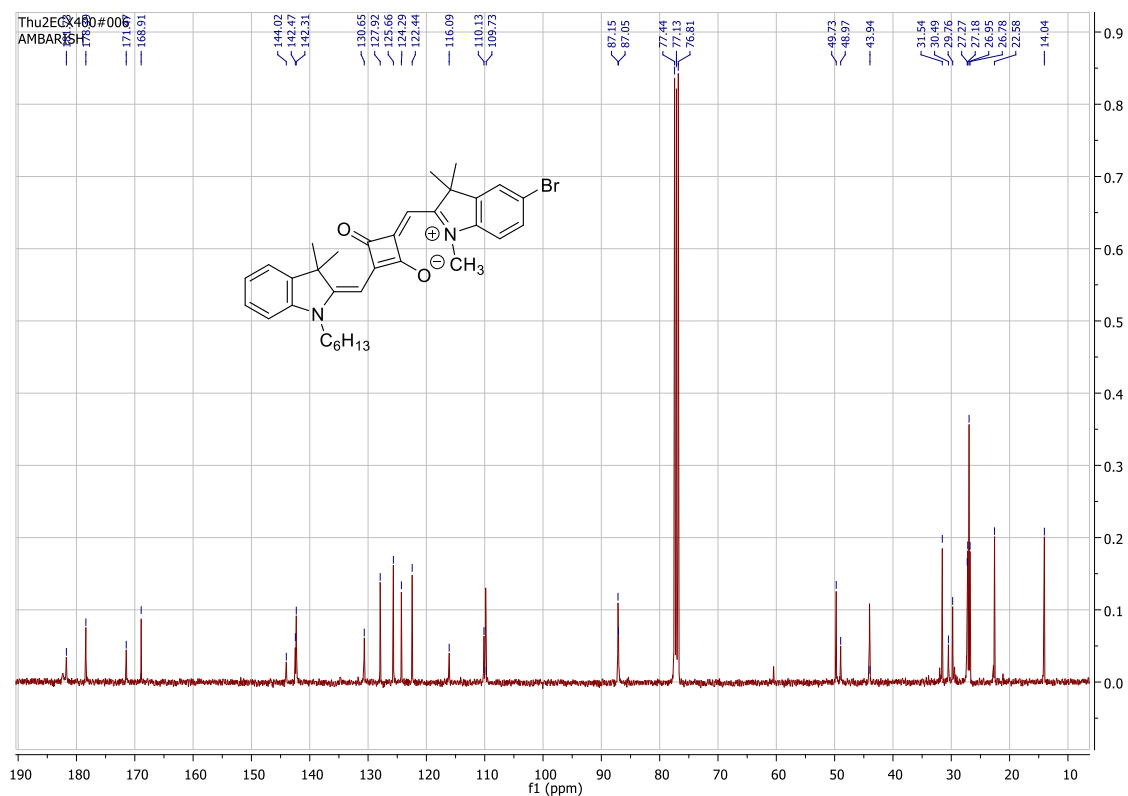
Figure 2. ^{1}H and ^{13}C NMR (CDCl$_3$) 4-((5-bromo-1,3,3-trimethyl-3H-indol-1-ium-2-yl)methylene)-2-((-1-hexyl-3,3-dimethylindolin-2-ylidene)methyl)-3-oxocyclobut-1-en-1-olate (**3**).
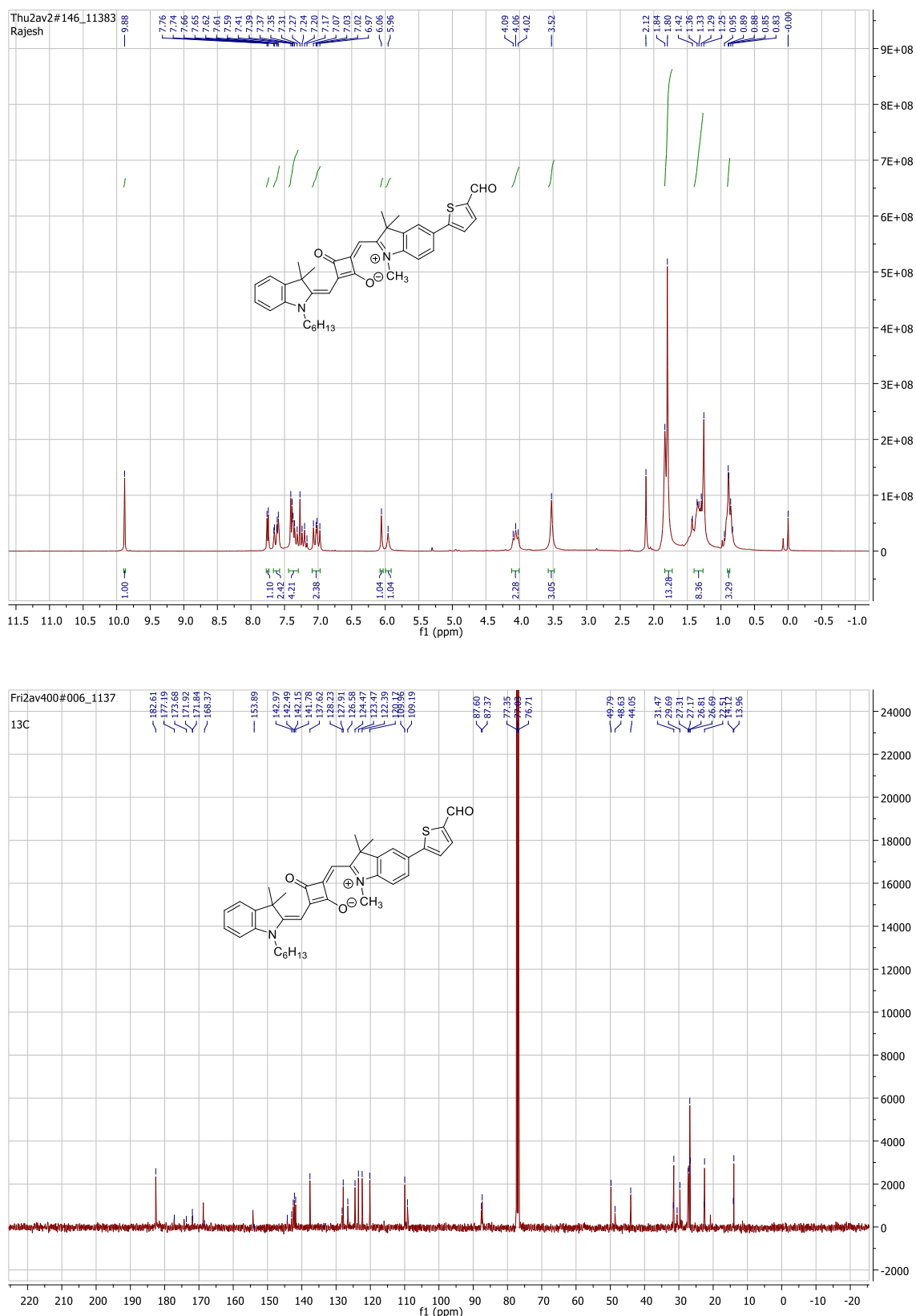
Figure 3. ^{1}H and ^{13}C NMR (CDCl₃) of (E)-4-((5-(5-formylthiophen-2-yl)-1,3,3-trimethyl-3H-indol-1-ium-2-yl)methylene)-2-(((E)-1-hexyl-3,3-dimethylindolin-2-ylidene)methyl)-3-oxocyclobut-1-en-1-olate (**4**).
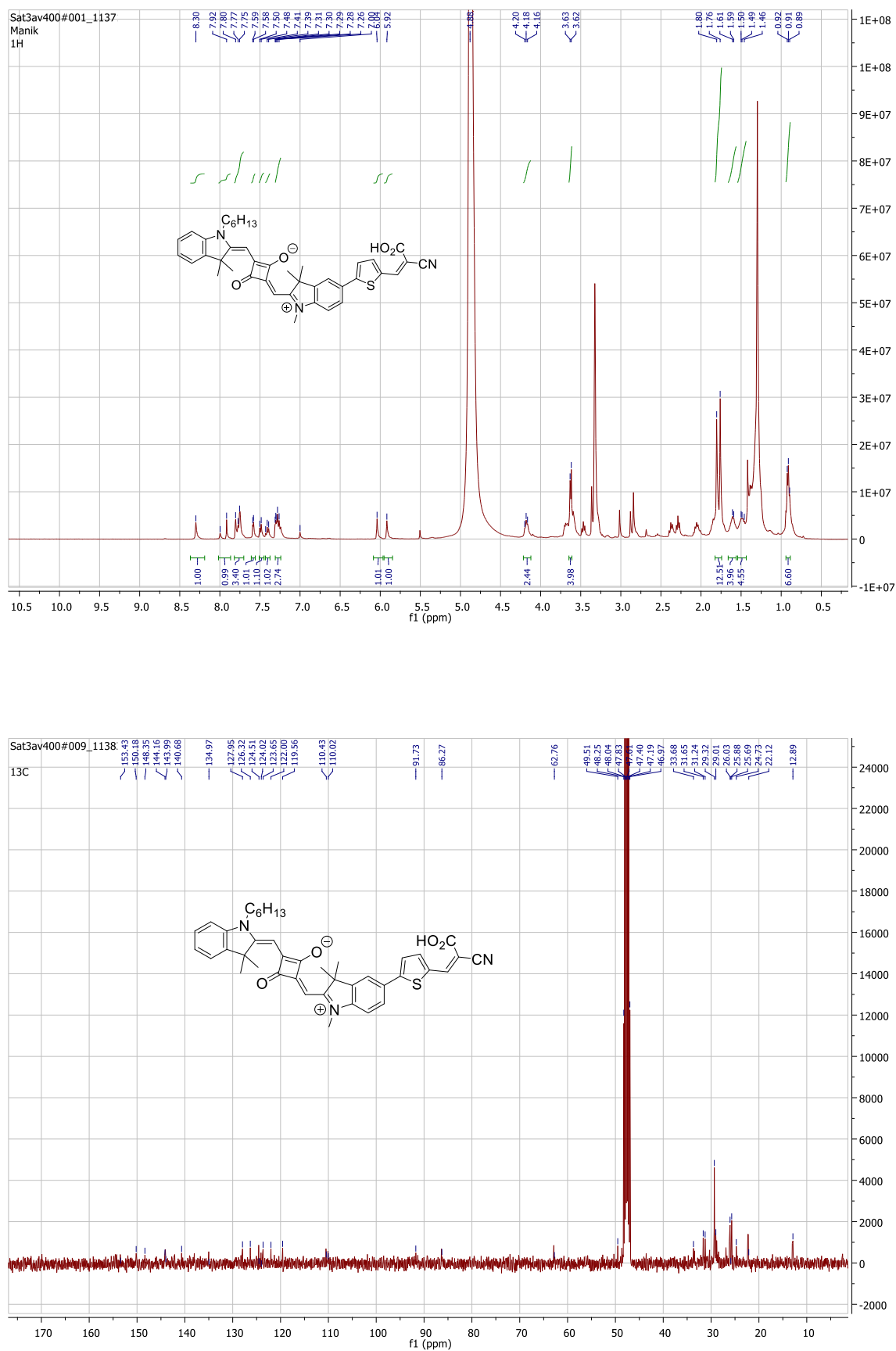
Figure 5. ^{1}H and ^{13}C NMR (CDCl$_3$) spectra of **D$_{sq}$, 5**.
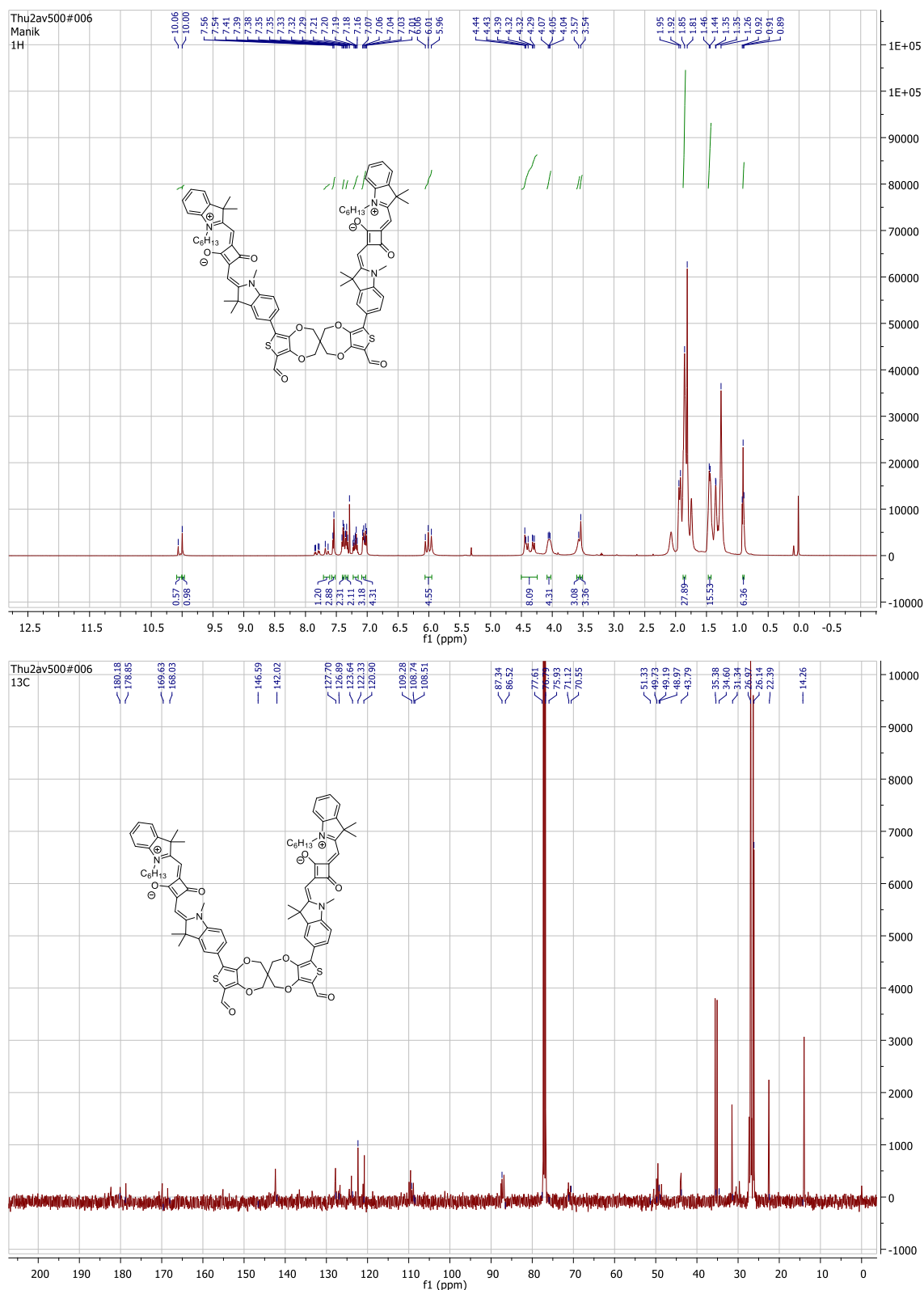
Figure 6. ^{1}H and ^{13}C NMR (CDCl₃) of (4E,4'E)-2,2'-(((2Z,2'Z)-(6,6'-diformyl-2H,2'H,4H,4'H-3,3'-spirobi[thieno[3,4-b][1,4]dioxepine]-8,8'-diyl)bis(1,3,3-trimethylindoline-5-yl-ylidene))bis(methanylylidene))bis(4-((1-hexyl-3,3-dimethyl-3H-indol-1-ium-2-yl)methylene)-3-oxocyclobut-1-en-1-olate (**7**).
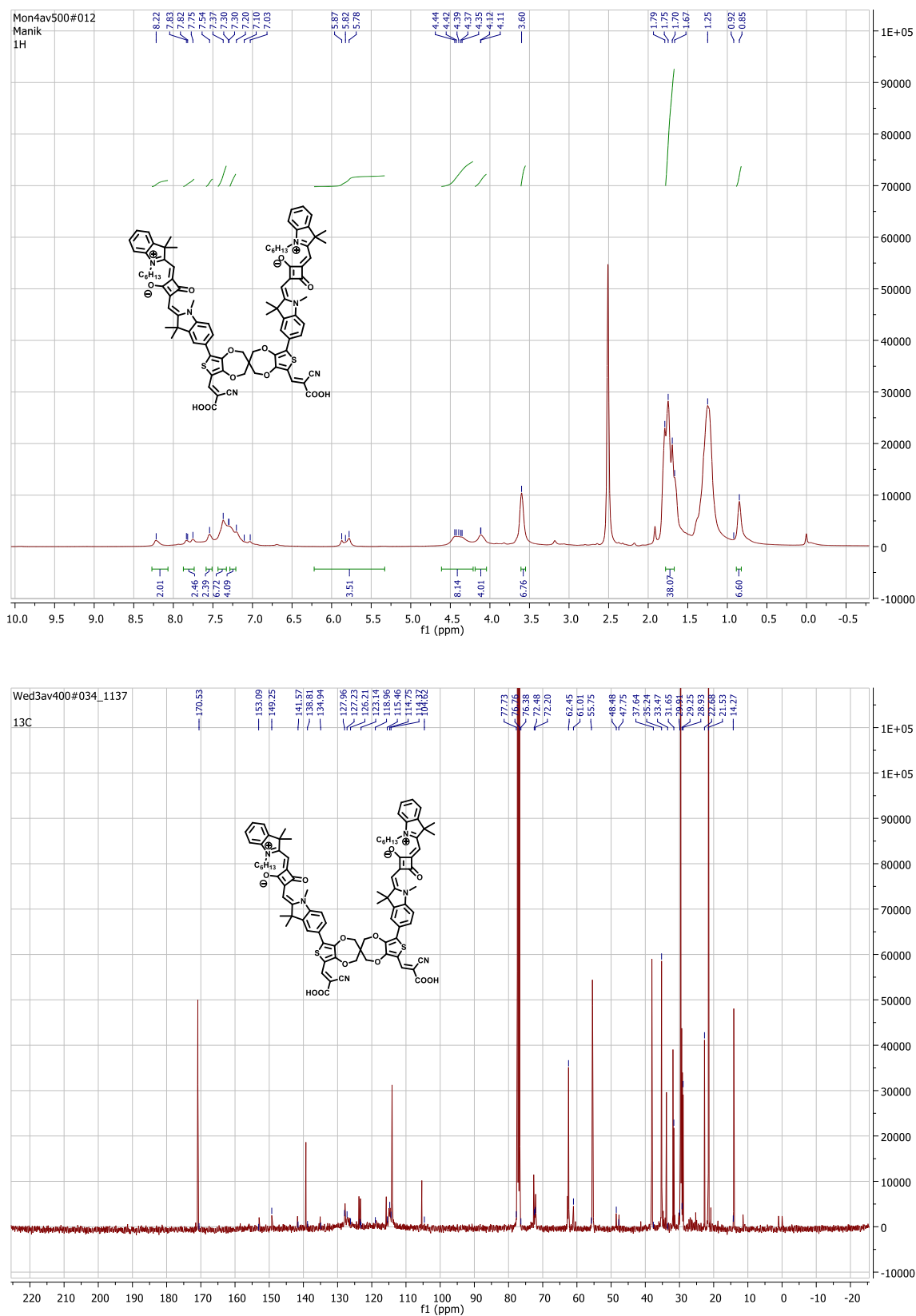
Figure 7. ^{1}H and ^{13}C NMR (DMSO-d_6) of D$_{sq}$-D$_{sq}$, **8**.
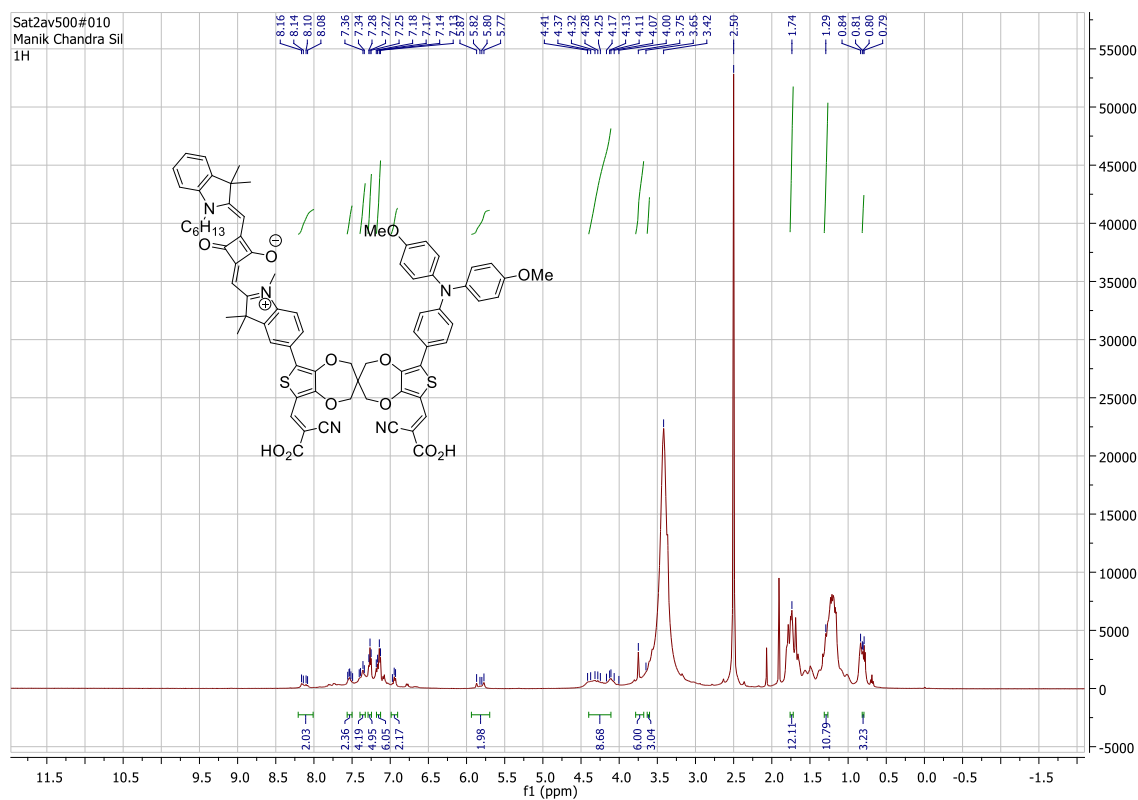
Figure 7. ^{1}H NMR spectrum (DMSO-d_6) of **D$_1$-D$_{sq}$, 12**.

Proton and 13 C NMR of chapter 4
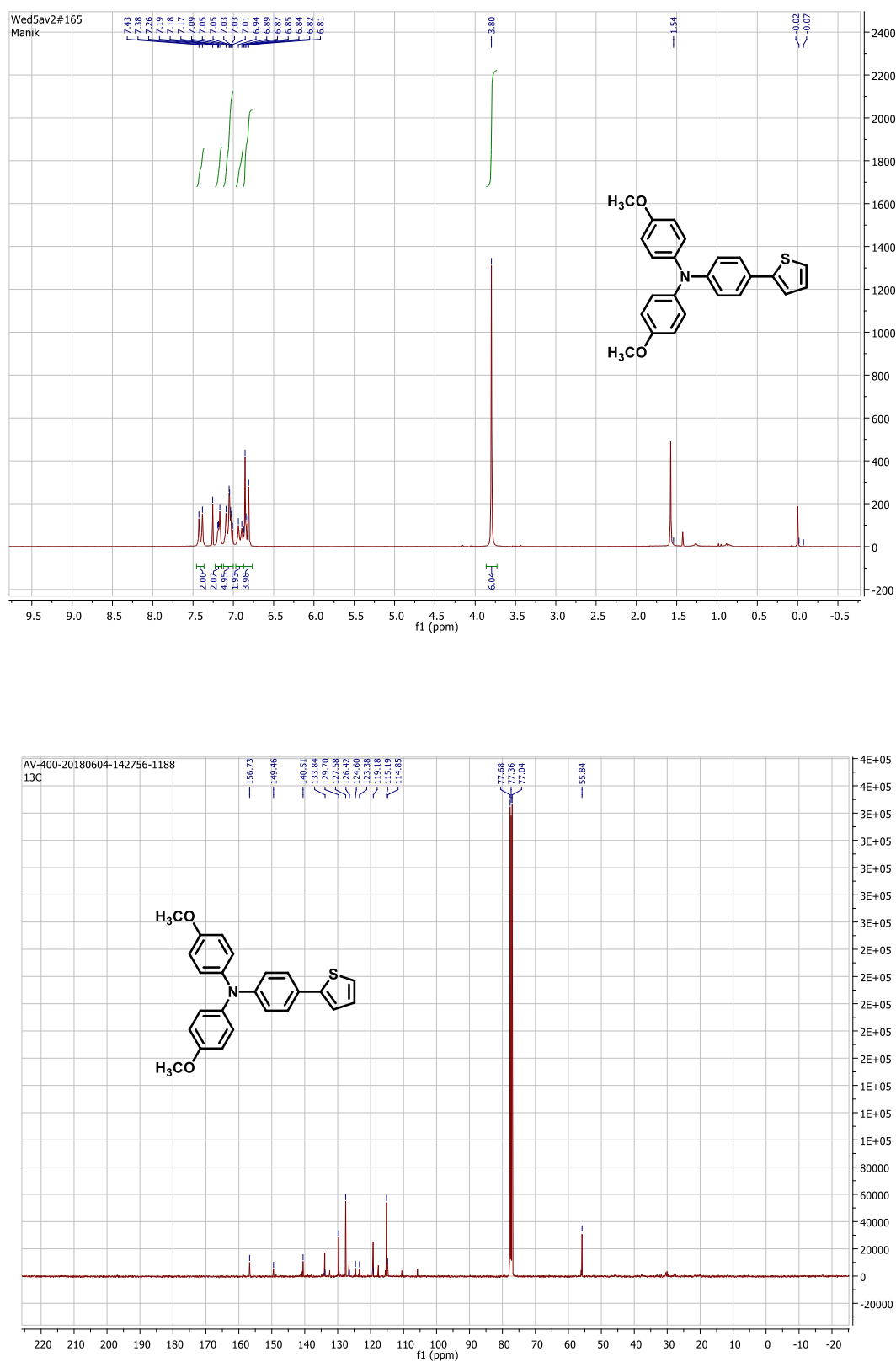
Figure 1. ^{1}H and ^{13}C NMR Nspectrum (CDCl$_3$) of 4-methoxy-N-(4-methoxyphenyl)-N-(4-(thiophen-2-yl) phenyl) aniline (**3**).
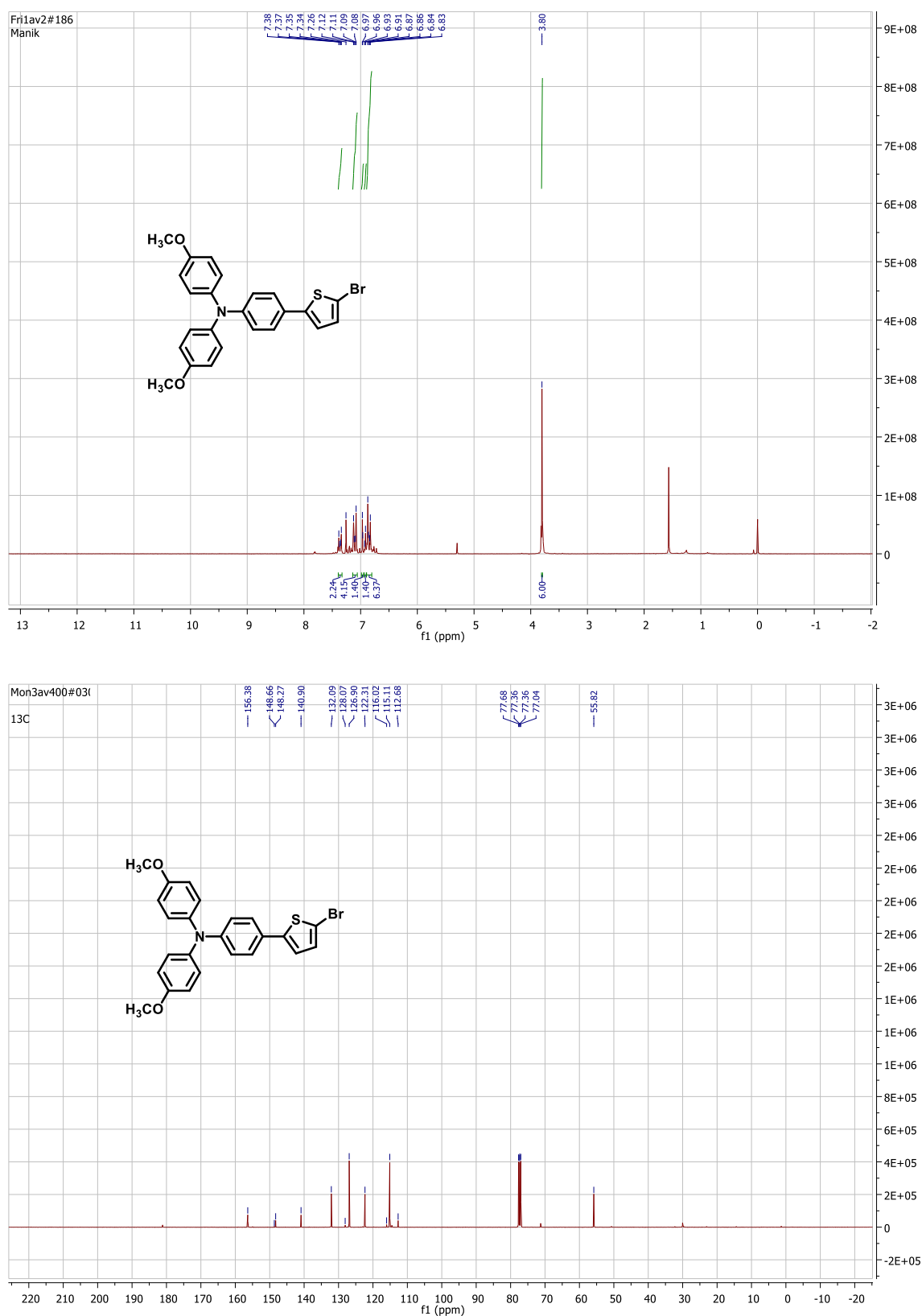
Figure 2. ¹H and ¹³C NMR spectrum (CDCl₃) of 4-methoxy-N-(4-methoxyphenyl)-N-(4-(thiophen-2-yl) phenyl) aniline (**4**).
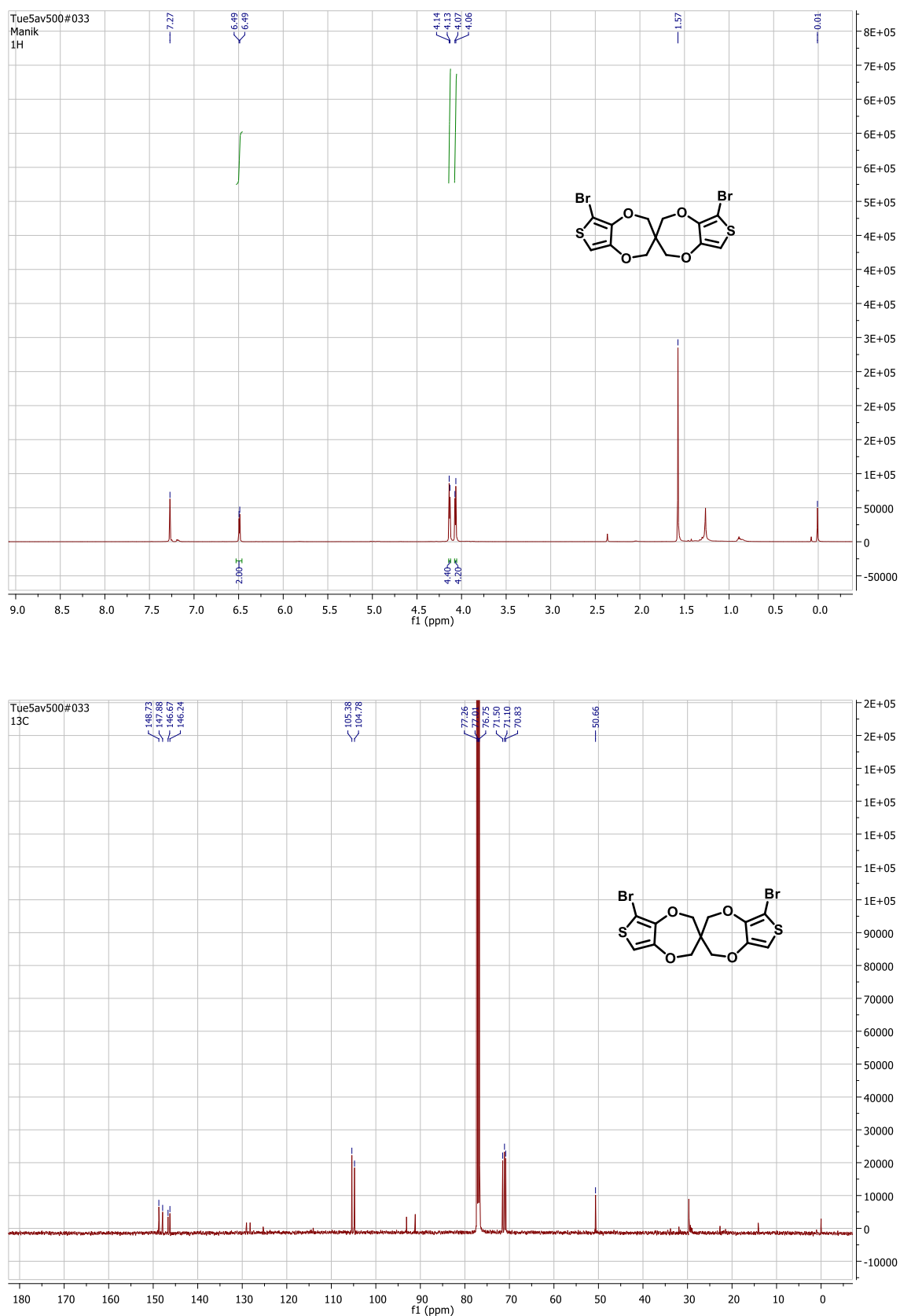
Figure 3. ^{1}H and ^{13}C NMR (CDCl$_3$) of 6,6'-dibromo-2H,2'H,4H,4'H-3,3'-spirobi[thieno[3,4-b][1,4]dioxepine] (**6**).
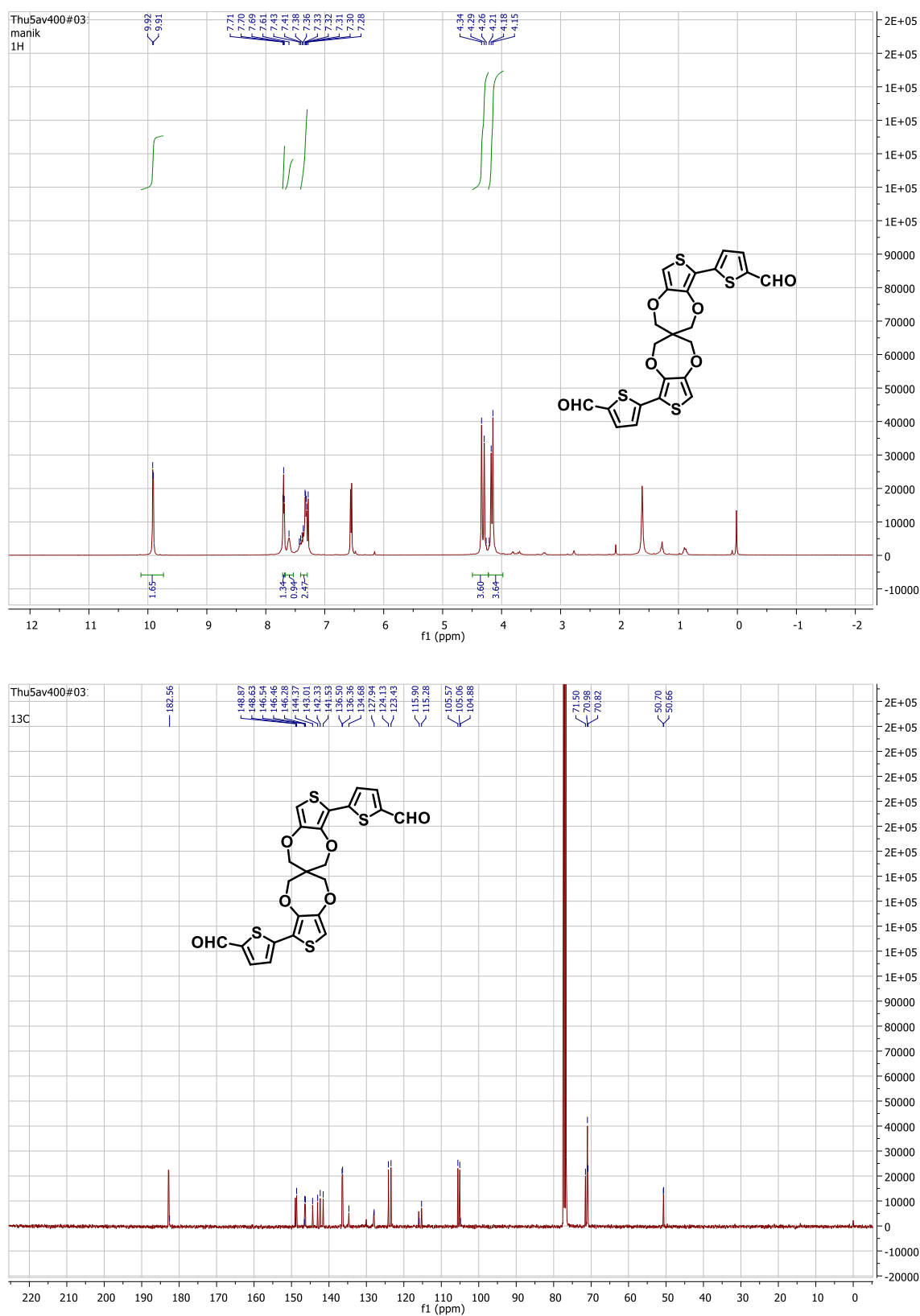
Figure 4. ^{1}H and ^{13}C NMR (CDCl$_3$) 5,5'-(2H,2'H,4H,4'H-3,3'-spirobi[thieno[3,4-b][1,4]dioxepine]-6,6'-diyl)bis(thiophene-2-carbaldehyde) (**7**).
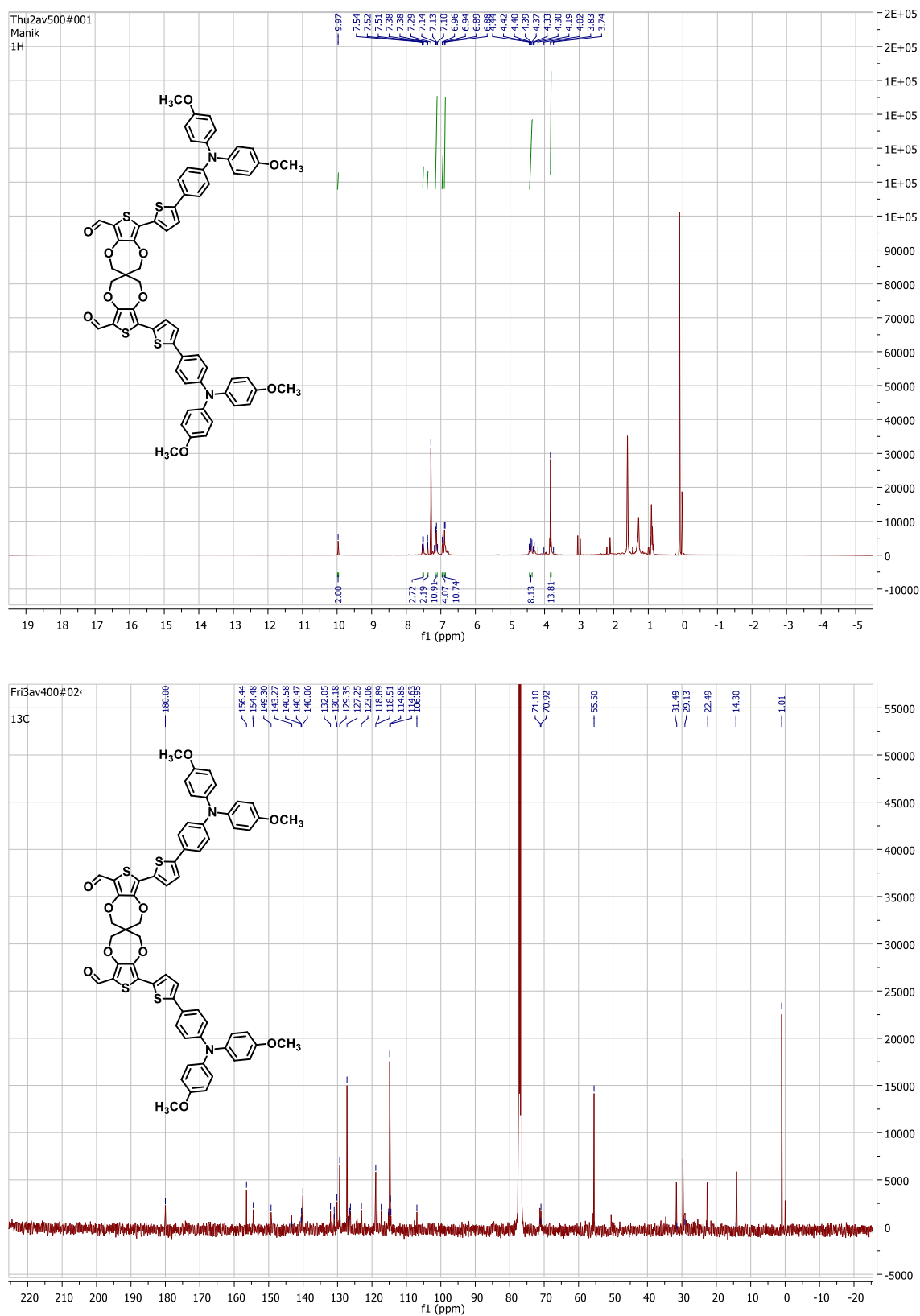
Figure 5. ^{1}H and ^{13}C NMR (CDCl₃) of 6,6'-bis(5-(4-(bis(4-methoxyphenyl)amino)phenyl)thiophen-2-yl)-2H,2'H,4H,4'H-3,3'-spirobi[thieno[3,4-b][1,4]dioxepine]-8,8'-dicarbaldehyde (**9**).
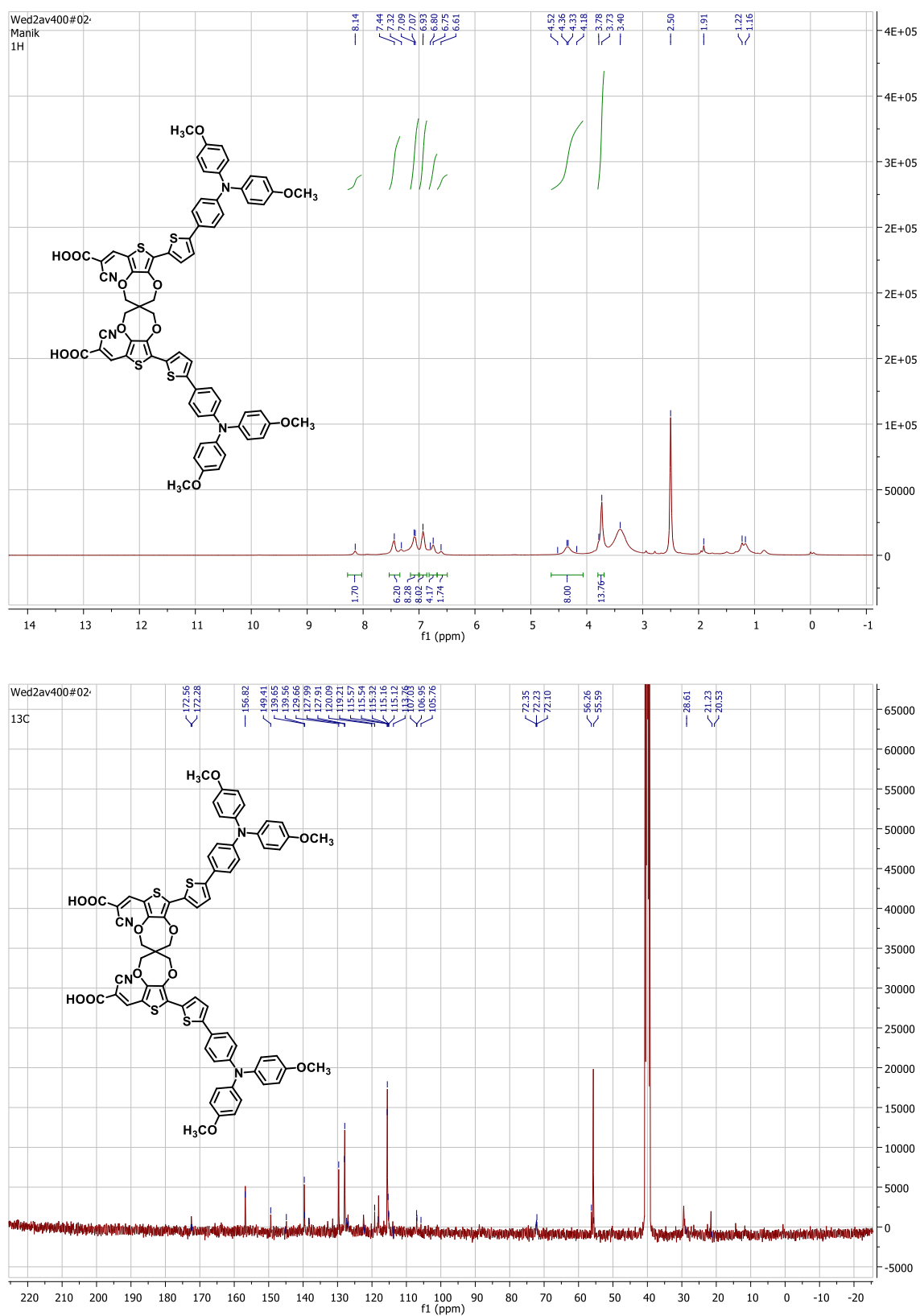
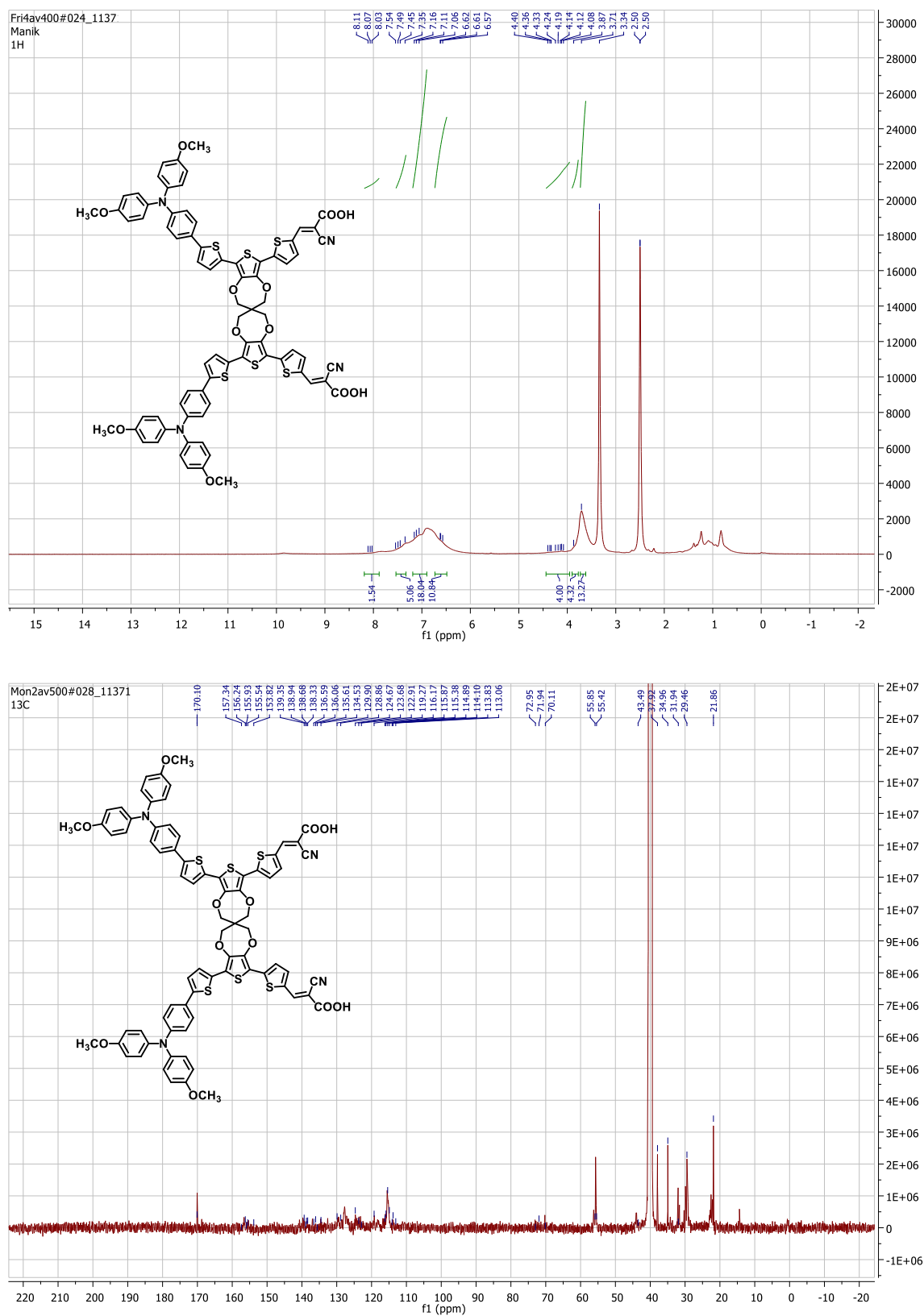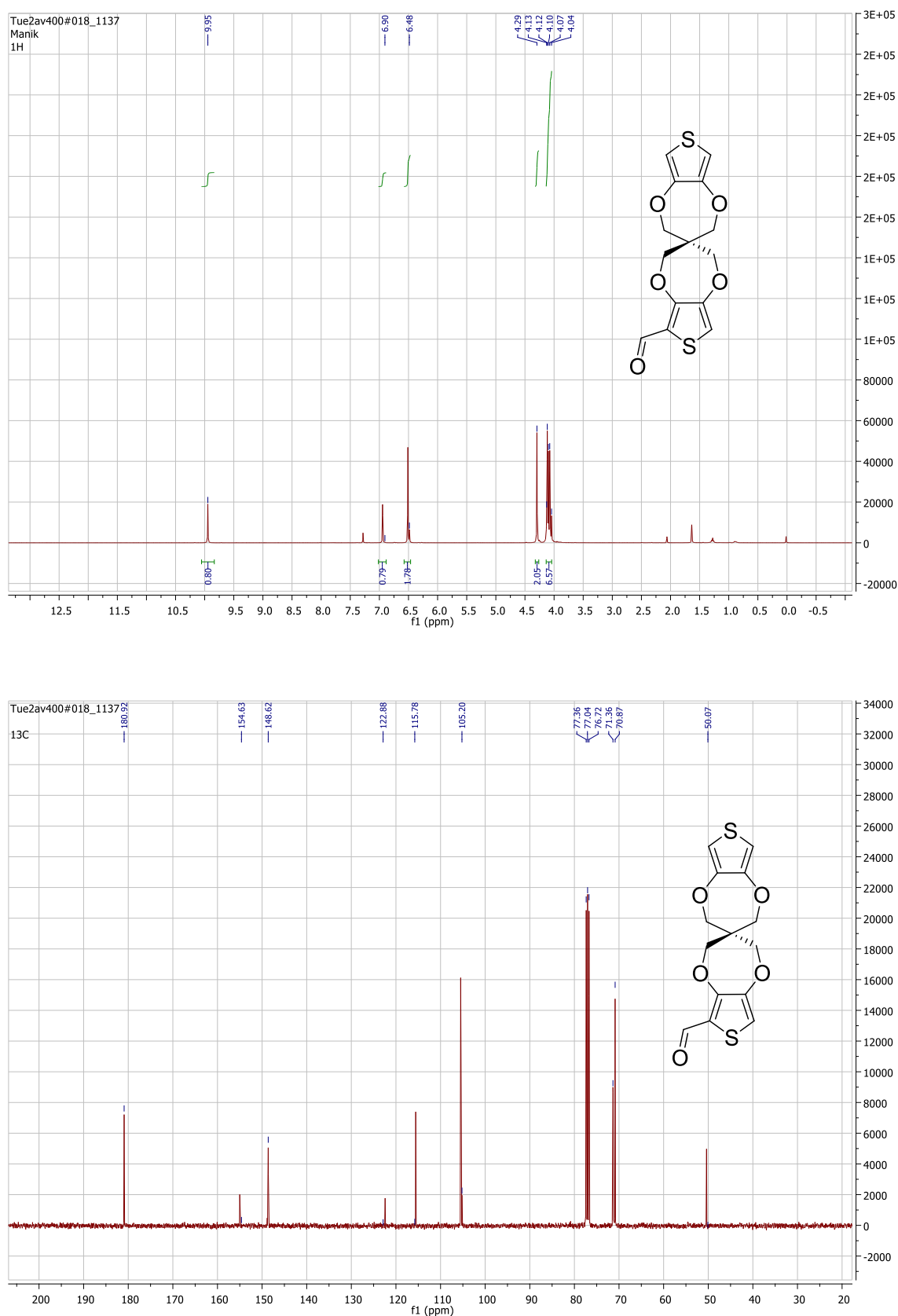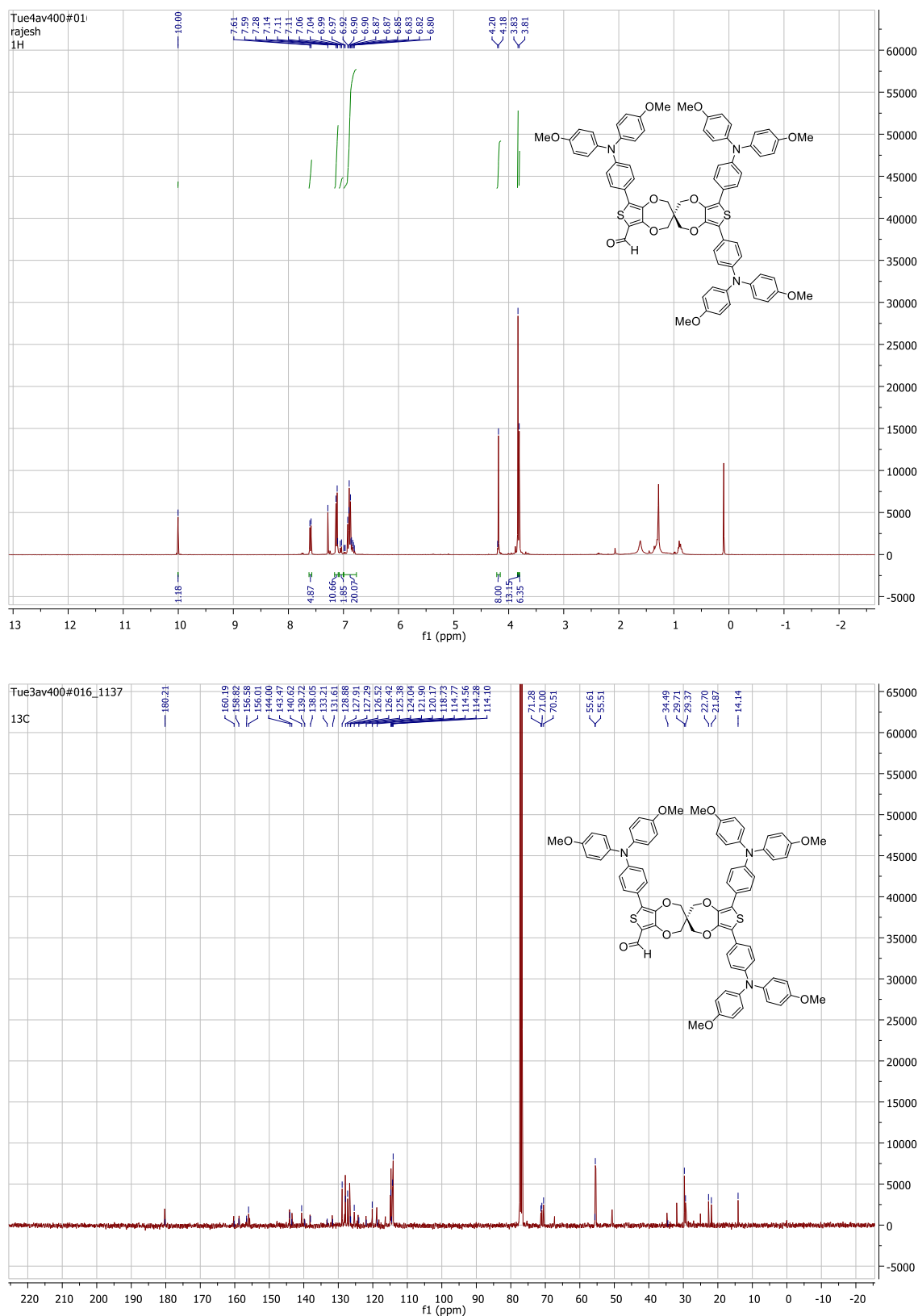**Figure 6.** ^{1}H and ^{13}C NMR (DMSO-d_6) of **TT$_1$, 10**.
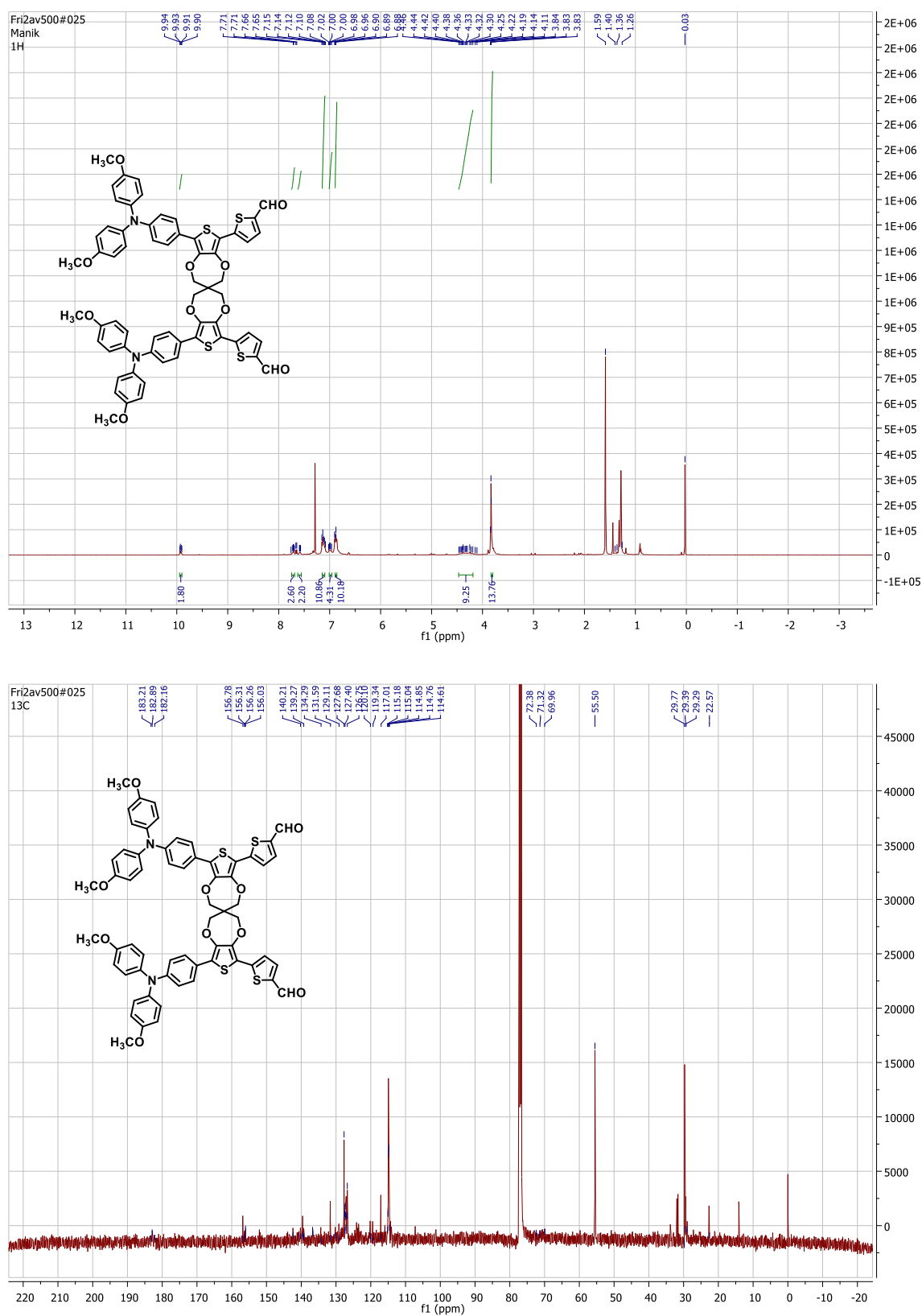
Figure 7. ^{1}H and ^{13}C NMR (CDCl₃) of 5,5'-(6,6'-bis(4-(bis(4-methoxyphenyl)amino)phenyl)-2H,2'H,4H,4'H-3,3'-spirobi[thieno[3,4-b][1,4]dioxepine]-8,8'-diyl)bis(thiophene-2-carbaldehyde) (**11**).
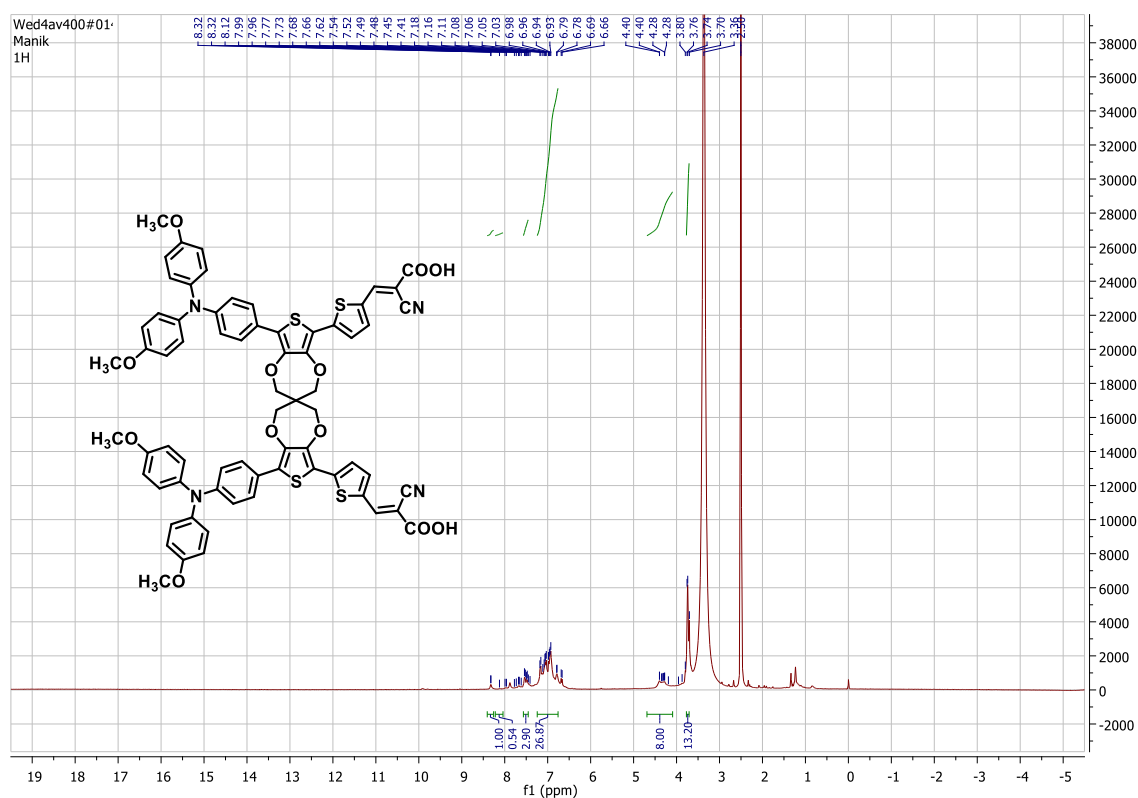
Figure 8. ^{1}H NMR of **T₁T**, **12**.
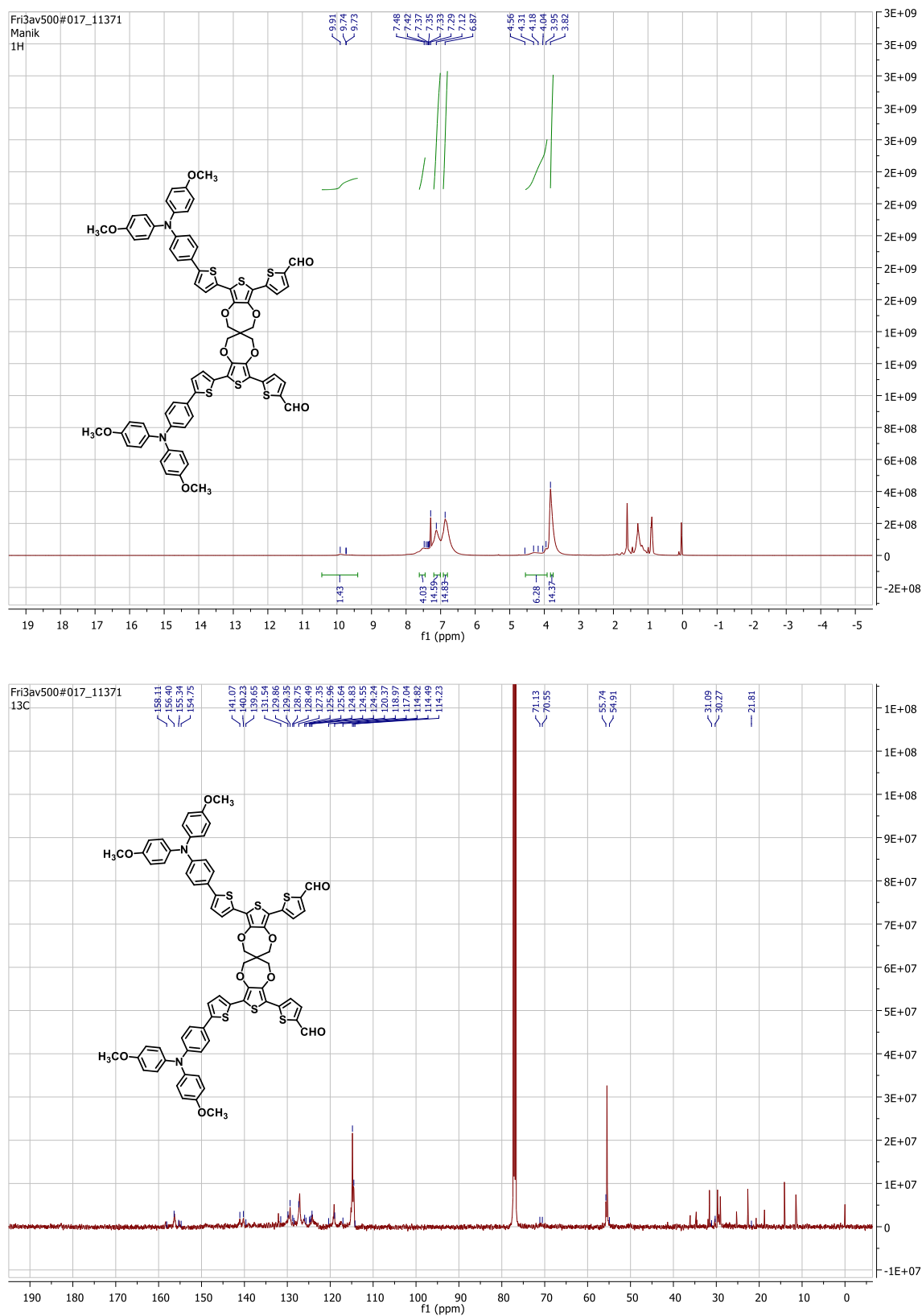
Figure 9. ^{1}H and ^{13}C NMR (DMSO-d_6) of 5,5'-(6,6'-bis(5-(4-(bis(4 methoxyphenyl)amino)phenyl)thiophen-2-yl)-2H,2'H,4H,4'H-3,3'-spirobi[thieno[3,4-b][1,4]dioxepine]-8,8'-diyl)bis(thiophene-2-carbaldehyde) (**13**).

Figure 10. ^{1}H and ^{13}C NMR (DMSO-d_6) of **TT$_1$T, 14**.

¹H-, ¹³C- NMR spectra of 5ᵗʰ chapter

Figure 1. ¹H and ¹³C NMR (CDCl₃) of 2H,2'H,4H,4'H-3,3'-spirobi[thieno[3,4-b][1,4]dioxepine]-6-carbaldehyde (**1**).

Figure 2. ^{1}H and ^{13}C NMR (CDCl3) 6,6',8'-tris(4-(bis(4-methoxyphenyl)amino)phenyl)-2H,2'H,4H,4'H-3,3'-spirobi[thieno[3,4-b][1,4]dioxepine]-8-carbaldehyde (**3**).
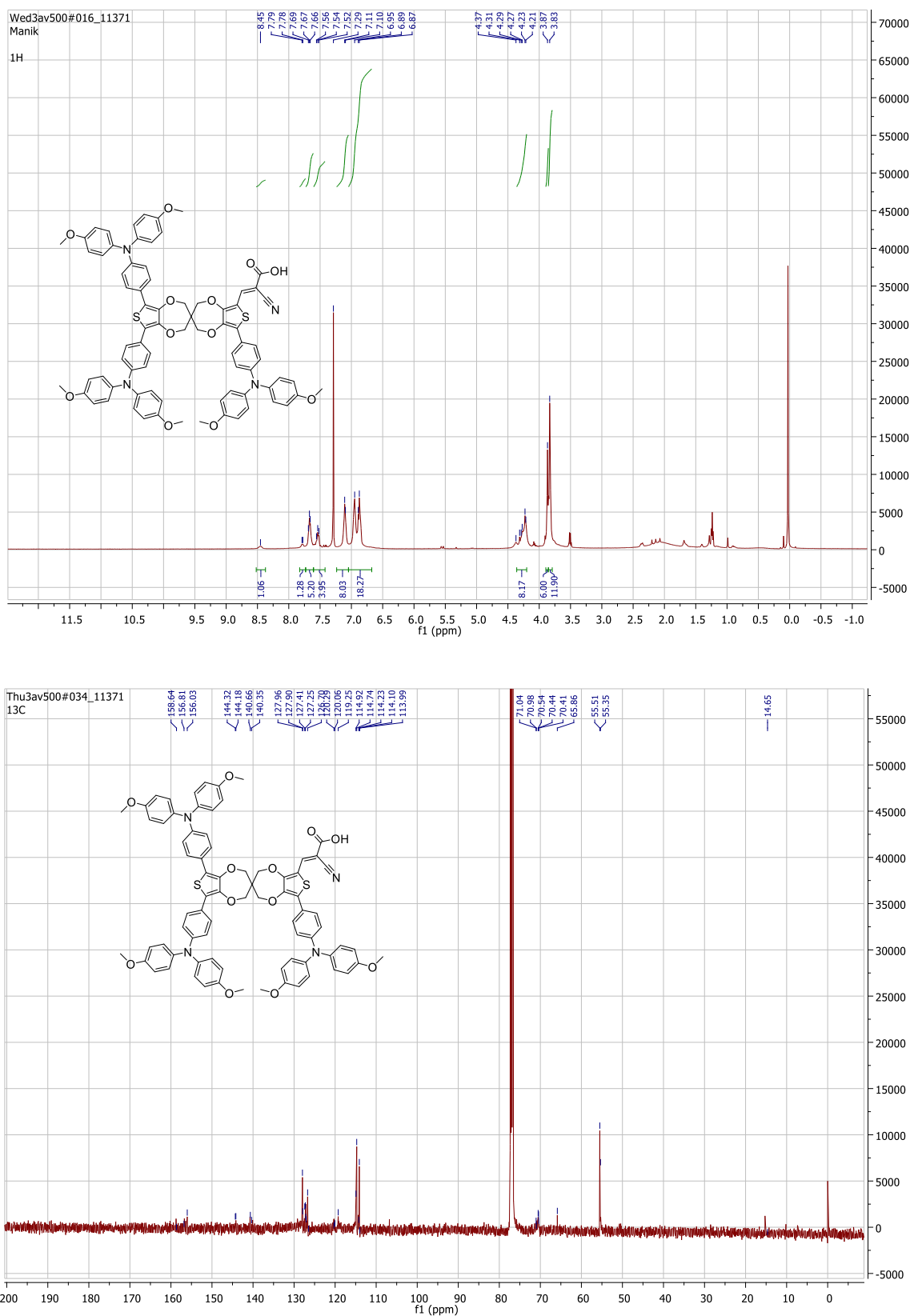
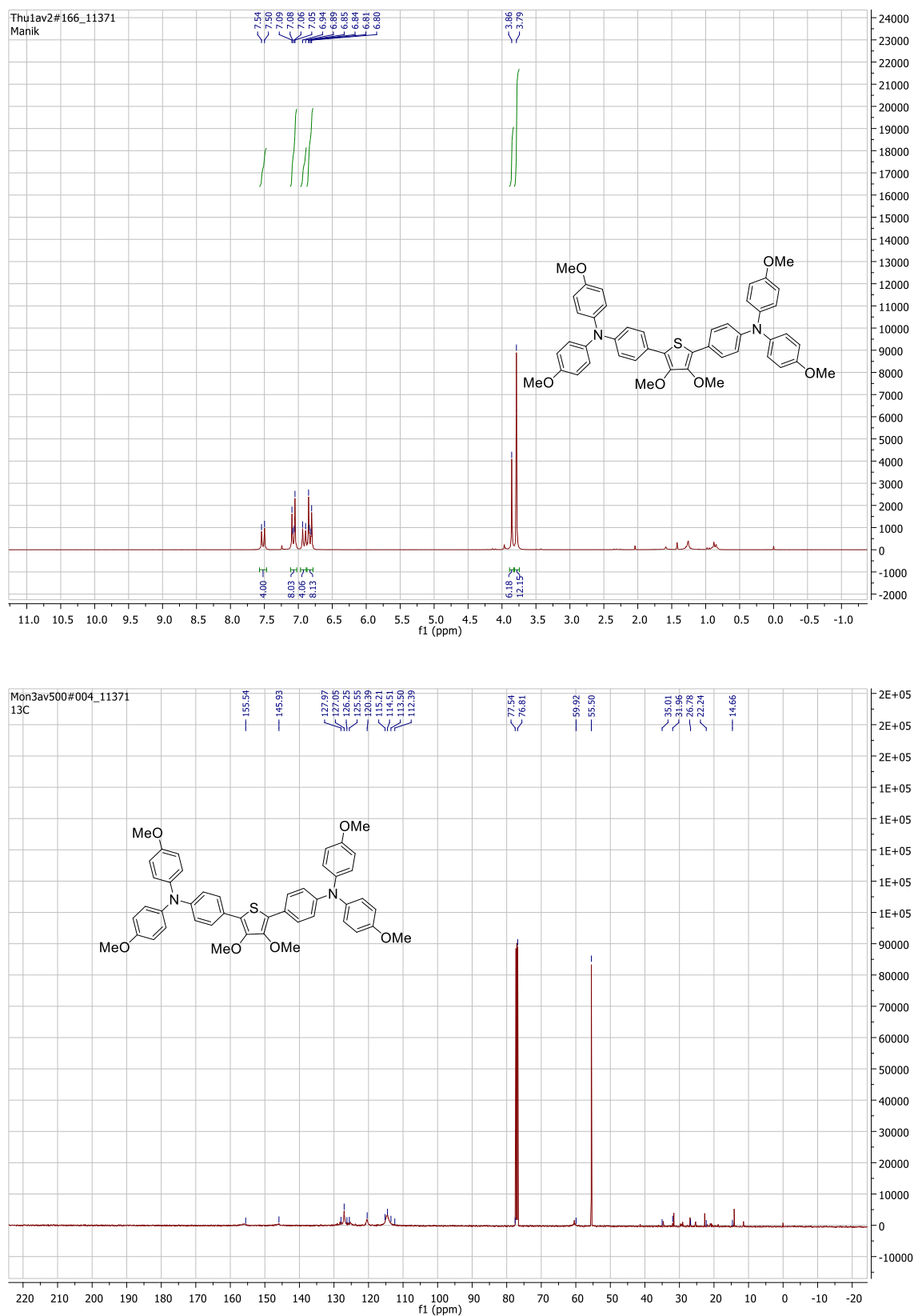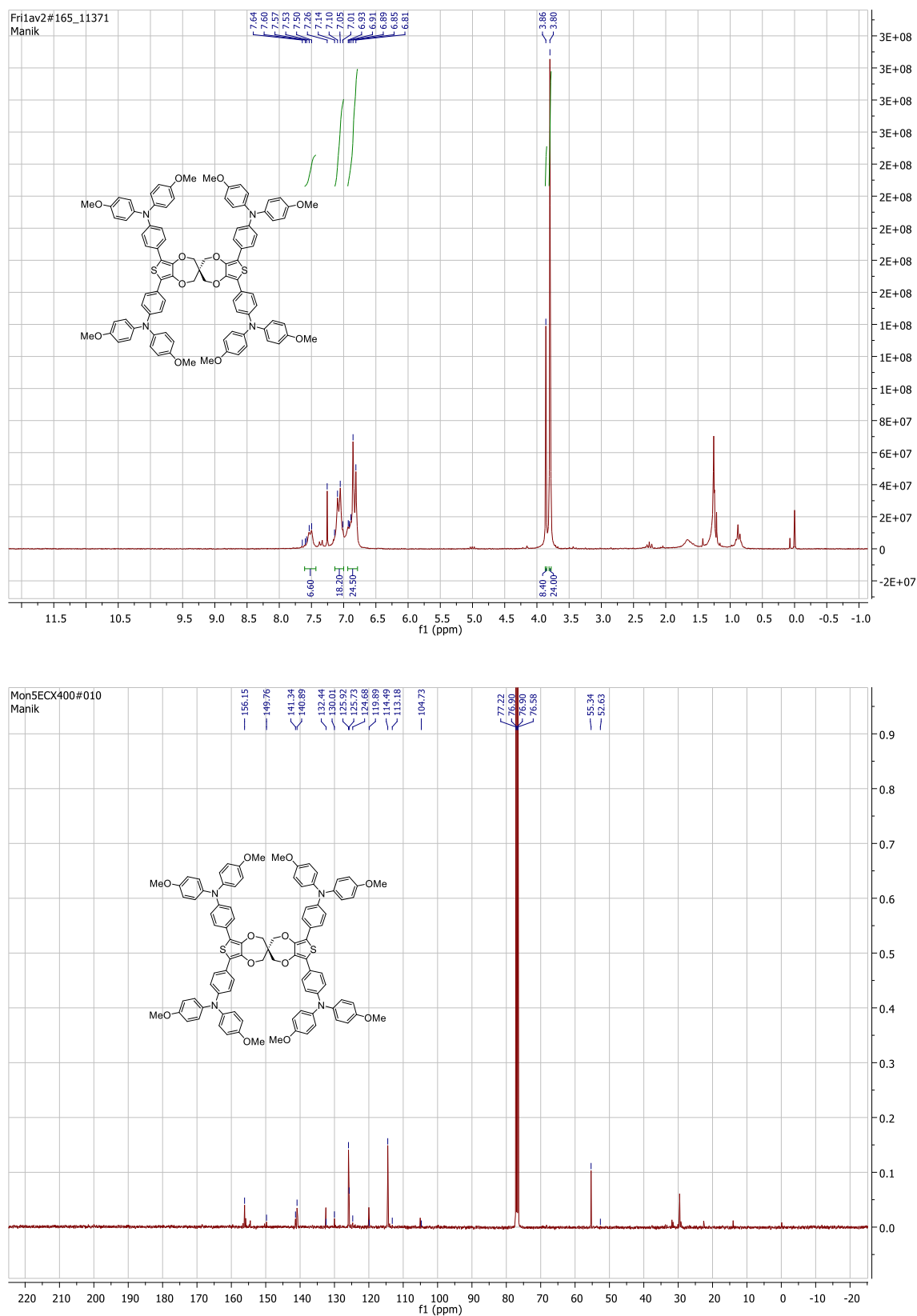**Figure 3.** ^{1}H and ^{13}C NMR (CDCl$_3$) of **D$_1$-HTM, 4**.

Figure 4. ^{1}H and ^{13}C NMR (CDCl$_3$) spectra of **HTM-1**.

Figure 5. ^{1}H and ^{13}C NMR (CDCl$_3$) spectra of **PTS1**.